Environmentally Friendly Medium-Range Aircraft

Final Report

Design Synthesis Exercise (AE3200)

Group 26

Delft University of Technology

TU Delft

Environmentally Friendly Medium-Range Aircraft

Final Report

by

Group 26

Student Name	Student Number
Dhierin-Perkash Bechai	4134303
Douwe den Blanken	4843940
Tomas Dundulis	4813618
Andrada Gheorghe	4651995
Valentine Laruelle	4645782
Lennert Luyckx	4671864
Georgiana-Mălina Mătieş	4780159
Noah Tarbah	4874285
Jaimy Thielen	4853784

Tutors:	Feijia Yin & Roberto Merino-Martinez
Coaches:	Erdem Turan & Jingyi Liu
Teaching Assistant:	Liam Megill
Institution:	Delft University of Technology
Place:	Faculty of Aerospace Engineering, Delft
Project Duration:	April, 2021 - July, 2021
Version:	2.0

Cover Image: own work

TU Delft

Summary

In this report the preliminary design of Zephyr One, an environmentally friendly medium range aircraft, is presented. This design was done by splitting the aircraft into systems: aerodynamics, propulsion, structures, weight, stability and controllability, and configuration. Each of these systems were designed to meet the requirements set out in the Baseline report. With the design space restricted, codes to size each aircraft system and subsystem were made and connected. These codes were iterated to reach a final design.

As with any complex engineering object, a solid design strategy has been developed and used. In this report, Multidisciplinary Design Optimization in the form of Differential Evolution [1] coupled with a custom-built iterator are used to optimise the design. The optimisation revolves around changing four key design parameters, the best combination of which should give the lowest total fuel mass.

The internal layout of the Zephyr One was constructed such that requirements set in the Baseline [2] and Midterm reports [3] are satisfied. The cross-sectional cabin configuration was first determined, after which the top-view configuration was set. The final design of the aircraft is able to carry a total of 203 passengers, of which 23 are business class and 180 are economy class. In addition to the passengers' luggage, the Zephyr One is able to transport up to 4.3 tons of cargo. The internal layout was also constructed such that the required number of lavatories, galleys, and emergency exits is satisfied.

The aerodynamic design of the aircraft was split up in to three main tasks; airfoil selection, planform generation, and aerodynamic characteristics determination. The airfoil selection consisted of picking a set of airfoils differing in thickness to chord ratios, while maintaining optimal cruise characteristics. Each of these selected airfoils were used to size the aircraft in the planform generation task. The planform was generated by first fitting the cabin in to the airfoil geometry, and subsequently sizing the inboard and outboard wing. The aerodynamic characteristics were analysed for each planform using AVL (Athena Vortex Lattice), an aerodynamic analysis program using the Vortex Lattice Method. The configuration of airfoil and planform with the highest L/D during cruise was chosen as the final aerodynamic configuration.

The propulsion system is designed for minimum fuel consumption during cruise, since this is the dominant flight phase for fuel consumption. A full thermodynamic model of a turbofan engine was developed, including a method for NO_x emission calculation. A design with a two stage compressor was chosen. Since emissions were a key constraint on the engine design, a method for core exhaust filtering was included. Using constraints on the design parameters, an optimiser was run to determine the optimal parameters. The fuel tanks and system were designed to meet the needs of the engines. Furthermore, an electric taxiing system was designed, to facilitate the emission-free taxiing requirement.

The structural design is optimised for a given cruising altitude, the objective of the structural analysis being the minimization of the aircraft weight. There are three main interconnected variables that dictate the entire process: the skin thickness, number and cross-sectional of the stringers. For structural purposes, the cross-section is idealised as a perfect ellipse, as the cabin is the main load carrying component. As the cabin is elliptical and not circular, massive bending loads develop in the skin, in addition to normal tension, pressurization becoming the main contributor to critical loads, neglecting the aerodynamic loads for obtaining final results, this assumption being validated. A preliminary trade-off between aluminum and carbon composites has been conducted before choosing the specific material, Al 7075-T6 being eventually the material used for the main structure, but composites are utilised for elevons.

The noise analysis is assessed in a semi-analytical manner, that is, where possible, a quantitative analysis was conducted, while qualitative methods were used otherwise. The Zephyr One is expected to positively surpass the noise requirements set out by Flightpath 2050, exceeding the required values. The noise shielding capabilities allow for a reduction of up to 22.5 dBA for the lateral case, while the engine noise is lowered significantly through the use of Geared TurboFans (GTFs) with Ultra Hight ByPass Ratio (UHBPR). To reduce airframe noise, Low Noise Technologies (LNTs) are implemented for the landing gear. Finally, continuous descent and climb operations are expected to be implemented by the time the aircraft enters into service, and will further contribute to noise reduction on an operational level.

The design of most systems was successful, except for the elevon and landing gear sizing. Due to limitations on the elevon size the rolling requirement during take-off was not met, and due to the tipback requirement the landing gear height of 5 m was chosen, which is too high for current airports. In future work the design of these systems will have to be analysed more in detail and solutions have to be found for these problems.

After obtaining the final design of the aircraft, the performance analysis, sensitivity analysis, operational analysis, and financial analysis were conducted. Zephyr One showed a better performance compared to competing aircraft, especially for sustainability. Additionally, the aircraft is flexible with its fuel and can be run on LNG (Liquid Natural Gas), if synthetically produced methane is not available. In case of synthetic methane, during the operation of the aircraft, zero carbon emissions are produced, due to the CO_2 absorbed during production, and the nitrogen oxides emissions are reduced by about 95% compared to the A321ceo. Moreover, besides its great performance, the aircraft features a competitive price and operational cost, having 8% lower direct operating costs per seat per hour on a 1,907 km flight. When carbon taxes of 20% are considered, the advantage over the A321ceo grows to 16%.

While challenging, recyclability of the Zephyr One could be profitable while further incentives such as overhaul and exchange programs could boost part re-use. On the other hand, the aircraft operations are more complex compared to competing aircraft. The market space for the Zephyr One is estimated to be 4,750 units with profit margins of 19% and a 24% return on investment justifying the $9.3 billion development budget and up to 15 years development time. Finally, the future project development was presented and the compliance matrix was constructed. The aircraft met most of the set out requirements and all of the project goal requirement. The final parameter specifications of the Zephyr One are shown in Table 1. All in all, Zephyr One is an aircraft, which can adapt to various customers needs and most importantly it can achieve great sustainability performance leading to a greener aviation future.

Table 1: Aircraft specifications.

Dimensions	
Wingspan	36 m
Length	34 m
Height	12.77 m
Capacity	
Max seating	260
Typical seating 2-class	203
Max payload	25.3 ton

Performance	
Range	6,482 km
MTOM	81 ton
Max fuel mass	13.5 ton
Max thrust	240 kN
NO_x	2.4 g/km
Maximum noise	67 dBA (at approach)
Cruise speed	869 km/h
Cruise altitude	12.9 km

Contents

Nomenclature

Abbreviations

Abbreviation	Definition
ACN	Aircraft Classification Number
AL	Aircraft List Price
AM	Additive Manufacturing
AMS	Amsterdam Airport Schiphol (Airport Code)
APU	Auxiliary Power Unit
ASP	Aircraft Sales Price
ASL	Average Stage Length
AVL	Athena Vortex Lattice
BH	Block Hour
Capt.	Captain
CBS	Cost Breakdown Structure
CC	Cargo Compartment
CFD	Computational Fluid Dynamics
VLM	Vortex Lattice Method
CO_2	Carbon Dioxide
CG	Center of Gravity
COG	Cost of Goods
$COG_{program}$	Program Costs
DAPCA	Development And Procurement Cost of Aircraft
DoD	Depth of Discharge
D&R	Disposal & Recycle
EASA	European Union Aviation Safety Agency
EoL	End-of-Life
EPNL	Effective Perceived Noise Levels
FAA	Federal Aviation Administration
FEM	Finite Element Method
FC	Flight Cycle
FH	Flight Hour
FO	First Officer
GPWS	Ground Proximity Warning System
GTF	Geared TurboFan
HLD	High Lift Device
HPC	High Pressure Compressor
HPT	High Pressure Turbine
IAS	Indicated Air Speed
ICAO	International Civil Aviation Administration
ISA	International Standard Atmosphere
LD	Load Device
LHV	Lower Heating Value
LNG	Liquid Natural Gas
LNT	Low Noise Technology
LPC	Low Pressure Compressor
LPT	Low Pressure Turbine

Abbreviation	Definition
MAC	Mean Aerodynamic Chord
MDO	Multidisciplinary Design Optimization
MLG	Main Landing Gear
MOI	Moment Of Inertia
MTOM	Maximum Take-Off Mass
MTOW	Maximum Take-Off Weight
NACA	National Advisory Committee for Aeronautics
NLG	Nose Landing Gear
NO_x	Nitrogen Oxides
OASPL	Overall Sound Pressure Level
OEI	One Engine Inoperative
OEM	Operational Empty Mass
PQ	Production Quantity
PEST	Political, Economic, Sociological, Technological
RAMS	Reliability, Availability, Maintainability and Safety
ROI	Return on Investment
req.	Requirement
SA	Single-Aisle
SCR	Selective Catalytic Reductor
SWOT	Stength, Weakness, Opportunity, Threats
TA	Twin-Aisle
TRL	Technological Readiness Level
TSFC	Thrust Specific Fuel Consumption
ULD	Unit Load Device
VS	Versus
WTC	Wake Turbulence Category

Symbols

Symbol	Definition	Unit
A	Aspect ratio	[-]
ac	Aerodynamic center	[-]
A_m	Cross-sectional area	[m^2]
a	Acceleration	[m/s^2]
b	Wingspan	[m]
$b_{stringers}$	Stringer Pitch	[m]
b_{aft}	Outer wing span	[m]
b_e	Spanwise position	[m]
b_N	[FILL IN]	[m]
C_a	Airframe costs	[$ mio]
C_e	Engine costs	[$ mio]
C_D	Drag coefficient	[-]
C_{D_i}	Induced drag coefficient	[-]
C_{D_0}	Zero lift drag coefficient	[-]
C_d	Airfoil drag coefficient	[-]
$C_{l_{d_0}}$	Airfoil zero lift drag coefficient	[-]
C_f	Skin friction coefficient	[-]
C_L	Lift coefficient	[-]
$C_{L_{aft}}$	Outer wing lift coefficient	[-]

Symbol	Definition	Unit
$C_{L_{max}}$	Maximum lift coefficient	[-]
$C_{L_{\alpha_{aft}}}$	Outer wing lift slope	[rad^{-1}]
C_{l_p}	Roll damping coefficient	[-]
C_{l_α}	Airfoil lift slope	[rad^{-1}]
$C_{l_{\delta\alpha}}$	Aileron control derivative	[-]
C_m	Airfoil moment coefficient	[-]
C_{M_α}	Aircraft coefficient slope	[-]
$C_{p,g}$	Isobaric heat capacity	[kJ/kg K]
c	Chord	[m]
c	Speed of sound	[m/s]
c_r	Root chord	[m]
c_t	Root chord	[m]
D	Drag	[N]
DoD	Depth of discharge	[%]
d	Separation distance standard	[m]
E_{bat}	Battery energy required	[kWh]
e	Oswald efficiency factor	[-]
e	Eccentricity	[-]
f_{centre}	Centre frequency of noise source	[Hz]
F_{ff}	Ground friction	[N]
FF	Form factor	[-]
h	length of the common final path	[m]
I_{yy}	Mass moment of inertia	[kgm^2]
k	Buckling coefficient	[-]
L	Lift	[N]
L_h	Elevon generated lift	[N]
$L_{A,max}$	Maximum A weighted sound pressure level	[dBA]
L_p	Sound pressure level	[dB]
M	Mach number	[-]
M_{ac}	Moment of aerodynamic center	[Nm]
M_{mlg}	Moment around main landing gear	[Nm]
m	Mass	[kg]
$\dot{m}$	Mass flow	[kg/s]
N	Fresnel Number	[-]
n	Load factor	[-]
n_daily	daily flights	[-]
$n_{passengers}$	Number of passengers	[-]
o	Increase in separation on the common final path	[m]
P	Rotational speed	[rad/s]
P_{bat}	Battery charging power	[kW]
p	Pressure	[Pa]
q	Shear flow	[N/m]
r	Radius	[m]
Re	Reynolds number	[-]
S	Surface area	[m^2]
S_{ref}	Reference surface area	[m^2]
S_{wet}	Wetted area	[m^2]
T	Temperature	[K]
T_B	Buffer time	[s]
T_N	Thrust	[N]
T_S	Minimum permitted separation time	[s]

Symbol	Definition	Unit
T_{SIA}	Scheduled interarrival time between two successive aircraft at the runway threshold	[s]
V	Velocity	[m/s]
V_{cargo}	Volume of the cargo	[m^3]
V_D	Dive Speed	[m/s]
V_L	Approach speed of the leading aircraft	[m/s]
V_s	Stall Speed	[m/s]
V_T	Approach speed of the trailing aircraft	[m/s]
W	Weight	[N]
x	Longitudinal position	[m]
y	Lateral position	[m]
z	Vertical position	[m]
δ_{max}	Maximum deflection	[rad]
δ_w	Turbulent boundary layer thickness	[m]
η	Efficiency	[-]
$\ddot{\theta}$	Angular acceleration	[rad/s^2]
κ	Specific heat ratio	[-]
Λ	Sweep angle	[rad]
$\Lambda_{0.5}$	Half chord sweep angle	[rad]
λ	Taper ratio	[-]
λ	Differential parameter	[-]
ν	Poisson ratio	[-]
ρ	Density	[kg/m^3]
τ	Control surface efficiency	[-]
ψ	Turnover angle	[rad]

1 Introduction

In today's world, sustainability, waste, and the mitigation of pollution are becoming matters of paramount importance in all industries and especially in the aviation industry. The latter accounted for 2% of the global CO_2 emissions in 2019[1] and 3% of the global NO_x emissions [4]. These emissions do not only come from burnt fuel during flight but also from processes happening before an aircraft takes to the skies, such as manufacturing. Additionally, with increasing number of flights the noise produced by aircraft is becoming a major concern for people living around airports and their health [5]. Thus, with a desire of consumers to fly more but with the interest of society to decrease environmental impact, companies in the aviation industry are aiming for sustainability while still being competitive.

Even though the aviation industry is showing an annual growth rate of 5%[2], most emerging sustainable concepts are based on very small aircraft, while fewer options appear for small-to-medium aircraft. On the other hand, a significant part of commercial aviation relies on medium-range aircraft, which account for around 90% of the market [6]. Thus, the aim of this project is to design a sustainable medium-range aircraft.

In previous reports, the mission need statement of this project was formulated: "*to design a medium-range, 200 passenger airliner that is considerably quieter and more environmentally friendly than the Airbus A320 family, achieving the goals of 'Flightpath 2050'*". Additionally, the project objective statement was "*to design 75% of the aircraft out of recyclable materials, reduce the NO_x and CO_2 emissions by 90% and 75% respectively, and mitigate the noise pollution by 65%*". The requirements were then established to meet certain performance and safety standards, while also complying with the users, the Flightpath 2050 goals, airport limitations, and financial aspects. After the Midterm report [3] a concept was chosen, and in this report, a more detailed design of this concept is given.

The goal of this report is to present the preliminary design of the aircraft, Zephyr One. This is usually done by designing for each system and subsystem and iterating the system parameters till they converge to a final design, capable of achieving the set out goals. Additionally, to show the benefits of the Zephyr One compared to competing aircraft a performance, operations and financial analysis should be completed.

The report is structured as follows. The summary of the steps taken in the Baseline and Midterm reports is given in Chapter 2, followed by the design methodology in Chapter 3. After this the aircraft configuration is presented in Chapter 4, following with the design of each system: aerodynamics - Chapter 5, propulsion - Chapter 6, structures - Chapter 7, weight estimation - Chapter 8, and stability and controllability - Chapter 9. Sensitivity analysis of the design is presented in Chapter 10. Next, the noise analysis is conducted in Chapter 11 and the remaining performance analysis is presented in Chapter 12, followed by operations and logistics in Chapter 13. A financial analysis is performed in Chapter 14 and the risk analysis is presented in Chapter 15. Furthermore, the future development of the project is given in Chapter 16 and aircraft validation is performed in Chapter 17. Finally, the conclusions are presented in Chapter 18.

[1] https://www.atag.org/facts-figures.html [cited 19 April 2021]

[2] https://www.statista.com/statistics/278372/revenue-of-commercial-airlines-worldwide/#:~:text=For%20instance%2C%20revenue%20in%20the,billion%20U.S.%20dollars%20in%202019. [cited 26 April 2021]

2 Concept Selection

In this chapter mainly the overview of the work done in Baseline and Midterm reports is presented [2, 3]. This overview will focus on the functional analysis presented in Section 2.1, requirements discussed in Section 2.2, the four concepts discussed in Section 2.3 and the trade-off process summarized in Section 2.4.

2.1. Functional Flow Diagram and Functional Breakdown

A functional breakdown structure and functional block diagram are useful tools to identify the functions the aircraft needs to perform and in turn the requirements the aircraft has to fulfill. These diagrams were made for the Baseline report and are presented in Figure 2.1 and 2.2 [2].

2.2. Requirements

The full list of requirements is presented in Table 2.1 and 2.2. The driving requirements, which influenced design options the most, have been highlighted. Additionally, some of the requirements have been removed, as they were no longer relevant for the Zephyr One aircraft.

Performance requirements		**Origin**
EFMRA-SYS-PF-01	The aircraft shall have a range of at least 6,150 km.	User req.
EFMRA-SYS-PF-02	The aircraft shall have a endurance of at least 6 h.	User req.
EFMRA-SYS-PF-03	The aircraft shall have a cruise speed of at least 830 km/h.	User req.
EFMRA-SYS-PF-04	The aircraft shall have a cruise altitude of at least 9,144 m.	User req.
EFMRA-SYS-PF-05	The aircraft shall have a take-off distance of at most 2,100 m.	User req.
EFMRA-SYS-PF-06	The aircraft shall have a landing distance of at most 1,500 m.	User req.
EFMRA-SYS-PF-07	The aircraft shall be able to carry at least 200 passengers and their luggage.	User req.
EFMRA-SYS-PF-08	The aircraft shall operate up to a Mach number of 0.8.	Functions
EFMRA-SYS-PF-09	The aircraft shall have a rate of climb of at least 12.7 m/s.	Functions
EFMRA-SYS-PF-10	The aircraft shall have a stall speed in landing configuration of no more than 55.8 m/s.	Functions
EFMRA-SYS-PF-11	The aircraft shall be able to carry up to 4.5 tons of cargo.	Market analysis
Safety requirements		**Origin**
EFMRA-SYS-SF-01	The aircraft shall comply with CS-25 climb gradient requirements.	Regulations

Table 2.1: Aircraft Requirements.

EFMRA-SYS-SF-02	The aircraft shall be stable and controllable.	Regulations
EFMRA-SYS-SF-03	The aircraft shall be capable of safely landing and taking-off with at most 37 km/h crosswind.	Regulations
EFMRA-SYS-SF-04	The aircraft shall comply with CS-25 loading requirements.	Regulations
EFMRA-SYS-SF-05	In case of one aisle the aircraft shall not have more than 3 seats abreast on each side of the aisle in any one row.	Regulations
EFMRA-SYS-SF-06	The aircraft shall comply with CS-25 climate control requirements.	Regulations
EFMRA-SYS-SF-07	The aircraft shall have an emergency fuel pump in case of failure of the main pump.	Regulations
EFMRA-SYS-SF-08	The engine of the aircraft shall be separated by a firewall from the rest of the aircraft.	Regulations
~~**EFMRA-SYS-SF-09**~~	~~The aircraft shall comply with CS-25 propeller clearance requirements if propellers are used.~~	~~Regulations~~
EFMRA-SYS-SF-10	The aircraft shall comply with CS-25 emergency exit requirements.	Regulations
EFMRA-SYS-SF-11	The aircraft shall comply with safety rules for reserve fuel/energy.	Regulations
EFMRA-SYS-SF-12	The aircraft shall be able to achieve an ETOPS 180 certification.	Market analysis
Flightpath 2050 requirements		**Origin**
EFMRA-SYS-FP-01	The aircraft shall be at least 75% recyclable.	User req.
EFMRA-SYS-FP-02	The aircraft shall comply with Flightpath 2050 goals for noise.	User req.
EFMRA-SYS-FP-03	The aircraft shall comply with Flightpath 2050 goals for emissions.	User req.
Airport requirements		**Origin**
EFMRA-SYS-AP-01	The aircraft shall be able to operate at a 4C type aerodrome.	Market analysis
EFMRA-SYS-AP-02	The aircraft shall have a turnaround time of no more than 52 min.	Market analysis
EFMRA-SYS-AP-03	The aircraft shall be compatible with existing ground material for the loading and unloading of passengers.	Market analysis
Financial requirements		**Origin**
EFMRA-SYS-FR-01	The aircraft shall cost not more than 100 million euros.	User req.
EFMRA-SYS-FR-02	The aircraft's operations shall cost not more than 2,700 euros per block hour.	Functions
EFMRA-SYS-FR-03	The aircraft shall be available by 2036.	Market analysis
EFMRA-SYS-FR-04	The aircraft shall be able to perform 4 flights per day for medium haul operations.	Market analysis
EFMRA-SYS-FR-05	The aircraft shall have an operational life of at least 30 years.	Market analysis

Table 2.2: Aircraft Requirements continued.

2.3. Concepts

Four concepts were created to enter the trade-off phase. Each of them featured a different aircraft configuration, energy source and propulsion system. The four concepts are described below [3]:

Concept 1
The first concept consists of a narrow-body box wing aircraft utilising a set of geared turbofans as the

propulsion system. This configuration allows for the reduction of induced drag by merging the wingtips and the tail in a box-like structure, while the geared turbofans allow for both noise and emissions reduction. In an effort to further reduce emissions, this concept implements bio-fuel as an energy source.

Concept 2
Concept 2 brings forward the double bubble fuselage, featuring a conventional wing configuration with morphing airfoil technology. The latter feature is implemented in order to optimise the lift-to-drag ratio at all times during the flight, while also reducing noise. This concept is propelled by a distributed propulsion system powered by hydrogen fuel cells.

Concept 3
Concept 3 combines the aerodynamic benefits of a blended wing body configuration with the environmental advantages of a turbofan-powered by hydrogen combustion. The combination of these two effects can help greatly reduce NO_x and CO_2 emissions as well as fuel consumption and noise.

Concept 4
Concept 4 is a sub-category of concept 3, making use of a Flying-V configuration, which is a specific shape of the blended wing body that allows for a shorter wingspan. The noise shielding capabilities of the airframe, together with the distributed ducted fans are expected to contribute to the achievement of Flight Path 2050 requirements. This concept also features methane as an energy source.

2.4. Trade-off

In order to fairly choose the best concept, a trade-off was performed. The trade-off was conducted by defining criteria to evaluate for each concept and giving each criteria a weight. The total weight was 1000 and the chosen criteria and the weight of them was: emissions (324), noise (245), RAMS (186), cost (123) and technology readiness level (TRL) (123). Weight was given out by comparing each criteria by their importance. As sustainability is one of the most important aspects of this project, emission and noise criteria got the highest weights. Emissions were evaluated quantitatively and were split into CO_2 and NO_x emissions. Noise was evaluated qualitatively and was split into propulsion system noise, airframe noise and noise shielding capabilities. RAMS was evaluated qualitatively and was divided into availability, maintainability and safety. The reliability of the aspect was evaluated for TRL. Cost criteria was split into the direct operating cost and sale price and it was graded quantitatively. Finally, the TRL consisted the wing, fuselage, energy source and engine type TRL. The grades were given from one to five, one being the worst performance and five the best.

Concept 4 won the preliminary trade-off, however, it was concluded that the energy source has a big influence on the trade-off results, so a more detailed trade-off was done. The four airframes remained the same with each of them utilising a geared turbofan. However, each of them was evaluated for three different energy sources: liquid hydrogen, liquid methane and hybrid liquid hydrogen. In total 12 concepts were evaluated, and the concept 4 airframe powered by methane won the further trade-off. This design not only won the trade-off, but also

posed an interesting design challenge for the group, and thus it continued to the final phase for a more detailed design.

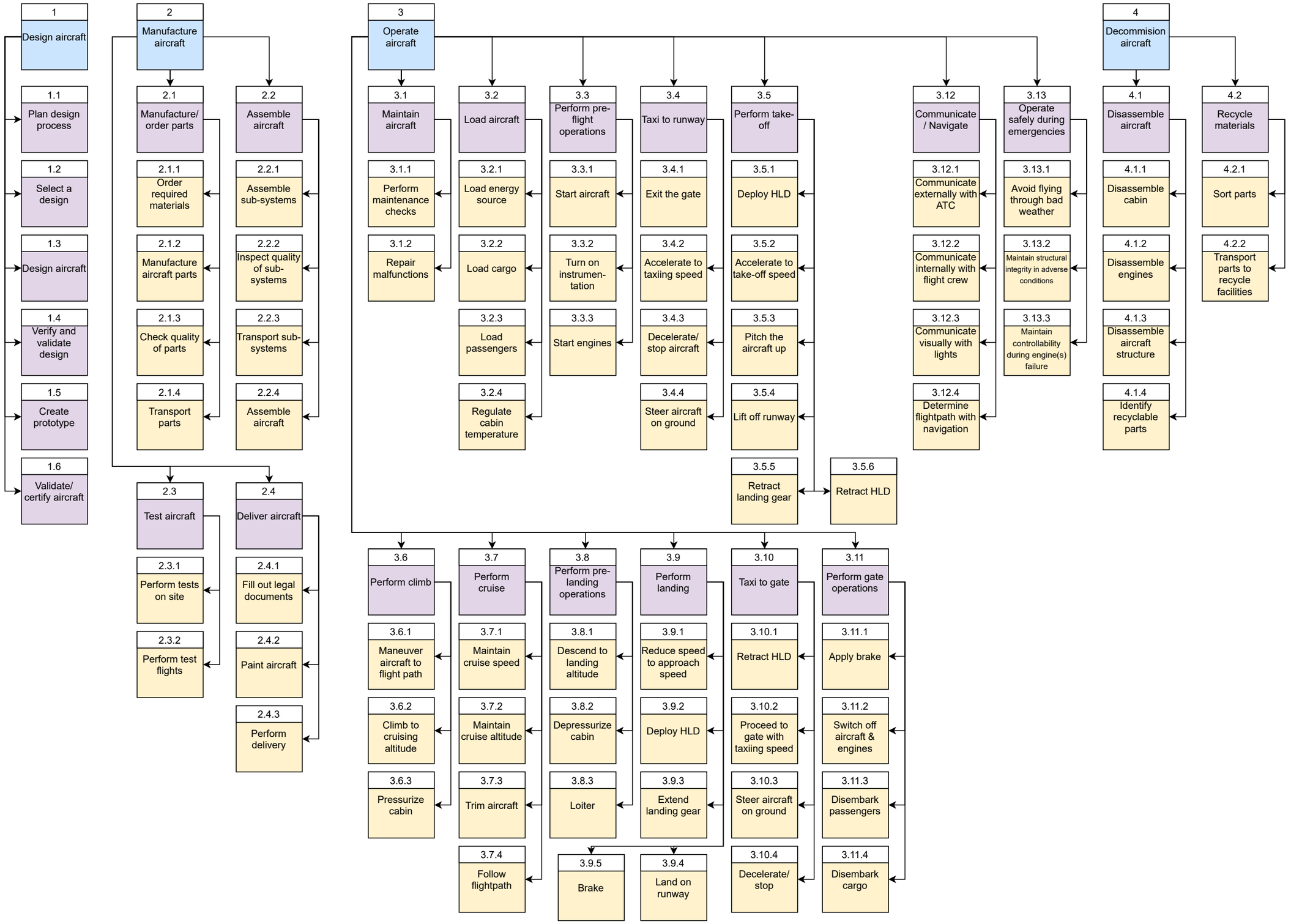

Figure 2.1: Functional breakdown structure of the aircraft.

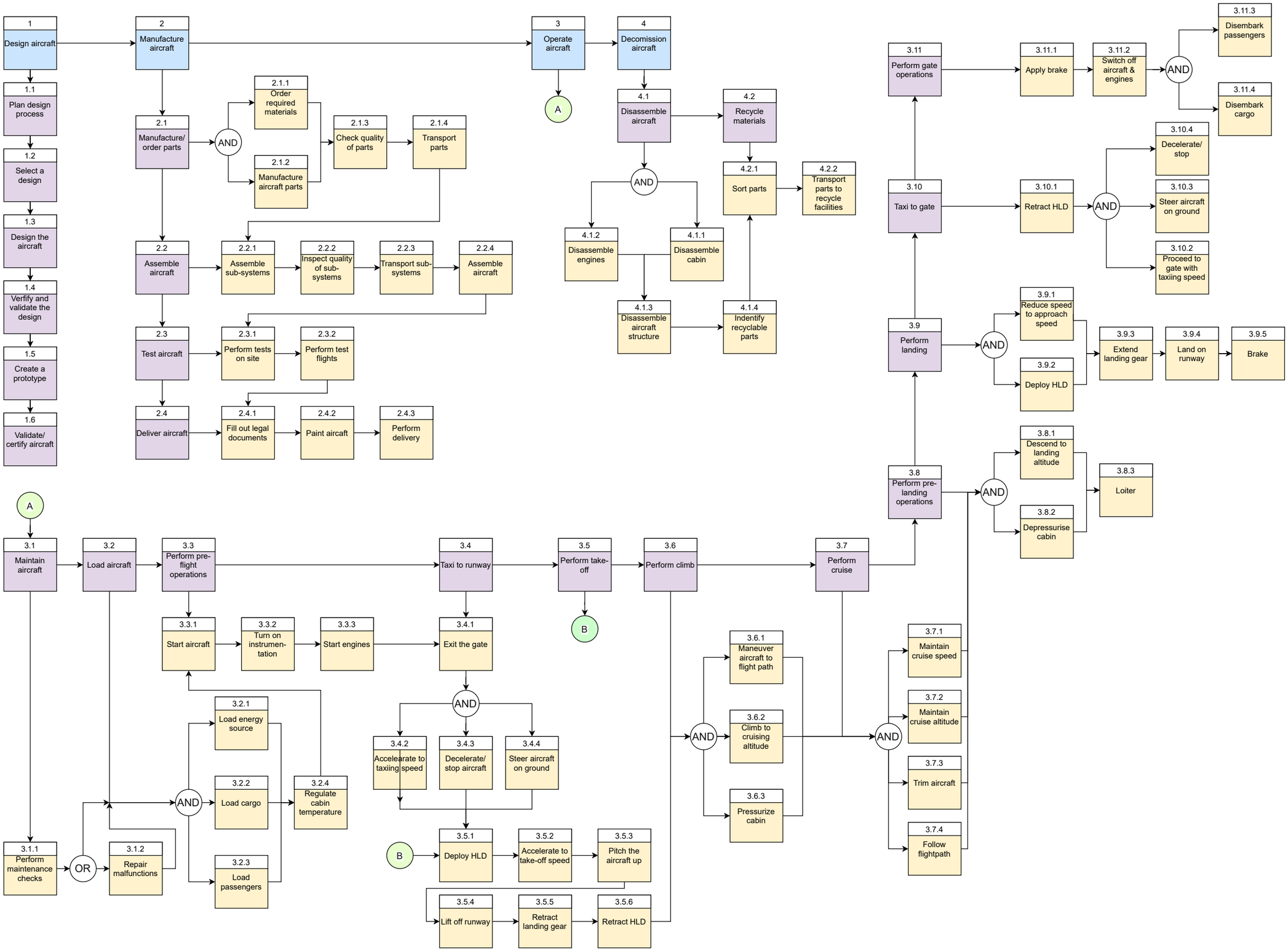

Figure 2.2: Functional flow block diagram of the aircraft.

3 Design Methodology

In this chapter, the holistic approach towards designing and optimising the aircraft will be explained. First, in Section 3.1, the procedure of generating a single design will be discussed. Then, in Section 3.2, the way the entire aircraft design is optimized will be presented. Next, the actual implementation of the optimisation is presented in Section 3.3. Finally, some recommendations are given in Section 3.4.

3.1. Design Procedure

Aircraft design is a hugely interdisciplinary effort, with couplings between almost all the engineering design components. The result of this is that a single part cannot be designed without having all the other parts designed, as all of them impose certain limits and constraints on each other. As such, an iterative procedure is applied to come to a final converging design. Using a set of initial values, every iteration will cause the aircraft design to reach closer to a final set of design parameters. An important detail of this method however is to ensure that all parts of the aircraft design are completely automatised and no further human input and interference is required. As such, the challenge of the design for the Zephyr One is to guarantee that every subsystem design process is entirely automatised and that all required parameters can flow in to the next subsystem design. The process and sequence of the aircraft design is shown in Figure 3.1.

The first step of the aircraft design is establishing a Class I weight estimation. The Class I weight estimation is a simple procedure which results in the mass components of the aircraft, an important parameter which will become an input for almost all of the steps afterwards. The next part of the design process is sizing the cabin. The cabin size is an important input for the aerodynamic design, as it will serve as a baseline for the aircraft airfoil size and planform. As such, the cabin sizing is followed by the aerodynamic design of the aircraft. The aerodynamic design is one of the crucial steps in the design process during which the entire aircraft is sized and its aerodynamic characteristics are determined.

The design of the propulsion system is performed after the aerodynamic design. The propulsion system design sizes the engine, from which a fuel consumption can be determined. The propulsion design is followed by the structural design. In the structural design process, the required structure for the aircraft is calculated, from which a structural weight of the aircraft is found. This then flows in to the Class II weight estimation, where a more accurate weight estimate is found and the center of gravity is established. Using the center of gravity positions, stability of the aircraft can be ensured and the control surfaces can be sized.

At the end of a single loop, the entire aircraft is designed. The process can be repeated, using the results from the previous iteration as inputs for the new iteration. The process is repeated until a final convergent design is found. For the Zephyr One, the aircraft design was deemed converged once the fuel mass of the aircraft changed by less than 1 % compared to the previous iteration. As an extra safety measure, the design is iterated once more after convergence and then checked for convergence again, to make sure that the generated design is 'stable'.

3.2. Design Optimization

As explained in the previous section, an iterative procedure is used for convergence towards a stable design. However, this iteration is a part of a bigger loop: the optimisation loop, which aims to optimise the entire aircraft design.

It is important to realize that optimising the performance of a single component or part, does not automatically improve the performance of the entire aircraft. The best-performing aircraft is not the sum of all individually best-performing components, i.e., the most aerodynamic aircraft will not fit even a single passenger.

Because of this, a type of Multidisciplinary Design Optimization (MDO) has been used in this project to find the optimal aircraft design. Multiple optimisation methods exist for these type of problems: generally, the methods can be split in two categories: gradient-based methods and non-gradient based methods.

The disadvantage of gradient-based methods is that they can get stuck in a local minimum, although they are reasonably quick, which is not always the global minimum. This is a problem for aircraft design, as there as so many interdependent variables, that a lot of local optima (minima in this case) exist.

Non-gradient based methods, do not, as the name implies, require the gradient of the cost function, in order to find the minimum. There are multiple methods, examples of which include ant colony algorithms, genetic algorithms or reinforcement learning. In this project, Differential Evolution (DE), as developed by Storn and Price [1], implemented in SciPy[1], is used. DE is an algorithm capable of finding the global minimum of a function, within certain bounds (limits on the input) and constraints (limits on the output or intermediate values).

DE is chosen over other methods for the following reasons:

- Implementation was readily available in Python
- Support for parallel computation due to the nature of the algorithm
- Good convergence properties [1]
- Ability to handle non-differentiable cost functions [1]

3.3. Implementation

Building on top of this already existing optimiser, the iterator as discussed in Section 3.1 was also implemented. The complete MDO architecture can be seen in Figure 3.1. The implementation of this architecture is fully developed in Python and heavily relies on high-performance numerical packages such as SciPy and NumPy. The entire optimiser can be run in parallel, greatly speeding up the procedure.

The MDO architecture developed is set up in such a way that it is easy to change which parameters are used to optimise the aircraft. These parameters are referred to (also in Figure 3.1) as x. For the research done here, the following variables were used to optimise the design:

$$x = (h, V_c, \Lambda_{inboard}, \Lambda_{outboard}) \tag{3.1}$$

The optimizer is currently used, as can be seen in Figure 3.1, to minimize the total fuel mass. It does this by changing four variables shown in Equation 3.1: the cruise altitude (h), cruise velocity (V_c), inboard wing sweep ($\Lambda_{inboard}$), and outboard wing sweep ($\Lambda_{outboard}$). Also, every time the aerodynamic block is run, the optimal airfoil for the current conditions is determined.

Furthermore, please note that the aforementioned variables can take any value, as long as they are in between the bounds shown in Equation 3.2. These bounds are based on drag divergence due to reaching the critical Mach number (for V_c, $\Lambda_{inboard}$ and $\Lambda_{outboard}$) and user requirements for the minimum h.

[1] `https://docs.scipy.org/doc/scipy/reference/generated/scipy.optimize.differential_evolution.html` [cited 22 June]

$$
\begin{aligned}
9144 \leq h \leq 13,500 \text{ [m]} \\
830 \leq V_c \leq 870 \text{ [km/h]} \\
58 \leq \Lambda_{inboard} \leq 65 \text{ [deg]} \\
30 \leq \Lambda_{outboard} \leq 45 \text{ [deg]}
\end{aligned}
\tag{3.2}
$$

There are a few reasons that the fuel mass was chosen as the value to optimize. First of all, it is one of the few parameters that almost every subsystem has an influence on. A few examples: a higher lift over drag (better aerodynamic performance) leads to a lower total required fuel, a higher cruise altitude leads to higher cabin Δp, leading to a heavier structure, which then leads to more fuel needed to perform the mission. Also, the fuel mass used because it is just a single parameter, making it easier to optimise with, compared to for example optimising for both L/D and c_j at the same time. Furthermore, a lower fuel mass does not only mean lower operating costs, it has a 1:1 relationship to the emissions from the aircraft. Half the amount of fuel used means half the CO_2 and NO_x emissions.

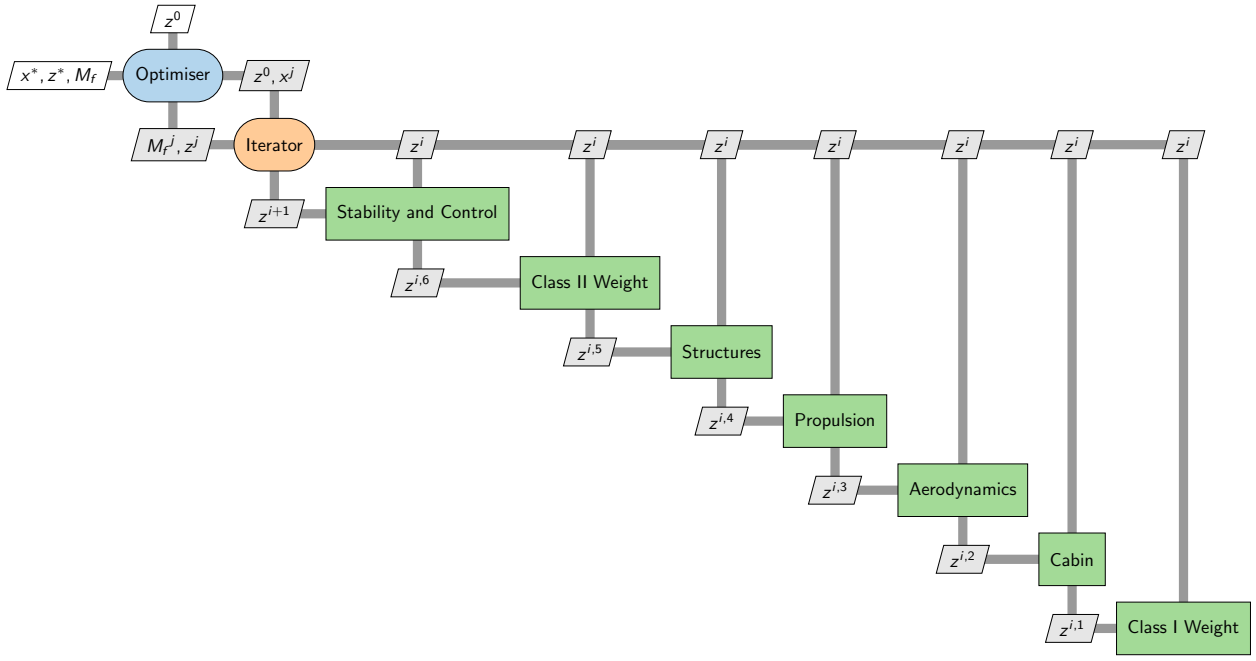

Figure 3.1: MDO architecture used. z is a set containing all the aircraft design parameters. Index i indicates the number of steps during iteration. Index j indicates the jth version of the aircraft created by the optimiser. Superscript i, x indicates that each block adds certain new and updated values for the next block to use, but does not update the set of z values.

The total runtime of an optimisation procedure as depicted in Figure 3.1 is about 15-20 minutes on an AMD Ryzen 5 4500U, having 6 cores and a boost clock of 4.0 GHz[2].

3.4. Recommendations

Although the tool is flexible in its inputs, function to optimize and outputs, there are still multiple improvements and additions that can be made.

First of all, it is important to be more aware of the computational speed of the tool that is being built. Some sections of the design iteration procedure would take orders of magnitude longer than others while being not as important or impactful. If from the start, a more proactive focus would have been present on raw runtime, it would have helped to decrease the total running time of the tool by a lot.

[2] `https://www.amd.com/en/products/apu/amd-ryzen-5-4500u` [cited 28 June]

Next, for further developments of the tool, tighter integration with the structural analysis is preferred. Because the weight of the structure (i.e. fuselage/wing) accounts for the majority of the weight of the aircraft, it is important to consider this in a precise manner. However, at the moment, the calculations of the structural properties and the resulting total structural mass only happen after an optimized design was found. This can lead to possible lower actual performance than what the optimizer found.

Furthermore, while the design optimisation tool is already very flexible, it does currently not support configurations with, for example, two galleys. Adding features would make the tool more suitable for the field of family aircraft design or even for designing an entire fleet of aircraft.

Another interesting and worthwhile field that has not been explored in this project (due to time constraints) is the parametrisation of the airfoils used in the aircraft. As the main planform characteristics are already parametrised, a parametrisation of the airfoils would lead to a fully parametrised aerodynamic aircraft shape. Various techniques for doing this exist, such as NURBS [7] or CST [8]. Using these kind of methods, an even more optimal aerodynamic design can be achieved, as the shape of the airfoil at each section can be altered to reduce the drag even more.

4 Aircraft Configuration

In this chapter, various elements that are part of the internal layout are discussed. In Section 4.1 are stated followed by a discussion of the methodology for the cabin sizing in Section 4.2. Subsequently, the flight deck layout in Section 4.3, the door layout in Section 4.4.1, and the sizing and positioning of the cargo holds in Section 4.4.2 are discussed. Finally, the cabin layout and fuel tank sizing and positioning are described in Section 4.4.4 and Section 4.4.5, respectively. Ideally, the sizing of the cabin, fuel tanks and cargo area is performed such that the requirements are met. Alternatively, the aircraft configuration can portray space constraints which could lead to iterations of the design parameters or requirements. In Section 4.5, the verification and validations has been discussed followed by a discussions of the aircraft system interactions in Section 4.6.

4.1. Requirements

The requirements set by the internal configuration of the aircraft are displayed in Table 4.1.

Table 4.1: Requirement for the internal layout of the aircraft.

EFMRA-SYS-AP-02	The aircraft shall have a turnaround time of no more than 52 min.
EFMRA-SYS-PF-07	The aircraft shall be able to carry at least 200 passengers and their luggage.
EFMRA-SYS-PF-11	The aircraft shall be able to carry up to 4.5 tons of cargo.
EFMRA-SYS-SF-10.3	The aircraft exits shall be designed for a 240 passenger capacity in one class configuration.
EFMRA-SYS-SF-13	Each passenger can be seated at a maximum angle of 18 degrees from the centre line without any special safety equipment.

4.2. Methodology

For sizing the radome, flightdeck, door layout, cabin, cargo compartment and fuel tank a multi-disciplinary approach shown in Figure 4.1 has been used. Using the inputs derived from requirements, the aircraft layout has been established. For sizing of the cabin, the number of passengers was used to define a two-class seating plan with accompanying seat widths, seat pitches, galleys and lavatories. Additionally, the door layout has been designed such that one-class seating is possible, maintaining sufficient exit limit for the aircraft. Because the surface area where the two cabin sections join, referred to as the joint forward compartment, is a function of sweep and the fineness ratio of the nose section, the calculated cabin lengths l_{cabin} were communicated to the aerodynamics department. The aerodynamics department recalculated the surface of the joint forward compartment which was then used by the configuration department to recalculate the cabin length. This was iterated several times to establish a cabin length and layout that considers the aerodynamic requirements of the design while also providing a spacious cabin layout. Using requirements on cargo capacity, passenger luggage in the cargo compartment and the width of the cabin, the cargo compartment was sized. Finally the fuel tanks were sized to accommodate sufficient fuel to perform the mission profile. In Figure 4.1, the red blocks are inputs derived from requirements represented in a blue block, the green blocks provide intermediate results that serve as input for the sizing of the layouts presented in the yellow blocks. The purple blocks represent aerodynamic parameters that played a role in determining the sizing the cabin. The aforementioned elements have been combined in an aircraft layout shown in Figure 4.4.

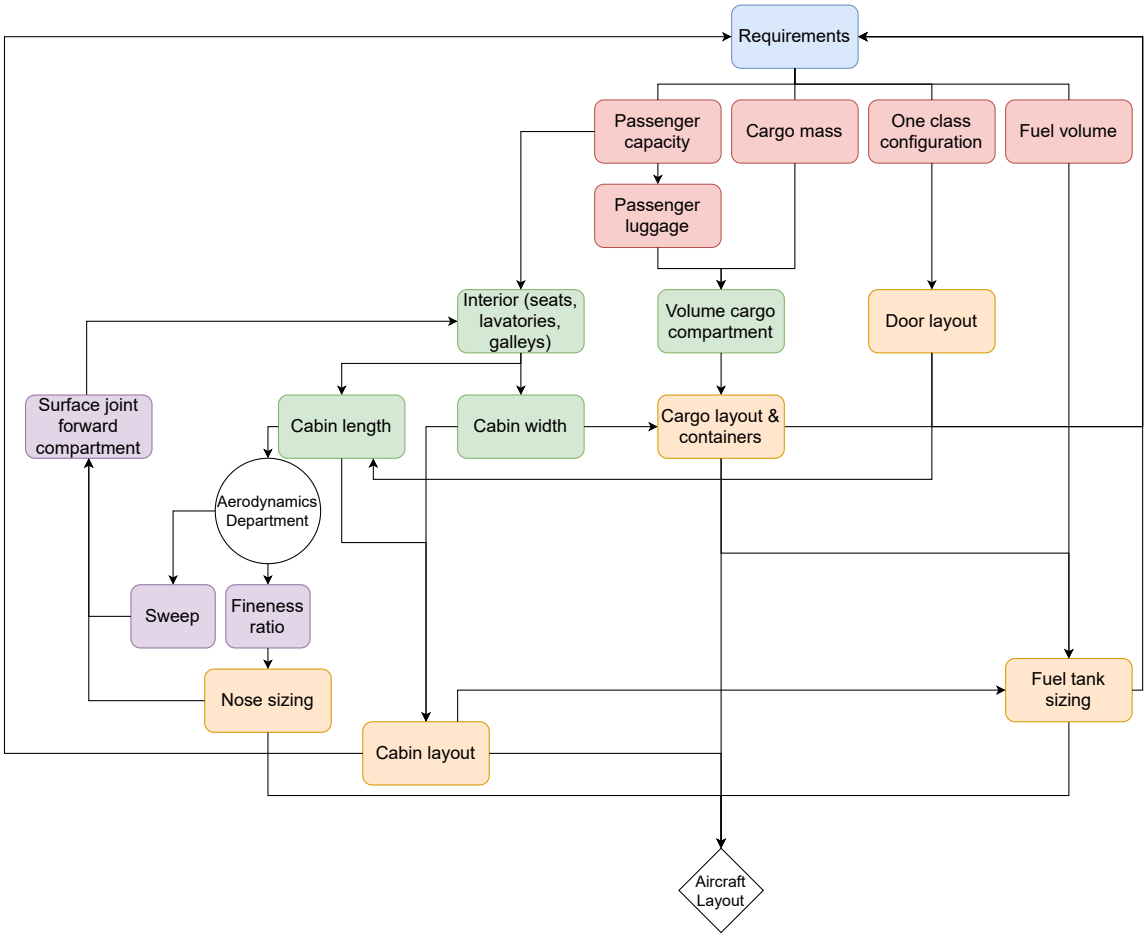

Figure 4.1: Multi-disciplinary configuration methodology.

4.3. Flight Deck

The length of the flight deck is measured from the bulkhead after the radome of the aircraft until the flight deck door. The length from the radome will be 1.35 m in line with single aisle aircraft [9] [10]. The radome houses the weather radar, ground proximity warning system (GPWS), localiser, the glide slope antenna and the flight director signal. The Zephyr One is flown by a flight deck crew of two and its flight deck does not differ from flight decks of comparable aircraft with exception for the implementation of controls for the electric taxi capability. The aircraft has been divided in a Capt. side (Captain) and the side of the FO (First Officer). For each side, the aircraft is equipped with side sticks for pitch and roll motion, rudders for yaw motion and a tiller for nose wheel steering.

Between the seat of the captain and first officer a unit is mounted to the floor which holds the following items:

- Engine start and ignition panel
- Throttle quadrant
- Trim wheel
- Speed brakes
- Radio panel
- Two flight management systems
- Lever to control flaps setting
- Control unit for electric taxi
- Standby air data inertial reference unit

Each side is equipped with a primary flight display and a navigation display. In between, two shared monitors to display aircraft and engine information and a lever to operate the landing gear are positioned. On top of the row of monitors, the flight control unit is located to (dis)engage and set up the autopilot to take inputs for the velocity, auto throttle, heading, altitude and climb rate. Additionally, the

flight control unit has a button to engage the localiser and the approach mode for autolanding.

Above the flight deck crew, the overhead panel is situated, allowing for the control of hydraulics, fire suppression, cabin pressure, anti-ice, exterior lights, ventilation, cargo heating, fuel flow, air conditioning, two air data inertial reference units and circuit breakers. Behind the flight crew, the panel with circuit breakers continues. The flight deck is also equipped with an electronic flight bag to navigate through charts.

These systems are fitted in a flight deck compartment with a length of 2.5 m[1] [9] bringing the length from tip to flight deck door 3.85 m.

4.4. Flight Deck and Aircraft Layout

In this section door, cargo, galley, lavatory, cabin and fuel tank layout is discussed.

4.4.1. Door Layout

The aircraft has been sized for two configurations. One configuration allows for 200 passengers to be seated in a spacious two-class layout, while the other has a capacity of around 260 passengers in an ultra-dense configuration and around 245 passengers in a typical one-class configuration. Having a dense configuration fits the market trend of low-cost carriers expanding market share. For the Zephyr One to benefit from his trend, the cabins and door layout have been designed with this trend in mind. Therefore, the door configuration has been determined using the critical case, which is the high density seating. The number of exit doors has been determined using CS-25 regulations [11] (**CS 25.807**). In compliance with **CS 25.807**, the door layout shown in Table 4.2 was selected. This results in an exit limit of 260 passengers meaning that a dense configuration with around 240 passengers (**EFMRA-SYS-SF-10.3**) is possible.

Table 4.2: Exit limit Zephyr One.

Door type	Pairs	Exit limit
Type B	2	150
Type C	2	110
Total	**4**	**260**

4.4.2. Cargo Layout

To ease loading and unloading of the aircraft, the Zephyr One will be loaded using containers called unit load devices (ULDs) behind the cabin. This aids the Zephyr One achieving the desired turnaround time of at most 52 minutes (**EFMRA-SYS-AP-02**). The ULDs carry passenger luggage and revenue generating cargo (**EFMRA-SYS-PF-11**). The aircraft uses standardised ULDs meaning that no new ULDs need to be developed and distributed around the globe for operations. The aircraft makes use of LD-26 containers, optimally using the width of the inboard wing while providing minimal addition to the length. Information used for sizing of the cargo compartment and selection of the LD-26 container is provided in Figure 4.2[2] and Table 4.3. Furthermore, a standardised mass of 17 kg was used for luggage in the cargo compartment (CC), in line with recommendations from EASA (European Union Aviation Safety Agency) [12].

[1] `http://www.737ng.co.uk/B737%20measurements.pdf` [cited 31st May 2021]

[2] `https://www.searates.com/reference/ld26/` [cited on 25 June 2021]

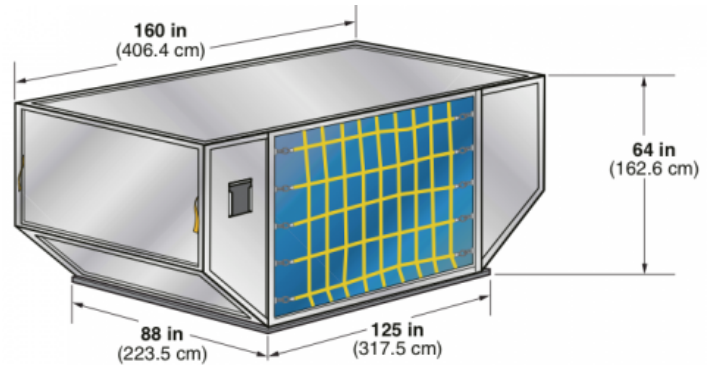

Figure 4.2: Dimensions of LD-26.

Table 4.3: Characteristics LD-26 container.

	Value
Max. gross weight [kg]	6,033
Tare weight [kg]	250
Volume [m^3]	13.3
Width [m]	4.064
Height [m]	1.626
Depth [m]	2.235

Using Equation 4.1a and Equation 4.1b [13], the volume for the luggage to be carried in the CC, $V_{luggage\,in\,CC}$ and the revenue generating cargo V_{cargo} were calculated from their respective masses m and densities ρ.

$$V_{luggage\,in\,CC} = \frac{m_{luggage\,in\,CC}}{\rho_{luggage\,in\,CC}}, \text{ typical } \rho_{luggage\,in\,CC} = 170 \text{ kg/m}^3 \tag{4.1a}$$

$$V_{cargo} = \frac{m_{cargo}}{\rho_{cargo}}, \text{ typical } \rho_{cargo} = 160 \text{ kg/m}^3 \tag{4.1b}$$

Table 4.4 shows the obtained volumes and required number of LD-26 units. Initially, the cargo compartment had been sized to hold 4.5 tons of cargo (**EFMRA-SYS-PF-11**) and luggage. However, the requirement states an upper limit and it was found that sizing for 4.5 tons of cargo would add to the length of the cargo compartment while not fully utilizing the volume of the third LD-26 container required for cargo. Therefore, the cargo compartment has been sized for a volume of 26.6 m^3 equivalent to 4.3 tons plus containers required for luggage. In total, four LD-26 containers are used while still meeting the set requirements for carrying cargo. Two containers are stored on each side of the aircraft, which results in a length of the cargo compartment of 4.5 m on each side.

Table 4.4: Cargo compartment sizing.

	Value	**LD-26**
Luggage in cargo compartment [m^3]	20.0	2
Cargo [m^3]	26.6	2
Total [m^3]	**46.6**	**4**

4.4.3. Galley and Lavatory Layout

The next aspects of the cabin to be investigated is the positioning of the galleys and lavatories. The range of acceptable amounts for each aspect is presented by D. Raymer [14]. An average of each of the ranges is applied for the cabin dimension computations. These averages are presented in Table 4.5.

Table 4.5: Lavatory and galley requirements based on Raymer [14].

	Economy class	**Business class**
Passengers per lavatory [-]	50	15
Galley volume per passenger [m^3/pax]	0.045	0.185

Based on these values, the number of lavatories required for the economy class and business class passengers are 4 and 2 respectively. For economy class, the lavatories are grouped at two per row, where a row of lavatories is present in each fuselage side. The business class lavatories are placed in the front central section of the fuselage.

For the galleys, a volume of 8.1 m ^{3} and 3.7 m^3 is required for the economy and business class passengers respectively, for a total of 11.8 m^3. The dimensions of a galley are obtained from the Aerospace Design and Systems Engineering Elements lectures [13], where the width of a galley is determined to be 0.76 m. This is for a galley with a quarter-circle cross-section, which suits the cabins for traditional aircraft. For the Zephyr One, a galley with a rectangular cross-section that fits within the cabin dimensions and has a width of 30 inches is utilised. A galley is placed at the end of each individual fuselage sections, which means that no aisle passing through them is required. In addition to these galleys, a third galley section is added at the beginning of the front center section, adjacent to the cockpit, with an aisle passing through for the pilots.

With the dimensions determined in Section 4.4.4, Table 4.6 can be constructed demonstrating that the galley and lavatory requirements are met.

Table 4.6: Checking fulfillment of lavatory and galley requirements.

	Zephyr One	**Raymer**
Lavatories [-]	6	6
Galleys [m^3]	12.71	11.8

4.4.4. Cabin Layout

The cabin layout must be designed to fit at least 200 passengers with their luggage, as stated by requirement **EFMRA-SYS-PF-07**. For the main design, a two-class configuration is decided upon, however, a one-class configuration layout that allows for a greater number of passengers is also considered. This would allow to introduce the Zephyr One to a larger market space. Note that in the case of a dual class configuration, the percentages of passengers in business and economy class are initially assumed to be 10% and 90%, respectively, as stated in D. Raymer [14].

The first step in constructing the cabin design is to define the cabin cross-section. As per CS25.785d [11], passenger seats are allowed to have a maximum inclination of 18° with respect to the vertical plane containing the aircraft centre line, i.e. the flight direction, without any safety equipment. Furthermore, with the aisle being parallel to each fuselage's length, this means that given a sweep of the inboard wing λ, the angle between the seats and the aisle is as described by Equation 4.2.

$$\theta = 90 - \Lambda - 18 \tag{4.2}$$

This angle is taken into account when computing the width of the cabin. Subsequently, using the values for the parameters in Table 4.7, the cabin cross-section dimensions can be computed.

Table 4.7: Parameters for computing the cross-section dimensions [14, 15].

Parameter	**Economy Class**	**Business Class**
Seat width [m]	0.50	0.61
Armrest width [cm]	5.00	5.00
Aisle width [m]	0.64	0.64
Clearance width [cm]	3.00	3.00
Seat pitch [m]	0.89	0.99
Aisle height [m]	1.93	1.93
Headroom height [m]	1.65	1.65
Shoulder height [m]	0.80	0.80
Floor height [m]	0.24	0.24

Using the values from this table, the cross-section perpendicular to the aisle and fuselage length could be drawn as shown in Figure 4.3, for economy class. Note that, because of the angle from

Equation 4.2, the widths of the seats, armrests, and clearances are slightly different from the ones in Table 4.7 and may appear to be wider.

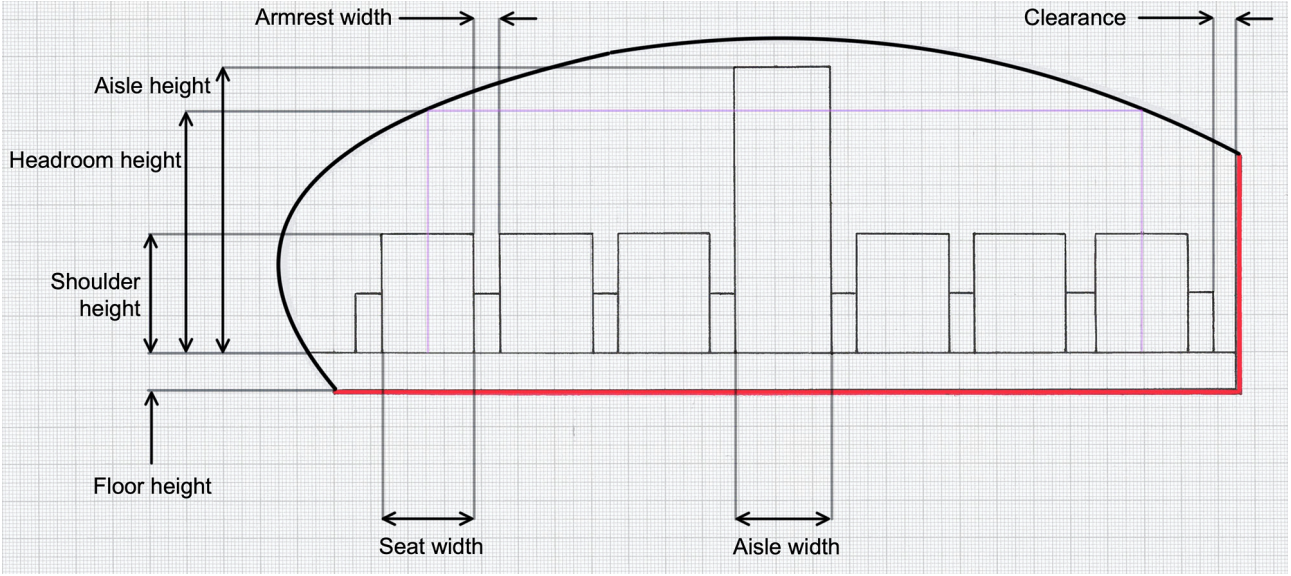

Figure 4.3: Internal layout of the cabin for economy class (scale 1:25).

There are three main sections in the Zephyr One: two fuselage sections and one front central section behind the cockpit. The two fuselage sections are at an angle (the sweep) with respect to the vertical symmetry plane containing the aircraft centre line. Their respective lengths can be calculated based on the placement of galleys, lavatories, and seat pitch - still keeping in mind the angle from Equation 4.2. Initially, only economy class passengers were considered to be placed in the two fuselages, while the business class passengers would be located in the front central section. Furthermore, six seats abreast were chosen for the fuselage parts. With this configuration, a first estimate of the respective cabin lengths were calculated, these were found to be 13.35 m each.

Next, it was attempted to fit the remaining 10% of passengers, namely the 20 business class passengers, into the central section. For the latter, the business class dimensions from Table 4.7 were considered. Additionally, to avoid rotating the seats with respect to the aisle, the aisles in the front central area are oriented at exactly 18° with respect to the vertical plane containing the aircraft centre line. In this way, a total of 11 passengers could fit in this section of the Zephyr One. Since this is less than the required 10% i.e. 20 passengers, three additional rows of business class seats were added to the front of each fuselage section, with two seats abreast. This resulted in 23 business class passengers in total. Adding these rows increased the lengths of the fuselage sections to 19.43 m each. With the total number of passengers i.e. 200, this also lead to 177 economy class passengers. However, with six seats abreast in the economy class, it was possible to fit up to 180 economy class passengers without increasing the lengths of the cabins, leading to a total of 203 passengers in a two-class configuration. This resulted in updated percentages of 11.33% and 88.67% for business and economy class passengers, respectively. All dimensions, seat, lavatory, and galley placement can be seen in Figure 4.4 showing the top view of the overall cabin configuration.

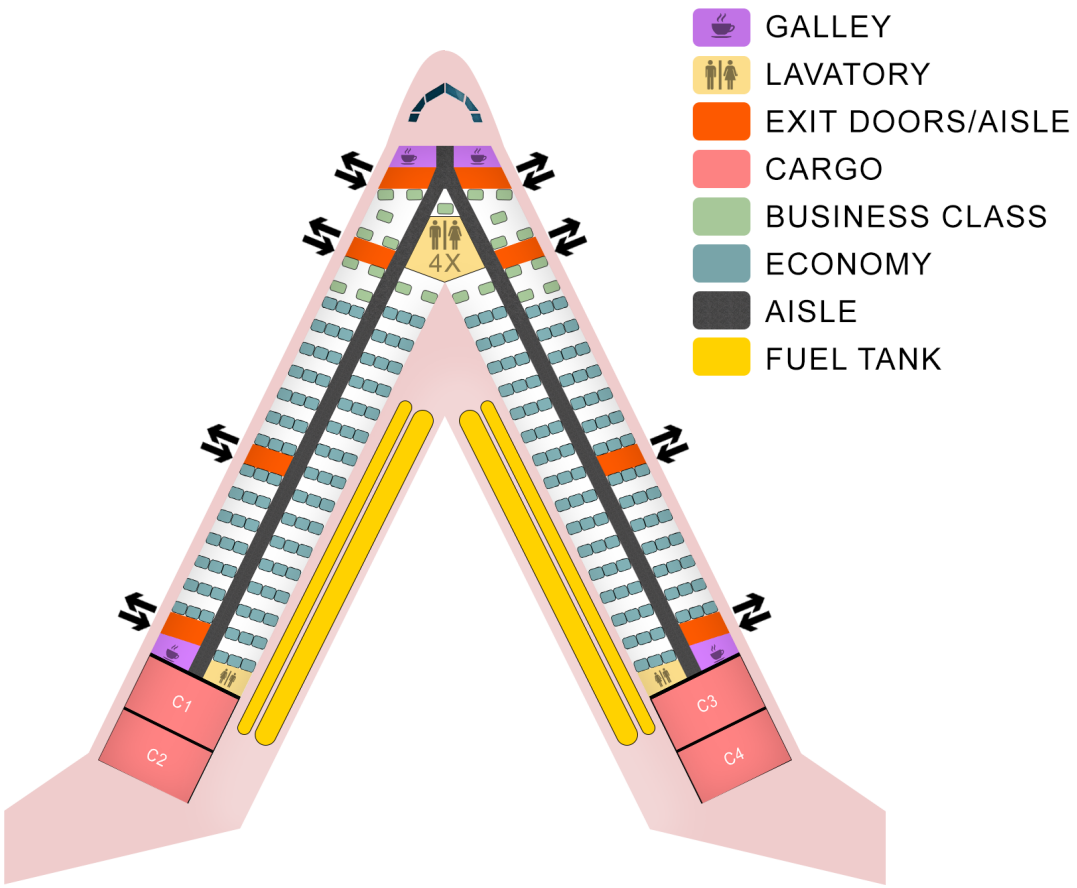

Figure 4.4: Aircraft layout Zephyr One.

The door layout discussed in Section 4.4.1 has been designed such that next to a spacious two-class cabin layout, a one-class cabin layout is also possible. For the one-class configuration, the pitch of the economy cabin has been reduced from 34 to 30 inches allowing for 24 additional seats in the economy cabin. Changing the seat pitch from 39 inches in business class to 29 inches allows for the addition of 11 seats, while adding narrower and more seats abreast compared to the business class section would add another 8 seats. This increases the number of seats for a one-class Zephyr One configuration to at least 246 seats with an average seat pitch of around 30 inches. This roughly matches the maximum capacity for the Airbus A321neo[3]. The average seat pitch of 30 inches is well above the minimum required seat pitch of 28 inches found on aircraft from low-cost carriers such as Wizz Air[4]. Using slimline seats, the Zephyr One still offers a spacious cabin experience in a dense one-class configuration and opportunities exist to opt for an ultra dense configuration pushing the capacity to 260 passengers. Increases in seating capacity could require the cargo weight to be reduced. Combined with strict baggage allowance polices for low-cost carriers, the cargo capacity would be reduced by 2.6 tot 4 tons. This is considered acceptable given that low cost carriers do not have cargo transport as an integrated part of their business model.

4.4.5. Fuel Tank Configuration

The sizing and placement of the fuel tanks will be discussed in Sections 6.3 and 8.2. For now, there is no exact position for this sub-system, since it is largely influenced by control and stability. However,

[3] https://www.airbus.com/content/dam/corporate-topics/publications/backgrounders/techdata/aircraft_characteristics/Airbus-Commercial-Aircraft-AC-A321.pdf [cited 2 June 2021]

[4] https://www.seatguru.com/airlines/Wizzair/Wizz_Air_Airbus_A321.php [cited 2 June 2021]

it is expected that the tanks will be positioned behind the cabin, somewhere along the yellow section shown in Figure 4.4. More specifically, the tanks will be placed right in front of the trailing edge of the airfoil, as seen in the cross-sectional view in Figure 4.5 below.

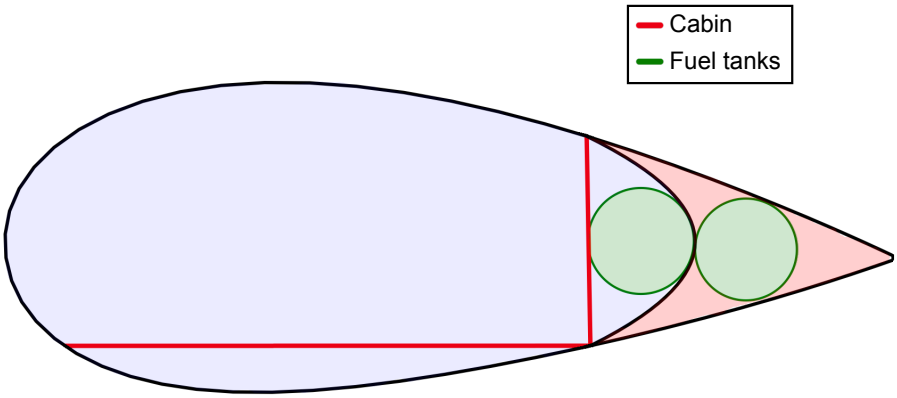

Figure 4.5: Fuel tank configuration.

4.5. Verification & Validation

To verify the Python scripts used for the Zephyr One's configuration, a set of unit tests were carried out for each defined function. The inputs were altered in order to facilitate hand calculations and the calculated outputs (known) were compared against the outputs given by the Python scripts. An absolute margin of 10^{-5} was used and all functions tested were proven to comply with that degree of accuracy.

Due to the novel nature of the design, no validation processes could be carried out, as there is no data for Flying-V aircraft other than conceptual prototypes. These concepts feature a tapered aircraft structure, leading to variable cabin width, which is not comparable to the Zephyr One's design. Furthermore, the design of the front centre section is generated using the dimensions provided by the aerodynamics department, as well as a unique predetermined general layout, making it difficult to compare to said prototypes. Conventional aircraft may also not be used for validating the sizing of the cabin as the code is customized for a Flying-V design, considering sweep, tilted seating, and a pentagonal front section. Therefore, during further work, a more general script for the internal design will be constructed to attempt validation with conventional aircraft designs.

4.6. Aircraft System Interactions

In this section the aircraft system interactions are presented. These include the electrical block diagram, which is given in Figure 4.6, hardware block diagram, which can be seen in Figure 4.7, and software and data handling diagram, which is presented in Figure 4.8.

Zephyr One features the more electrical architecture, which is explained more in depth in Section 6.4. Thus, most of the aircraft systems are powered by electricity. In Figure 4.6 the aircraft electrical system is split into three parts: main, left, and right parts. Everything is powered by a central battery, which is charged by the electric generators located in the engines. Then the electricity is distributed by the main power bus to the cockpit and other centered electricity sources. Left and right power bus distribute the power to the left and right fuselage electric systems, respectively.

Hardware and software diagrams feature the aircraft computer, through which most of the information passes, as seen in Figure 4.7 and 4.8. The navigation of the aircraft is done by flight sensors, GPS, and radar. The communication is done via the radio and radar. Climate control is responsible for keeping the cabin at right pressure and temperature. All of the data flows through the aircraft computer, to check the inputs.

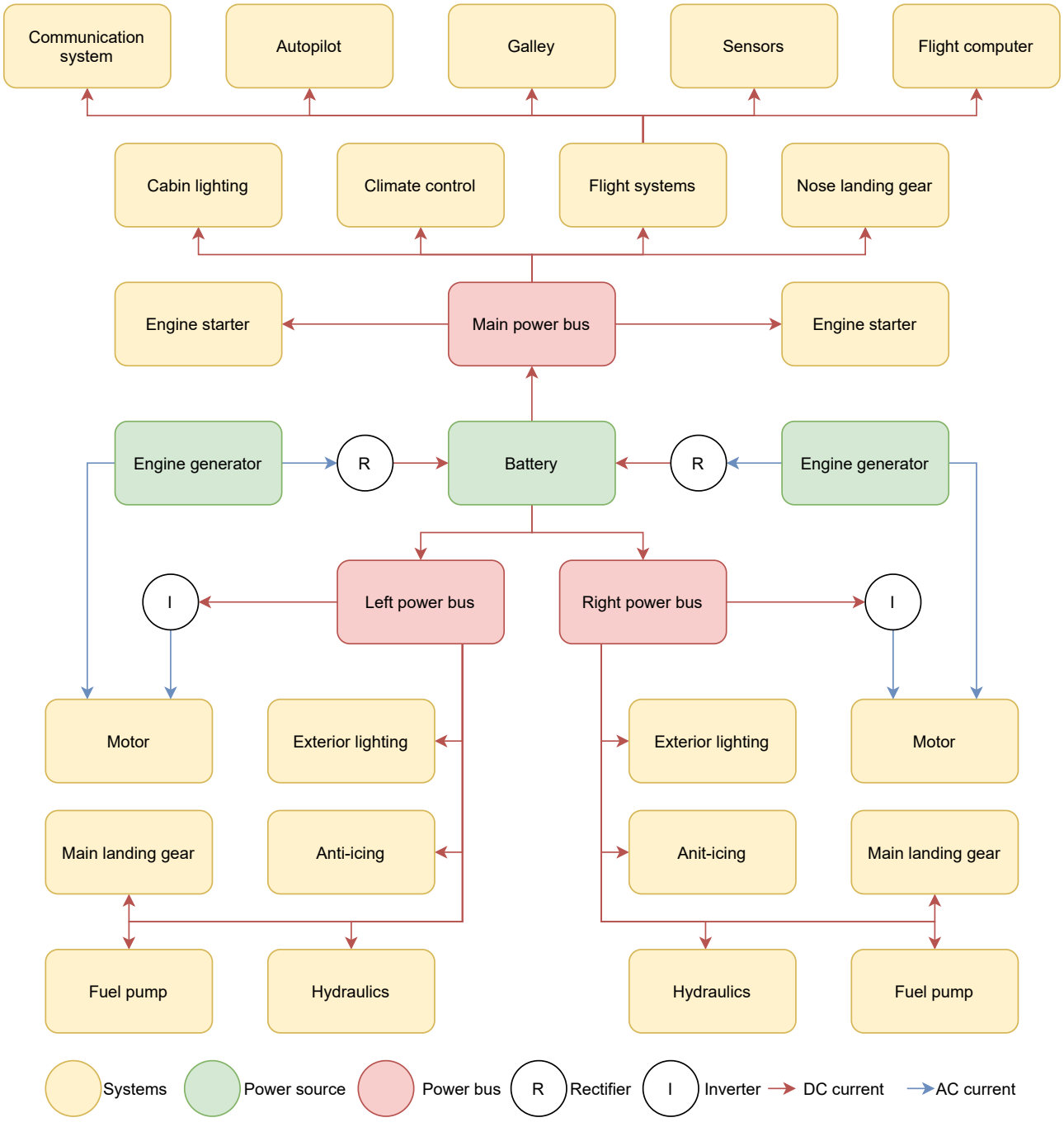

Figure 4.6: Electrical block diagram of the aircraft.

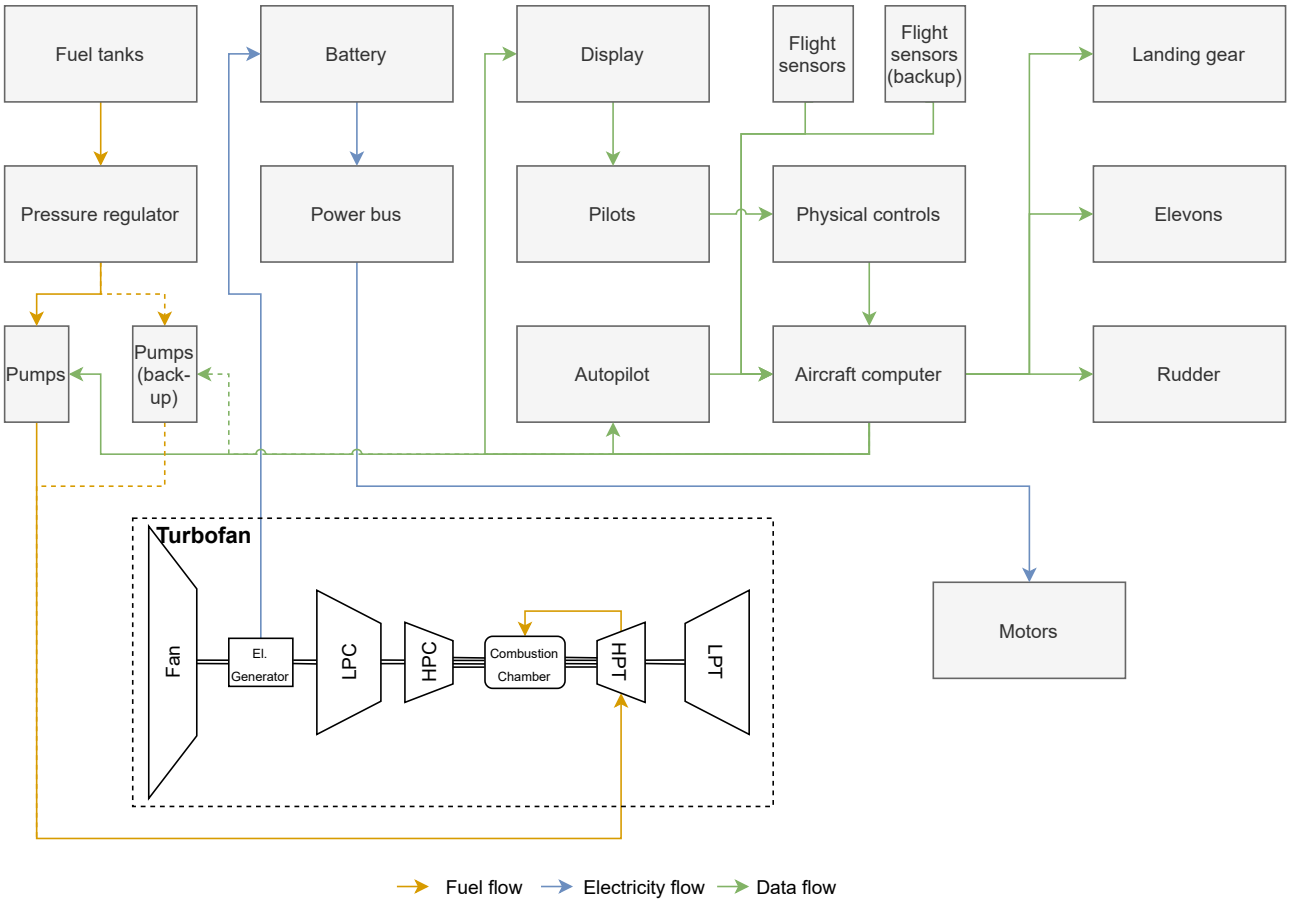

Figure 4.7: Hardware block diagram of the aircraft.

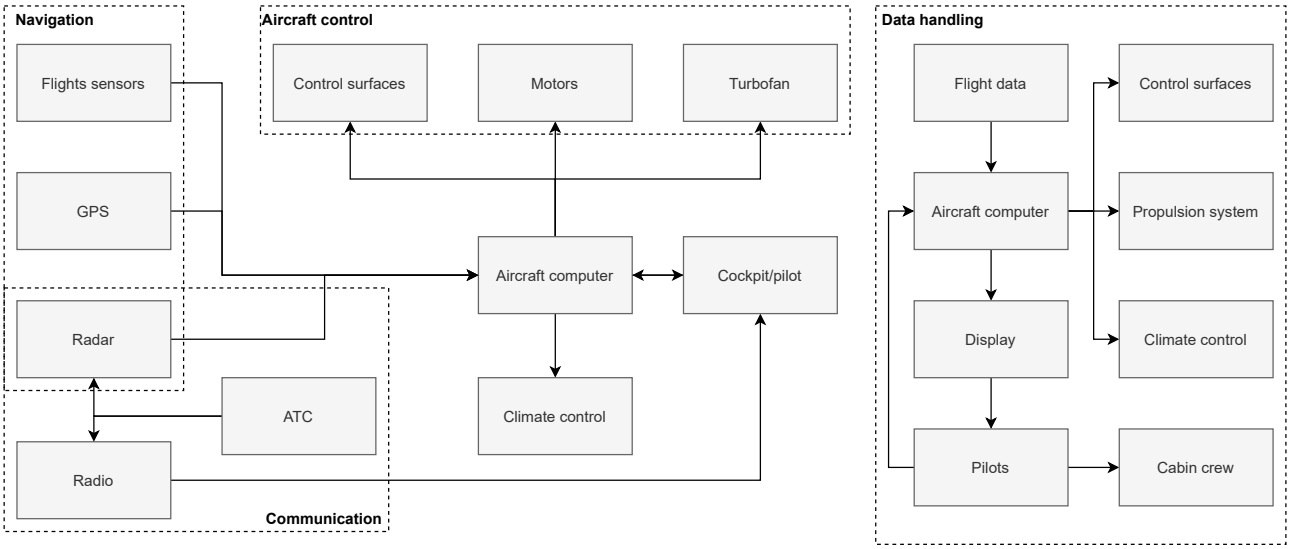

Figure 4.8: Software and data handling block diagram of the aircraft.

5 Aerodynamic Design

In this chapter, the process of the aerodynamic design of the Zephyr One is discussed. Consequently, results stemming from the final design are shown and the accuracy of the methods used are discussed. In Section 5.1, additional requirements and constraints that were set for the aerodynamic design are shown. In Section 5.2, the methodology for the aerodynamic design by means of a design loop is explained. The airfoil selection is discussed in Section 5.3, while the planform generation is described in Section 5.4. The analysis of the planform is performed in Section 5.5. The methods used are verified and validated in Section 5.6, while the results obtained from the methods are shown in Section 5.7. Finally, recommendations are made in Section 5.8.

5.1. Requirements

Requirements are set to constrain the design and set design goals that need to be achieved. Listed below are the requirements for the aerodynamic design, some originating from the Baseline Report [2], while the last five requirements are new. These new requirements are more technical and provide constraints on the performance of the aircraft.

Table 5.1: Aircraft Requirements for aerodynamic design.

EFMRA-SYS-PF-03	The aircraft shall have a cruise speed of at least 830 km/h.
EFMRA-SYS-PF-04	The aircraft shall have a cruise altitude of at least 9,144 m.
EFMRA-SYS-AP-01.1	The aircraft shall have a wingspan no larger than 36 m.
EFMRA-SYS-AE-01	The aircraft shall have a maximum lift coefficient of minimum 1.1.
EFMRA-SYS-AE-02	The aircraft shall have a negative C_{m_α}.
EFMRA-SYS-AE-03	The aircraft wing surface shall satisfy the minimum required wing loading.
EFMRA-SYS-AE-04	The airfoil shall be able to fit the cabin.
EFMRA-SYS-AE-05	The angle of attack at CL design shall be between 0° and 4°.

5.2. Aerodynamic Design Methodology

The aerodynamic design is a process that is heavily optimised and iterated during the design of the aircraft. The overall goal of the aerodynamic design is maximising the lift over drag during a cruise. The design loop is shown in Figure 5.1. The design loop can be split into three main sequences. The first sequence is determining valid airfoils for the design. Secondly, the geometry of the planform of the Flying-V is generated. The last sequence consists of analysing the aerodynamic properties of the design. These last two sequences are performed for each suitable airfoil found in sequence 1. Each sequence is described in more detail in the subsections below.

5.3. Airfoil Selection

Selecting the airfoil is the first phase of the aerodynamic design and forms the base for the entire loop as it initialises the inputs. The initial set of inputs come from the requirements set and from the optimisation parameters described in Chapter 3. With these inputs, and using variables determined during the Midterm Phase, an initial set of aerodynamic properties are determined. The loading diagram of the aircraft can then be constructed using the set of inputs and aerodynamic properties. From the maximum wing loading obtained from the loading diagram, a required wing area is established, which

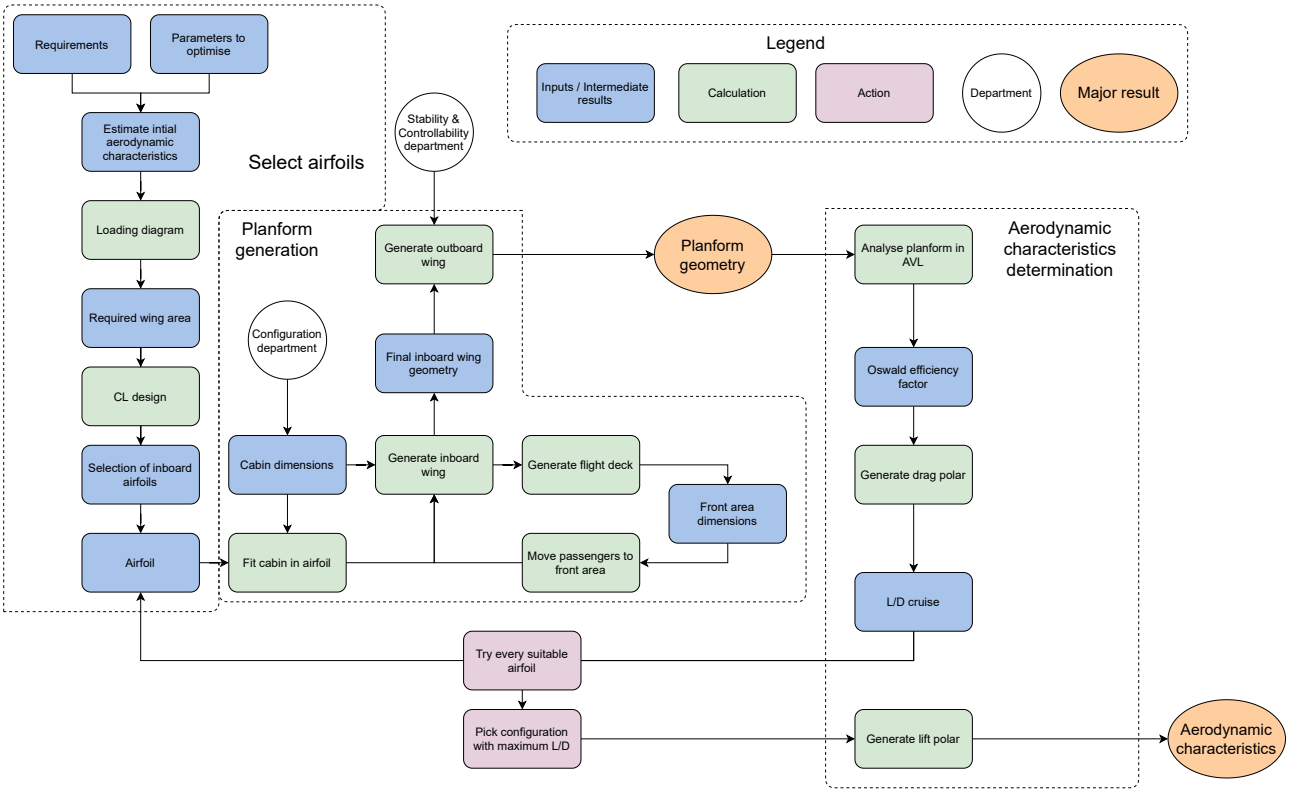

Figure 5.1: Aerodynamic design loop.

will be used to size the planform. $C_{L,\,des}$ is the lift coefficient required for the wing during cruise flight, and is obtained by using Equation 5.1. The required lift coefficient generated by the swept airfoil is then determined using Equation 5.2. The Flying-V uses different airfoils for the inboard and outboard wing, however, as they have different sweep angles. As such to determine the C_l of the separate airfoils, the lift coefficient is scaled based on the fraction of the surface area.

$$C_{L,des} = \frac{2}{\rho v^2} \cdot \frac{1}{2}\left\{\left(\frac{W}{S}\right)_{start} + \left(\frac{W}{S}\right)_{end}\right\} \quad (5.1)$$

$$C_{l,des} = \frac{C_{L,des}}{cos^2\Lambda} \quad (5.2)$$

$$C_{l,des_{inboard}} = \frac{C_{L,des}}{cos^2\Lambda_{inboard}} * \frac{S_{inboard}}{S_{total}} \quad (5.3)$$

$$C_{l,des_{outboard}} = \frac{C_{L,des}}{cos^2\Lambda_{outboard}} * \frac{S_{outboard}}{S_{total}} \quad (5.4)$$

A suitable set of airfoils can be determined using the design lift coefficient. Suitable airfoils should experience minimum drag at $C_{l,des}$ and have a negative moment slope, C_{m_α}. More emphasis is put on picking the airfoil of the inboard wing as this airfoil has more significance for the design. Due to the high sweep of the inboard wing, the airfoil does not have to be supercritical, and as such a standard NACA 5 or 6 digit airfoil can be chosen. During the design process it was noted that the available space in the airfoil can be utilised more efficiently with NACA 5-digit airfoils, and as such, this is the category from which the airfoil is chosen. Javafoil was used to generate the airfoil geometries. The airfoils were split up into subcategories, defined by the $C_{l,des}$ of the airfoil, ranging from 0 to 1.4. For these subcategories of airfoils, the thickness to chord ratio and maximum camber location was varied to find the optimal airfoil. During the design, it became obvious that a maximum camber location of 40% is optimal, as this is close to the cabin aisle location. Six different thickness to chord ratios were used per subcategory, ranging from 20% to 35%. As such, a total of 60 different airfoils were generated. The six airfoils corresponding to the current $C_{l,des}$ of the design iteration were then used as input to the planform generation. A planform was generated for each airfoil and subsequently evaluated using the lift over drag during cruise as the deciding metric.

The outboard wing selection is less detailed, as no significant performance difference can be identified with the currently used tools. A supercritical airfoil is being used for the outboard wing due to the decreased sweep compared to the inboard wing. The airfoil that was chosen for the outboard wing is the NACA-SC20714.

5.4. Planform Generation

The planform generation sequence consists of fitting the cabin in the airfoil and sizing the external geometry of the aircraft. Almost the entire planform can be generated based on an airfoil and constraints originating from the configuration department.

5.4.1. Airfoil Sizing

The first step is fitting the cabin in the airfoil, with cabin dimensions taken from Section 4.4.4. The cabin is first approximated to be a square inside the airfoil geometry, as visualised in Figure 5.2. The goal is to determine the square that minimises the airfoil chord length after being scaled to real dimensions, as this results in a minimal drag and mass. The airfoil is scaled by applying the wall dimensions obtained from Section 4.4.4. Before being considered a valid solution, however, the cabin needs to adhere to two more requirements.

- The width of the square needs to exceed the minimum cabin width.
- At the centre of the square, the distance from the bottom of the square to the upper airfoil geometry needs to exceed the minimum aisle height.

The solution that results in the minimum chord length, while fulfilling these two constraints, is then chosen as the final cabin configuration. This results in the first parameter of the Flying-V planform, the chord of the wing perpendicular to the wing sweep. Together with more constraints from the cabin configuration, the planform of the aircraft can now be realised.

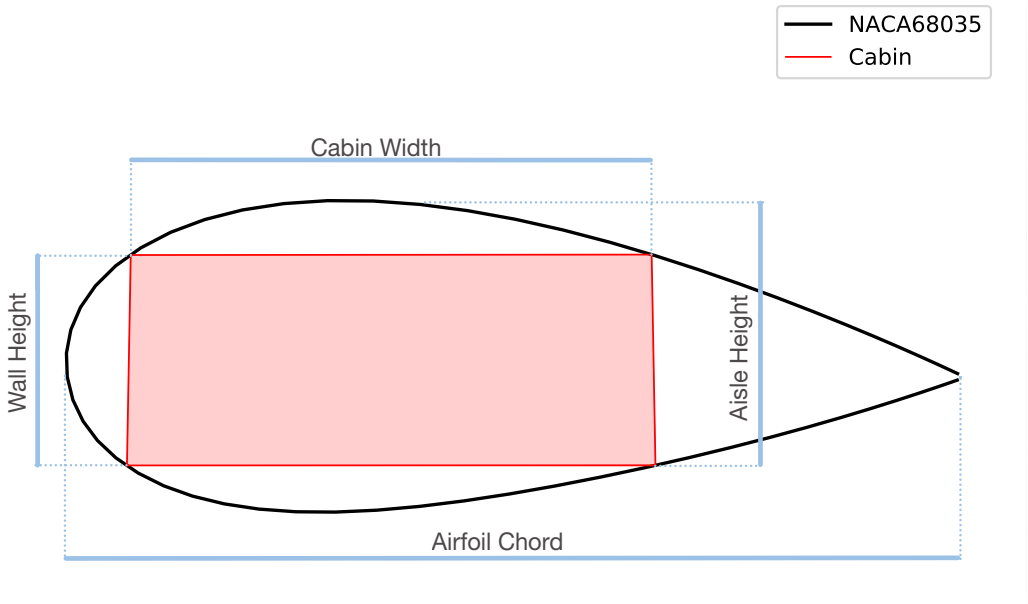

Figure 5.2: Cabin sizing using airfoil geometry.

5.4.2. Inboard and Outboard Wing Sizing

Figure 5.3 shows a top view of the Flying-V planform, with seven parameters defined. These are the only parameters required to generate the entire wing planform. Furthermore, three areas are defined in Figure 5.3; the flight deck, the inboard wing and the outboard wing. The first step of determining the planform is sizing the inboard wing. The three parameters required to size the inboard wing are the inboard sweep angle $\Lambda_{inboard}$, the airfoil chord length $c_{inboard}$, and the fuselage length $l_{fuselage}$. The sweep angle is one of the parameters which is optimised, as described in Chapter 3. The airfoil chord length is shown in Figure 5.2, and the fuselage length is determined in Section 4.4.4.

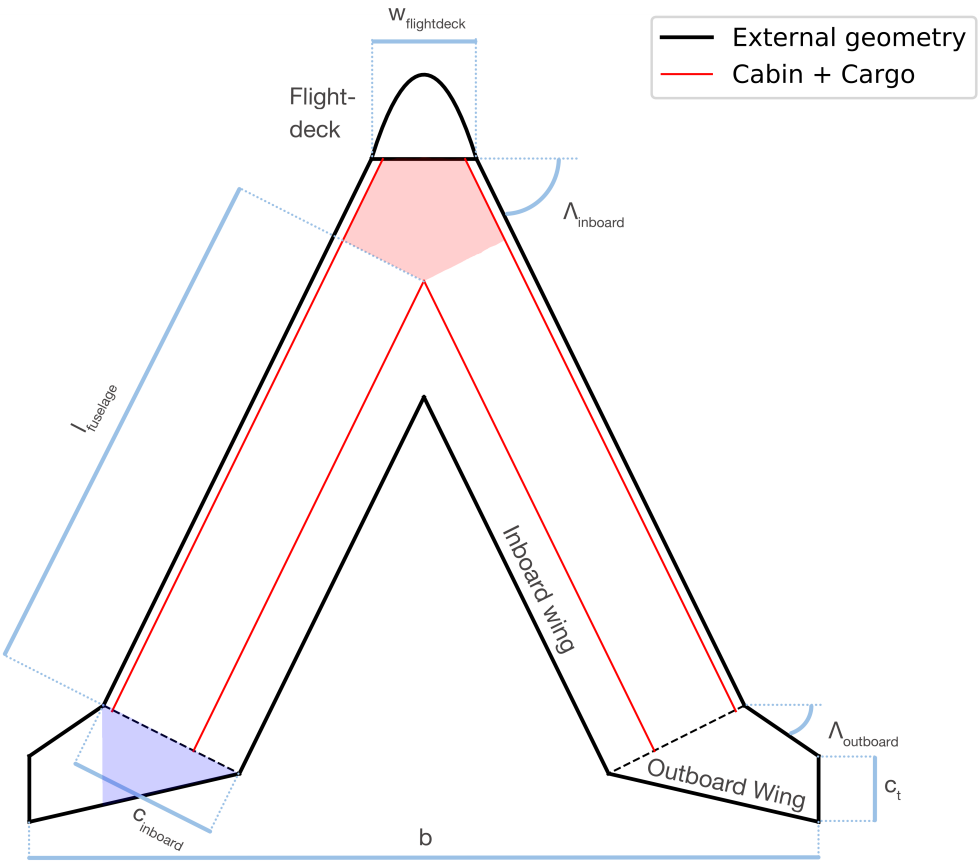

Figure 5.3: Top view of the aircraft with all the parameters used for planform generation.

The inboard wing is completed by placing the flight deck at the front, which has been sized in Section 4.3. Placing the flight deck leaves an open front area, shaded red in Figure 5.3. A small iteration is performed between the planform sizing and the cabin configuration, as passengers and galleys/lavatories can be moved from the fuselage to the front area, consequently reducing the fuselage length. The result is a final inboard wing and flight deck geometry, after which the outboard wing can be sized.

The outboard wing can be generated using three parameters of the aircraft planform. The first parameter used to size the outboard wing is the outboard sweep angle $\Lambda_{outboard}$. The outboard sweep angle is optimised to find the optimal solution, as described in Chapter 3. The second parameter to use is the wingspan of the entire aircraft, b. In combination with the span of the inboard wing, the remaining span of the outboard wing is determined. Increasing the wingspan increases the aspect ratio, which in turn reduces the drag of the aircraft. It was thus seen that using the maximum allowed wingspan provides optimal aerodynamic characteristics. The maximum wingspan is set by requirement **EFMRA-SYS-AP-01.1**, stating that the span shall not exceed 36 meters, and as such, this is the span used for this aircraft. The last parameter used to create the outboard wing is the tip chord c_t.

This parameter can flow from either of two sources. Initially, a tip chord is obtained from the control and stability department. In Section 9.3 the sizing of the vertical tail is described, from which a root chord of the vertical tail originates. The vertical tail is placed on the tip chord of the outboard wing, and thus the root chord of the vertical tail becomes the tip chord of the aircraft. Requirement **EFMRA-SYS-AE-03** sets a constraint on the wing surface area of the entire aircraft, however. Currently, the only parameter that can be adjusted to increase the wing area is the tip chord of the outboard wing. The tip chord of the aircraft will thus initially be set to be the root chord of the vertical tail, if this planform does not satisfy the minimum required wing area, however, the tip chord length will be increased. A transition of the inboard airfoil and outboard airfoil is located at the blue shaded area in Figure 5.3.

The final result of the planform generation is a complete planform. The next step is analysing the aerodynamic characteristics of the aircraft to determine the optimal configuration and airfoil.

5.5. Planform Characteristics

In the final sequence of the aerodynamic design loop, the aerodynamic characteristics of the planform, generated in the previous sequences, are determined. The aerodynamic characterisation consists of analyzing the lift and drag polar of the aircraft. First, in Section 5.5.1, the approach to find the drag polar is explained. Then, in Section 5.5.3, the method for determining the lift polar is discussed. Finally, the pitching moment of the aircraft is discussed in Section 5.5.4. To perform these tasks, first, a simplification of the planform is made.

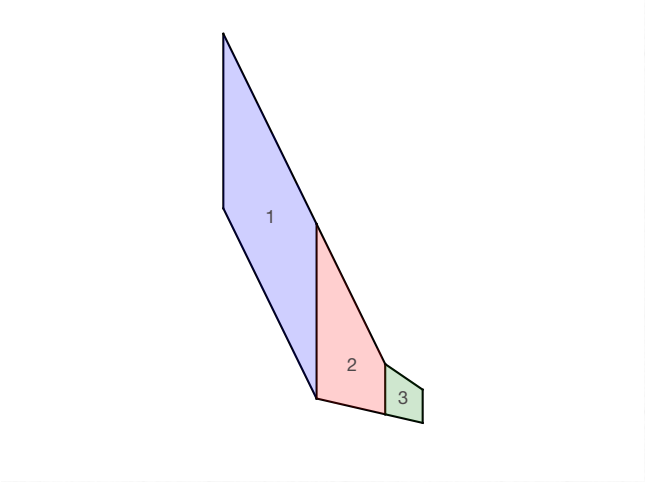

Figure 5.4: Simplification and division of the wing planform.

As shown in Figure 5.4, two adjustments are made to the wing planform. First, the flight deck is simplified by straightening the nose cone curve, making the leading edge of the wing a straight line. Additionally, the wing is split up into three segments, each having its own root and tip chord. Each of these segments has a clearly defined sweep angle, root and tip chord. These simplifications help with modelling the wing and determining aerodynamic characteristics per segment.

5.5.1. Drag Polar

In order to determine the drag polar of an aircraft, the contribution of various factors to the total drag should be considered. Looking at Equation 5.5, two contributions can be identified: zero-lift drag (C_{D_0}) and lift-induced drag (C_{D_i}).

$$C_D = C_{D_0} + C_{D_i} = C_{D_0} + \frac{C_L^2}{\pi A e} \tag{5.5}$$

In this equation, A is the aspect ratio of the (wings of the) aircraft and e is the Oswald efficiency factor. First, in Section 5.5.1, the zero-lift drag will be analyzed, after which in Section 5.5.1, the lift-induced drag will be computed.

Zero-Lift Drag

C_{D_0} is determined using methods presented in the AE2111-II Aerospace Design & Systems Engineering Elements course, which are mostly taken from Raymer [14]. For the C_{D_0}, the contributions of the wing, the nacelle and the pylons are considered. The contribution of the winglets/fins is neglected, as they contribute to a higher lift coefficient, but also to higher viscous drag, resulting in little impact on the total lift of drag ratio [16].

The approach used here for the zero-lift drag is also referred to as the component drag build-up method. The formula used for this approach can be seen in Equation 5.6. The first term, C_f, is the flat plate skin friction coefficient as calculated in Equation 5.7. The second and third term, FF and IF, are the form and interference factor, respectively. The form factor is computed using Equation 5.9 or using Equation 5.10. For all components discussed in this section, the IF is set to 1, as it is assumed that the flow past the engine does not interfere with the flow over the wing.

$$C_{D_0} = \frac{1}{S_{ref}} \sum_c C_{f_c} \cdot FF_c \cdot IF_c \cdot S_{wet_c} \tag{5.6}$$

Two values of the flat plate skin friction coefficient are obtained: one for the laminar portion of the flow, and one for the turbulent portion. The final C_f value is the weighted average of both. For a commercial aircraft, it is determined that 10% of the flow over the airfoil is laminar [14].

$$\begin{aligned} C_{f,\text{laminar}} &= \frac{1.328}{\sqrt{Re}} \\ C_{f,\text{turbulent}} &= \frac{0.455}{(\log_{10}(Re))^{2.58} \cdot (1 + 0.144M^2)^{0.65}} \end{aligned} \tag{5.7}$$

The Reynold's number used in Equation 5.7 is detailed in Equation 5.8. It is unsurprisingly dependent on the air density, the free-stream velocity and the length of the body immersed in the flow. The factor k is a surface parameter indicating roughness. In the case of the Flying-V, a value of $0.634 \cdot 10^{-5}$ was taken (value for smooth paint on the surface [14]). A preliminary estimate was thus made for the design that the surfaces of the Flying-V will be on the smoother side.

$$\begin{aligned} Re_{M<0.75} &= \min\left(\frac{\rho V l}{\mu}, 38.21\left(\frac{l}{k}\right)^{1.053}\right) \\ Re_{M\geq 0.75} &= \min\left(\frac{\rho V l}{\mu}, 44.62\left(\frac{l}{k}\right)^{1.053} M^{1.16}\right) \end{aligned} \tag{5.8}$$

Using Equation 5.9, the form factor of the wing is computed [17]. $\Lambda_{0.5}$ refers to the half chord sweep angle. This equation was chosen based on its proven accuracy [18].

$$FF = 1 + \left(2.7 \cdot \frac{t}{c} + 100 \cdot \left(\frac{t}{c}\right)^4 \cdot \cos^2\left(\Lambda_{0.5}\right)\right) \tag{5.9}$$

For a nacelle, the following equation is used for the component form factor:

$$FF = 1 + \frac{0.35}{f} \tag{5.10}$$

$$f = \frac{l}{d} = \frac{l}{\sqrt{\left(\frac{4}{\pi}\right) \cdot A_{max}}} \tag{5.11}$$

The total CD_0 contribution for the nacelles is multiplied by two, as there are two engines on this aircraft.

Finally, the wetted area of each component depends on the type of component. For the nacelles, the total surface area of the engine, approximated as a cylinder, is taken as the wetted area. For the wing, Equation 5.12 is used. The subscript exp refers to the exposed wing area.

$$S_{wet_w} = 1.07 \cdot 2 \cdot S_{exp_w} \tag{5.12}$$

Finally, the zero-lift drag coefficient for the pylons is taken to be $3 \cdot 10^{-}4$ [19]. Summing all of these contributions, the total C_{D_0} of the aircraft can be calculated.

Lift-Induced Drag

As could be seen in Equation 5.5, the lift-induced drag depends on three factors: C_L, e and A. The latter can be calculated as follows, where b is the wingspan and S the wing surface area:

$$A = \frac{b^2}{S} \tag{5.13}$$

The Oswald efficiency factor was determined by performing an analysis on a digital model of the Zephyr One using a Vortex Lattice Method called AVL, developed by MIT[1]. AVL was chosen because of its computational speed (time to convergence is less than a second), its accuracy and, due to its command-line style usage, the possibility to automate its running.Figure 5.5 shows a sample (not the actual geometric characteristics of the final aircraft) Zephyr One as seen in AVL.

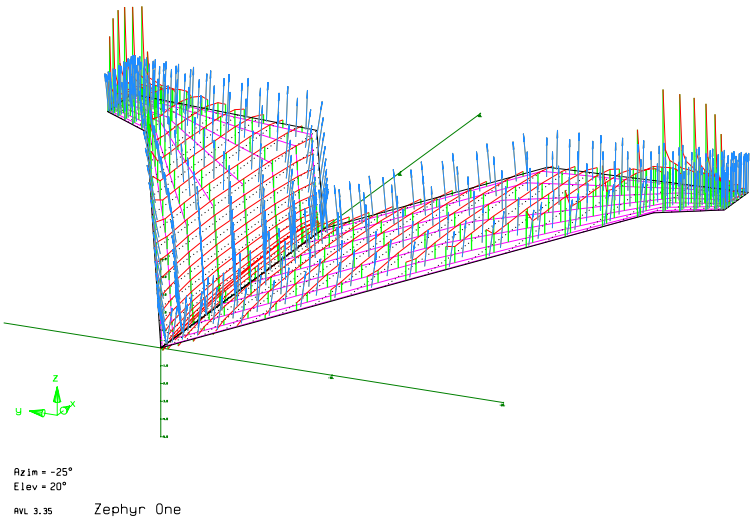

Figure 5.5: Example Zephyr One planform modelled in AVL, with blue arrows indicating normal vectors and red lines indicating the local aerodynamic loading. Purple grid indicates the panels used for the analysis.

The actual value of e resulted from trimming the aircraft (finding the correct angle of attack) in AVL for $C_{L_{des}}$, with the program returning the value of the efficiency factor.

[1] `https://web.mit.edu/drela/Public/web/avl/` [cited 21 June]

5.5.2. Lift Over Drag

Using the total drag coefficient, the L/D of the aircraft during the cruise phase is determined using Equation 5.14.

$$\left(\frac{L}{D}\right)_{cruise} = \frac{\frac{1}{2}\cdot\rho\cdot V^2\cdot C_{L_{des}}\cdot S}{\frac{1}{2}\cdot\rho\cdot V^2\cdot C_D\cdot S} = \frac{C_{L_{des}}}{C_D} \tag{5.14}$$

$\left(\frac{L}{D}\right)_{cruise}$ is the parameter used to select the best airfoil. The airfoil has a great and complicated impact on the lift over drag. From thisEquation 5.9, it can be seen that increased airfoil thickness increases the drag of the aircraft. Thinner airfoils require a larger wing surface area however as a larger airfoil chord is required to fit the cabin in the airfoil. Increasing the surface area of aircraft also increases the drag, as shown in Equation 5.6. Due to this complicated relationship between the airfoil and the total aircraft drag, every airfoil was evaluated at planform level, instead of just at airfoil level during the airfoil selection. The airfoil which resulted in the highest lift over drag during cruise was chosen to be the best airfoil.

5.5.3. Lift Polar

The final step of the aerodynamic design is constructing the lift curve of the aircraft. The lift curve can be constructed using four defining parameters; α_{0L}, C_{L_α}, $C_{L_{max}}$ and α_{stall}. The angle of attack at zero lift, α_{0L}, is an airfoil characteristic and thus is easily determined using JavaFoil [20]. The rest of the parameters are determined using DATCOM methods [21]. DATCOM uses semi-empirical methods to estimate aircraft performance [21]. The slope of the lift curve, C_{L_α}, is calculated using the following equation[21]:

$$C_{L_\alpha} = \frac{2\pi A}{2+\sqrt{4+\left(\frac{A\beta}{\eta}\right)^2\cdot\left(1+\frac{tan(\Lambda_{0.5C})^2}{\beta^2}\right)}} \tag{5.15}$$

The aspect ratio used in Equation 5.15 is increased by 20% as the use of winglets on the tip chord of the aircraft increases the effective aspect ratio [22]. The sweep angle is taken to be the angle between half chord at the root of the aircraft, and half chord at the tip of the aircraft. The linear part of the lift polar can be constructed using α_{0L} and C_{L_α}.
The maximum lift coefficient and the corresponding stall angle are determined again using methods from DATCOM [21]. DATCOM uses separate methods for high aspect wings and low aspect wings, as for low aspect wings the 3d effects are amplified, reducing the impact of the chosen airfoil [22]. Equation 5.16 is used to determine if the aircraft is considered high or low aspect ratio, where C_1 is a function of the wing taper.

$$A \leq \frac{3}{(1+C_1)cos\Lambda_{LE}} \tag{5.16}$$

Due to the small wingspan of the planform, the Zephyr One is considered to be a low aspect ratio according to DATCOM, and as such the low aspect ratio method is applied. The simplifications described Section 5.5 are applied to determine the maximum lift coefficient of each separate section. The weighted average of the three wing sections is then taken to be the final value. Only the stall parameters in landing configuration (low Mach number) are determined, as the aircraft can not handle the aerodynamic loads at stall conditions at higher cruise velocity.

The DATCOM method utilises Equations 5.17, 5.18 to determine the maximum lift coefficient and stall angle respectively.

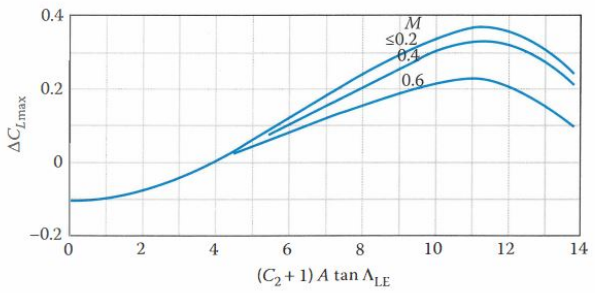

Figure 5.6: DATCOM plot for determining $\Delta C_{L_{max}}$ [21].

$$C_{L_{max}} = (C_{L_{max}})_{base} + \Delta C_{L_{max}} \quad (5.17) \qquad \alpha_s = (\alpha_{CL_{max}})_{base} + \Delta\alpha_{CL_{max}} \quad (5.18)$$

The parameters in Equations 5.17, 5.18 are determined from plots provided by DATCOM [21], one of which is shown in Figure 5.6. These plots were converted to data files and interpolated so that the calculation of the stall characteristics was automatised.

A lift polar can be constructed using all the calculated parameters. The trim angle of the aircraft can consequently, the angle at which the aircraft is flying during cruise. Requirement **EFMRA-SYS-AE-05** states that the angle of attack during cruise shall be between 0 to 4 degrees, to ensure passenger comfort. The trim angle is found by determining the angle of attack required to achieve $C_{L_{des}}$.

5.5.4. Moment Coefficient

Although not of high importance for the aerodynamic performance, in order to guarantee the stability of the aircraft, the derivative of the moment coefficient with respect to the angle of attack ($dC_m/d\alpha$) should be negative. After an optimal design is found using the optimiser, whether or not this required is fulfilled by hand, by running an AVL simulation for 0 and 10 degrees angle of attack. The requirement is considered fulfilled when the moment coefficient at 10 degrees is lower than the one at 0 degrees.

5.5.5. Mean Aerodynamic Chord

Similarly to the moment coefficient, the location of the MAC (Mean Aerodynamic Chord) is essential to for stability reasons. The surface area of the Zephyr One produces positive lift, as such the MAC of the entire aircraft has to be determined. The length of the MAC is calculated using Equation 5.19, while the position of the MAC is determined using Equation 5.20 [2]. These equations use integrations along the half span of the wing planform. The simplified planform shown in Figure 5.4 is used. The location of aerodynamic centre, ac_x, is assumed to be located at 25 % of the mean aerodynamic chord.

$$c_{MAC} = \frac{2}{S}\int_0^{b/2} c^2 dy \quad (5.19) \qquad y_{MAC} = \frac{2}{S}\int_0^{b/2} c \cdot y dy \quad (5.20)$$

5.6. Verification and Validation

In this section, the Verification and Validation of the methods used for the aerodynamic analysis of the Zephyr One are performed.

5.6.1. Lift Polar

The lift polar is verified and validated to ensure valid results are retrieved. The determination of stall characteristics was automatised by interpolating the graphs found in DATCOM [21], it is thus

[2] `https://www.fzt.haw-hamburg.de/pers/Scholz/HOOU/AircraftDesign_7_WingDesign.pdf` cited on 18 June 2021

crucial to thoroughly verify the results found from these interpolations to ensure no mistakes are made. First off the graphs were all checked manually to ensure the data used was accurate compared to the DATCOM plots [21]. Furthermore unit and system tests were performed which consists of manually determining the stall characteristics from the plots and comparing it with the results found by the interpolated data. Finally, the stall characteristics of the final aircraft were verified manually by calculating the stall characteristics by hand.

The method of determining the stall characteristics is validated using wind tunnel experiment data on a Flying-V model. A highly swept flying wing model was analysed experimentally in a wind tunnel by R.A. Viet [23]. A lift curve was constructed using this experimental test, resulting in clearly defined stall characteristics for the model. To validate the method used to determine the stall characteristics of the Zephyr One, the same method is applied to the experimental model used by R.A. Viet [23]. Similarly to the method described in Section 5.5.3 and shown in Figure 5.4, the model is then split into three sections, each with parallel chords. The maximum lift coefficient and stall angle are then determined per section using the DATCOM methods [21]. The weighted average is taken to find the stall characteristics of the entire model.

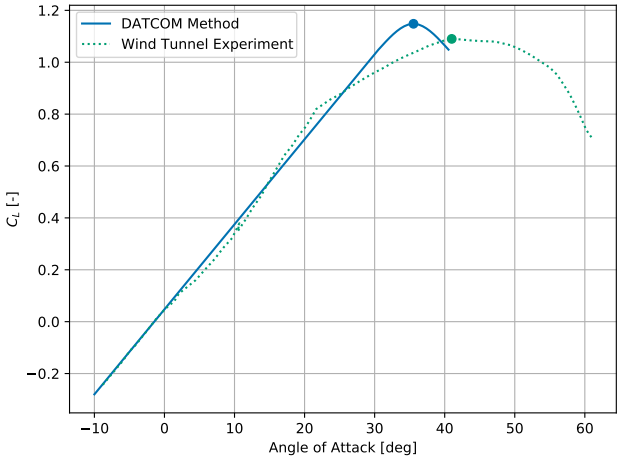

Figure 5.7: Graphical comparison of DATCOM method and experimental wind tunnel results.

Table 5.2: Numerical comparison of the DATCOM method and experimental wind tunnel results.

	Wind tunnel data	**DATCOM method**	**Relative difference [%]**
C_{L_α} [1/rad]	1.9	1.88	1.1
$C_{L_{max}}$ [-]	1.09	1.15	-5.2
α_{stall} [deg]	41	36	13.9

Figure 5.7 shows a graphical comparison of the DATCOM method and the experimental data, Table 5.2 represents a numerical comparison. It can be seen that the biggest discrepancy occurs for the stall angle of attack, as this is underestimated by 13.9%. The maximum lift coefficient determined using the DATCOM method is only slightly overestimated compared to experimental data. Finally, discrepancies start to occur between the lift curve slopes for higher angles of attacks. This is due to leading edge vortices starting to occur at an angle of attack of 10 degrees and onward for the wind tunnel data [23]. These leading edge vortices generate extra so-called vortex lift [23]. These effects are not accounted for in Equation 5.15. Though the method of DATCOM seems quite accurate compared to experimental wind tunnel tests, determining the stall characteristics still remains highly unreliable [22]. Wind tunnel experiments have to be performed to more accurately determine the stall characteristics of the Zephyr One planform. These wind tunnel experiments still however also lack accuracy as usually small scale models are analysed at vastly different Reynolds number compared to real life.

5.6.2. Zero-Lift Drag

The zero-lift drag will be both verified and validated, as there is both other theoretical as well as practical (in this case, wind tunnel) data available. Verification is performed by comparing the result of the C_{D_0} calculation procedure with the result of Faggiano [18], as he approaches the zero-lift drag coefficient estimation in the same way. The exact conditions and (approximate) geometry for which Faggiano calculated the C_{D_0} were used as inputs to the C_{D_0} method presented here. The result of this procedure can be found in Table 5.3.

Table 5.3: Reference verification data for zero-lift drag estimation methods.

	Faggiano	**DSE26**	**Relative difference [%]**
C_{D_0} [-]	0.00572	0.00598	-4.3

As can be seen in Table 5.3, Faggiano's finds the zero-lift drag coefficient to be slightly lower than what results from the method presented in this chapter. A possible reason for this discrepancy can be the absence of exact geometrical values as used by Faggiano, as he does for example not disclose his precise MAC, t/c or $\Lambda_{0.5}$, the latter two having a large impact via the wing form factor (see Equation 5.9) on the final result. These geometric properties thus had to be estimated to a certain degree.

Next, validation is performed by comparing the results of this method with actual wind tunnel data from Palermo [24]. Palermo performed wind tunnel tests with a scaled model of a Flying-V and recorded and reported extensively on his results.

Table 5.4: Reference validation data for zero-lift drag estimation methods.

	Palermo	**DSE26**	**Relative difference [%]**
C_{D_0} [-]	0.015	0.011	36.4

Looking at the results in Table 5.4, it can be seen that there is a more substantial difference between the two results than for verification. Again, some of it is due to having to guess engine radius and length as well as various other parameters. However, even when these inputs are set to their worst case (resulting in higher C_{D_0}), the 0.015 reported by Palermo cannot be reached. The 0.011 obtained here also includes a laminar flow fraction of 10%, however, this value should probably be higher in case of the model aircraft. The author's best guess is that this method does not work very accurately (although resulting in same order of magnitude values) for small-scale aerodynamics, as the empirical relationships used are for large scale subsonic aircraft. It can thus be concluded that this method is reasonably correct for large-scale aircraft analysis, but starts to fail for lower speeds/smaller aircraft and should be not be used in the latter case.

5.7. Results

The aerodynamic parameters for the final aircraft are discussed in this section. The airfoil used for the inboard wing is the NACA68035, as it was found that the thicker airfoils were able to achieve a higher L/D during cruise, despite their increased thickness.

The lift polar curve of the Zephyr One is shown in Figure 5.8. Similarly to what was seen in the wind tunnel experiment by R.A. Viet, the stall angle is very high. A significantly higher $C_{L_{max}}$ of 1.39 is achieved however, in combination with an increased C_{L_α}. Differences between the wind tunnel test and the Zephyr One can be attributed to compressibility effects and the use of actual dimensions. The linear part of the lift polar during cruise is plotted with the green line. The trim angle of attack is determined by taking the required angle of attack to achieve $C_{L,des}$. The trim angle is marked with the red 'x' in Figure 5.8, and is equal to 2.6 degrees.

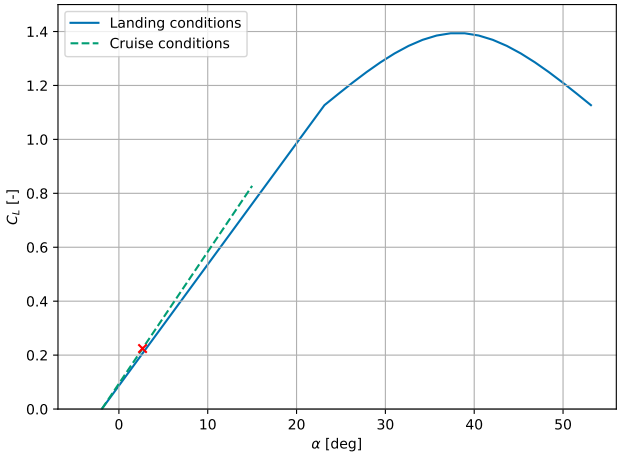

Figure 5.8: Lift polar of the Zephyr One.

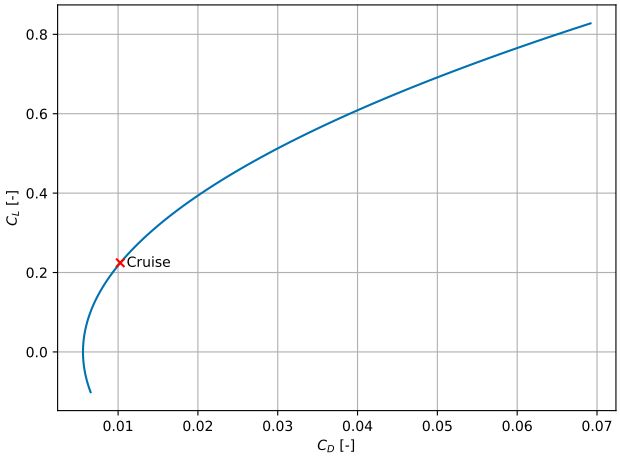

Figure 5.9: Drag polar of the Zephyr One.

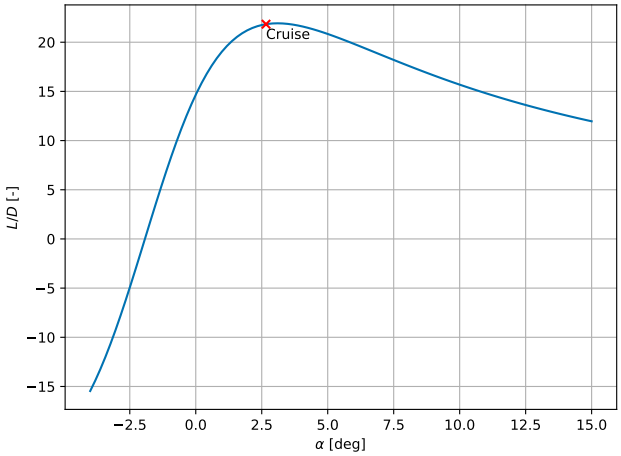

Figure 5.10: Lift over Drag for varying Angle of Attack.

The drag polar is shown in Figure 5.9. As expected, the drag polar shows that the drag coefficient increases for increasing lift coefficients. Figure 5.10 shows the lift over drag of the Zephyr One for varying angles of attacks. The cruise conditions are marked with the red 'x'. Within the range of $\alpha = 1.8$ and $\alpha = 4.8$, the L/D only decreases by a maximum of 5%. Showing that there is a wide range of angle of attacks available to fly at during cruise, while still maintaining high aerodynamic efficiency.

Finally, a complete overview of all the aerodynamic characteristics of the Zephyr One aircraft can be found in Table 5.5.

Table 5.5: Final aerodynamic characteristics for cruise configuration.

Parameter	Value
C_{D_0} [-]	0.005602
e [-]	0.9186
A [-]	3.73
$\Lambda_{inboard}$ [deg]	63.9
$\Lambda_{outboard}$ [deg]	34.3
ac_x [m]	19.85

Parameter	Value
$C_{L_{des}}$ [-]	0.22
α_{trim} [deg]	2.6
α_0, L [deg]	-1.9
$C_{L_{\alpha,landing}}$ [1/deg]	0.0450
$C_{L_{\alpha,cruise}}$ [1/deg]	0.0489
$C_{L_{max}}$ [-]	1.39
α_{stall} [deg]	38

5.8. Recommendations

In this section, various recommendations for further research into the aerodynamics of the Zephyr One will be presented.

To achieve optimal reduction of wasted space, it is advised to generate an airfoil geometry that is able to fit all required components within the wing, instead of using predefined airfoils from the NACA series. With an airfoil specifically generated for the Zephyr One, it is possible to decrease the airfoil chord length, while also achieving more beneficial aerodynamic characteristics. Modifications to the airfoil can be made to achieve trim angles closer to zero angle of attack, which improves passenger comfort.

Finally, more analysis should also be performed to find the optimal outboard airfoil: currently used aerodynamic characteristic estimation methods and tools do not perform well with transonic flows over this low-sweep part of the wing. This, in combination with the effect of transitioning from the thick, inboard cabin airfoil to the thin outboard airfoil could lead to a drop in performance which can not be foreseen at the moment.

Generally, it is advised to run a CFD analysis as an extra step after the results of AVL deem satisfactory, as done by Faggiano [18]. Since a VLM method like AVL neglects the influence of thickness [25] and with the Zephyr One being a relatively thick wing itself, a CFD analysis will make sure that the aerodynamic design does not move towards a design that in reality is not performant. However, since CFD both computationally and timewise expensive, this activity should only be performed on already well-performing design variations.

Regarding the zero-lift drag, comparisons with CFD results could lead to better analytical predictions of this value, as the method presented here was not originally designed to work in the transonic flow regime.

Furthermore, the influence of winglets on the lift over drag has been neglected, as explained in Section 5.5.1. However, in order to find a suitable airfoil for this part of the wing, CFD could be used, but preferably, a cheaper computational method is to be used if one wants to evaluate more than just a few airfoils.

Finally, two design parameters that have not been investigated but that are worthy of a proper analysis, are the twist and dihedral of the wing. In the original article on the Flying-V [26], a twist ranging from 1.5 to 3.5 degrees was used to make the lift distribution fully elliptical. Although the authors have used the twist in the design exploration phase and saw the value of e go up, it was not included in the design optimization due to lack of time. The same goes for the dihedral of the wing: this would dramatically increase lateral stability (higher C_{n_β}) at little cost. The influence of both of these can be explored in AVL and it is thus advised to do so in next phases of the design.

6 Propulsion System Design

In this chapter the aircraft's propulsion system's design is discussed. First of all, the turbofan design is presented in Section 6.2. Then the fuel system design is given in Section 6.3. After this the electrical propulsion and electrical system design of the aircraft is presented in Section 6.4. Finally, the propulsion system mass is estimated in Section 6.5. The overview of the propulsion system can be seen in Figure 6.1. As can be seen, fuel is pumped through the HPT first. This is done in order to cool the HPT's blades, whilst also heating up the fuel in order to evaporate it, for use in the combustion chamber.

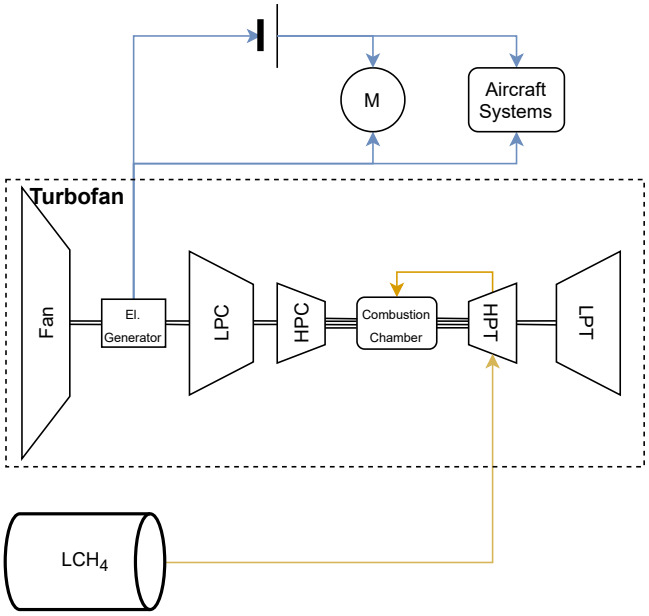

Figure 6.1: Overview of the propulsion system.

6.1. Requirements

A number of requirements are set for the propulsion system. The list of requirements originates from the top-level systems requirements determined in the Baseline report [2]. The requirements are listed in Table 6.1.

Table 6.1: Requirements set for the design of the propulsion system.

EFMRA-SYS-PF-01	The aircraft shall have a range of at least 6,150 km.
EFMRA-SYS-PF-02	The aircraft shall have an endurance of at least 6 h.
EFMRA-SYS-PF-03	The aircraft shall have a cruise speed of at least 830 km/h.
EFMRA-SYS-PF-04	The aircraft shall have a cruise altitude of at least 9,144 m.
EFMRA-SYS-PF-05	The aircraft shall have a take-off distance of at most 2,100 m.
EFMRA-SYS-PF-09	The aircraft shall have a rate of climb of at least 12.7 m/s.
EFMRA-SYS-SF-7	The aircraft shall have an emergency fuel pump in case of failure of the main pump.
EFMRA-SYS-FP-03.01	The aircraft shall produce no more than 2.917 kg/km of CO_2 emissions for its mission range.
EFMRA-SYS-FP-03.02	The aircraft shall produce no more than 0.0057 kg/km of NO_x emissions for its mission range.
EFMRA-SYS-FP-03.03	The aircraft shall produce no emissions while taxiing.

No precise limits on minimal thrust at sea-level or cruise conditions can be derived from this, since these are dependant on the final aerodynamic properties. Therefore, these constraints will be included in the optimisation program, and will be updated in each design iterations.

6.2. Turbofan Design

In order to determine the optimal design for the propulsion system, an engine model is developed first, in order to analyse engine performance. In Section 6.2.1 the engine model itself will be detailed. Afterwards, emissions are calculated, and the maximum allowable amount of LNG used is considered. Finally, the results of the optimisation are presented in Section 6.2.5.

6.2.1. Methodology

In order to calculate the fuel burned, the thrust produced, as well as estimate the NO_x emissions, a thermodynamic model of a turbofan engine has been developed. For this engine model, the engine is split into a number of stages, which are considered separately.

The first stage encountered by the air flowing through the engine is the inlet. This inlet has no effect on total temperature. However, there is a small drop in total pressure, due to the efficiency of the inlet. The efficiency of the inlet is assumed to be 0.98. At this point of the calculations, environmental pressure and temperature are converted to total pressure and temperature, using Equation 6.1 and Equation 6.2. The pressure drop due to the isentropic efficiency of the inlet is taken into account directly when converting from static to total conditions. κ_a Refers to the specific heat ratio of air, which is assumed to be constant with temperature.

$$\frac{T_t}{T} = 1 + \frac{(\kappa_a - 1)}{2} M^2 \tag{6.1}$$

$$\frac{p_t}{p} = \left(1 + \eta_{is_{inlet}} \frac{\kappa_a - 1}{2} M^2 \right)^{\frac{\kappa_a}{\kappa_a - 1}} \tag{6.2}$$

Next, a number of compressor stages is encountered. The fan is treated like a compressor in the calculations. The total pressure after a compressor stage is calculated by multiplying the total pressure in front of the compressor with the design pressure ratio. The total temperature rise across a compressor stage is governed by Equation 6.3. The power required by a compressor stage is calculated using Equation 6.4. The mass flow for the fan is the complete mass flow through the engine. For the

LPC and HPC, only the mass flow through the core is considered. $C_{p,a}$ Refers to the specific heat of air, which is assumed to be constant with temperature.

$$\frac{T_{t\ ,2}}{T_{t,1}} = 1 + \frac{1}{\eta_{is}} \left[\left(\frac{p_{t,2}}{p_{t,1}} \right)^{\left(\frac{\kappa_a - 1}{\kappa_a}\right)} - 1 \right] \tag{6.3}$$

$$P_{compressor} = \dot{m}\, C_{p,a} \left(T_{t,out} - T_{t,in}\right) \tag{6.4}$$

The next step of the model is the combustion chamber. The model is flexible in having either the fuel flow, or the combustion outlet temperature specified. Using Equation 6.5, the other of the two can then be calculated. LHV Refers to the calorific value of the fuel, and $C_{p,g}$ refers to the specific heat of the gas after the combustion. This is different from the specific heat of air, since the composition of the gas changes throughout the combustion process. The total pressure after the combustion chamber is obtained by multiplying the total pressure before combustion with the combustion chamber pressure ratio.

$$\dot{m_f} = \frac{\dot{m_a} \cdot C_{p,g} \cdot \left(T_{t,out} - T_{t,in}\right)}{\eta_{cc} \cdot LHV} \tag{6.5}$$

After combustion, the flow passes through the turbine stages. The high pressure turbine (HPT) delivers the power required for the high pressure compressor (HPC). The low pressure turbine (LPT) delivers the power to the low pressure compressor (LPC) and the fan. The power delivered by the turbine is calculated using Equation 6.6. The power supplied by the turbine should equal the power used by the compressors it is connected to, divided by the mechanical efficiency. Using this equation, the total temperature after the turbine is determined. Using Equation 6.7, which can be rewritten to Equation 6.8, the total pressure after the turbine is determined.

$$P_{turbine} = \dot{m} \cdot C_{p,g} \cdot \left(T_{t,in} - T_{t,out}\right) \tag{6.6}$$

$$\frac{T_{t,2}}{T_{t,1}} = 1 - \eta_{is} \left[1 - \left(\frac{p_{t,out}}{p_{t,in}} \right)^{\left(\frac{\kappa_g - 1}{\kappa_g}\right)} \right] \tag{6.7}$$

$$\frac{p_{t,2}}{p_{t,1}} = \left(1 - \frac{1}{\eta_{is}} \left(1 - \frac{T_{t,2}}{T_{t,1}} \right) \right)^{\frac{\kappa_g}{\kappa_g - 1}} \tag{6.8}$$

Finally, The flow passes through the nozzle, here the total thrust is calculated using Equation 6.9. This is done for the bypass flow as well as for the core flow.

$$T_N = m \left(v_{exhaust} - v_{inf}\right) + A_{exhaust} \left(p_{exhaust} - p_{inf}\right) \tag{6.9}$$

A block diagram of the engine model can be found in Figure 6.2.

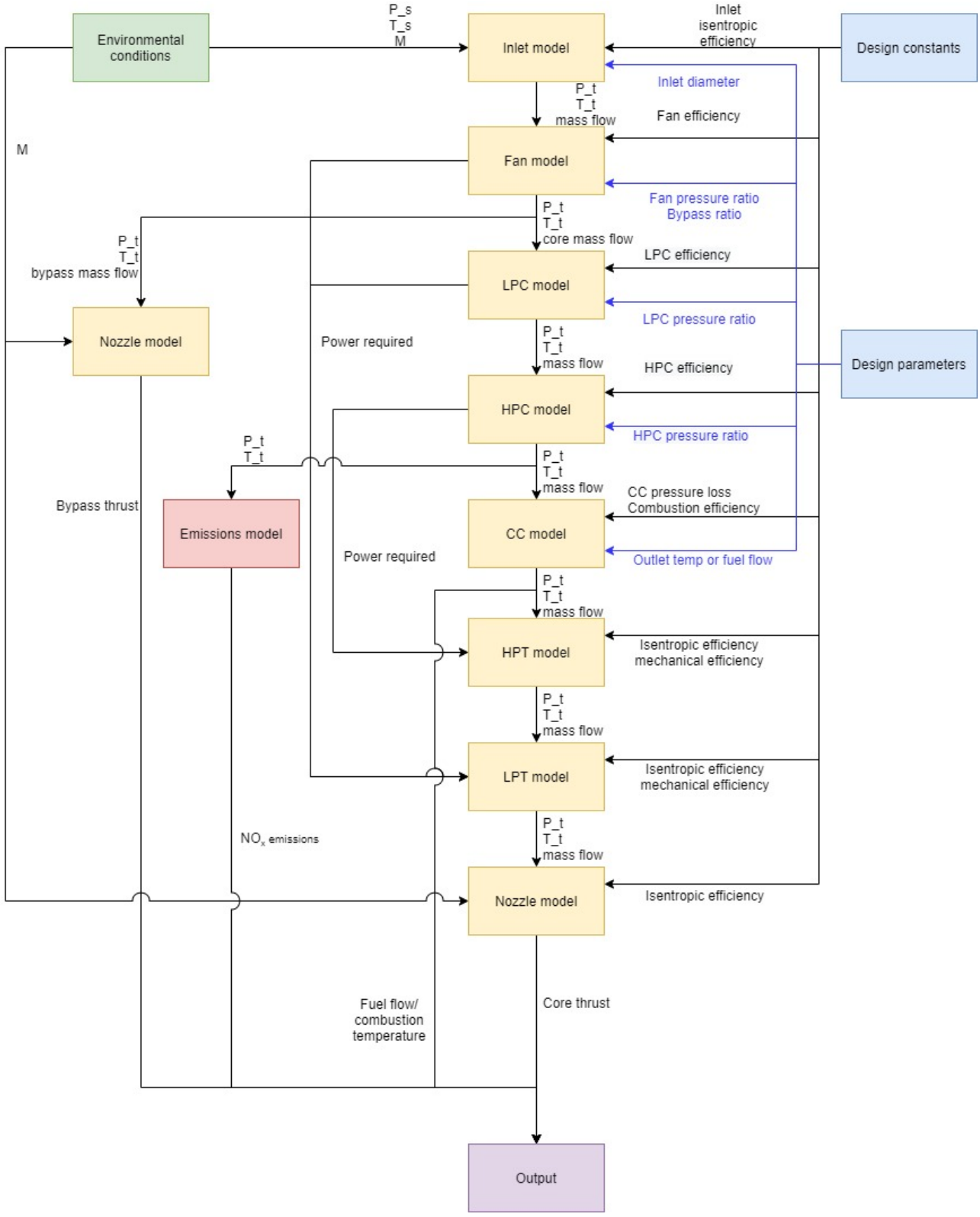

Figure 6.2: Flowchart of the engine model.

6.2.2. NO_x Emissions

The Flightpath 2050 guidelines stipulate a 90% reduction in NO_x emissions. This requirement will be one of the driving constraints of the propulsion system design. In order to evaluate this requirement, an unbiased method for determining the emissions index will be used. Due to the preliminary nature of the design, more elaborate methods are not yet feasable. Therefore, Equation 6.10 [27] will be used.

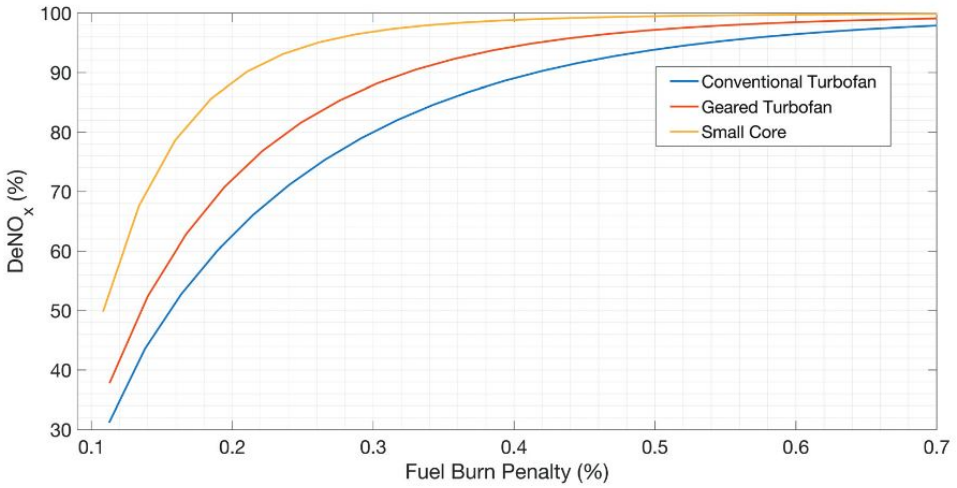

Figure 6.3: No$_x$ reduction to fuel burn penalty.

$$EINO_x = 2 + 28.5 \cdot \sqrt{\frac{P_3}{3100}} \cdot exp(\frac{T_3 - 825}{250}) \tag{6.10}$$

In modern day aircraft engines, there is a push for maximising overall pressure ratio's, as this increases fuel efficiency. However, the increase in pressure and temperature before combustion, leads to higher NO_x emissions [28]. From initial runs of the optimisation algorithm, it was clear that it was impossible to meet the emission requirement, whilst having an acceptable fuel consumption. Therefore, alternate solutions were investigated.

With ever increasing bypass ratio's, and consequently lower core mass flow rates, emissions control on the exhaust stream becomes a serious option [29]. For the Zephyr One, it was decided to go with a selective catalytic reductor (SCR). A reducing agent is introduced into the exhaust flow, before it is pushed trough a catalyst. This catalyst triggers a reaction, converting NO_x and the reductor into pure nitrogen gas and water vapour.

A SCR will reduce the NO_x significantly. However, it also comes at a cost. SCR systems are relatively heavy and large, and require reductor fluid in order to function. Furthermore, forcing the core flow through the SCR will cause a pressure drop in the core flow. Therefore, the thrust specific fuel consumption (TSFC) of the engine will increase slightly. The magnitude of this increase in fuel burn has been approximated in a study conducted by Prashanth et al [29]. The results of that study can be seen in Figure 6.3. From this graph, the increase in fuel burn for a given reduction in NO_x emissions can be estimated. The design point used for the Zephyr One is chosen at a 95% reduction in NO_x emissions, for a 5% increase in fuel burn. This loss in efficiency is more then compensated by the higher pressure ratios that can be used.

The reduction reaction requires a reducting agent to be injected into the exhaust flow. In current road-based SCR's a mixture of ammonia and water, known under the brand name AdBlue is used. However, for usage in an airliner, purer forms of urea or ammonia can be considered, since it can be assumed the fluid will be handled by professionals. The main advantage of using pure anhydrous ammonia is the lower weight and volume required. However, it needs to be stored cold or under high pressure and handled with care due to its toxic nature.

The amount of reductor fluid required will be dependant on the NO_x emissions without SCR. Using anhydrous ammonia, approximately 0.37 grams of reductor will be required for every gram of NO_x emitted. This reductor will have to be stored in a pressure vessel capable of handling pressures up to 17.2 bars. Furthermore, only 85% of the tank can be filled, to allow for expansion of the gas[1]. This

[1] https://www.ag.ndsu.edu/publications/crops/anhydrous-ammonia-managing-the-risks#:~:text=and%

tank will be placed in the trailing edge. Since the tank is relatively small, it's precise placement will only be considered later. However, the tank must be placed outside the pressurised cabin, to avoid ammonia leaking into the cabin in case of a leak.

6.2.3. Fuel Mixture

In order to save costs and allow the Zephyr One to fly into airports where no synthetic methane is available, a mixture of LNG and synthetic methane can be used. Technically, the Zephyr One can fly on pure LNG. However, this would mean emission requirements are not met.

In order to meet the CO_2 emission requirements set by Flightpath 2050, a limit on the usage of grey methane has to be set. From the methane burning chemical reaction, seen in Equation 6.11, it is clear that one mole of methane burned will produce one mole of CO_2. Therefore, taking into account the molar masses of CH_4 and CO_2, a maximum of 1.06 kg of LNG can be used per kilometer of flight distance.

$$CH_4 + 2O_2 \rightarrow CO_2 + 2H_20 \tag{6.11}$$

6.2.4. Other Emissions

The requirements specify maximum emission rates for CO_2 and NO_x. However, other greenhouse emissions might be present and will therefore be considered.

One of the emissions considered will be methane emissions. It is important to consider these emissions, since methane is a very powerful greenhouse gas. Over a 100 year period, methane has approximately 30 times the greenhouse potential of CO_2. Over a 20 year period, this ratio is even higher at approximately 85[2]. Since no emissions data for methane turbofan engines is available, data gather from ground based, industrial gas turbines will be used. Research conducted by D. Kristian et al [30] shows methane emissions of approximately -0.039 % to 0.204% of fuel used. The negative values can be explained by methane in the atmosphere being burned together with the fuel. Assuming the worst case scenario, and the fuel mass estimated in class I weight estimation, approximately 0.0051 kg of methane would be emitted per km. This has an equivalent greenhouse potential over 20 years to 0.4335 kg/km of CO_2 emissions, which equates to approximately 1/7 of the emissions requirement. This can be compensated by emitting less carbon dioxide. Furthermore, special care should be taken in tank and refueling system design, to minimise leakage.

Another important type of emissions to consider is the emission of water vapor in the form of contrails. These contrails have a significant impact on global warming. Whilst depending on the weather conditions and the location, the effect of sunlight reflecting on the trails and the trails trapping heat at the surface might approximately cancel out during the day, they have a significant warming effect at night, when the surface heat trapping is no longer canceled out by the added reflection of solar radiation. Whilst the warming effect of a contrail is less permanent then that of greenhouse gasses, they still pose a significant threat. If no action is taken to mitigate the effect of contrails, their effects might add up to 0.1°C of global warming[3]. Most research conducted so far has focused on reducing the impact of contrails by means of route planning, which has no impact on design. However, burning methane will have an impact in lowering contrail effects, as the lower soot emissions will contribute to the formation of shorter-lasting contrails[4], which will more then offset the slightly higher number of contrails due to the higher water vapor emissions of methane combustion.

20suffocation%20results.-,Pressure%20for%20Storage,can%20be%20available%20for%20use. retrieved 15 June

[2] https://unece.org/challenge

[3] https://e360.yale.edu/features/how-airplane-contrails-are-helping-make-the-planet-warmer

[4] https://e360.yale.edu/features/how-airplane-contrails-are-helping-make-the-planet-warmer retrieved 15 June

6.2.5. Turbofan Design Results

After global optimisation of the entire aircraft, and optimisation of the turbofan engine, a final design has been obtained. For this optimisation, a number of bounds was set on the design parameters. These bounds are detailed in Table 6.2. Furthermore, constraints where set to limit the NO_x emissions, as well as the cruise thrust, and the sea-level thrust required. This resulted in a twin-spool turbofan, with the fan and low pressure compressor run on the low pressure turbine, and the high pressure compressor run on the high pressure turbine. The core flow is run through an SCR, in order to reduce the NO_x emissions. The final design parameters for the engine can be found in Table 6.3.

Table 6.2: Turbofan bounds.

Bypass	0-20
Fan pressure ratio	1-1.8
LPC pressure ratio	1-3
HPC pressure ratio	1-60
Total pressure ratio	1-70
Combustion temperature	$T_{out,HPC}$-2200K
Engine radius	0.5-2 m

Table 6.3: Final turbofan parameters.

Bypass	18.34
Fan pressure ratio	1.4
LPC pressure ratio	2.246
HPC pressure ratio	22.2603
Combustion temperature	1700 K
engine radius	1.00 m
TSFC cruise	10.6 g/N s
Cruise fuel flow	0.178 kg/s

6.3. Fuel System Design

In this section the design of the fuel tanks is discussed. Fuel tanks have to be designed to withstand the high pressure and temperature differences. First of all, the strength of the fuel tank is analysed and then the insulation of it.

As the fuel tanks will be cylindrical the needed thickness for the cylindrical part and the cap is found using Equation 6.12 and Equation 6.13, respectively [31]. The inputs used for the fuel tank aluminium casing calculations are presented in Table 6.4. As two tanks are used on each side of aircraft, and one of them is placed inside the pressurised cabin, two different pressure differences are used.

$$t_w = \frac{D_0 \Delta p FoS}{2\sigma_a e_w - 1.2\Delta p FoS} \tag{6.12}$$

$$t_w = \frac{D_0 \Delta p FoS}{4\sigma_a e_w - 0.4\Delta p FoS} \tag{6.13}$$

Table 6.4: Tank wall design properties.

Parameter	Value
σ_a	172.4 MPa
ρ	2840 kg/m3
FoS	2.2
Δp_{in}	26.06 kPa
Δp_{out}	84.58 kPa
e_w	0.8

Table 6.5: Tank insulation design properties.

Parameter	Value
k	0.0046 W/mK
ρ	49.8 kg/m3
ΔT	181 K
t	30,000 s

The tanks also needs to be thermally insulated to ensure low boil-off rates. Polyvinylchloride is a very good option for the insulation material, it has a density of 49.8 kg/m3 and a thermal conductivity of 0.0046 W/mK. A temperature difference of 181 K is taken, as liquid methane is stored at 112 K and standard atmosphere conditions are assumed (293 K). Of course, the fuel tanks might experience a higher temperature difference, however, this does not affect the structure of the tank, only the amount of boiled-off methane. During cruise the boiled-off methane will be used to power the engines, as the rate of boil-off is much lower compared to fuel consumption. At ground when the boil-off increases and the fuel consumption decreases, the boil-off will be released or could be stored in extra tank, which would contain boiled-off methane and it would be used during cruise. This boil-off will be accounted for

by ensuring extra storage for it. The main inputs used for the fuel tank insulation sizing are presented in Table 6.5.

The code was run for two iterations to account for the extra volume needed for the boiled-off methane. The results are presented in Figure 6.4. For lower thickness of insulation the boil-off mass increased, meaning more fuel is needed to be carried and for higher insulation thickness the insulation mass increased. The increasing casing mass at low insulation thickness is due to increased fuel volume due to boil-off, as it is an iterated process. From Figure 6.4 the optimized mass of all fuel tanks is 451.8 kg and the total length of the fuel tank is 15.23 m.

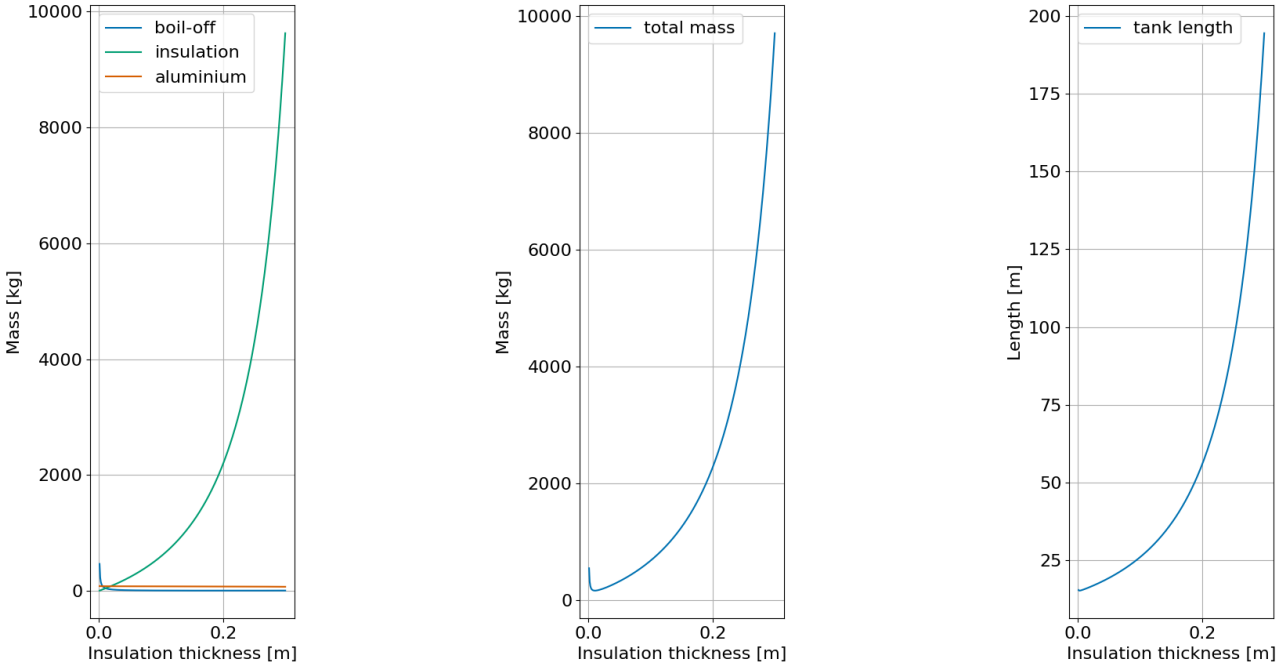

Figure 6.4: Fuel tank component masses and length versus insulation thickness.

6.4. Electrical System Design

This section will deal with the preliminary design of the electrical systems of the aircraft. The electrical system and propulsion system are interlinked, since the propulsion system will supply the electrical power, and electrical propulsion will be used for the emission free taxiing. This section first discusses the emission-free taxiing, and later deals with a general electrical budget.

For the entire aircraft, a more electrical architecture, or MEA is used. This means as many systems as possible are driven electrically, and no bleed air from the engines is used. This increases overall efficiency, as well as reducing the number of moving parts and reducing the risk of a leak in one of the hydraulic or pneumatic systems.

6.4.1. Emission-Free Taxiing

In this section, the aircraft's taxiing configuration will be discussed. Requirement **EFMRA-SYS-FP-03.3** indicates that the taxiing of the vehicle shall be emission-free. This leaves the regular jet-thrust assisted taxiing immediately out of the options, as running the main engines would produce CO_2 and NO_x. External solutions (an electric vehicle pulling the aircraft) are not considered for the Zephyr One, as it would severely limit the aircraft's autonomy. The remaining design options can be found in Figure 6.5

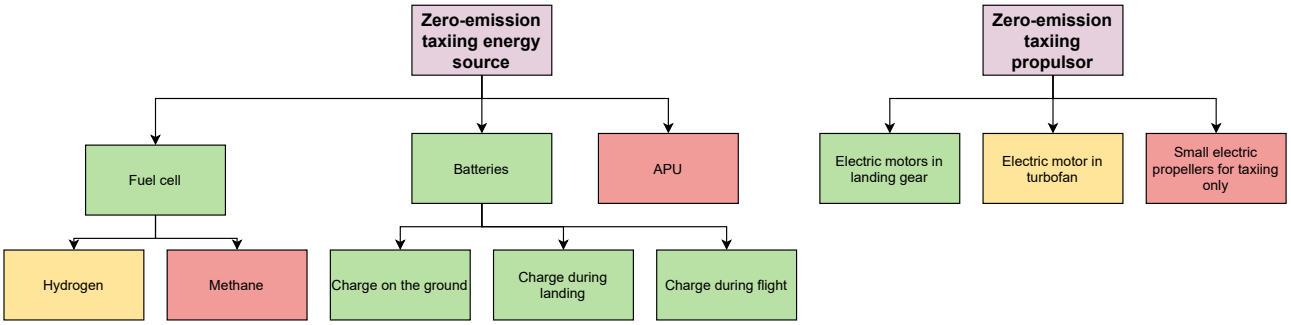

Figure 6.5: Design option tree for emission-free taxiing. Green indicates a feasible option, yellow indicates possible but not meeting the zero-emission requirement, red means too complex or too environmentally unfriendly to implement.

In the end, it was chosen to opt for electric motors in the main landing gear, powered by batteries. This is due to its ease of integration with existing landing gear designs and due to its simplicity in both design and usage. Adding a battery to the aircraft is not a major change and electric motors in itself are very simple with very little moving parts, both leading to simpler and thus more reliable designs. The decision for positioning in the MLG instead of the NLG, was taken based on two things: the fact that the majority of the weight of the aircraft is supported here, leading to higher traction; and, the possibility to install more than one motor [32]. Furthermore, the electric motor will be connected directly to the wheel, without a gearbox. This yields even higher reliability and also results in lower maintenance cost [32].

Generally speaking, an electric taxiing system has numerous advantages compared to the use of the jets in taxiing. Not only is the aircraft more autonomous, as no pushback tractor is required, the possible fuel (thus cost) savings and emission-reductions are also non-neglible [33]. This is because jet engines are optimized for cruise speed, leading to a very low efficiency at taxiing speeds. Disadvantages include higher weight, but this is mostly offset by the lower total fuel consumption.

To estimate the weight of such a system, the maximum required torque and the total required energy has to calculated. This is done by using a simple model [32], taking into account the forces on the wheels of the aircraft while moving it. The governing equations in this model are Equations 6.14 - 6.18.

$$F_{road} = c_{rr} \cdot mg \cdot \cos(\alpha) + mg \cdot \sin(\alpha) + \frac{1}{2} \cdot \rho \cdot C_D \cdot S \cdot V^2 \tag{6.14}$$

$$J_t = J_{motor} + J_{wheel} + \frac{1}{n_m} \cdot m \cdot r^2 \tag{6.15}$$

$$J_{total} \cdot \frac{d\omega_m}{dt} = T_{em} - \frac{1}{2} \cdot r \cdot F_{road} \tag{6.16}$$

$$P_{em} = T_{em} \cdot \omega_m \tag{6.17}$$

$$E_{em} = \int_0^{t_{taxi}} P_{em} dt \tag{6.18}$$

Where c_{rr} is the rolling resistance coefficient, α the slope of the taxiway, T_{em} is the developed electromagnetic torque, ω_m the angular velocity of the landing gear wheel, r the radius of the landing gear wheel, J is the moment of inertia and n_m is the number of motors installed on the aircraft.

For these equations, the following assumptions are made: the losses in the mechanical drivetrain are negligible and the entire aircraft mass is assumed to create a normal force on the wheels for which the torque is calculated.

Two simulations, one of taxi-out at Schiphol (AMS) and one of taxi-in at London Heathrow (LHR), were performed in order to determine the total required energy. The velocities used for these simulations come from Lukic [33]. Lukic chose these airports as they are both busy airports where the taxiing procedure can be up to one hour in length [33].

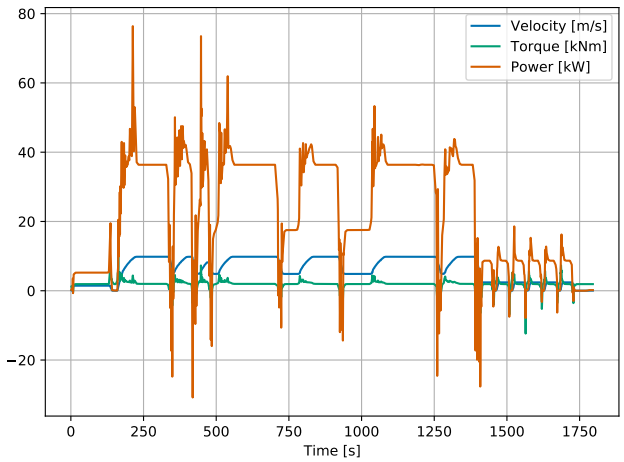

Figure 6.6: Simulation of taxi-out at Schiphol

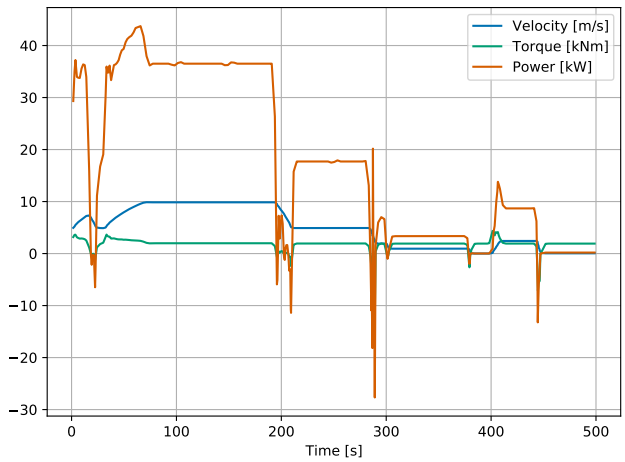

Figure 6.7: Simulation of taxi-in at London Heathrow

For the simulations seen in Figure 6.6 and Figure 6.7, regenerative braking is also taken into account. This is a procedure where braking the aircraft charges the batteries. An efficiency of 50% is assumed for this process. Furthermore, the simulations are performed at MTOW, with one motor per MLG, a c_{rr} of 0.009 [33] and a wheel radius of 0.535 m [33], which is equal to that of a Boeing 737-400.

It can be seen that taxi-out is the most demanding procedure, both in terms of total energy and in terms of peak power. For the higher total energy, this is due to the fact that the taxi-out phase simply takes longer. Regarding the higher peak power in Figure 6.6, this is most likely due to the aircraft first performing a pushback, having to come to a halt and then accelerate towards the runways.

6.4.2. Electrical Motors

To taxi electrically the aircraft has to have electric motors installed. Due to the large weight of the aircraft and wheel diameter, high torque motors have to be chosen. In Section 6.4.1 a peak torque of about 10 kNm was found, however, this value only occurred once. Thus, looking at lower peaks about 6 kNm motor should suffice. It was also decided to have two motors. This decision lead to the choosing of higher torque motors, however, it would save space compared to a four motor configuration. DST2-200BO hollow shaft motor fits the needs of an aircraft best. It can offer a maximum torque of 3230 kNm and it weights 325 kg [34]. It has a diameter of 0.4 m and a length of 0.556 m, so it should fit in the landing gear with the wheel. As two motors will be used a maximum torque of 6460 kNm can be achieved and weight of this systems is 650 kg.

6.4.3. Aircraft Power Budget

In the Baseline report a power budget was estimated to be 1.25 MW [2]. However, this is the peak power (without the electric motors). Looking again at Table 6.6, the flight control (low average value), landing gear (low operational time), engine start (low operational time) and auxiliary hydraulic pumps (low average value) can be neglected for average power use. This results in an average power of 0.725 MW. This is a quite high value, however, a bleed-less engine was chosen, so higher amount of electrical power is needed for the cabin climate control. Additionally, a peak power of 1 MW is expected, as engine starter will not operate at the same time with wing de-icing.

Table 6.6: Power budgeted to main electrical loads [2].

	Cabin pressurisation & air conditioning	Flight controls	Fuel pump	Wing de-icing	Landing gear	Engine start	Auxiliary Hydraulic pumps	Cabin power	Lights	Other
Power budget	300kW	50kW	10kW	250kW	75kW	250kW	150kW	50kW	15kW	100kW

6.4.4. Battery Sizing

From Section 6.4.3 a maximum power of 1 MW can be expected. Additionally, from Section 6.4.1 the total power needed for the electric taxi is 24.74 kWh. During taxi the turbofan engines will not operate, thus, the battery will need to provide energy during taxi for other systems. In Section 6.4.1 a taxi out time of 1800 s and taxi in time of 500 s was used. This means that the battery should be capable of providing 105.42 kWh for other systems required during taxi and 24.74 kWh for electric motors: a total of 130.16 kWh. A depth of discharge of 80% and an efficiency of 90% are assumed [32]. This results in a total energy of 180.78 kWh. Current state of the art lithium batteries have an energy density of 240 Wh/kg and power density of 1.9kW/kg [32]. Taking both values to find the battery weight, the critical weight is achieved for the energy density, and is found to be 753.25 kg.

6.5. Propulsion System Mass

In order to estimate the mass of the engines to be used in further design iterations, a method based on statistical data will be considered. The design parameters considered for the mass estimation are the bypass ratio, the overall pressure ratio, and the mass flow through the core [35]. The equations used can be seen in Equation 6.19 - Equation 6.22. This equation is to be used with imperial units. Furthermore, 180 kg are added to each engine to account for the SCR. This value is based on the design of a similar system [29].

$$m_{eng} = a \cdot \left(\frac{\dot{m_{core}}}{100}\right)^{b} \cdot \left(\frac{OPR}{40}\right)^{c} \tag{6.19}$$

$$a = 18.09 \cdot BPR^2 + \left(4.769 \cdot 10^2\right) \cdot BPR + 701.3 \tag{6.20}$$

$$b = \left(1.077 \cdot 10^{-3}\right) \cdot BPR^2 - \left(3.716 \cdot 10^{-2}\right) \cdot BPR + 1.190 \tag{6.21}$$

$$c = \left(-1.058 \cdot 10^{-2}\right) \cdot BPR + 0.232 \tag{6.22}$$

6.6. Verification and Validation

Extensive verification and validation has been performed for the engine model and the engine mass estimation. The verification and validation of the engine model will be detailed first, later the verification and validation of the engine mass model will be worked out.

For verification purposes, a number of unit tests, as well as a system test were performed. For this, reference values obtained for a worked out example for a GE90 engine where used. Each component is verified separately using a unit test. Then, a broad system test is performed for the entire model. These steps where automated, so that after each update of the engine model the model can be rapidly verified. The model passed all tests to within 1%.

For validation purposes, the model was compared with data from the CFM56-5B3 engine, for sea-level static conditions. The model predicted a sea-level thrust of 143.4 kN, whilst the actual engine is rated at 142.3 kN of thrust. Since the engine model requires detailed input that is not publicly available for most engines, only one engine can be used for validation purposes. However, since the results are so similar, the model is assumed valid.

For the engine mass model, verification was performed by a syntax check, as well as a simple check against hand calculations, since the model is so simple. For validation purposes, the mass of a number of reference engines was computed using the engine mass model, and subsequently compared to

the actual engine mass. In case the engine mass flow was not given, it was calculated using the fan diameter, assuming air enters into the engine at mach 0.45.

The results of this comparison can be seen in Table 6.7. As can be seen in the table, the maximum error is 34.4 % for the LEAP-1A. This can be attributed to the weight saving measures employed in the design of the LEAP-1A.

The largest negative difference can be observed for the RB211-535. This is to be expected, since the first model of this engine entered into service in 1972 on the Lockheed L-1011 tristar. From this one can conclude that the model will slightly underpredict the mass of older engines, whilst slightly overpredicting for newer engines. Therefore, care should be taken when using this model for ultra high bypass ratio's, and in case the engine mass becomes unrealistically high, the results from the model should be discarded.

Table 6.7: Comparison of real world data with engine mass model.

Engine model	OPR	Bypass ratio	Mass flow [kg/s]	Fan diameter [m]	Dry weight [kg]	Calculated weight [kg]	Difference [kg]	Relative difference [%]
CFM-56-7B22	32.7	5.3	355	1.55	2370	2043	-327	-13.8
CFM-56-5B3	35.5	5.4	439	1.73	2380	2577	197	8.3
GE90-76B	40	8.4-9	1426	3.1	7893	8626	733	9.3
LEAP-1A	50	11	582	1.98	2990	4019	1029	34.4
TRENT 1000	50	10	1206	2.85	6120	7685	1565	25.6
PW4000-94	27.5-32.3	5	848	2.39	4273	4985	712	16.7
PW4000-112	34.2-42.8	5.8-6.4	1197	2.84	7375	7322	-53	-0.72
PW2000	27.6-31.2	6	680	2.14	3221	3933	712	22.1
RB211-535	25	4.4	525	1.88	3705	2904	-801	-21.6

Regarding the electric taxiing simulations, verification was performed by comparing the output of the model with the results of the reference article [33]. Due to having a much simpler model than the original authors, both the taxi in and taxi-out simulations' total energy usage was lower than the reference data. The simpler model used here was, on average, off by about 10%. For that reason, a factor of 1.1 was applied to the total energy usage.

6.7. Recommendations

In this section, recommendations for further work into designing the propulsion system of the Zephyr One are presented.

First, a new prediction model for engine mass should be determined, in order to get more accurate results for ultra high bypass ratio's, as well as account for future development in engine mass reduction.

It is advised to move on into the detailed design of the propulsion system. Whilst optimal compression ratio's, and work required from the turbines have been determined, the detailed design of the compressors and turbines remains unknown. It is therefore recommended to start the aerodynamic design of rotor and stator blades, using CFD for detailed design.

Furthermore, detailed design of mechanical components, as well as the combustion chamber still has to be performed. Furthermore, structural analysis on all detailed parts of the propulsion system will have to be performed.

In a later stage, ground testing on the power plant will have to be performed, before integration into an existing airframe for airborne testing. Later on it can be fully integrated into a full prototype of the Zephyr One for flight testing.

7 Structural Design and Materials

This chapter is dedicated to the structural design and analysis of the aircraft, which presents different challenges compared to conventional aircraft. While a regular aircraft encounters problems due to aerodynamic loading, the Flying-V does not, as the main structure, which is the heaviest, is also the lift generating surface. However, for this particular aircraft design, the cabin pressurization is the main load inducer due to the elliptical shape of the cabin, as in this case the cabin pressurization entails a bending stress in addition to tension. The structural design is optimised for the lowest aircraft weight, while maintaining its integrity for the most critical loads. In Section 7.1 the functional analysis, requirements, structural idealization and assumptions are presented, which enable the computation of the loads as presented in Section 7.2 and Section 7.3. Subsequently, a trade-off between metals and composites is conducted in Section 7.4, which enable detailed structural design described in Section 7.5. Before presenting the final design in Section 7.7, the verification and validation of the used codes and methods is performed in Section 7.6. Lastly, a fatigue analysis is conducted in Section 7.8 and the chapter ends with a series of recommendations described in Section 7.9.

7.1. Functional Analysis and Assumptions

The main load-carrying structure is represented by the cabin, which is designed as a torsion box, fulfilling various functions: provide structural integrity by possessing capabilities of safely carrying the critical loads, carry payload (passengers and cargo) safely (including adequate pressure provisions), provide support for the other subsystems, and allow for maintenance. Based on these functions, a list of requirements can be generated, as presented in Table 7.1.

Table 7.1: Aircraft Requirements for Structural Design.

EFMRA-SYS-SF-04.1	A safety factor of 1.5 shall be applied for prescribed limit loads.
EFMRA-SYS-SF-04.2	The aircraft shall not yield under a maximum load factor of 2.5.
EFMRA-SYS-SF-04.3	The aircraft shall not yield under a maximum load factor of -1.
EFMRA-SYS-SF-06.2	The aircraft shall be capable of maintaining a cabin pressure altitude of at most 2438 m
EFMRA-SYS-STRUCT-01	The aircraft shall not buckle under critical loading.
EFMRA-SYS-STRUCT-02	The aircraft shall not flutter.
EFMRA-SYS-STRUCT-03	The aircraft shall allow maintenance.
EFMRA-SYS-FP-01	The aircraft shall be at least 75% recyclable.

Considering that at this stage of the project a preliminary design is the point of concern, a series of assumptions is set at the beginning of the analysis in order to ease the calculations, as enumerated below:

- The cross section is modeled as a perfect ellipse, symmetrical around the horizontal and vertical axis. The major axis is equal to summation of the cabin width and two times the distance from the first seat to the leading edge, and the semi-minor axis is represented by the maximum distance from the major axis to the airfoil, which is found to be the distance to the upper skin of the airfoil. This is not the reality as the airfoil is not symmetrical, but is a reliable approximation.
- Thin wall assumptions apply during the structural analysis, as the thickness of the skin and stiffeners is undoubtedly much smaller than the other aircraft dimensions (e.g width, length).
- The stringers are modeled as boom areas, evenly distributed along the shape, considering that they only carry bending stress.

- The contribution of the stringers to the center of gravity is neglected, as they are attached to the skin and have small dimensions compared with the rest of the structure.
- Due to the thin wall assumptions, the stringers only contribute with the Steiner terms to the moment of inertia (MOI).
- The shear is carried solely by the skin and spars, as the skin is the main structure responsible for the transmission the shear loads.
- A constant skin thickness is assumed, as variations in thickness lead to stress concentrations, and can only be accurately modeled by a FEM (Finite Element Method) analysis.
- Bending due to pressurization loads is assumed around the vertical symmetry axis [36], and bending due to aerodynamic loads is assumed around the horizontal symmetry axis of the ellipse.
- Location of the center of gravity (cg) is assumed to be fixed. Even though the location of the center of gravity slightly changes locally due to the mass distribution, for the preliminary structural analysis of the aircraft the location of the center of gravity is considered constant through the section. This is a valid simplification, as most of the weight is concentrated in the cylindrical section due to the big share of the OEW, presence of the fuel tanks, cargo, and most of the passengers.
- The aerodynamic loading acts at the quarter chord length of the airfoil
- Weight is assumed to be distributed uniformly, with different magnitudes, depending on the payload and OEW distribution
- Only one material is used for the main structure, in order to avoid stress concentrations.

As there are two major loading cases, the structural analysis is split in two: loads induced by the pressurisation of the cabin, and aerodynamic loads. Note that the cargo hold is also pressurized, resembling the conditions of any other airliner.

7.2. Pressure Loads

A circular fuselage only experiences tensile stress in the membrane, as the pressure vector is aligned with the radius vector, both perpendicular to wall. However, in the case of an elliptical shape, the fuselage has the tendency of reaching the equilibrium point by changing the shape to a circular one, generating shear and bending loads due to pressurization in addition to tensile loads. Thus, this section analyses the loads induced by the cabin pressurisation.

The first step is represented by the computation of the pressure difference between the cabin and the air at the cruising altitude. According to regulations [2], the pressure in the cabin is assumed to be the International Standard Atmoshphere (ISA) pressure corresponding to 8,000 ft (2,438 m), which is the maximum altitude that ensures a comfortable air pressure for passengers, but also allows for slight load alleviation. The maximum cruising altitude is 13,000 m, thus the pressure difference is given by Equation 7.1. Because the cabin carries the passengers and cargo, it is an extremely sensitive and important structural element. Hence, a load factor of 1.5 is applied, as prescribed by regulations and stated by **EFMRA-SYS-SF-04.1**. This means that the pressure difference is multiplied by 1.5.

$$\Delta p = n(p_{2438} - p_{13000}) = 1.5(70104 - 22625.8) = 47478Pa \tag{7.1}$$

As the shape is symmetric in two directions, the calculations only have to be performed for a quarter of the shape. It is known that pressure vector always acts perpendicular to the surface. However, in an elliptical shape, the radius vector acts at a different angle than the pressure vector, as depicted in Figure 7.1. As the two vectors are not aligned anymore, other loads than tension develop in the skin. Thus, the pressure angle must be expressed as a function of the radius angle , which allows the integration required to find the induced forces. Knowing the polar form of the ellipse radius, as

expressed in Equation 7.3, and the tangent equation, as given by Equation 7.2(x_1 and y_1 represent known coordinates, chosen conveniently), a relation between angles θ and ϕ is obtained as stated in Equation 7.4. The surface of the ellipse is discretised in many nodes, where the pressure vector is decomposed in vertical and horizontal components. This enables the computation of the vertical and horizontal components of the resulting force through numerical integration, as presented in Equation 7.5 and Equation 7.6.

$$\frac{x_1}{a^2}x + \frac{y_1}{b^2}y = 1 \tag{7.2}$$

In order to obtain the force components at each node, firstly the boundary force at the horizontal extremity of the ellipse is computed by integrating Equation 7.5 on the interval (0, $\pi/2$), yielding the magnitude of the vertical boundary force. As at this point the pressure vector is aligned with the radius vector, the boundary force in the horizontal direction is zero. At each node the integration is performed between two consecutive nodes (expressed as angles) for both components and the value of the integral is added to value obtained at the previous node. Thus, the force values at each node represent the cumulative sum of the integrals beginning from the boundary. After the vertical and horizontal force components have been obtained at each node, the magnitude and orientation of the local resultant is computed. Subsequently, the resultant force is decomposed on perpendicular and tangent components to the surface. The tangent force to the surface gives the normal tension stress in the shell, and the perpendicular component is responsible for the bending.

$$r(\phi) = \frac{b}{\sqrt{1 - e^2 \cdot cos^2(\phi)}} \tag{7.3}$$

$$\theta = \frac{\pi}{2} - arctan\left(\frac{tan(\phi)}{\frac{a^2}{cos^2(\phi)r^2} - 1}\right) \tag{7.4}$$

$$F_y = \int_i^{i+1} n\Delta p \cdot sin(\theta) \cdot r(\phi) d\phi = n\Delta p \int_0^{\pi/2} cos(arctan(\frac{tan(\phi)}{\frac{a^2}{cos^2(\phi)r^2} - 1})) \cdot \frac{b}{\sqrt{1 - e^2 \cdot cos^2(\phi)}} d\phi \tag{7.5}$$

$$F_x = \int_i^{i+1} n\Delta p \cdot cos(\theta) \cdot r(\phi) d\phi = n\Delta p \int_0^{\pi/2} sin(arctan(\frac{tan(\phi)}{\frac{a^2}{cos^2(\phi)r^2} - 1})) \cdot \frac{b}{\sqrt{1 - e^2 \cdot cos^2(\phi)}} d\phi \tag{7.6}$$

The normal tension stress is obtained by dividing the tangent force by the thickness, as indicated in Equation 7.7. However, the computation of the bending stress is not straight forward, as the location of the neutral axis is unknown. Usually, a FEM model yields an accurate bending stress distribution. However, during the structural design, the maximum stress is the point of concern, as eventually the structure must be designed to withstand the most critical loads.

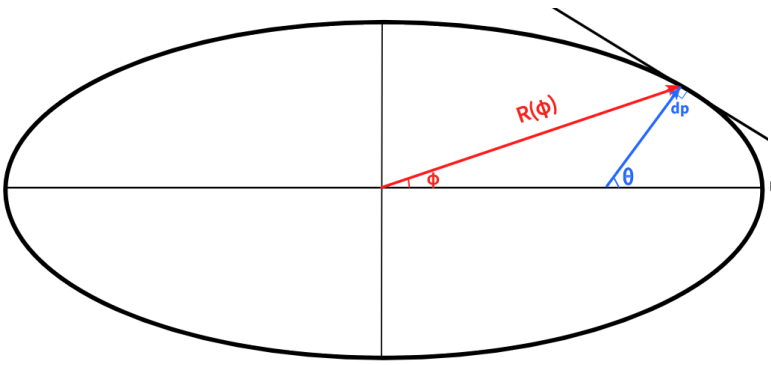

Figure 7.1: Pressure and Radius vector in an Ellipse.

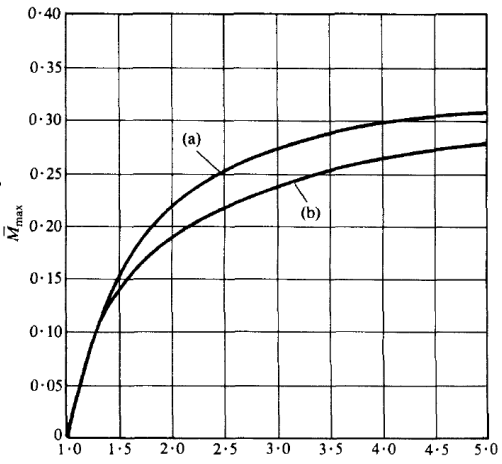

Figure 7.2: Normalised bending vs ellipse aspect ratio [36].

Through literature research, an analytical expression for the maximum bending stress in a pressurized ellipse is identified, as given by Equation 7.8. The maximum bending stress occurs at the most extreme points on the ellipse, which are the ends of the major axis [36]. Figure 7.2 givens the value of the maximum normalised bending stress as a function of the aspect ratio of the ellipse, which is the ratio between the major and minor axis. Curve (a) corresponds to the elliptical shape and is the plot of interest in the current analysis, while curve (b) corresponds to the a curved shape that is able to minimise the bending stress in the structure for a given aspect ratio. As curve (b) corresponds to a mathematical concept that does not suite the shape of the airfoil, it is not further investigated. The maximum bending moment occurs at the locations of the ends of the major axis and is given by Equation 7.8. It is important to note that the bending moment is highly influenced by the aspect ratio of the cabin and the length of the fuselage. In the current case, the aspect ratio of the cabin is 2.4, entailing a maximum normalised bending moment of 0.24 [36]. Hence, the maximum bending stress can be obtained through Equation 7.10, assuming the maximum distance from the neutral axis can not supersede the major axis. The total maximum stress is represented by the sum of the maximum tension stress and maximum bending stress. The moment of inertia of a thin walled ellipse [37] and the Steiner terms of the stringers determine the moment of inertia as given in Equation 7.9. The shape idealization entails a conservative approach for bending moment calculations, as the utilized MOI is smaller than the real one.

$$\sigma = \frac{F_y}{t} \tag{7.7}$$

$$M_{max} = \bar{M_{max}} \cdot n \cdot dp \cdot a^2 \cdot l_{fuselage} \tag{7.8}$$

$$I_{xx} = \frac{\pi}{4} a^3 t (1 + 3\frac{b}{a}) + \sum_{1}^{n} A dy^2 \tag{7.9}$$

$$\sigma_{max} = \frac{M_{max} a}{I_{xx}} \tag{7.10}$$

$$\sigma_{total} = \sigma_y + \sigma_{bend,max} \tag{7.11}$$

Through this approach it is desired to investigate whether the cabin design is feasible without vertical separating walls (which would take the role of spars), as this would create discomfort for passengers. Furthermore, the shear flow distribution, normal tension in the shell and maximum bending stress without contribution of stiffening walls due to pressurisation are obtained. From preliminary calculations it can be deduced that the bending due to cabin pressurisation is the dominant load, as just the bending moment takes the values of 3.57 MNm.

7.3. Aerodynamic Loads

Due to symmetry, only one half of the wing is analysed, as the loads and deflections would be the same in the other half. Because at the symmetry line where the two halves are joined the aircraft is restricted from moving, each half of the wing can be modeled as a clamped beam.

The aircraft may be subjected to different magnitudes of the aerodynamic load and weight, depending on the flight phase. However, the aircraft must be able to withstand the most critical load cases. Thus, the aircraft is designed for the maximum possible loading that can occur. This means that a case where the maximum load occurs is analysed, multiplying the lift by the maximum load factor, which is 2.5, as indicated by regulations. Because of symmetrical stringer distribution, if the 2.5 requirement is met, so is the -1, because the magnitude of compression decreases, only the location where it occurs changes. But since even distribution of the stringers accounts for all areas, the -1 is not a concern. The 2.5 load factor is not achieved during take-off and initial climbing manoeuvres. Thus, only 90% of the MTOW is considered, accounting for the fuel consumption [13].

For weight considerations, the wing planform is divided in four regions, each having a different magnitude for the distribution of the weight. Firstly, the engine weights is subtracted from the total OEW, because they are considered point loads. The inboard wing has three components, and the outboard wing is considered a separate component. Each component is assigned an OEW proportional to the

surface area of the region, as given by Equation 7.12.

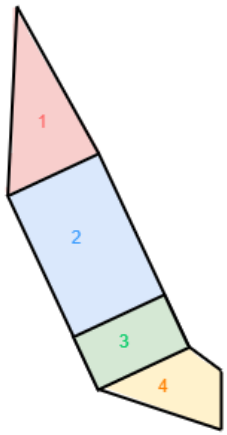

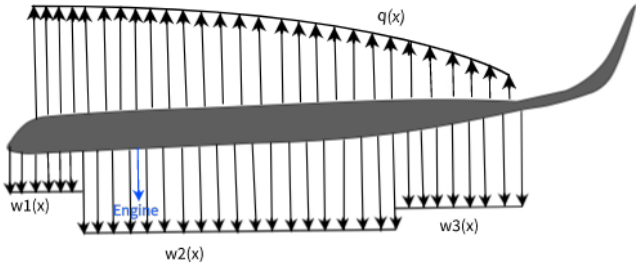

Figure 7.4: Inboard free-body diagram.

Figure 7.3: Regions considered for the free-body diagram.

Region one corresponds to the front of the aircraft, which is from the cockpit to the rectangular region. The weight for this region is the sum of the OEW for this part and the weight of 6 passengers and their cabin luggage. The uniform load is expressed in Equation 7.13. Region number two begins where the rectangular region begins, which also corresponds to the location where the fuel tanks begin, and ends at the point where the cargo hold begins. This region includes the weight of 96 passengers with cabin luggage and the weight of the fuel tanks. The length of the fuel tanks is slightly larger than the cabin, but the difference is very small (0.3m) and it can be considered that the fuel tanks contribute with their entire weight in the second region. In this region the weight of an engine is introduced as a point load. The uniform load is expressed in Equation 7.14. The third region corresponds to the cargo hold, marking the end of the inboard wing. It contains the OWE assigned for this region and the weight of the cargo hold. The uniform load is expressed in Equation 7.15.

$$OEW_{region} = \frac{S_{region}}{2 \cdot S_{total}} \cdot \frac{OEW_{total} - W_{engine - W_{tanks}}}{2} \tag{7.12}$$

$$W_{region1} = OEW_{region1} + 6 \cdot 88 \cdot 9.81 = 38.8kN \rightarrow w(x) = 6.5kN/m \tag{7.13}$$

$$W_{region2} = OEW_{region2} + 96 \cdot 88 \cdot 9.81 + 0.5(W_{fuel} + W_{tanks}) = 189.2 \rightarrow w(x) = 14.55kN/m \tag{7.14}$$

$$W_{region3} = OEW_{region3} + W_{cargo} = 45.65kN \rightarrow w(x) = 10.14kN/m \tag{7.15}$$

Since the outboard wing is tapered, the weight is considered to decrease linearly. The free-body diagram is depicted in Figure 7.4.

The aerodynamic loading has an elliptic distribution, given by Equation 7.16, expressed in kN. The free-body diagram for the inboard wing is depicted in Figure 7.4, which enables the computation of the shear force distribution. As the structure is symmetrical, the shear center is located at the intersection of the symmetry axis, which is the ellipse origin. The lift obtained from the aerodynamic analysis is transformed for the corresponding angle of attack.

$$q(x) = \sqrt{42.58^2(1 - \frac{x^2}{26^2})} \quad (7.16) \qquad q = \frac{T}{2A_m} \quad (7.17)$$

The shear center is located at the intersection of symmetry axis, which is also the location of center of gravity. Since the weight acts at the center of gravity and the aerodynamic loading acts at a quarter chord, the only contributor to the torque is the lift. The shear flow induced by torque can be approximated utilising Equation 7.17.

7.4. Materials

Before selecting the specific material for the main structure, a preliminary trade-off between aluminium alloys and composites must be conducted, as these two materials have very different behaviour under different types of loads, but both are still capable of providing high stiffness. Moreover, the aluminium alloys have similar properties among themselves and can be generalised [2].

7.4.1. Aluminium VS Composite Trade-off

There are four main considerations when it comes to the current material trade-off: recyclability, structural integrity fatigue and costs. Each criterion will be further compared for the two materials.

Recyclability Considerations

EFMRA-SYS-FP-01 states that the aircraft should be at least 75% recyclable, and as a consequence, it is the main driver in material selection. While aluminium alloys are relatively fully recyclable, carbon laminates are not fully recyclable, because the theromset resin can not be recycled due to cross-linking, which is an irreversible process. In carbon laminates, only the fibers can be recycled by evaporating the resin. A common fiber volume is 60%, meaning that maximum 60% of the carbon laminate is recyclable. However, not 100% of the fibers can be recycled, as there might exist small portions of delaminations or damaged fibers. Broken fibers tend to remain impregnated in the resin, and flaws might be discovered, as the resin is evaporated. The interiors of the aircraft also can not be fully recycled, due to use of thermosets or wear. Titanium, which is fully recyclable, is used in engine pylons and as a reinforcement material for both aluminium and carbon composites, but the percentage differs. Aluminium usages requires 7% titanium, but composites require more, about 15% (weight-wise) [38]. Even though it is not impossible to make a composite aircraft 75% recyclable, this number is much harder to achieve, and a preliminary assessment based on the information mentioned above shows that only 66% of the aircraft can be recycled. Given the fact that preliminary analysis shows that aluminium can better fulfill the recyclability requirements, metals are preferred over composites for recyclability purposes.

Structural Considerations

During the designing process, the strength of a material is considered to be the maximum stress, above which the material is not able to carry loads properly anymore. In the case of metals, this is represented the yield strength, as plastic deformations drastically affect the load carrying capabilities. Composites are brittle materials, that do not exhibit plastic behaviour, only linear elastic. This aspect makes them very notch sensitive, as there is no possibility to reduce the peak stress, as there is for metals, through the formation of the plastic zone. Thus, this effect is incorporated by using only 30% of the ultimate strength of the composite as the design limit, which is an industry standard, and the reasons is represented by the fact that circular holes locally increase the stress by a factor of 3. In order to be able to use composites in the aircraft design, quasi carbon laminates must be utilized, as they provide the same mechanical properties in all directions. It must have at least 4 layers of composite, with fibers generally oriented 0,90,+45 and -45 deg. In composites damage forms due to cyclic compression, shear ,and bending, and in metals damage forms due to cyclic tension [39]. As seen from the previous preliminary calculations, bending is the most critical loading in the aircraft. Considering the 70% drop in design strength in composites due to brittle behaviour and their sensitivity

to damage due to cyclic bending, which is the main load in the structure, aluminium alloys are preferred over composites in structural performance.

Fatigue Considerations

When considering fatigue, three aspects are investigated: S-N curves (which depict number of loading cycles until failure vs. load amplitude), damage tolerance (resistance to crack propagation), and corrosion. The S-N curves are highly influenced by the notch factor, as the tolerable load amplitudes decrease for a given number of cycles for both materials. However, the curve drops more for composites than for metals [39]. Despite this fact, even with the notch effect, carbon composites seem to have slightly higher S-N curves than aluminium [40, 41]. Generally, the fracture toughness (which is the parameter utilised to compare the crack propagation performance) is smaller for composites than for aluminium alloys. However, if the fibers break, they have the tendency to remain stuck in the resin, preventing delaminations or further crack propagation [39]. The first considerations make aluminium alloys and composites perform equally good, but what differentiates the two is the fact that composites are corrosion resistant[1]. Even though aluminium alloys perform well in fatigue, the fact that composites do not corrode makes them be preferred over metals.

Cost Considerations

The cost assessment is a very broad and complex process. The production cost of the composite aircraft is higher than for aluminum as carbon composites are more expensive[2] [3], but cost is also influenced by weight, because lighter aircraft can increase their range and payload capacities. While the use of composites entails more use of titanium, the final structure can still be lighter[4]. However, real cost assessment is heavily dependent on undisclosed information from the manufacturers (such as material discount) or detailed FEM analysis (to determine the amount of reinforcement). At a first glance the composites seem to outperform aluminium due to the reduced weight.

Conclusions

Because the trade-off is conducted only for two types of materials, for each criteria it is considered that there is only one winning material. Thus, a score of 1 is awarded to the chosen material, and a score of 0 is awarded to the material that is disregarded, based on the brief analysis performed above. Because recyclability is one of the mission objectives, it is considered the most important criteria. Secondly important are the structural considerations, as the integrity of the aircraft is a top priority in the designing process. Real cost assessment is heavily dependent on undisclosed information from the manufacturers (such as material discount) or detailed FEM analysis (to determine the amount of reinforcement). At a first glance the composites seem to outperform aluminium on the long run, but the amount of unknowns raises many uncertainties, and for this reason the cost is considered the least important criteria. As fatigue considerations are only differentiated by corrosion, it is considered the third most important criteria. The trade-off process is summarised in Table 7.2, the final result indicating the fact that the material that will be used for the main structure is represented by aluminium.

Table 7.2: Material trade-off.

Property	Aluminium	Composites	Weight
Recyclability	1	0	0.4
Structural	1	0	0.3
Fatigue	0	1	0.2
Cost	0	1	0.1
Total	**0.7**	**0.3**	**1**

[1] http://compositeslab.com/benefits-of-composites/corrosion-resistance/ [cited 21 June 2021]
[2] https://nl.rs-online.com/web/ [cited 21 June 2021]
[3] https://www.onlinemetals.com/en/buy/aluminum-sheet-plate-7075-t6-t651 [cited 21 June 2021]
[4] https://www.airbus.com/aircraft/passenger-aircraft/a350xwb-family.html [cited 21 June 2021]

As the material that will be used for the main structure is represented by aluminium, a specific alloy has to be chosen. Analysing the alloys presented in the previous report [2], the choice of the alloy is not very difficult, since the chosen one should have relatively high stiffness, yield strength and fracture toughness. The alloy that best fulfills these aspects is AL 7075 T6, especially due the higher fracture toughness (the yield stress and E-modulus do not vary considerably from the other alloys). Even though the primary structure is made out of aluminium, the use of carbon composites is not totally disregarded. Secondary structures, such as elevons, can still make use of the weight saving capabilities and will be manufactured out of quasi-isotropic carbon. The engine pylons will be made out of titanium, in order to withstand the high point loads induced by the weight of engines. Table 7.3 summarizes the properties of considered materials, and data was collected from material databases such as Knovel[5] Matmach[6], which can be used simultaneously to confirm the mechanical properties of the material. Different maintenance methods apply for different materials, and are further explained in Section 13.3.3.

Table 7.3: Metals Mechanical Properties.

Material	**E [GPa]**	**Yield [MPa]**	**G [GPa]**	**K_{1c} [MPa $m^{1/2}$]**	**ρ [g/cm^3]**
Al 7075 T6	71.7	470	26.9	27.5 [42]	2.7
Ti 6Al 4V	110	880	40	-	4.43
Quasi-isotropic carbon[7]	70	570	30	15	1.6

7.4.2. Sustainability of Materials [2]

A sustainable design strategy implies sustainable considerations from incipient stages of aircraft existence, which is the manufacturing phase, extending to the entire operational life and retirement stage. The choice of materials is the main factor that has a direct impact on the manufacturing methods, durability of the aircraft and recycling capabilities.

Current studies focus on determining mechanical properties of recycled fibres. Even though they provide lower mechanical strength than virgin carbon fibres, they also present lower weight and could be used in the aircraft interiors, such as the arm-rests [43]. In order to encourage the use of recycled materials, the properties of rCF must be researched in order to decide whether they can be used in the aviation industry or not. Furthermore, the identification of other markets where rCF would be relevant is going should be searched, as ensuring the existence of a viable market that can successfully utilise rCF would make the use of carbon fibres sustainable. Active use of recycled materials must be encouraged.

Organic composites are gaining more and more popularity, as they pollute less during the manufacturing process and are bio-degradable. Currently, in the aviation industry, synthetic fibres are used for composite manufacturing, which generate CO_2 emissions during manufacturing. They could be substituted by natural fibres extracted from water algae or basalt, which do not undertake the carbonisation process. Additionally, bio-resins could be used as the matrix base. Bio-composites could be utilised for the cabin, cargo holds and structural components. Advantages of using bio-composites are lower weight than synthetic composites, biodegradability and availability. On the other hand, there are some major drawbacks that require further research on bio-composites: they absorb moisture, leading to lower mechanical performance, delamination, there is a variety in properties depending on the soil they grew in, and they present flammability issues [44], as big quantities of smoke are generated in case of a fire.

Nowadays, between 80% and 90% of the aircraft can be recycled[8]. Parts made out of aluminium are reused in electronics; seats, flaps and control surfaces are investigated, repaired and then sold on

[5] `https://app.knovel.com/kn` [cited 21 June 2021]

[6] `https://matmatch.com/` [cited 21 June 2021]

[8] `https://airlines.iata.org/analysis/aircraft-recycling-the-life-and-times-of-an-aircraft` [cited 19 May 2021]

the second-hand market [9]. But eventually, all components reach a point where the product can not be used anymore and it can either be recycled, or is left in a landfill. Hence, it is the responsibility of the aircraft designer to ensure that most of the aircraft components can be eventually recycled. Another difficulty when recycling is represented by combinations of different materials arranged in layers, as it is difficult to separate. Metal alloys can easily be melted and reused for instance in electronics, the most challenging materials to recycle being composites. As the main structure is made out of aluminium, it is expected that for least 80% of the design to be recyclable, as composites are only used for elevons and interiors.

7.5. Effect of Stiffeners

By implementing the pressure difference and the cabin dimensions in Equation 7.11, it resulted that the cabin design is not structurally feasible without vertical and horizontal stiffeners, as it would require very thick stringers and a skin thickness of 8 mm in order for the structure to be able to withstand the high bending load due pressure. While the floor and ceiling might take the role of the horizontal stiffeners, the high loads induced by bending also require the presence of vertical stiffeners, which could be represented by separating walls, that could have holes and cut outs in order to reduce weight. However, with the introduction of the stiffeners, the bending moment and stress calculations change and are not straightforward, requiring FEM models in order to obtain the stress distribution and required thickness. Hence, in order to obtain a realistic value for the thickness of the structure, the method presented in Schmidt's paper [45] is adopted and performed, as this approach takes into consideration the presence of the stiffeners. In this approach, the ellipse is modeled as two circle arcs, as depicted in Figure 7.7.

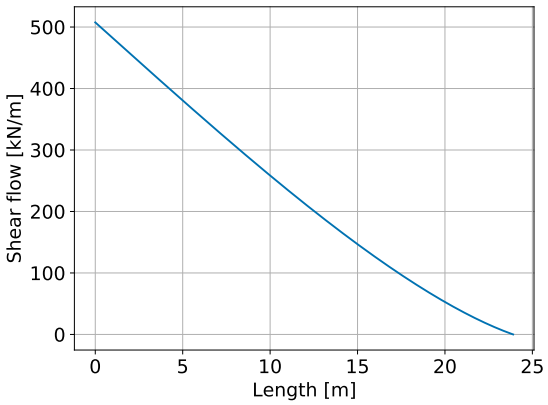

Figure 7.5: Torque distribution.

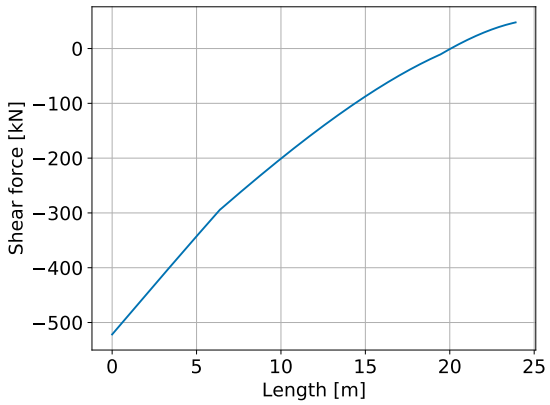

Figure 7.6: Shear force distribution.

The shear force distribution due to aerodynamic loading has also been performed, results for the inner wing being depicted in Figure 7.6. Slight changes in slope are in two locations due to the change in value of the weight distribution (at the transition between regions). As the internal forces are lower than in regular aircraft due to a more even distribution of the weight and lift where they tend to cancel out, their contribution to the total stress considered for designing is neglected in further calculations. This assumption will be checked for the final design. Low shear forces would also generate low shear flow (compared with the one due pressurization), and the torsion would give small values as well. Figure 7.5 depicts the torque distribution, as an indicator for the expectation of low shear flows. Furthermore, the contribution of vertical spars to shear flow alleviation is not accounted mathematically, reinforcing the reasoning for neglecting of shear flow due to aerodynamic loading.

Since the vertical coordinate of the vertical stiffeners' centroid is on the symmetry axis, the Steiner

[9] `https://www.airbus.com/company/sustainability/environment/product-responsibility.html` [cited 30 April 2021]

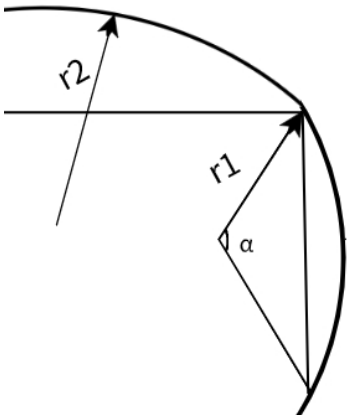

Figure 7.7: Cabin idealization as two circle arcs.

terms becomes zero. However, high loads are expected to develop in the upper and lower skin, because in this regions the radius of the considered arc is the largest. The larger the radius, the worse for the load carrying capacities due to pressure (a flat plate has an infinite radius, which performs very badly for pressure loads). Thus, the presence of the vertical stiffeners (represented by walls) is very vital to keep the ellipsoidal shape, as it is the main carrier of the shear loads. The horizontal stiffeners (floor and ceiling) are assumed to contribute with 0.08 m^2 to the MOI, assuming a preliminary thickness of 1 cm in order to avoid big stress concentrations.

Equation 7.19 gives an expression for normal stress due to pressurization that takes into consideration the contribution of the vertical walls, through the radii of the two arcs and the position of the walls [45]. The value of the radii is measured geometrically, and the value of α is computed with the cosine rule, thus, for the current design, r_2 equals 1.45, and r_1 1.3, yielding a value of 0.95 for α and a value close to 1 for $cos\beta$, as the walls are placed almost vertically in the current design. Equation 7.20 gives the maximum bending moment in the cross-section as a result of a differential equation explained in Schmidt's paper [45], making use of differential parameters given by Equation 7.21 and Equation 7.22. The maximum bending moment is dependent on the maximum shear flow obtained with Equation 7.5, and the calculations are conservative because the maximum shear flow is obtained without accounting for the presence of stringers. Note that this approach also demonstrates the stress dependency on the length of the fuselage through the parameter L.

$$\sigma = \frac{N}{2t_{skin}} + \frac{Ma}{I_{xx}} \tag{7.18}$$

$$N = \Delta p(r_2 - r_1)\frac{sin(\alpha)}{cos(\beta)} \tag{7.19}$$

$$M_{max} = N(\delta + e) + \frac{qL^2}{2} - \frac{qL}{2} \tag{7.20}$$

$$\lambda = \sqrt{\frac{N}{EI}} \tag{7.21}$$

$$\delta = \frac{q}{EI\lambda^4}\left(sec\frac{\lambda}{2} - 1\right) - \frac{qL^2}{8EI\lambda} \tag{7.22}$$

Another structural load which must be accounted for is represented by buckling. Buckling is a phenomenon that occurs only when the structure is loaded in compression, and is expressed by Equation 7.23. The critical load is given by the maximum compression stress that occurs in the skin. Note that this equation is defined for a thin plate loaded in pure, normal compression. This equation is highly dependent on the buckling coefficient, k, which is defined by the type of support the stiffening structures provide. In the current case, the stringers are considered to provide simple support, entailing a value of 4 for k [46].

$$\sigma_{cr} = \frac{k\pi^2 E}{12(1-\nu^2)}\left(\frac{t_{skin}}{b_{stringers}}\right)^2 \tag{7.23}$$

Because the force and pressure vectors align at the minor and major axis, it is known that at those location the ellipse is loaded in tension, and compression can only occur between the two regions. The compression load is reduced furthermore because of the normal stress developing in the skin due to pressurization. The magnitude of the compression load is also smaller than the tension, because the extreme points, which correspond to the highest ellipse radius, are loaded in tension. With all of these factors in mind, the location of the maximum compression is expected to occur between the extremities of the ellipse, and the distance from the neutral axis is substituted with the radius corresponding to an angle of $45°$ (1.42) in Equation 7.20. Thus, the maximum compression stress can be found, which becomes the critical stress for buckling. Note that this value is not constant through the skin, but it is an approximation for the highest compression load that can occur, making the undertaken approach, again, conservative. For a given thickness, by rearranging the terms of Equation 7.23, the stringer pitch b can be obtained, which will give the number of stringers.

The buckling factor could be increased, if separating walls would be used in the cabin, taking the role of ribs. However, the aspect ratio of each section should be smaller than one in order to significantly increase the buckling factor, requiring separating walls every 2.3 m, which in return would add weight and make the passengers feel uncomfortable. Thus, a factor of 4 is used without requiring any additional separating walls and further attempts to increase the bucking factor are disregarded.

7.6. Verification and Validation

Verification is performed in order to ensure the correct implementation of the analytical and numerical formulas. One way to verify that the code is set up correctly is to check the value for the horizontal boundary force through another method. If the code is implemented correctly, the integration on the interval (0, $\pi/2$) for the horizontal force should yield the same result as the cumulative sum of the integrals performed between each two nodes. The first integral is 82,029.703 N/m, and the second one is 82,029.702 N/m. The difference between the two is 0.001, which gives a relative error of 1.28 $\cdot 10^{-6}$%. To achieve this accuracy, 15,708 nodes were utilised. For the calculations of moment of inertia, since the stringers are placed evenly, this results in a symmetric structure, if an even number is used. Thus, the Steiner term for all stringers should equal the doubled Steiner term for only half of stringers. For 100 stringers with area 0.05 m^2, the MOI equals 5.49287411 m^4, and the double of the MOI using 50 stringers of the same area is 5.49287410 m^4. All computational results for analytical formulas that have been provided through out this chapter have been double checked by hand calculations, and the relative error is within 1%.

After ensuring that the analytical and numerical models were correctly implemented in the code, validation of the utilised methods can be performed. As there is no Flying-V built to scale, the validation solely relies on comparison with results and methods presented in other papers. However, the resources are very scarce. Schmidt's paper [45] studies the stress distribution in an oval fuselage, which is the most resembling analysis to the elliptical fuselage, and Osterom's paper [16] presents values for shear forces. For the same cabin inputs, stresses are compared. Slightly higher errors than the ones encountered during verification occur in the case of validation, but this was expected since the number of stringers is not reported in the master thesis, and values are read from plots. In the current model the number and dimension of the stiffening elements have been set in order to comply with structural integrity requirements. Further validation is recommended as more data becomes available.

Table 7.4: Validation structural stress.

Property	Zephyr One	Data	Relative error
Maximum stress [MPa]	178	169	5.3%
Shear [kN]	170	160	6.25%

7.7. Final Structural Design

Three main variables dictate the structural design for a given altitude, as these parameters have a direct impact on both yield and buckling loads: stringer area, number of stringers (and implicitly the stringer pitch), and the skin thickness. Cabin dimensions and stiffening wall locations are limited by the cabin sizing and do not represent variables in the current designing set-up. The objective of the structural design is to minimise the final weight. In order to get the optimal combination of skin thickness, number and cross-sectional area of stringers, the weight index, represented by the summation of skin volume and stringer volume, is computed for different combinations, as given by Equation 7.24. The combination that yields the minimum weight index is the final one. Combinations are limited by strength and buckling considerations. While computing the weight index, it has been observed that thickness is the main contributor to the weight, thus a thin skin is desired. However, reducing the skin also reduces the MOI, which has to be compensated with a higher number of stringers, which in exchange increases the weight. For a given thickness, the number of stringers is fixed due to buckling constraints. As the number of stringers becomes fixed, their surface area is determined by the failure stress calculation (due to their contribution to MOI). Figure 7.8 depicts the shear flow distribution in the skin due to pressurization, identifying the maximum shear flow as 75,525.33 N/m at the location where the resultant force is oriented in the same direction as the radius vector. The optimal values for the structural design are summarised in Table 7.5.

$$W_{index} = 2\pi\sqrt{\frac{a^2+b^2}{2}} \cdot l \cdot t_{skin} + n_{stringer} S_{stringer} \cdot l = 295.5 \cdot 4t_{skin} + 0.001434 \cdot n_{stringer} \tag{7.24}$$

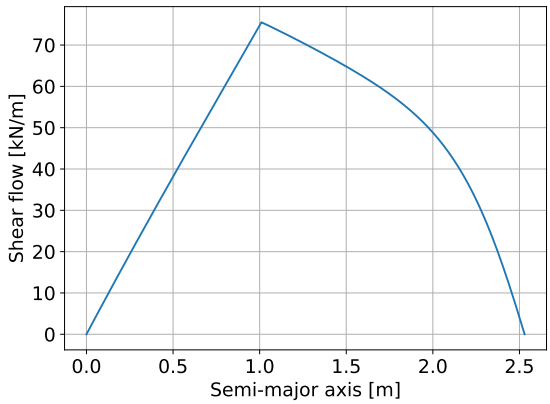

Figure 7.8: Shear flow distribution.

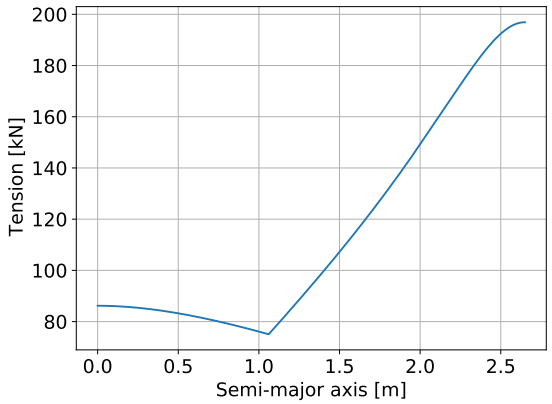

Figure 7.9: Tension distribution.

Table 7.5: Summary table structural design.

Skin thickness [m]	Number of stringers	Area stringers[mm^2]
0.003	515	60

The contribution of the aerodynamic loads given the final dimensions is 9 MPa, which confirms the assumption made in Section 7.5. Because of the buckling loads, which determined the number stringers, the maximum tensile load that occurs in the structure is lower than yield strength, being equal to 290 MPa. Figure 7.9 depicts the tension distribution due to pressurization, confirming the fact that the maximum loads are expected at the horizontal extremities of the cabin. The zero coordinate corresponds to the origin of the ellipse. Figure 7.10 confirms the assumption that the shear flow due to torque is much smaller than the one generated by pressurization, as its maximum is only around 26 kN/m. As the loads decrease in the outboard wing and the critical ones occur in the inboard wing, the outer region is not accounted in the plots.

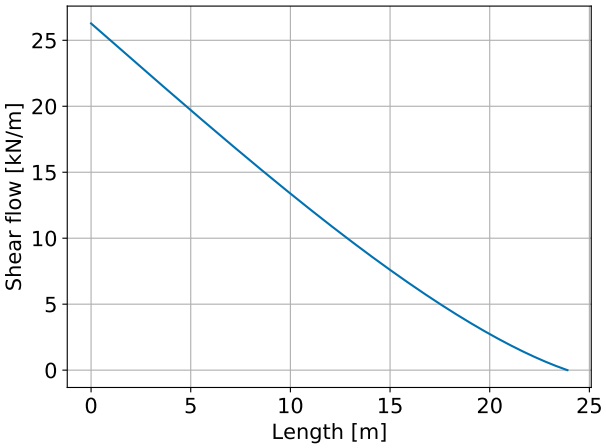

Figure 7.10: Shear flow distribution due torque.

7.8. Fatigue Analysis

In the aerospace industry there are two main design philosophies when considering fatigue: safe life and damage tolerance. Safe life is based on S-N curves, which are obtained experimentally, but often show very scattered data for the same material. For this reason, safety factors up to 5-6 are applied, which makes the structure over designed. Hence, this approach is generally only applied in detailed landing gear design. When assessing the main structure, the damage tolerance approach is utilised, as this method does not have the tendency to over design the structure. It is built around the crack propagation theory.

Once aluminium has been chosen as the main structural material, the maximum stress allowed in the structure can be determined based on the cycles between maintenance and crack propagation behaviour. Because crack propagation is not influenced by compression loads in aluminium alloys, the load amplitude for fatigue calculations is considered to be equal to the maximum tension loading during flight, which was reported to be about 300 MPa. Paris law will be used as in Equation 7.25, where the stress is used in MPa units, and thus is corrected with a factor of 10^4, allowing the use of the stress in Pascals. For aluminium, A is set to 10^{-12} and m is set to 3 [47]. The minimum crack length that can be detected is 2 mm [48], and in Equation 7.25, c denotes half of the crack length, thus $c_{initial}$ is set to 1 mm. However, in order to account for a variety of testing methods, a higher crack length will be assumed (for some methods the minimum crack length that can be detected is 4 mm). Because the maintenance is performed by humans, errors can occur and cracks might go by unidentified. Thus, a factor of 5 is applied to the fatigue cycles (industry standard). Note that this method does account for the notch effect.

$$\frac{dc}{dN} = 1.1A(\sigma\sqrt{\pi \cdot c})^m \rightarrow dN = \frac{dc}{A(1.1\sigma\sqrt{\pi \cdot c})^m} \xrightarrow{\int} N = \frac{c_{critical}^{1-m/2} - c_{initial}^{1-m/2}}{A \cdot 1.1^m \sigma^m (1-m/2)\pi^{m/2}} \tag{7.25}$$

$$c_{critical} = \frac{K_{1c}^2}{1.1^2\sigma^2\pi} \tag{7.26}$$

$$N = 2 \cdot 10^{24} \frac{\frac{1}{\sqrt{c_{initial}}} - \sqrt{\frac{1.1^2\sigma^2\pi}{K_{1c}^2}}}{10^{-12} 1.1^3 \sigma^3 \pi^{3/2}} \tag{7.27}$$

By substituting the number, the results indicate up to 10^8 cycles without fatigue damage. This is because the amplitude of the maximum tension is low, it never reaches the yield strength, because of the design limits imposed by buckling. Thus, maintenance checks can be performed every 2.5 years.

7.9. Recommendations

The preliminary analysis indicates that the aircraft concept is feasible. However, it must not be forgotten that a number of assumptions have been generated, and more in depth structural analysis is required. Thus, this section is dedicated to further recommendations that should be taken into account in the next design steps.

Both maximum bending stress and tension occur at leading edge, which is the most extreme point of the cabin. Thus, significant care and reinforcements are needed, if windows and doors are implemented in the structure, as cuts are performed exactly at the location of maximum internal loading. The loads can be decreased significantly, if the length of the fuselage is reduced, as the bending moment induced by pressurization is dependent on the axial length, or if the aspect ratio of the elliptical cabin is decreased, as it would more resemble a circle, alleviating the loads due to pressurization. For structural purposes it is highly recommended to model the cabin with a small aspect ratio for the ellipse and reduce the length of the fuselage as much as possible.

The cabin design requires the presence of vertical stiffeners in order to deal with the high pressure loads. FEM is required in order to determine the stress distribution, exact maximum stress, exact maximum compression load and the influence of the ceiling, floor and other possible vertical stiffeners. FEM models should also yield more accurate values for the torsion in the cross-section, and also generate realistic deflection distributions. Due to the high loads and sweep, special care and detailed calculations are also highly recommended in joints and fasteners.

After the stress distribution is obtained as a result of a FEM analysis, stringers should be positioned at a smaller pitch in the regions where compression occurs in order to counter the buckling load. The size of the stringers might also be subjected to investigation, but it must be noted that variations in stringer pitch and size entails stress concentrations. It is highly important to determine the exact maximum compression load, because in the end buckling proved to be more critical. If the compression loads are lower, this would further decrease the weight. Flying-V features curved skin plates, thus further buckling calculations have to be performed, as the utilised relations are valid for a flat plate loaded in pure compression.

Changing the dimensions of the supporting walls might decrease the number of stringers, as it would reduce the critical buckling loading, increasing the stringer pitch. However, this might have a negative impact on the weight and might create stress concentrations. Moreover, as indicated by Equation 7.19, the orientation of the walls also plays a role in the final magnitude of the stresses.

Furthermore, a detailed analysis should include an aeroelastic analysis. Aeroelasticity concerns the coupling between aerodynamic forces and the structure, aeroelastic phenomenons that could occur being: divergence, when the aerodynamic load increases the angle of attack, which leads to further load increments, control reversal, when the deployment of control surfaces leads to a decrease in control properties or even reversal of the desired action, and flutter, which represents a self-oscillation state that might lead to structural failure. The analysis should include an accurate flutter speed calculation. The aeroelasticity of a Flying-V is again not very straightforward, as regular analysis do not involve wings with high sweep, thus a regular approach can not be undertaken. Dynamic instabilities might couple with the structure of the aircraft contributing to the initiation of flutter.

Lastly,there might be other shapes that can better distribute the bending stress [36], and a fatigue model that accounts for the notch effect should be considered, and eventually the fatigue performance should be proven experimentally for small components. The shape of the stringers should also be investigated in order to maximise their efficiency. Nonetheless, a more detailed structural idealization could consider the landing gears as point loads as well.

8 Aircraft Weight Estimation

The weight of the aircraft is estimated multiple times during the design iteration. At the start of the iteration the weight of the aircraft is estimated using a Class I weight estimation, shown in Section 8.1. A Class II weight estimations is performed towards the end of the design iteration, which is discussed in Section 8.2. A center of gravity excursion diagram is constructed in Section 8.3, which helps determine the shift of center of gravity.

8.1. Class I Weight Estimation

The Class I weight estimation method used is the identical method used in the Midterm Report [3]. The estimation method is based on fuel fractions to determine the total fuel mass. The fuel fractions for the constant flight phases are determined statistically, while fuel fractions for cruise and loiter phases are calculated using the Breguet Range and Endurance equations, shown below [49]:

$$R_{jet} = \frac{V}{g \cdot c_j} \left(\frac{L}{D}\right)_{cruise} \ln\left(\frac{W_n}{W_{n+1}}\right) \qquad (8.1) \qquad E_{jet} = \frac{1}{g \cdot c_j} \left(\frac{L}{D}\right)_{loiter} \ln\left(\frac{W_n}{W_{n+1}}\right) \qquad (8.2)$$

Table 8.1 shows the fuel fractions used for the constant flight phases. These fractions come from an A320 [50], and have been adjusted for liquid methane, as explained in the Midterm Report [3]. In addition to this, the fuel fraction of the taxi phase has been set to 1, as the aircraft uses batteries for taxiing and thus does not burn any fuel during this phase. The final fuel fraction relating to landing, taxi and shutdown has also been adjusted to accommodate the electric taxiing.

Table 8.1: Fuel fractions for methane powered aircraft.

Flight phase	Methane
Start up	0.999
Taxi	1
Take-off	0.996
Climb 1	0.996
Descent 1	0.994
Climb 2	0.996
Descent 2	0.994
Landing, taxi, shutdown	0.997

The maximum take off weight of the aircraft is calculated using Equation 8.3, which shows the buildup of weights of the aircraft.

$$W_{MTOW} = W_{OEW} + W_{PL} + W_{Fuel} = W_{OEW} + W_{PL} + 1.05(1 - M_{ff})W_{MTOW} \qquad (8.3)$$

8.2. Class II Weight Estimation

A Class II weight estimation is performed by using empirical relations to find the weight of the aircraft components. The Flying-V is an unconventional aircraft however for which most of these empirical relations do not apply. Thus, a different approach is applied. To estimate the weight of a Flying-V, a method described by Oosterom was used [16]. Equation 8.4 shows that the Operational Empty Weight is split up in to the following components: fuselage, outboard wing, vertical tail, landing gear, propulsion system, operational items, furniture, aircraft systems, battery, and landing gear motor.

$$W_{OEW} = W_{fuselage} + W_{aft} + W_v + W_{lg} + W_p + W_{op} + W_{furniture} + W_{sys} + W_{battery} + W_{motor} \quad (8.4)$$

The fuselage weight is the weight of the inboard wing, and the flight deck. It mainly consists of the primary structure, which comes from the structure designed in Chapter 7. The weight of the structure is calculated by finding the total volume of the structure and multiplying it with the material density. The primary (fuselage) structure weight is multiplied by 1.2 to account for joints and cutouts and other structural parts [16]. The weight of the non-pressurised trailing edge is also added by determining the total volume of the trailing edge. The remaining weights are the pressure bulkhead weight, windscreen weight, door and miscellaneous item weight, window weight, aperture weight, freight door weight, paint weight and radar weight, as seen in Equation 8.5. These weights are all determined using empirical equations from Torenbeek [17].

$$W_{fuselage} = 1.2W_{primary} + 0.8W_{fus_{TE}} + W_{pb} + W_{ws} + W_{doors,misc} + W_{windows} + W_{apt} + W_{fd} + W_{paint} + W_{radar} \quad (8.5)$$

The outer wing weight and vertical tail weight is found using Equation 8.6, which is an equation from Torenbeek [17]. For this formula imperial units need to be used. For Zephyr One K is equal to 1 for outer wing and vertical tail [16].

$$W = KS_{h,v}\left(\frac{3.81S_{h,v}^{0.2}V_D}{1000\sqrt{\cos\Lambda_{0.5h,v}}} - 0.287\right) \quad (8.6)$$

The landing gear weight is found using Equation 8.7. The coefficients A to D are empirical values determined from Torenbeek [17], and dependent on which type of landing gear is used.

$$W_{lg} = k_{uc}(A + BW_{MTOW}^{3/4} + CW_{TO} + DW_{TO}^{3/2}) \quad (8.7)$$

The operational item weight consists of crew provisions, passenger supplies, potable water and safety equipment, as seen in Equation 8.8. The weights of these elements are determined using simple empirical relations based on the total number of passengers and flight crew [17].

$$W_{op} = W_{crewprov} + W_{paxsup} + W_{potwater} + W_{emergency} \quad (8.8)$$

The furniture weight consists of flight deck accommodation weight, seat weight, galley weight, sound proofing weight, lavatory weight, floor weight, cargo provision weight, oxygen system weight, fire provision weight and escape provision weight, as seen in Equation 8.9. Again, these are all simple empirical relations which are valid to use for the Flying-V, as it was assumed that the total fuselage length is the sum of both fuselage tubes of the aircraft.

$$W_{furniture} = 0.72(W_{fd} + W_{seats} + W_{galley} + W_{sp}) + W_{lav} + W_{floor} + W_{prov} + W_{ox} + W_{fireprov} + W_{escape} \quad (8.9)$$

The system weight consists of air conditioning system weight, flight control system weight, electric system weight and instrument weight, as seen in Equation 8.10 [17].

$$W_{systems} = W_{api} + W_{fc} + W_{el} + W_{iae} \quad (8.10)$$

Each of the subsystems weights described above are added together to form the final empty operating weight using Equation 8.4. The weight estimation resutls are presented in Figure 8.1. Next the center of gravity is estimated for the operational empty weight aircraft. First the location of each subsystem is determined separately, by defining locations of each element using the aircraft planform. Locations of items such as seats and floor weights are assumed to be located at the center of the cabin. Items such as crew provisions are located in the front section. The flight control and instrument systems, in addition to the battery, are placed in the flight deck. Equation 8.11 is used to calculate the location of the subsystems, and for the final center of gravity location for the operational empty weight aircraft. Fuel tanks and engines are moved to the most forward possible location due to stability.

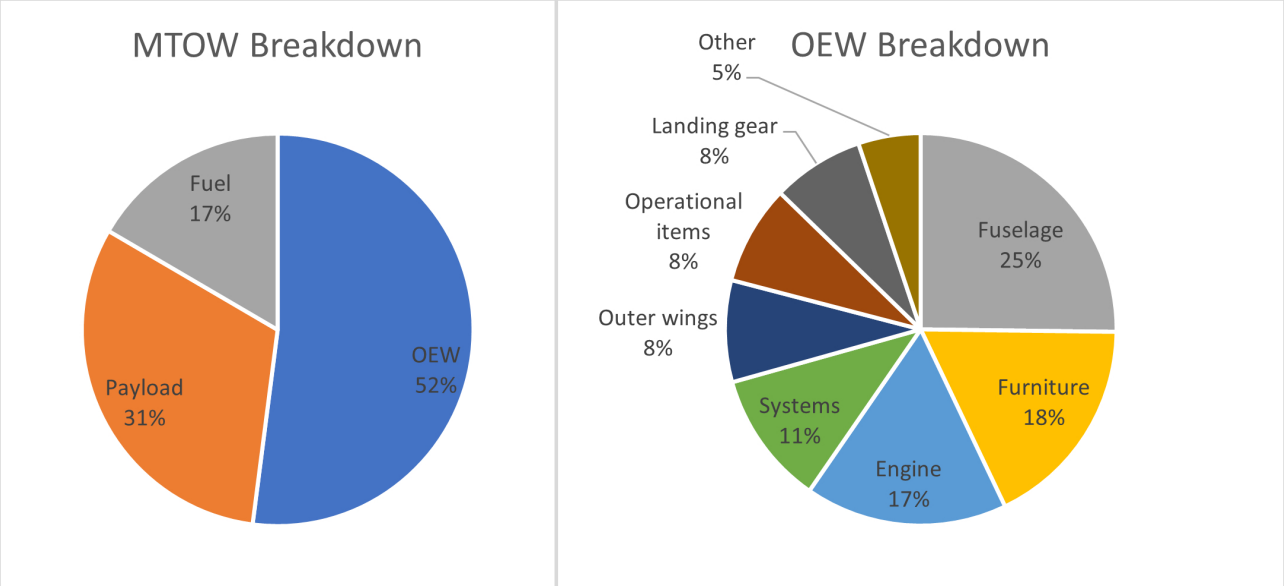

Figure 8.1: Aircraft weight breakdown.

$$x_{cg} = \frac{\sum_{i=1}^{N} W_i x_i}{\sum_{i=1}^{N} W_i} \tag{8.11}$$

8.3. Center of Gravity Excursion Diagram

With a center of gravity excursion diagram the shift of the center of gravity is determined for different loading cases of the aircraft.

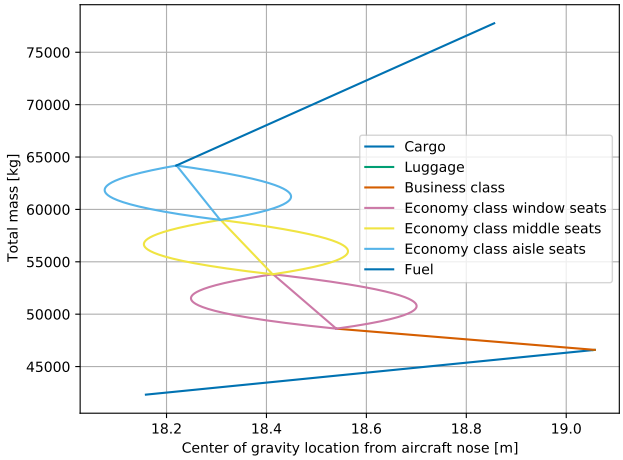

Figure 8.2: Center of gravity plot for the Zephyr One.

Figure 8.2 shows the center of gravity range of the Zephyr One aircraft. It is assumed that the cargo is loaded first, after which the passengers are loaded. Lastly the aircraft is fuelled up. Figure 8.2 shows that the cargo moves the center of gravity of the aircraft aft, while loading the passengers moves the center of gravity back forwards. As the fuel tanks are located more towards the rear of the aircraft, they also move the center of gravity aft. The center of gravity shift is taken to be the minimum and maximum locations seen in the center of gravity excursion diagram, to which a 2% safety margin is added.

8.4. Verification and Validation

Due to limited resources the verification of the model is not possible, however, it will be validated using existing aircraft data.

In Figure 8.1 the weight breakdown of Zephyr One is presented and it is comparable to the A321 weight breakdown [9]. Both aircraft feature the same ratio of empty operational weight, however, Zephyr One has a heavier battery, motors and a heavier fuel tank. On the other hand a Flying-V aircraft should feature a lower empty operational weight compared to a conventional aircraft [16]. Thus, the lower operational empty weight is compensated with additional aircraft systems. Moreover, Zephyr One features a 4% lower fuel fraction. This is because methane has a higher energy density and the Flying-V features a more aerodynamic design. This also enables Zephyr One to carry a higher payload ratio compared to the A321. Due to the similar results to the A321 weight and logical differences in the weights the weight estimation model is validated.

8.5. Recommendations

The recommendations for future work for the weight estimation of Zephyr One are as follows:

- The verification of model should be done. At this moment the model cannot be verified due to limited resources. In the future this should be looked into.
- After the preliminary design phase, when all the subsystem weight are known, a very detailed weight estimation should be done.

9 Stability and Controllability Design

To be able to operate the aircraft safely, it has to be stable and controllable at all flight conditions. The longitudinal stability of the aircraft is discussed in Section 9.1 where the X-Plot of the aircraft is also presented. After this the longitudinal and lateral controllability of the aircraft is explained in Section 9.2. The directional stability and controllability is discussed in Section 9.3. Finally, the landing gear positioning is given in Section 9.4.

9.1. Longitudinal Stability

The requirements for longitudinal stability are presented in Table 9.1. This requirement comes from CS-25. Zephyr One is an aircraft without a horizontal tail and does not produce negative lift. Thus, for it to be stable during flight, the center of gravity has to always be in front of the whole aircraft aerodynamic center. The location of the aerodynamic center is discussed in Section 5.5.5. The range of center of gravity has been found from the potato diagram in Section 8.3. The stability margin is determined for the most critical cg position, which is the most aft position. The aerodynamic center of the aircraft is located at 19.84 m, meaning that there is a stability margin of 5.1%. As such the Zephyr One is deemed to be longitudinally stable.

Table 9.1: Longitudinal stability requirements.

EFMRA-SYS-SF-02	The aircraft shall be stable and controllable.

9.2. Elevon Design

Elevator control surfaces are used to rotate the aircraft and ailerons are used to roll the aircraft. Usually, these two control surfaces are separate, however, due to limited span length of the outer wing, both control surfaces have to be combined into one. This control surface combination is called an elevon. The requirements set out for this subsystem are presented in Table 9.2. Small transport aircraft have a rotational acceleration of 6-8 deg/s^2, while large transport aircraft have a rotational acceleration of 4-6 deg/s^2 [51]. The aircraft to be designed fits between these two group, so an acceleration requirement of 6 deg/s^2 is chosen during take-off (most critical flight condition for elevator design [51]). The aircraft fits into Class III aircraft [51]. This means that the aircraft is required to achieve a 30° bank angle in at least 1.5 s at approach conditions [51]. Finally, the elevon shall not exceed an effectiveness of 0.8, as seen in Figure 9.2. A higher value would make it not possible to implement the control surface in the wing, as the control surface chord would be too big.

Table 9.2: Elevon requirements.

EFMRA-SYS-SC-01	The elevon shall provide an angular acceleration of 6 deg/s^2 during take-off.
EFMRA-SYS-SC-02	The elevon shall provide a roll rate of at least 20 deg/s during approach.
EFMRA-SYS-SC-03	The effectiveness of elevon shall not exceed 0.8.

First of all, the elevon will be sized for rotation. The free body diagram of the aircraft during a rotation at take-off is presented in Figure 9.1. This leads to a moment equilibrium around the point of the main landing gear, as presented in Equation 9.1. While in general aircraft rotate at speed of 1.1-1.3 V_s, the elevator has to be designed to rotate the aircraft at the stall speed.

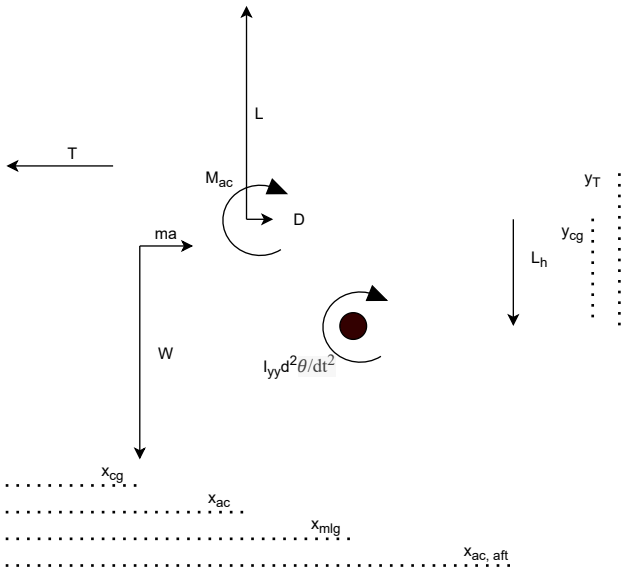

Figure 9.1: Free body diagram of aircraft during rotation.

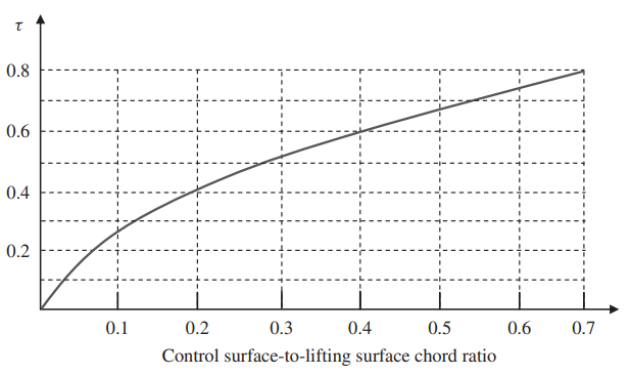

Figure 9.2: Control surface angle of attack effectiveness parameter [51].

$$\sum M_{mlg} = I_{yy}\ddot{\theta} = -W(x_{mlg} - x_{cg}) - T_N z_T + M_{ac} + L(x_{mlg} - x_{ac}) + Dz_{ac} + may_{cg} + L_h(x_{ac,aft} - x_{mlg}) \tag{9.1}$$

From Equation 9.1 the needed lift produced by the elevon can be found. This required lift will lead to a change of lift coefficient of the outer wing. Finally, the needed aileron effectiveness can be found using Equation 9.2. This effectiveness determines the control surface chord to wing chord ratio, as shown in Figure 9.2.

$$\Delta C_{L_{aft}} = C_{L_{\alpha_{aft}}} \tau \delta_{max} \tag{9.2}$$

The outer wing of the aircraft are also producing positive lift, thus, an immense force needs to be generated by the elevator to rotate the aircraft. This moment generated by the elevons can be adjusted by the placement of the main landing gear. Thus, a program sizing the elevon outputs the possible control surface effectiveness at each location of the main landing gear. The final chosen inputs and outputs are presented in Table 9.3.

Table 9.3: Elevator sizing inputs and outputs.

Inputs	
$\ddot{\theta}$	6 deg/s2
δ_{max}	40 deg
$b_{e,\,start}/b_{aft,\,1/2}$	0
$b_{e,\,end}/b_{aft,\,1/2}$	0.95
I_{yy}	8,247,255 kgm^2
W	795,261 N

M_{ac}	-65,991 Nm
L	127,920 N
D	5,859 N
F_{ff}	6,006 N
Outputs	
x_{mlg}	20.42 m
τ	1.17

As seen in Table 9.3, the effectiveness of the elevon needs to be at least 1.17 for a landing gear position of 20.42. This effectiveness is not possible, thus, design improvements have to be made to allow the aircraft to rotate during take-off. One suggestion would be to convert the outer wing to a stabilator (fully moving outer wing), so the whole surface could be used as an elevon. However, this solution should be analysed with CFD, to see how the stabilator affects the vertical tail and rudder performance. This problem will have to be fixed in future work.

Elevon sizing for rolling is done using Equation 9.3-9.6. These equations will be solved to find the needed control surface effectiveness.

$$C_{l_{\delta\alpha}} = \frac{2c_{l\alpha}\tau}{S_{ref}b}\int_{b_1}^{b_2} c(y)ydy \quad (9.3) \qquad C_{l_p} = -\frac{4(c_{l\alpha}+c_{d_0})}{S_{ref}b^2}\int_0^{b/2} y^2c(y)dy \quad (9.4)$$

$$P = -\frac{C_{l_{\delta\alpha}}}{C_{l_p}}\delta_{max}\left(\frac{2V}{b}\right) \quad (9.5) \qquad c(y) = c_r\left(1+\frac{\lambda-1}{b_{aft,1/2}}(y-b_e)\right) \quad (9.6)$$

Equation 9.4 is used to calculate the roll damping coefficient of the aircraft. The aircraft is made out of two wing sections, so two roll damping coefficients need to be calculated and added up for the total roll damping coefficient. For the outer wing Equation 9.6 is used to determine the chord along the wingspan. The needed aileron control derivative is found using Equation 9.5 and then the required control surface effectiveness is found with Equation 9.3. The inputs and outputs of the aileron sizing code are presented in Table 9.4.

Table 9.4: Aileron sizing inputs and outputs.

Inputs	
P	20 deg/s
δ_{max}	30 deg
$b_{a,\,start}/b_{aft,\,1/2}$	0
$b_{a,\,end}/b_{aft,\,1/2}$	0.95

Outputs	
C_{l_p}	-0.211
$C_{l_{\delta\alpha}}$	0.031
τ	0.106

The needed control surface effectiveness is much lower for rolling requirement, thus, the elevon design for rolling during flight is possible.

9.3. Vertical Tail and Rudder Design

The sizing of the vertical tail and rudder were performed by implementing the method presented by Faggiano [18]. In his thesis, the vertical tail is sized according to three critical conditions flight conditions which are listed below.

- Directional static stability
- Stability with one engine inoperative (OEI) at take-off
- Cross-wind landing

Table 9.5: Vertical tail and rudder requirements.

EFMRA-SYS-SF-02	The aircraft shall be stable and controllable.
EFMRA-SYS-SF-03	The aircraft shall be capable of safely landing and taking-off with at most 37 km/h crosswind.

9.3.1. Directional Static Stability

The main condition for directional static stability is that the aircraft has to return to its original state after a disturbing force is applied. This means that the aircraft needs to have an overall positive yawing moment coefficient derivative with respect to sideslip β. According to Roskam [52], this coefficient must be at least 0.001 per deg. In radians, this requirement is as follows.

$$C_{n_\beta} \geq 0.0573 \text{ rad}^{-1} \quad (9.7)$$

Next, the yaw moment equilibrium around the aircraft center of gravity is taken. The simplification of the equations of motion is presented by Dr. Scholz in his book on aircraft design [53]. Note that since

the Zephyr One does not have a separate fuselage and two different wing influences (the inboard and outboard wing), a yawing moment derivative for the fin-less aircraft is used. This coefficient can be determined via AVL modelling of the aircraft. The final equilibrium equation can be seen below

$$C_{n_\beta} = C_{n_{\text{fin-less}}} + C_{n_{\beta_v}} \tag{9.8}$$

$C_{n_{\beta_v}}$ is the yawing moment derivative of the fins evaluated with Equation 9.9

$$C_{n_{\beta_\text{v}}} = C_{L_{a_v}} \left(1 + \frac{d\sigma}{d\beta}\right) \frac{q_v}{q} K_{\text{FV}} \frac{S_\text{v} l_{x_v}}{Sb} \tag{9.9}$$

Here, $C_{L_{a_v}}$ is the slope of vertical tail lift curve, σ is the sidewash experienced by the fins, and $\frac{q_v}{q}$ is the ratio between the dynamic pressure experienced by the fins and the freestream, K_{FV} quantifies the effect of a fuselage, and l_{x_v} is the moment arm of the fins with respect to the most aft center of gravity. For a Flying-V, the sidewash, pressure ratio, and fuselage effects can be neglected [16, 18]. By implementing the simplified version of Equation 9.9 in Equation 9.8, an equation for sizing the required vertical tail area for this condition can be determined.

$$S_v = \frac{Sb(C_{n_\beta} - C_{n_{\beta_{\text{fin-less}}}})}{C_{L_{a_v}} l_{x_v}} \tag{9.10}$$

9.3.2. OEI Stability at Take-off

The fins of the aircraft must be able to counteract the yawing moment generated by the thrust difference produced by having one engine inoperative during take-off. In particular, the aircraft must sustain a zero angle of sideslip during this condition, while the maximum rudder deflection is at most $20°$[18]. By taking the moment equilibrium around the most aft center of gravity, the rudder defection can be related to the thrust difference as follows.

$$\delta_r = -\frac{T_\text{max} y_\text{eng}}{C_{n_{\delta_r}} qSb} < 20° \tag{9.11}$$

In this equation, the thrust difference is T_max, y_eng is the moment arm of the thrust force and equivalent to the distance from the engines to the plane's central axis. Finally, $C_{n_{\delta_r}}$ is the yawing moment derivative with respect to rudder deflection and is equivalent to:

$$C_{n_{\delta_\text{r}}} = -C_{L_{\alpha_\text{v}}} \frac{S_\text{v} l_{x_\text{v}}}{Sb} \frac{q_\text{v}}{q} \tau_\text{r} \frac{b_r}{b_v} \tag{9.12}$$

τ_r is the control surface angle of attack effectiveness of the rudder as presented in Figure 9.2, where for the rudder, the chord ratio is taken to be 0.3, leading to a τ_r of 0.530. The ratio of rudder to vertical tail span is taken to be 0.95. Substituting Equation 9.12 in Equation 9.11, the vertical tail area required for this situation is determined to be:

$$S_v = \frac{T_\text{max} y_\text{eng}}{\delta_r \tau_r \frac{b_r}{b_v} l_{x_\text{v}}} \tag{9.13}$$

9.3.3. Crosswind Landing

The final condition to be satisfied is that for crosswind landing, where the crosswind requirement is **EFMRA-SYS-SF-03**. This condition requires that the aircraft remains balanced under the influence of a sideslip due to the crosswind, all the while the rudder deflection does not exceed $20°$. Taking the moment equilibrium leads to Equation 9.14 for the rudder deflection. The sideslip angle can be obtained with Equation 9.15, where U is the crosswind velocity and V_land is the velocity during landing.

$$\delta_r = -\frac{C_{n_{\beta_{\text{fin-less}}}}\beta}{C_{n_{\delta_\text{r}}}} < 20° \tag{9.14}$$

$$\beta = \frac{U}{V_{\text{land}}} \tag{9.15}$$

The equation can be rearranged to obtain the vertical tail area as follows:

$$S_v = \frac{bSC_{n_{\beta_{\text{fin-less}}}}\beta}{l_{x_\text{v}}\tau_r\frac{b_r}{b_v}\delta_r C_{L_{\alpha\text{v}}}} \tag{9.16}$$

9.3.4. Sizing Procedure

Now that the equations used to determine the required vertical tail area for each condition, the optimal tail area can be determined by using a range of aspect ratios, sweep angles, and taper ratios as input. Each possible combination of the different ranges is analysed and the critical vertical tail area noted. Subsequently, the minimum critical vertical tail area of all the combinations is taken for the final design. Finally, the area is halved since the Zephyr One has a fin at the tip of each outboard wing. The range of inputs analysed is portrayed in Table 9.6

Table 9.6: Inputs for vertical tail sizing [18].

Input Parameter	Range
Aspect Ratio	0.1-2.5
Sweep Angle [deg]	0°-50°
Taper Ratio	0.45-0.7

Table 9.7: Outputs of vertical tail sizing.

Output	Values
Total Fin Surface Area [m^2]	36.72
Vertical Tail Height [m]	6.87
Taper Ratio	0.7
Aspect Ratio	2.5
Sweep[deg]	50°

The output obtained from the iteration is displayed in Table 9.7. The total fin surface area corresponds to singular fin with an area of 18.35 m^2. The root and tip chords of the fins can be obtained through simple planform geometry and are equal to 3.1 and 2.2 m, respectively. The output tends to the maximum values for the aspect ratio, sweep and taper ratio as l_{x_v} is maximised automatically, leading to a smaller surface area. In fact, by testing some larger, more unrealistic bounds, the program tends to a sweep of 60.9°, which leads to unreasonable weights. Further recommendations regarding vertical tail sizing are mentioned in Section 9.6.

9.4. Landing Gear Design

The requirements for the aircraft's landing gear is presented in Table 9.8. The longitudinal position of the aircraft main landing gear is limited by the center of gravity and the tipback angle, which determine the most forward position of the landing gear. The most aft position of landing gear is limited by the rotation elevon sizing. The lateral position is fixed by the turnover requirement. The nose gear longitudinal position is set by the 8%-15% load requirement.

The closest to the center lateral position of the main landing gear is found using Equation 9.17, where d is longitudinal distance from nose gear to main landing gear, z_{cg} is the height of center of gravity, b_N is the longitudinal distance form nose gear to center of gravity and ψ is the turnover angle, which should be at least 55°.

Table 9.8: Landing gear requirements.

EFMRA-SYS-SC-01	The aircraft shall not turnover during taxi.
EFMRA-SYS-SC-02	The landing gear shall allow for at least a 15° tipback angle.

$$y_{mlg} = d \tan \arcsin \left(\frac{z_{cg}}{b_N \tan \psi} \right) \tag{9.17}$$

The resulting position of the landing gear is 20.42 m in the longitudinal direction from the nose of aircraft and 3.1 m in the lateral direction form the center of aircraft. The most backward direction of center of gravity is 19.08 m, thus, the aircraft will not tip over at ground. The landing gear height resulted in 5 m, due to the tipback. This is a bit too high for aircraft operations and should be lowered in future work. Additionally, the loading of the nose gear was not analysed, as the aircraft can be steered with main landing gear powered by electric motors and the structure of the nose gear can be strengthened if the load increases.

9.5. Verification and Validation

The verification and validation for the control and stability model is done in this section. The verification and validation of elevon model, vertical tail and rudder model is presented here.

9.5.1. Elevon Design

The elevon sizing was done by sizing for elevators and ailerons. The elevator part was verified using an exercise presented in a book by Mohammad H. [51]. This verification was done for a conventional aircraft. The same inputs were used and the results are presented in Table 9.9. First of all, the results are match quite well. The model predicts the needed lift force and coefficient well in magnitude, however, the signs do not match. This is because in the model the elevator produced lift is assumed to act in different direction. This causes the coefficient to be positive and a positive deflection angle is used to get a positive efficiency. Furthermore, the small differences occur due to rounding errors made in the book. The efficiencies differ a bit, but it is due to the fact that in the book the downwash effect is assumed, while the model does not do this, thus, resulting in the higher needed efficiency. If the downwash effect is neglected in the book, the result is 0.522, exactly matching the model.

The aileron part was verified using data from a master's thesis of Resende G.J. [54]. In this thesis the same approach was used, as in the model made. Using the same variables, close results are achieved, as presented in Table 9.9. All in all, the elevon model predicts well the needed control surface efficiency, thus, it is verified.

Table 9.9: Elevon sizing model results compared to other source results.

	Elevator			**Aileron**
Parameter	L_h	C_{L_h}	τ	τ
Source results	−18348 N	−0.979	0.664	0.412
Model results	18354 N	0.980	0.522	0.417

9.5.2. Vertical Tail and Rudder Design

The Python scripts used for determining the size of the vertical tail, and thereby the rudder, were verified by performing a set of unit tests on each individual function within the script. The inputs for the functions were chosen to facilitate easier hand calculations. Subsequently, the output from the hand calculations are compared to the output of the function, where the absolute difference between

the two methods was at most 10^{-4}. Therefore the python functions are proven to be verified.

For the validation of the fin sizing, it was attempted to implement input from Faggiano and Oosteroom [18, 16]. However, some of the input and output needed was not reported. Therefore, the validation of the fin sizing results was performed via comparison against those of a similarly sized Flying-V aircraft, the Cryo-V [55]. As can be seen in Table 9.10, although different methods are used between the two aircraft, the required fin area is extremely similar. The other dimensions of the fins differ, however, this is possibly due to different constraints set on the input for either method.

Table 9.10: Fin sizing of the Zephyr One and Cryo-V.

	Zephyr One	**Cryo-V**
Singular Fin Area	18.35	18.45
Sweep	50	30
Aspect Ratio	2.5	3
Taper Ratio	0.7	1

9.6. Recommendations

The recommendations for future work for the stability and controllability of Zephyr One are as follows:

- The loading of the aircraft has to be analysed more in depth for the whole flight phase, as currently the aerodynamic center lies in the range of possible center of gravity locations and certain loading restrictions need to be made in the ground maintenance to ensure that the aircraft remains stable during flight.
- The flight phase during rotation at take-off has to be analysed again and innovative design need to be created to allow the aircraft to rotate at take-off. Currently the elevon cannot generate enough lift to rotate the aircraft.
- The dynamic stability and control of the aircraft during the different eigenmotions needs to be analysed. However, in order to perform this analysis, all the stability derivatives need to be obtained.
- The script used to determine the size of the vertical tail must also be optimised for minimising the weight of the vertical tail as well as tail area in order to provide more accurate results.
- Currently the landing gear height is 5 m. It is preferable to make the landing gear lower to make the aircraft more accessible. In the future a solution needs to be made to reduce the landing gear height.

10 Methodology Analysis

The methodology used for the design (optimisation) of the Zephyr One has to be verified to ensure that accurate results are obtained. In Section 10.1, an optimisation analysis is performed, in which the optimisation procedure is verified. A sensitivity analysis is performed in Section 10.2, in which the effects of altered system parameters are investigated. Both analyses use the fuel mass as a design-change indicator, for reasons discussed in Section 3.3.

10.1. Optimisation analysis

In the optimisation analysis, the optimisation parameters (set x as discussed in Section 3.3) are altered to verify if the optimisation method actually found the most optimal value. The analysis is performed by taking the final aircraft design, altering one of the parameters that were varied in order to find the optimal design (a single entry of x), and performing the iterative design loop until convergence. The parameters that are altered, one at a time, are the cruise altitude, cruise velocity, and the inboard and outboard wing sweep.

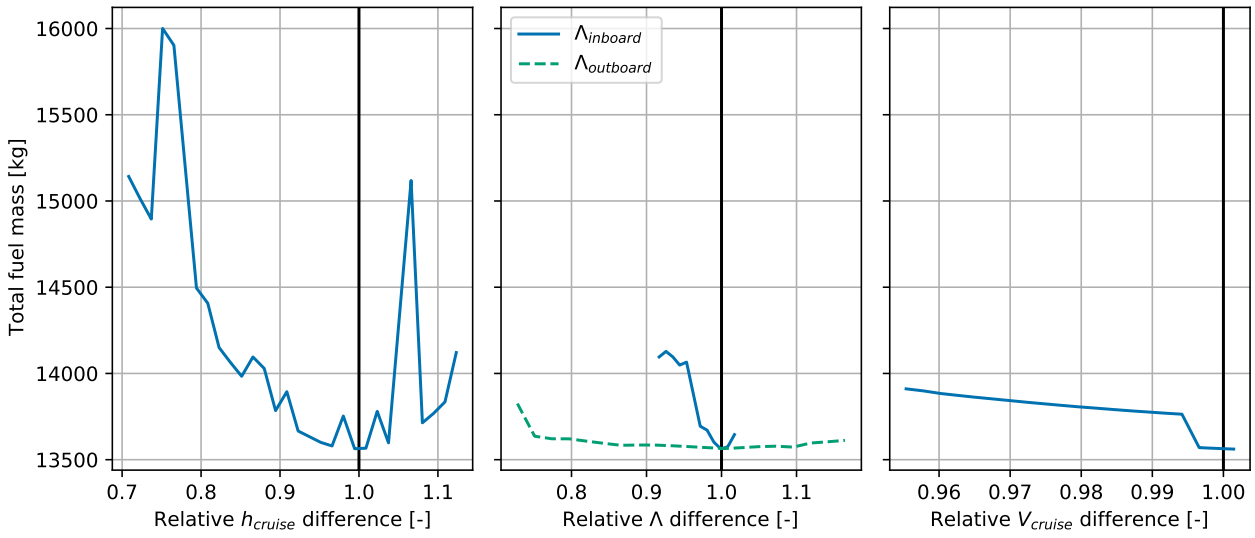

Figure 10.1: Resultant total fuel mass for alterations in optimisation parameters.

Figure 10.1 shows the results for this optimisation analysis. Please note that a smaller range of velocities and inboard sweep angles are used compared to the cruise altitude, because of the smaller design space available for these variables. The vertical black line in these plots indicate where the relative parameter difference is equal to 1.0, meaning that the value of that parameter is equal to the value of that parameter in the final aircraft design.

It is clear to see that the plots for cruise altitude, inboard sweep and cruise velocity all show a minimum occurring at the design point. These minima are also not local minima, as can be seen in, meaning that the optimiser found the actual global optimum. All in all, this shows that the optimisation software was indeed able to find the optimal values for the cruise altitude, the sweep angles and the cruise velocity.

Furthermore, it can be noticed from Figure 10.1, that the outboard sweep angle line shows that it has only a minor effect on the entire design of the aircraft. This is expected as the outboard wing only

forms a minor part of the aircraft and the evaluation of the performance of the outboard wing is limited with the currently used design tools.

10.2. Sensitivity analysis

A sensitivity analysis gives more insight into how the change of a system parameters affects the (entire) aircraft design. Again, also in this section, the total fuel mass is taken as the common reference point. Parameters that are interesting to change in order to investigate their effect on the design, are the cruise range, and the payload mass, as these will both have a major impact on the fuel mass of the aircraft. The latter is altered by changing the mass of the cargo payload. A likely outcome for this would be that the aircraft is not stable anymore, due to the shift of the center of gravity. This issue is however not accounted for in this sensitivity analysis.

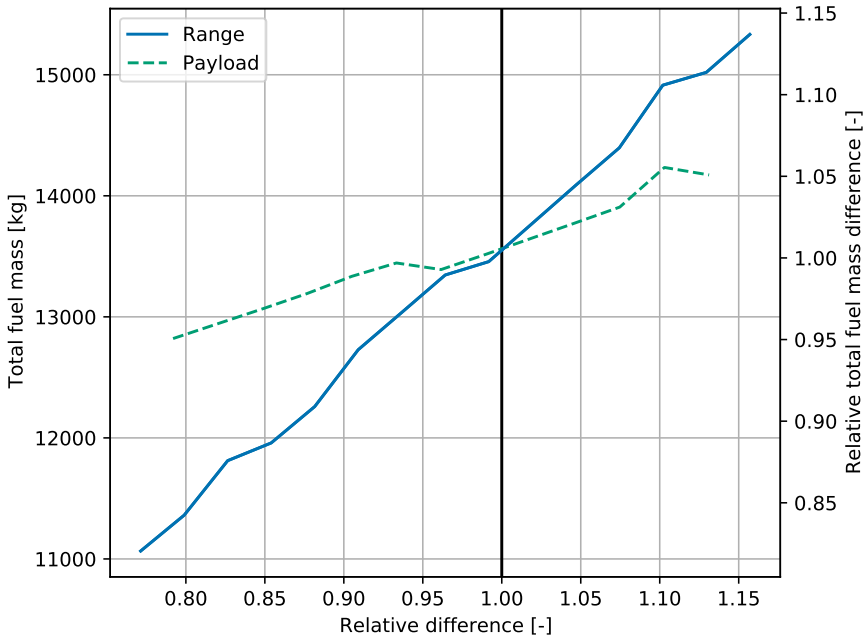

Figure 10.2: Resultant total fuel mass for alterations in input parameters.

The results of the performed analysis is shown in Figure 10.2. As expected, increasing the range or payload mass increases the required total fuel mass. One can also deduce that increasing the range of the aircraft has a bigger impact on the fuel required compared to increasing the payload. Furthermore, the lines describing the change in range and payload show quite linear behaviour and lack spikes or sudden jumps. All in all, this shows that the final aircraft design, is not very sensitive to changes in design and that the changes that do occur, are predictable. It can thus be concluded that the design iteration, connected with the optimiser, are verified.

11 Noise Analysis

The noise analysis of the Zephyr One is an important parameter for the performance of the design and must be carefully assessed. Since it is difficult to accurately evaluate noise emissions without experimental data, a semi-analytical analysis will be carried out i.e. where possible, quantitative estimations will be performed.

First, a recapitulation of requirements will be presented in Section 11.1, along with the three main measurement locations and the noise metrics used. Next, the noise will be assessed into four separate categories, namely engine, airframe, noise shielding, and operational procedures in Sections 11.2 through 11.5, after which the final values for the noise generation of the Zephyr One will be summarised in Section 11.6.

11.1. Noise Assessment, Requirements and Comparison

Before starting to estimate the noise levels for the different categories, it is crucial to have an overview of the noise assessment points as well as the metrics used. This section aims to give an overview of these parameters, followed by the Flightpath 2050 requirements and reference values used for the noise reduction capabilities of different noise reducing technologies.

11.1.1. Location of Measurements

As detailed in requirements **EFMRA-SYS-FP-02.1** to **EFMRA-SYS-FP-02.3**, there are three different measurements used for noise certification: fly-over, approach, and lateral noise. These are summarised in Figure 11.1a. Furthermore, the axis system used to assess the distance R between the noise source (the aircraft) and the observer (the reference point) is shown in Figure 11.1b.

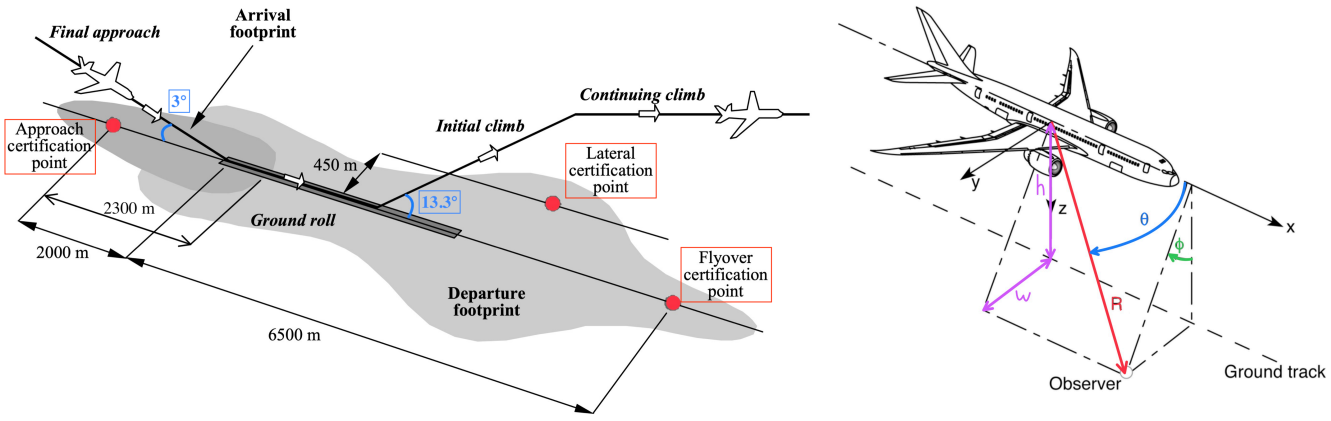

(a) Reference points for noise certification, dictated by ICAO [56].

(b) Axis system used for noise certification measurements [57].

Figure 11.1: Noise certification measurements and reference points.

The fly-over reference point is ”the point on the extended centre line of the runway and at a distance of 6,500 m from the start of roll” [56]. Consequently, the lift-off distance must be subtracted from the 6,500 m before calculating the height at this reference point, as can be deducted from Figure 11.1a. The approach noise is assessed similarly, with a different angle and ground distance. More specifically, the reference point for approach is ”the point on the ground, on the extended centre line of the runway

2,000 m from the threshold. On level ground this corresponds to a position 120 m vertically below the 3° descent path originating from a point 300 m beyond the threshold" [56]. Finally, the lateral noise reference point is "the point on a line parallel to and 450 m from the runway centre line, where the noise level is a maximum during take-off" [56].

The values for angles ϕ and θ from Figure 11.1b are given in Table 11.1, as well as the dimensions for the distance R, where w and h vary depending on the reference point being assessed.

Table 11.1: Parameters for estimating noise at the certification reference points.

	θ [°]	ϕ [°]	R [m]		
Fly-over	90	0	h	=	1,040
Approach	90	0	h	=	120
Lateral	90	$tan^{-1}(w/h)$ = 90	$\sqrt{w^2+h^2}$	=	450

11.1.2. Noise Metrics

Although the Effective Perceived Noise Level (EPNL) was used to assess noise in previous reports [2, 3], the A-weighted maximum sound pressure level ($L_{A,\,max}$), measured in dBA, will be used from now on. This was chosen for two main reasons. Firstly, the A-weighting filter is used to simulate the sensitivity of the human ear and consequently assesses the annoyance level of potential observers [58]. As a result, $L_{A,\,max}$ considers the frequencies which are more harming to the human ear, namely between 1 to 5 kHz, giving a more realistic standard for noise perception [59]. Secondly, assessing noise in EPNL poses some logistical problems. Indeed, most of the data in EPNL is not available to the general public at this level of detail as it is mainly accessible to aircraft companies. Therefore, it was decided to assess the Zephyr One's noise levels by means of $L_{A,\,max}$.

When the noise levels in dBA cannot be acquired, the Overall Sound Pressure Level (OASPL) measured in dB is computed and converted to $L_{A,\,max}$. For airframe noise, an empirical relation taken from Fink [60] may be used for this conversion. By subtracting 4.6 dB to the OASPL, as shown in Equation 11.1, one can convert this metric to $L_{A,\,max}$. Note that this may only be used for airframe noise estimation, since it is an empirical approximation.

$$L_{A,max}[dBA] = \text{OASPL}\ [dB] - 4.6[dB] \tag{11.1}$$

Another important assumption made is that even though exact values of noise differ between the various metrics, the *change* in EPNL, $L_{A,\,max}$, and OASPL is assumed to be constant. This assumption is summarised in Equation 11.2.

$$\Delta\text{EPNL} \approx \Delta L_{A,max} \approx \Delta\text{OASPL} \quad \text{but} \quad \text{EPNL}\ [EPNdB] \neq L_{A,max}[dBA] \neq \text{OASPL}\ [dB] \tag{11.2}$$

Finally, as the noise levels are assessed separately for the different noise sources, one must add them up to obtain the total noise level generated by the aircraft. Since noise is assessed in decibels (dB), or variants of it, the logarithmic scale must be used when adding or subtracting noise levels from different sources. This is done as shown in Equation 11.3, as explained by Ruijgrok [61], where N is the number of noise sources. As can be seen, the summation is performed similarly for any noise metric.

$$L_{A,max} = 10\log\left(\sum_{i=1}^{N} 10^{\frac{L_{A,max}}{10}}\right) \;;\quad \text{OASPL} = 10\log\left(\sum_{i=1}^{N} 10^{\frac{OASPL}{10}}\right) \;;\quad \text{EPNL} = 10\log\left(\sum_{i=1}^{N} 10^{\frac{EPNL}{10}}\right) \tag{11.3}$$

11.1.3. Flightpath 2050 Requirements

The noise requirements derived from Flightpath 2050 have previously been translated into three main noise limits corresponding to the three measurements described in Section 11.1.1 [2]. According to

Flightpath 2050, the Zephyr One shall reduce its noise pollution by 65% in comparison to the reference aircraft, which translates into lowering noise levels by 15 dB.

In the Baseline report [2], the chosen reference aircraft was the Airbus A321, which was found to generate 84 EPNdB during fly-over, 94 EPNdB for the lateral reference point, and 95 EPNdB during approach [1]. Consequently, the initial EPNL requirements were the ones shown in the first column of Table 11.2, and stated in requirements **EFMRA-SYS-FP-02.1** to **EFMRA-SYS-FP-02.3** [2].

Since the noise metric used for the final part of the project was changed to $L_{A,\,max}$, the noise requirements had to be updated to match this metric. That is, the EPNL values measured in EPNdB had to be converted to the updated unit: dBA. To do so, Eurocontrol's ANP database[2] was used to retrieve a list of total aircraft noise values in dBA for the Airbus A321. These values depended on the power setting and the distance to the observer r. Therefore, they were interpolated twice to obtain the exact values for the fly-over, approach, and lateral certification reference points. The A321 was found to generate 71 dBA during fly-over, 84 dBA for the lateral reference point, and 87 dBA during approach. Assuming that the change in EPNdB corresponds to the same change in dBA, as explained in Section 11.1.2, one could assess the final maximum noise requirements in dBA by subtracting 15 dBA to the $L_{A,\,max}$ values of the A321. The final results (in dBA) are listed in the second column of Table 11.2 and will be used as reference from now on.

Table 11.2: Flightpath 2050 requirements for maximum noise levels.

	Flightpath 2050 maximum noise levels	
	EPNL [EPNdB]	$L_{A,max}$ [dBA]
Fly-over	69	59
Lateral	79	69
Approach	80	72

In conclusion, the requirements for noise have been updated as listed in Table 11.3.

Table 11.3: Aircraft requirements for noise performance.

EFMRA-SYS-FP-02.1	The aircraft shall have a fly-over reference noise lower than 59 dBA.
EFMRA-SYS-FP-02.2	The aircraft shall have an approach reference noise lower than 72 dBA.
EFMRA-SYS-FP-02.3	The aircraft shall have a lateral reference noise lower than 69 dBA.

11.2. Airframe Noise

The noise generated by the airframe can be split into three separate components. These are the noise generated by the clean wing, landing gear, and trailing edge high lift devices. However, since the Zephyr One lacks HLDs, that component of the noise is zero. The contribution of the deployed HLDs to the airframe noise in a conventional aircraft accounts for an increase of 10 dB compared to its clean wing configuration [62]. The noise emissions of the other airframe components are evaluated using methods derived from M. Fink's report "Airframe Noise Prediction Method" [60]. Note that the equations used in Fink's book return the noise level as overall sound pressure level (OASPL), while the Flightpath 2050 requirements are expressed in dBA. Fink states that the total A-weighted noise level of the airframe is approximated to be 4.6 dB less than the OASPL, with a standard deviation 1.3 dB [60].

[1] `https://www.ana.co.jp/eng/aboutana/anaenvironment/pdf/e2003-5.pdf` [cited on 17 June 2021]
[2] `https://www.aircraftnoisemodel.org/` [cited on 16 June 2021]

11.2.1. Clean Wing Noise

The noise generated by the clean wing can be obtained using Equation 11.4.

$$\text{O A S P L}_w = 50 \log\left(\frac{V}{100}[kts]\right) + 10 \log\left(\frac{\delta_w b_w}{h^2}\right) + 8(\text{ND}) + 10 \log\left(\left(\cos\phi \sin\theta \cos\frac{\theta}{2}\right)^2\right) + 104.3 \text{ dB} \tag{11.4}$$

In this equation, V is the velocity of the aircraft at each noise measurement location measured in knots. ND is a constant set to zero in this case, as the Zephyr One is considered to be an aerodynamically clean aircraft (as it has no trailing edge HLD's). δ_w is the thickness of the turbulent boundary layer which is determined using Equation 11.5. The thickness is dependent on the wing structure, velocity, and the kinematic viscosity of air $\mu = 1.48 \cdot 10^{-5}$. With the exception of the logarithmic velocity term in Equation 11.4, all the units used are in S.I, since the units cancel out and the noise is dimensionless.

$$\delta_w = 0.37 \left(\frac{S_w}{b_w}\right) \left(\frac{V S_w}{b_w \mu}\right)^{-0.2} \tag{11.5}$$

11.2.2. Landing Gear Noise

The landing gear noise can be further split into two different sources, which are the nose landing gear and main landing gear. The landing gear configurations consist of a two-wheel configuration for the nose landing gear and a four-wheel main landing gear configuration as used in most jet aircraft.

$$\text{OASPL}_{\text{nlg}} = 60 \log\left(\frac{V}{194}[kts]\right) + 20 \log\left(\frac{D_n}{r}\right) + 10 \log\left(10^{12.52} + 10^{\text{G3}}\right) \tag{11.6}$$

$$\text{OASPL}_{\text{mlg}} = 60 \log\left(\frac{V}{194}[kts]\right) + 20 \log\left(\frac{D_m}{r}\right) + 10 \log\left(10^{12.79} + 10^{\text{G3}}\right) \tag{11.7}$$

As can be seen in Equations 11.6 and 11.7, the noise levels depend on the velocity, position with respect to the observer, and dimensions of the landing gear, where the strut height is incorporated in Equation 11.8

$$\text{G3} = 12.79 + \log\left(0.34 \frac{H_{\text{strut}}}{D}\right) (\sin(\phi))^2 \tag{11.8}$$

Since the diameters of the nose and main landing gear have not been calculated in this stage of the design, the dimensions used are the ones of the A320 as provided by Bridgestone[3].

In the midterm report [3], research has been performed into investigating Low-Noise Technologies (LNTs) that aim at "reducing the incoming flow velocity, suppress cavity resonance, shield small components, or prevent wake interactions" [63]. Due to the recirculation of the airflow underneath the wings, the Main Landing Gear (MLG) experiences a lower flow velocity than the nose landing gear, which leads to the two systems producing comparable amounts of noise [64]. Therefore, LNT applied to one system are assumed to lead to similar reductions in noise as the other.

R. Merino-Martínez *et al* examine the noise reduction effects of a set of LNT of medium to high TRL applied to a NLG system [63]. In particular, the following adjustments are analysed. A ramp door spoiler placed upstream of the NLG bay to deflect the airflow towards the outside of the landing gear. Next, a landing gear fairing is added to the NLG to improve its aerodynamic properties, and hence produce less noise. Hub caps placed on the inside and outside of the wheels are used to improve airflow and reduce noise. Finally, porous fairings that reduce flow velocity towards the sides of the fairings are investigated. These fairings do however increase the higher frequency noise due to

[3] `https://www.bridgestone.com/products/speciality_tires/aircraft/products/applications/pdf/tire_applications.pdf` [cited on 21 June 2021]

shearing flow around the porosities, which can be adjusted through design changes to increase the frequencies above the human hearing threshold. The effects of these individual adjustments, as well as multiple combinations, are examined in the article. A combination of the first three adjustments leads to the best results, a decrease of 4 to 7 dBA in noise emissions.

11.2.3. Total Airframe Noise

Now that the separate components of airframe noise are obtained, the total airframe noise can be obtained by adding up the individual components logarithmically, as explained by Ruijgrok [61]. This is displayed below, where n_m is the number of sets of four-wheel main landing gears.

$$\text{OASPL}_{\text{airframe}} = 10 \log \left(10^{\frac{\text{OASPL}_w}{10}} + 10^{\frac{\text{OASPL}_{\text{nlg}}}{10}} + + \sum_{i=1}^{n_m} 10^{\frac{\text{OASPL}_{\text{mlg}}}{10}} \right) \tag{11.9}$$

This noise value is converted to A-weighted decibels by subtracting by 4.6dB [60].

11.3. Engine Noise

It is difficult to estimate the noise emissions produced by the engine without a detailed analysis of the entire engine layout. According to Bertsch [65], the two most dominant noise sources of a turbofan are jet and fan noise. To estimate these, one would implement Stone's method and and Heidmann's methods respectively. However, since the input required to implement these methods is beyond the level of detail provided by this project, a simplified approach is required. In particular, a set of empirical relations between the noise level of a pre-existing engine and the one designed for the Zephyr One is established.

Using Eurocontrol's ANP database [4], the total aircraft noise for the Airbus A319 is determined at each measurement point. Note that the lateral and fly-over measurement points occur during departure, while the approach measurment point occurs during approach. In order to obtain the engine noise, the following relations between total aircraft noise and the fan and jet components of engine noise determined by Bertsch in his thesis [65] are used.

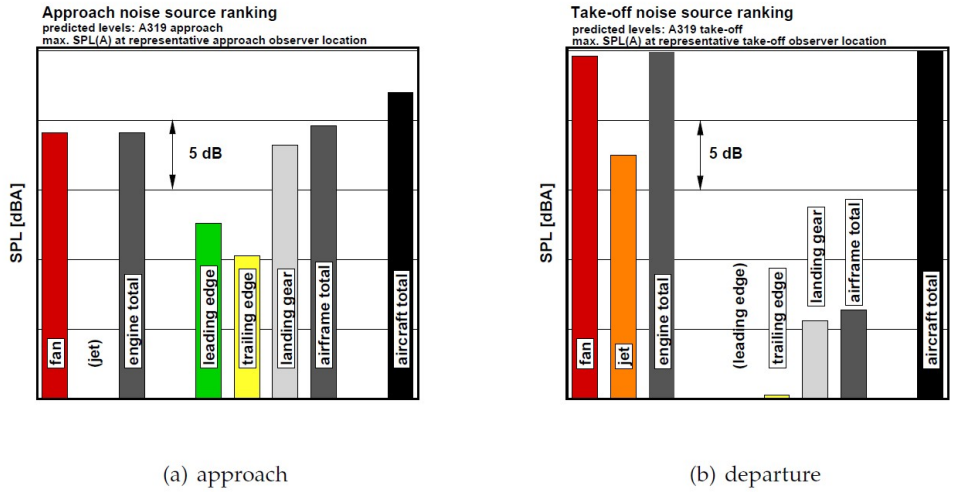

(a) approach (b) departure

Figure 11.2: Relations between different noise sources in an A319 [65].

By using the scale in Figure 11.2, the fan and jet noises are determined to be 0.4 and 7.6 dBA less than the total aircraft noise respectively during take-off, and 2.9 and 22.4 dBA less during approach

[4] `https://www.aircraftnoisemodel.org/` [cited on 16 June 2021]

respectively. While these noise level differences concern the Airbus A319, it is assumed that the Airbus A321 has similar noise level differences as it belongs to the same aircraft family.

Since the engines powering the A321 and the Zephyr One produce similar amounts of thrust, the main difference between the noise levels is due to the reduced fan rotation speed and higher bypass ratio [66]. Therefore, a correction for each of these effects is applied to the engine noise.

A relation between the bypass ratio and the noise level can be seen in Figure 11.3. This graph is for an engine with a thrust level of 178kN. While the thrust is larger than that of the engine used in the Zephyr One, the difference in engine noise levels due to a change in the bypass ratio is assumed to be the same. The bypass ratio of the A321 is 5.6 [67], while the bypass ratio of the Zephyr One is 18.3. This leads to noise reductions of 17.3 and 7.6 dBA for the jet and fan noise respectively.

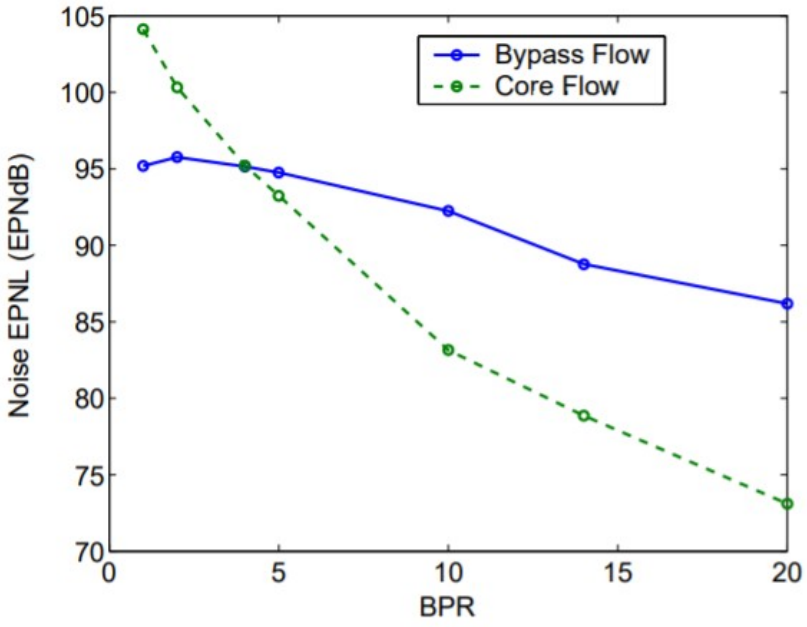

Figure 11.3: Relation between bypass ratio and engine noise level [68].

The noise reduction due to the engine being a Geared TurboFan (GTF) is conservatively estimated to be 3-4 dBA applied to the entire aircraft noise during departure procedures (fly-over and lateral), as determined by Bertsch [65]. This estimation is considered conservative due to the fact that the GTF considered is outdated with respect to newer GTF such as the PW-1000g, which reduces the engine noise footprint by up to 75% compared to its predecessors [5].

The final step is to add up the fan and jet noise emissions logarithmically similarly to the procedure in Section 11.2.3.

$$L_{A_{max},\text{Engine}} = 10\log(10^{\frac{\text{dBA}_{\text{fan}}}{10}} + 10^{\frac{\text{dBA}_{\text{jet}}}{10}}) \tag{11.10}$$

11.4. Noise Shielding

Noise shielding concerns the reduction in the noise produced from an energy source due to the shape of the aircraft and the location of the noise sources. In the case of the Zephyr One, noise shielding reduces the perceptible noise emissions produced by the engine. The method used to predict the noise shielding effect in this report is the Barrier Shielding Method (BSM) as presented by A. Vieira and F. Dewitte in their respective PhD and master theses [69, 70].

[5] `https://spinoff.nasa.gov/Spinoff2015/t_1.html` [cited on 16 June 2021]

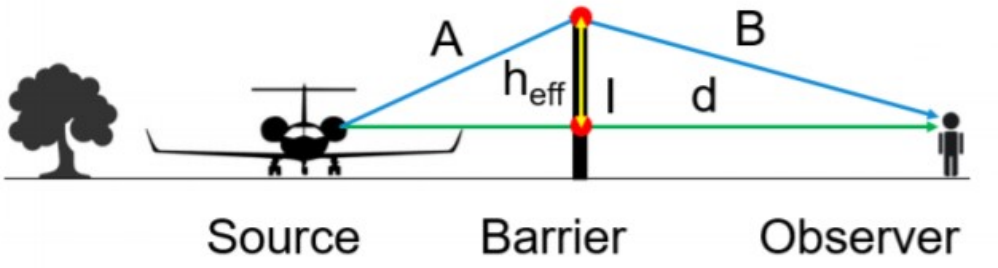

Figure 11.4: Diagram displaying the BSM [70].

The procedure for estimating the noise shielding via the BSM method is as follows. The Fresnel number (N) is computed via Equation 11.11. In this equation, f_{centre} is the centre frequency of the noise source, which in the case of an engine is its blade passing frequency. δ is the difference between the length of the shortest path around the shielding geometry and that of the straight line from the source to the observer as displayed in Figure 11.4. a_{sound} is the speed of sound in air. The Fresnel number is taken to be positive when the direct path to the observer is blocked and negative when it is not.

$$N = \frac{2 f_{\text{centre}} \delta}{a_{\text{sound}}} \tag{11.11}$$

Next, for a Fresnel value $N \geq -0.2$, the sound pressure level reduction ΔL_p is obtained using . For all other values of N, the reduction is zero.

$$\Delta L_p = 5 + 20 \log\left(\frac{\sqrt{2\pi N}}{\sqrt{\tanh 2\pi N}}\right) \text{ dB} \tag{11.12}$$

So far, the calculations are considering a singular edge. However, for the Zephyr One, the noise shielding area is assumed to be as portrayed in Figure 11.5.

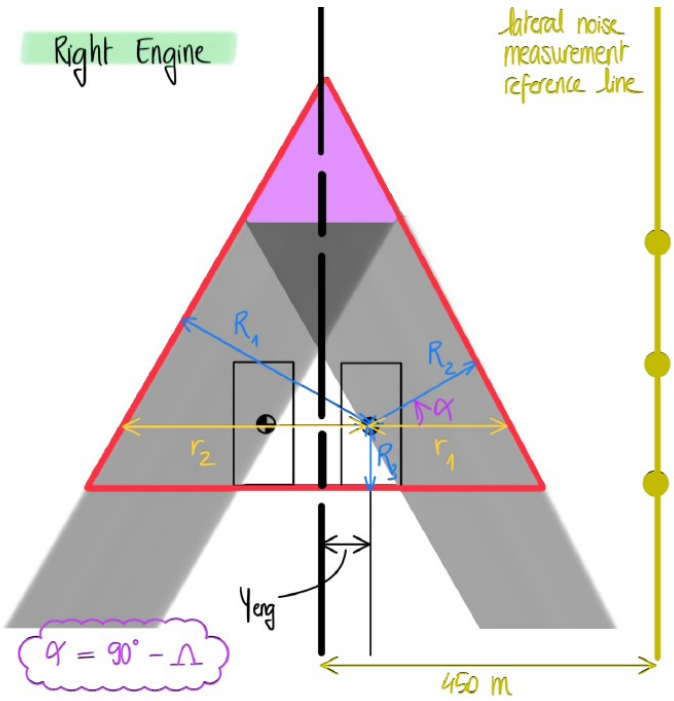

Figure 11.5: Top view of the noise shielding.

The shielding area is considered to be a triangle whose base coincides with either the rear of the engines (if there is an empty area between the engines) or the location where the two fuselages meet (if there is no empty area), and whose other sides are the edges of the planform. For the Zephyr One, the latter case is applicable. Given the locations of the observer obtained in Table 11.1, δ can be found for each edge, and subsequently the noise attenuation around each edge. Finally, the noise reductions around each of the three edges can be logarithmically added as in Equation 11.13.

$$\Delta L_{p_{tot}} = -10 \log \left(\sum_{i=1}^{3} 10^{\frac{\Delta L_{p_i}}{10}} \right) \tag{11.13}$$

11.5. Operational Procedures

So far, noise has been assessed at aircraft level, however one may also alter operational procedures in the effort of reducing generated noise. As already explained in the Baseline report [2], different noise mitigation measures already exist while some are still being implemented. Note that changing operational procedures may not deteriorate safety, under any circumstance.

Runway usage configurations are optimised to obtain the most efficient and least emitting arrangement. Noise simulations are carried out using software, such as FAA's *Integrated Noise Model (INM)* which allow for optimisation. These generate noise contour maps for a designated "peak day" based on scheduled flights, average usage of different runway configurations, and weather conditions (visibility) [71]. This is however highly dependent on the airport, air traffic, and runway configurations, therefore no fixed noise reduction value can be obtained by applying this optimisation.

Currently, one of the most promising and impactful solutions for noise reduction is the use of low-noise flight profiles, such as steeper climbing and descent rates. The concept is shown in Figure 11.6. Instead of having the conventional level flight segments, also known as "stepped" approach or climb, a continuous optimised segment is used instead. These would allow for increased distances between the noise source (the aircraft) and the residents living close-by the airport.

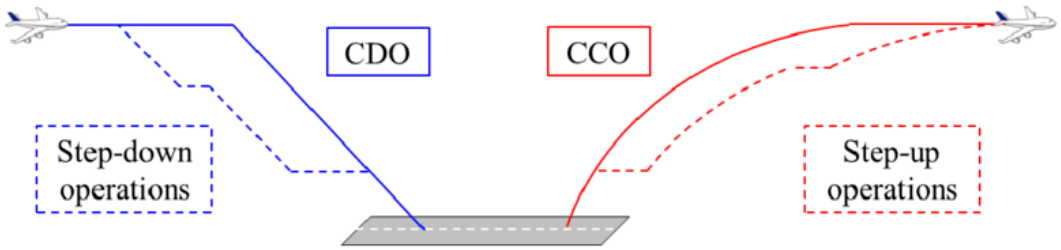

Figure 11.6: Continuous descent and approach operations [72].

With descent being the most noisy phase, NASA has developed a low-noise flight guidance concept, designed to aid the pilots in achieving a Continuous Descent Approach (CDA) [73]. The latter accounts for trajectory characteristics, time and fuel, ATC procedures, and pilot input. Eurocontrol is also investigating the implementation of Continuous Descent Operations (CDO) and Continuous Climb Operations (CCO), which are expected to reduce noise in all directions by 3 to 5 dB [74]. Furthermore, NATS has also looked into the issue, estimating the noise reduction of such operations between 1 to 5 dB. Not only will CDO and CCO reduce noise, they also minimise fuel consumption and in turn reduce CO_2 and NO_x emissions, thus improving the design's sustainabile strategy. Implementing CDO and CCO for the Zephyr One will allow to further reduce the overall noise levels of the aircraft, thus ameliorating its noise performance with respect to the A321 values, and consequently, achieve the Flightpath 2050 requirements.

11.6. Final Noise Assessment

After assessing the four noise categories in Sections 11.2 through 11.5, the total noise generation of the Zephyr One could be evaluated. To do so, the individual noise contributions were added logarithmically, as explained previously in Equation 11.3. The values generated by the airframe and the engines are summarised in Table 11.4, without taking into account the noise reduction achieved with noise shielding or any other LNTs. Note that for lateral noise, the reference point is taken on the right parallel line to the runway centre line, as shown in Figure 11.5. This explains why the right engine has a higher lateral noise level in comparison to the left one.

Table 11.4: Noise generated by the Zephyr One, without the implementation of LNTs.

Noise generated [dBA]	Airframe	Left Engine	Right Engine
Fly-over	51.6	45.7	45.7
Lateral	59.3	53.9	71.4
Approach	69.7	56.2	56.2

Table 11.5 contains the noise reduction values achieved with noise shielding and Table 11.6 lists the $L_{A,\,max}$ reductions achieved individually by the LNTs implemented in the Zephyr One. These include landing gear LNT, GTF usage with an Ultra High ByPass Ratio (UHBPR), and CDO/CCO operational procedures. Note that the reductions achieved with the implementation of GTFs and CDO/CCO apply to the overall noise level of the aircraft, while the rest are only valid per subcategory.

Table 11.5: Noise reduction from shielding applied to the engines at the measurement points.

Noise Shielding [dBA]	Left Engine	Right Engine
Fly-over	20.4	20.4
Lateral	22.5	4.97
Approach	20.5	20.5

Table 11.6: Noise reduction capabilities of LNTs applied.

Noise reduction [dBA]	Landing gear LNT	GTF	UHBPR (Fan)	UHBPR (Jet)	CDO/CCO
Per component	4 - 7	-	17.3	7.6	-
Overall	-	3 - 4	-	-	1 - 5

Finally, after applying the reductions from the previous table, the final noise values of the Zephyr One are found. They are shown in Table 11.7 where they are also compared against the required values from Flightpath 2050.

Table 11.7: Noise generated by the Zephyr One, with the implementation of LNTs.

Total noise generated [dBA]	Flighpath 2050	Zephyr One
Fly-over	59	44 - 51
Lateral	69	63 - 68
Approach	72	65 - 71

The results of this preliminary noise estimation portrayed in Table 11.7 show that the overall noise levels of the Zephyr One meet and exceed the requirements set by Flightpath 2050. The estimated noise levels are displayed as a range of values attributed to the best and worst case scenarios from the range of noise reduction seen in Table 11.6. However, it is not likely to reach the highest estimated levels, since future LNTs are expected to be even more effective at reducing noise. Further

improvements to the noise estimation methodology, as well as possible improvements to the design that lead to further noise reduction are described in Section 11.8.

11.7. Verification & Validation

After having generated the code used to assess the noise generation of the Zephyr One, it is important to verify and validate it to ensure the accuracy and correctness of the results. The verification procedure is explained in Section 11.7.1, while validation is explained in Section 11.7.2.

11.7.1. Verification

In order to verify the computations for the noise levels of the Zephyr One, a set of unit test was performed on each of the functions. In these unit tests, the input was changed to simplify hand calculations. The output of the hand calculations was compared to that of the Python script, where it was determined that the absolute difference between the two methods was at most 10^{-6}. As a result, the computations are considered to be verified.

11.7.2. Validation

In order to perform validation on the Python scripts used to generate the noise levels of the Zephyr One, the output of the code has to be compared to real life noise data. However, as this code is very specific to a Flying-V type aircraft, and there are no published noise estimation for such an aircraft, it is impossible to validate that way. On the other hand, in order to use the script for a conventional aircraft, it would require extensive modification which in turn defeats the purpose of validation. Therefore, in future work, a more general noise estimating procedure will be developed that encompasses both conventional and non-conventional aircraft.

11.8. Recommendations

While the preliminary noise estimation produced satisfactory results regarding the noise levels of the Zephyr One, more detailed methods for noise estimation must be investigated once more details about the design are available.

In terms of the engine noise prediction, a number of improvements can be made to the noise estimation method. In order to more accurately determine the noise generated by the fans, Stone's method as presented by Bertsch [65] can be used, as it takes into account the directivity as well as more detailed engine dimensions such as nozzle shape, exhaust jet velocity, and exhaust jet temperature to name a few. In addition to this, more accurate techniques for determining fan, combustion, and turbine noise as used by NASA's ANOPP can be examined [75].

The BSM used in this report for obtaining the noise reduction due to shielding, while easy to implement, is not very accurate. Therefore in future work, Kirchoff's theory of diffraction [69] will be implemented. The procedure for obtaining the airframe noise can also be improved, as more modern methods have been developed for determining clean wing and landing gear noise.

In addition to all these improvements, more research into noise reduction technologies can be performed. The implementation of boundary layer suction, as discussed in the Midterm report [3], can be considered for future design work. This mechanism allows to reduce the thickness of the boundary layer and consequently turbulent flow, thus further reducing noise.

Finally, concerning CDO and CCO, optimisations could be done based on different parameters, such as the airport location and population density, to find the optimal angle for take-off and approach.

12 Flight Performance

The performance of the Zephyr One during flight is examined in this section. First, a payload-range diagram is constructed in Section 12.1. Next, the loading diagram of the is presented in Section 12.2. Subsequently, Section 12.3 displays the manoeuvre and gust load diagrams.

12.1. Payload-Range Diagram

Figure 12.1 displays the payload-range diagram of the Zephyr One compared to that of the Airbus A321neo. It is clearly visible that the Zephyr One can carry a greater payload mass at every range inspected. In addition to that, the Zephyr One has a greater maximum range than the A321neo. The point at which the Zephyr One carries 200 passengers and their luggage, is displayed as a red cross, where the range is 7,249 km and the payload is 21,315 kg. At maximum payload, which includes passengers, luggage and cargo, the range is 6,482 km. The maximum possible range of the Zephyr One, without any payload, is 10,950 km.

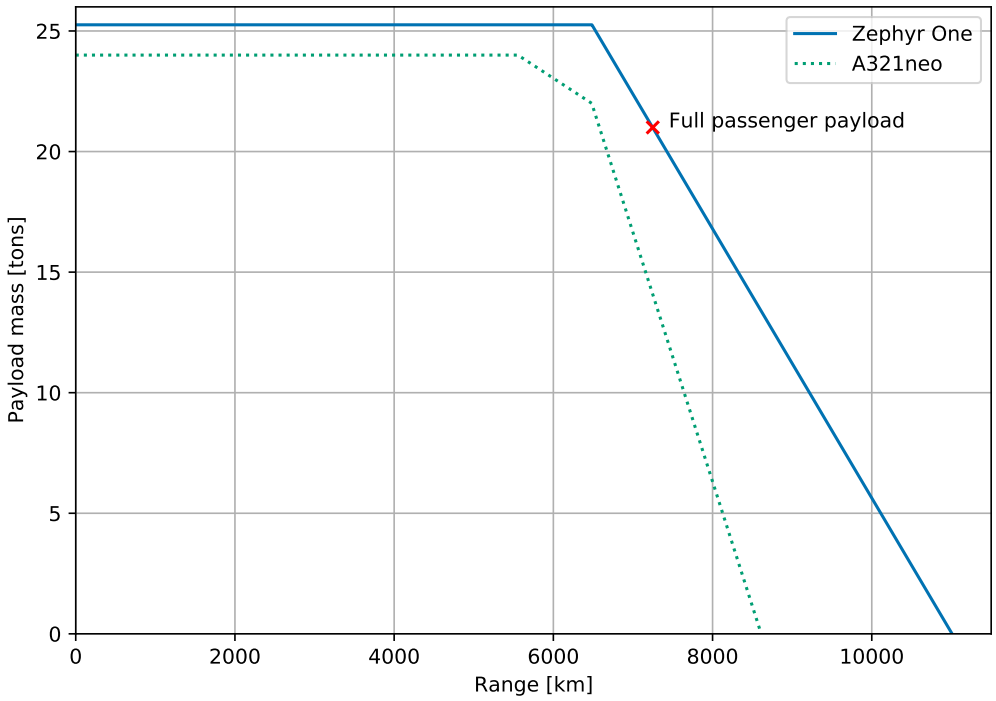

Figure 12.1: Payload-range diagram of the Zephyr One and A321neo.

12.2. Loading Diagram

The final loading diagram for the Zephyr One can be seen in Figure 12.2. Here the most bottom right point in the feasible space is selected as the optimal configuration, at which the wing loading is determined to be 1908.2 N/m^2 and the thrust loading is 0.203.

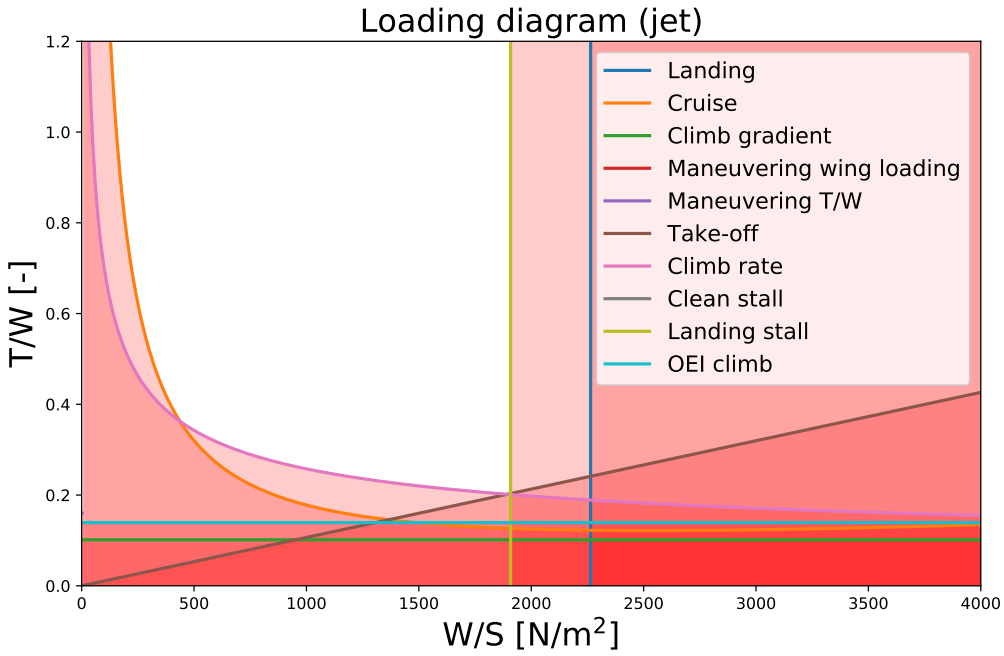

Figure 12.2: Loading diagram of Zephyr One.

12.3. Manoeuvre and Gust Load Diagram [3]

In this section, the manoeuvre and gust load diagrams are constructed. These are then displayed in Figure 12.3.

12.3.1. Manoeuvre Load Diagram

In this diagram, the load factor is depicted as a function of Equivalent Air Speed (EAS). These are converted from True Air Speed (TAS) using Equation 12.1. For the first part of the plot, Equation 12.3 is utilised to relate the load to the velocities, where the velocities range from zero to the manoeuvring speed at which the maximum load factor is equated to 2.5 taken from CS-25 regulations. The manoeuvring speed is computed via Equation 12.4. The graph is mirrored around the velocity axis until the maximum allowed negative load factor of -1. The velocity of the aircraft at that point corresponds to the stall speed. This can also be seen using Equation 12.3 with a load factor of 1. The maximum lift coefficient is 1.39 is determined in Section 5.5.3. The wing loading is determined from the loading diagrams in Section 12.2 is 1908.2 N/m^2.

On the top part of the graph, a line is drawn from the manoeuvring speed to the dive speed, which is defined as 1.25 times the cruise speed. On the bottom of the graph, the load factor stays at -1 between the cruise and dive speeds. Finally, a straight line connects the -1 load factor at cruise speed with 0 attained at the dive speed.

$$EAS = \sqrt{\frac{\rho}{\rho_0}} \cdot TAS \tag{12.1}$$

$$V_{C,EAS} = \sqrt{\frac{\rho}{\rho_0}} \cdot V_{C,TAS} = 113.1 m/s \tag{12.2}$$

$$n = \frac{L}{W} = \frac{\frac{\rho v^2}{2} C_{L,max}}{\frac{W}{S}} \tag{12.3}$$

$$V_A = \sqrt{\frac{2n\frac{W}{S}}{\rho_0 C_{L,max}}} = \sqrt{\frac{2 \cdot 2.5 \cdot 1908.2}{1.225 \cdot 1.39}} = 74.7 m/s \tag{12.4}$$

12.3.2. Gust Load Diagram

In addition to the manoeuvre loads, the aircraft should also be able to withstand the loads induced by gusts in different flight conditions, namely at cruise and dive velocities [76]. The values of the gusts are given by airworthiness authorities and are listed in Table 12.1.

Table 12.1: Gust speed at different flight conditions.

Flight condition	u [feet/s]	u [m/s]
Cruise	50	15.24
Dive	25	7.62

The load factor is computed for the cruise and dive velocities obtained in Section 12.3.1 using Equation 12.5. All velocities are in EAS converted from TAS at cruise conditions. The lift curve slope is obtained from Section 5.5.3, while the wing loading remains the same as in Section 12.3.1.

$$n = 1 + \Delta n = 1 + \frac{u \rho V C_{L_\alpha}}{2 \cdot (W/S)} \tag{12.5}$$

The manoeuvre and gust load diagrams can be seen in the figure below.

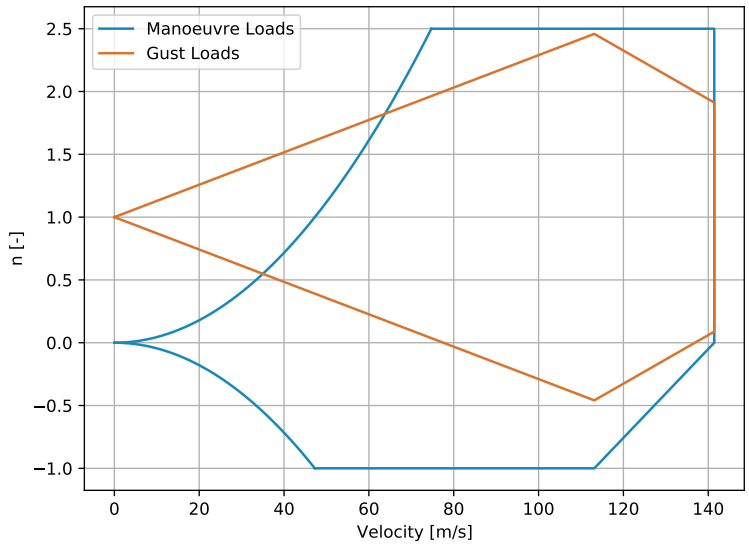

Figure 12.3: Manoeuvre and gust diagram of Zephyr One.

13 Operations & Logistics

For an aircraft to enter service, not only does it have to adhere to technical requirements, it must also comply with airport regulations and operational procedures dictated by various organisations, such as ICAO, FAA, and EASA. Therefore, performance aside, it is important to ensure that the aircraft is operationally feasible and advantageous for airports, airlines, and Air Traffic Services (ATS). This section will detail the operations and logistics associated to the Zephyr One, as well as the benefits brought by this revolutionary design.

The requirements related to operations and logistics are listed in Table 13.1 and will be expanded upon in the following sections.

Table 13.1: Airport requirements for operations & logistics.

EFMRA-SYS-AP-01	The aircraft shall be able to operate at a 4C type aerodrome.
EFMRA-SYS-AP-01.1	The aircraft shall have a wingspan not larger than 36.8 m.
EFMRA-SYS-AP-01.2	The aircraft shall have a tail height not larger than 13.7 m.
EFMRA-SYS-AP-02	The aircraft shall have a turnaround time of no more than 52 min.
EFMRA-SYS-AP-03	The aircraft shall be compatible with existing ground material for the loading and unloading of passengers.

13.1. Airport & Aircraft Classification Schemes

Most information stated in this section is taken from two courses of the Minor program *'Airport of the Future'* taught at Delft University of Technology. These courses are AE3502-14 *'Airport Planning, Design and Operations'* [77, 71, 78], coordinated by Ir. P.C. Roling, and AE3501-19 *'Air Transportation'* [79], coordinated by Dr. Ir. A. Bombelli.

Different organisations have different ways of categorising aircraft, hence many aircraft design classification schemes exist. The main ones, relevant to airport operations and aircraft performance are as follows:

- Aircraft design group classification
- Runway load classification
- Noise classification
- Wake-vortex classification
- Approach-speed classification

The first two are related to airport infrastructure and whether or not a certain aircraft is suited to operate at a particular airport, based on its dimensions, MTOM, and required maintenance. The last three points affect the airport's airside capacity, such as runway usage, approach speed, and noise regulations.

13.1.1. Airport Infrastructure

For an aircraft to make use of a particular airport, it is important for both parties to be compatible. This refers to geometrical aspects, size, and loads. Airports are designed to provide sufficient space for the movement of aircraft through a set of design standards driven by safety considerations. These relate to runways, taxiways, aprons, and gates, for which standardised dimensions dictated by ICAO or the FAA must be followed [77]. Consequently, the Zephyr One's category must be established in order to set the range of airports at which it could operate.

The ICAO aerodrome reference code (also included in ICAO Annex 14 [80]) is used to categorise aircraft based on their geometrical properties[1]. It contains two elements i.e. one number (1-4) and one letter (A-E), of which the first one determines the reference field length (take-off length), and the second element is attributed based on a combination of aircraft wingspan and outer main landing gear wheel span. Requirement **EFMRA-SYS-AP-01** states that the aircraft must be classified as type 4C to be comparable to the A320 family. This is partly confirmed by requirement **EFMRA-SYS-PF-05**, which states that the aircraft's take-off distance must not exceed 2,100 m, thus leading to the first digit of the ICAO aerodrome reference code: 4. The second element of the reference code, C, requires the Zephyr One to have a wingspan between 24 and 36.8 m and an outer main gear wheel span ranging from 6 to 9 m, as stated in ICAO Annex 14 [80]. These dimensions also correspond to those of the FAA Airplane Design Group (ADG) III [81], which comes with additional requirements for the tail height. The latter must be between 9 to 13.7 m, as stated in requirement **EFMRA-SYS-AP-01.2**. Since the Zephyr One does not have a tail, the lateral fins will be used instead to assess the compliance of this requirement [82].

The values needed for the operational aspects of the aircraft are shown in Table 13.2, where the MTOM, wingspan, and outer main gear wheel span all comply with the values stated previously. Therefore, the first three requirements from Table 13.1 may be considered to be fulfilled.

Table 13.2: Parameters needed for the operational & logistical aspects of the Zephyr One.

Parameter	Value	Requirement Value
Take-off length [m]	2,100	2,100
Wingspan [m]	36	24 - 36.8
Outer MLG wheel span [m]	6.21	6 - 9
Tail height [m]	12.77	9 - 13.7
MTOM [kg]	81,094.10	-
OEM [kg]	42,311.55	-
Approach speed [m/s]	61.44	-

The runway load classification is also important for operational aspects. Indeed, depending on the aircraft's MTOM, OEW, and the flexibility/rigidity of the runway, one can determine the Aircraft Classification Number (ACN). The latter describes the relative load intensity of an airplane's main landing gear. More specifically, the ACN *"is a number that expresses the relative effect of an aircraft at a given configuration on a pavement structure for a specified standard subgrade strength"*[2]. Aircraft manufacturers are required to calculate this number for any new aircraft coming into service, and ICAO has already calculated it for a number of selected aircraft. The A320's ACNs are shown in Table 13.3 for different runway pavement types, subgrade categories, and weights. The MTOM and OEM considered are 83,384 kg and 46,993 kg, respectively [83]. The flexible pavement subgrade is given in CBR, which stands for 'California Bearing Ratio', and the rigid runway subgrades are specified through k. While the latter is a measure of pressure per unit length, the CBR is *"a penetration test for evaluation of the mechanical strength of natural ground, subgrades and base courses beneath new carriageway construction"*[2].

Table 13.3: Aircraft Classification Numbers of the A320-200 for different runway pavement types [83].

	Flexible pavement subgrades - CBR [%]				**Rigid pavement subgrades - k [MPa/m]**			
	High	Medium	Low	Very low	High	Medium	Low	Very low
	A	B	C	D	A	B	C	D
	15	10	6	3	150	80	40	20
MTOM	45	48	53	59	51	54	57	59
OEM	23	24	26	30	26	28	29	31

[1] https://www.skybrary.aero/index.php/ICAO_Aerodrome_Reference_Code [cited on 7 June 2021]

[2] https://www.skybrary.aero/index.php/Aircraft_Classification_Number_(ACN) [cited on 8 June 2021]

Due to the similarity of the Zephyr One's MTOM and OEM with the A320-200 series presented above, its ACNs are expected to be very similar. Therefore, the numbers listed in Table 13.3 may be used to assess the runway load classification of the design.

With the geometrical aspects of the two aircraft being very close to each other, and considering that they both belong to ICAO group 4C, it is also assumed that all airport infrastructure, including gates, vehicles, and refueling facilities, will also be compatible with the Zephyr One. As the design complies with requirement **EFMRA-SYS-AP-01**, it is able to operate at a 4C type aerodrome, and according to the previous assumption, this means that requirement **EFMRA-SYS-AP-03** is also met. That is, the aircraft will be compatible with existing ground material for loading and unloading passengers. This is also logical since the ground material present at airports must be compatible with the operating aircraft, and vice versa.

13.1.2. Airport Capacity

The Zephyr One shall not, under any circumstances, negatively affect the capacity of the airport at which it operates, as that would not be beneficial for external parties. Airport capacity is affected by many factors including its infrastructure, the number of runways and their configuration (as well as usage configuration), but also aircraft approach speed, noise category, and wake-vortex classification. The Zephyr One is expected to facilitate airport operations and have minimal interference with other aircraft movements.

The wake-vortex classification of an aircraft is given by the ICAO Wake Turbulence Category (WTC), which is solely based on the aircraft's MTOM[3]. Table 13.4 shows the main wake turbulence categories with their corresponding weight ranges. Note that the "super heavy" category was only introduced recently with the appearance of the A380, which is currently the only civil aviation aircraft classified in this group. For safety reasons, the wake vortex generated by an aircraft when landing or taking off must be dissipated before the next aircraft lands or takes off. To ensure this, a minimum separation distance d is set by ICAO depending on the WTC of the leading and trailing aircraft, as shown in Table 13.5[4]. This is also illustrated in Figure 13.1, where the distance between the three main categories of aircraft is obvious.

Table 13.4: Aircraft wake turbulence categories[3].

WTC	Description	MTOM [kg]
J	Super (A380)	Max: 560,000
H	Heavy	$\geq$ 136,000
M	Medium	7,000 - 136,000
L	Light	$\leq$ 7,000

Table 13.5: Wake vortex separation distance [84].

Aircraft Wake Turbulence Separation				
Leading / Trailing	A380	Heavy	Medium	Light
A380	8 km	6 km	6 km	6 km
Heavy	12 km	8 km	6 km	6 km
Medium	13 km	10 km	6 km	6 km
Light	15 km	12 km	10 km	6 km

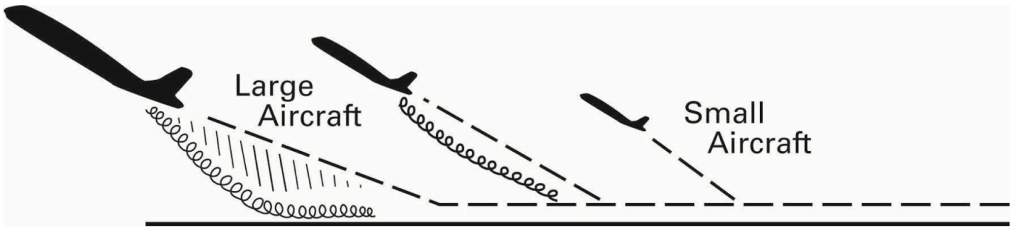

Figure 13.1: Wake turbulence separation distance, illustrated for take-off [85].

[3] https://www.skybrary.aero/index.php/ICAO_Wake_Turbulence_Category [cited on 8 June 2021]

[4] https://www.skybrary.aero/index.php/Mitigation_of_Wake_Turbulence_Hazard#Minimum_Distance_Separation [cited on 8 June 2021]

In addition to the separation distance, the minimum permitted separation time T_S is defined. The latter is obtained by converting the separation distance standard to time, as shown in Equation 13.1. To do so, the approach speeds of the leading and trailing aircraft (V_L and V_T, respectively) are used. Note that when the leading aircraft is faster than the trailing aircraft, an increase in separation distance (denoted by o) on the common final path is added to the separation distance standard d, to avoid them getting dangerously close to one another.

$$T_S = \frac{d}{V_T} \text{ , if } V_T \geq V_L \quad ; \quad T_S = \frac{d+o}{V_T} \text{ , if } V_T \leq V_L \tag{13.1}$$

This leads to the discussion of the approach-speed classification introduced earlier. ICAO's approach speed categorisation is used to differentiate aircraft based on the speed at which they fly during the approach phase. All five groups are shown in Table 13.6 with their corresponding IAS range.

Table 13.6: Approach speed categorisation[5].

Group	Approach IAS [kts]	Approach IAS [m/s]
A	< 91	< 46.8
B	91 - 120	46.8 - 61.7
C	121 - 140	62.2 - 72
D	141 - 165	72.5 - 84.9
E	> 166	> 85.4

The scheduled inter-arrival time T_{SIA} between two successive aircraft at the runway threshold is obtained by adding a buffer time T_B to T_S because of delivery uncertainty, i.e. $T_{SIA} = T_S + T_B$. Finally, the runway capacity C may be calculated as shown in Equation 13.2, where p_{ij} is the probability that a leading aircraft i (i = L, M or H) will be followed by a trailing aircraft j (j = L, M or H).

$$C = \frac{1}{T_A} \text{ , with } T_A = \sum_i \sum_j p_{ij} \cdot T_{SIA_{ij}} \tag{13.2}$$

p_{ij} is found based on the traffic composition or traffic mix p_{mix} at a specific airport, as shown in Equation 13.3. The latter consists of the three classes of aircraft from Table 13.4 (L, M, H) and their respective probabilities denoted by the matrix $[p_{mix}] = [p_L \quad p_M \quad p_H]$.

$$[p_{ij}] = [p_{mix}]^T [p_{mix}] \tag{13.3}$$

Even though the capacity is largely influenced by the traffic composition, it is important to reduce the separation distance d and minimum permitted separation time T_S to maximise runway capacity. This is possible when a more homogeneous traffic mix is achieved. The Zephyr One is classified as Medium (M) for its WTC and B for the approach speed category, according to the MTOM and approach speed listed in Table 13.2. Therefore, it will not largely alter p_{mix} by introducing a too heavy or too light aircraft in the traffic composition. On the contrary, for an airport mainly operating medium-range flights with a majority of medium aircraft, the Zephyr One actually contributes to the optimisation of the facility's runway usage. Looking at it on a more singular level (ignoring p_{mix}), such as shown in Figure 13.1, it is obvious that introducing a too heavy aircraft will be diminishing towards lighter aircraft, as it would only increase d and T_S. However, with the Zephyr One's WTC M and approach speed category B, a lower separation distance d and minimum permitted separation time T_S may be achieved, thus benefiting the airport's airside capacity.

[5] https://www.skybrary.aero/index.php/Approach_Speed_Categorisation#ICAO_Aircraft_Approach_Category [cited on June 8 2021]

13.1.3. Noise Classification

The noise levels presented in Table 11.7 have proven to comply with Flightpath 2050 requirements. Furthermore, since the reference values used for the derivation of these requirements were those of the A321, the Zephyr One has demonstrated that it performs better in that aspect. As a result, no constraints are expected to be applied to this aircraft regarding noise regulations.

As already explained in the Midterm report [3], Figure 13.2 shows the maximum Effective Perceived Noise Levels (EPNL) set by ICAO in its Annex 16 [86]. These depend on the MTOM of the aircraft as well as the number of engines.

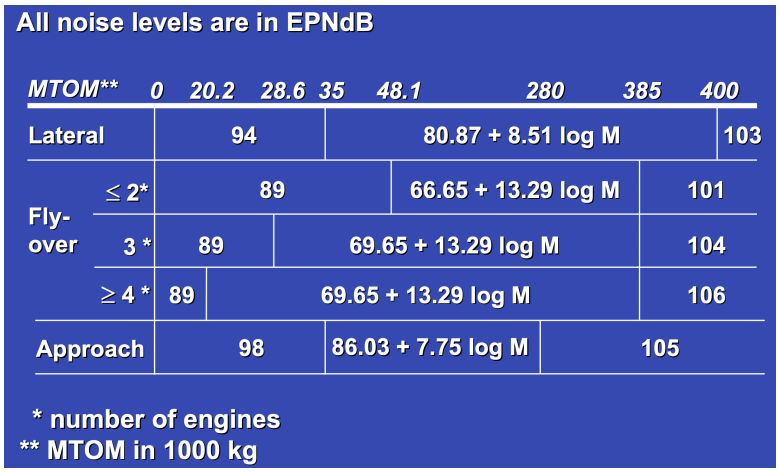

Figure 13.2: Maximum noise levels set by ICAO, Annex 16, Volume 1, Chapter 4 [56].

Since the MTOM has already been computed and it is known that a total of two GTFs are used for the design, the maximum noise levels dictated by ICAO can also be calculated based on the formulas from Figure 13.2. The results are shown in Table 13.7 and correspond to *current* maximum noise levels, used worldwide.

Table 13.7: Maximum noise levels set by ICAO stage 4, based on MTOM, number of engines, and Figure 13.2.

Max. EPNL [EPNdB]	Fly-over	Lateral	Approach
ICAO stage 4	92	97	100
Flightpath 2050	69	79	80
Zephyr One	44 - 51	63 - 68	65 - 71

As can be seen in Table 13.7, the maximum EPNL values derived from ICAO's Annex 16 [86] are much larger than those set for the Flight Path 2050 requirements. It is only logical that, in the future, the maximum noise levels dictated by ICAO will be lower, and consequently closer to those required by Flightpath 2050. Since the Zephyr One already complies with these requirements, it also complies with the maximum noise levels set by ICAO. Hence, as expected, there are no operational limitations for the design regarding noise standards.

Regarding surface operations, electrical power is preferred. In the Baseline report [2], it was advised to incorporate electric taxiing, set limits on outbound taxiing aircraft, and limit the number of engine run-ups and testing. Finally, the use of the Auxiliary Power Unit (APU) should be limited as it is a significant source of noise during ground operations [71]. These will be further detailed in the next section.

13.2. Logistics

After having analysed the airport and aircraft classification schemes, one must examine the logistical aspects related to the operation of the Zephyr One. These include refueling, turnaround, electric taxiing, and battery charging, which are detailed in Sections 13.2.1 through 13.2.4, respectively.

13.2.1. Refueling

With the Zephyr One's unconventional fuel source comes the logistical complexity of refueling operations. Indeed, airport infrastructure is not yet adapted to LNG, however, it may be feasible in the coming years, assuming airport infrastructure and pipeline system are adapted accordingly.

Although refueling operations vary depending on the size of the airport and its accessibility to different types of facilities, the outline of this procedure is as follows. Currently, refueling with kerosene is done as shown in Figure 13.3. First, the fuel arrives at the receiving facility where it enters a large pipeline system connected to the airport. At the airport, kerosene is stored in large tanks, located at a significant distance from the aircraft stands, due to safety considerations. A delivery pump and hydrant piping are then used to deliver the fuel to the aircraft. In some cases, there may not be a pipeline system between the storage facility and the aircraft. In that case, kerosene delivery is facilitated by tank trucks.[6]

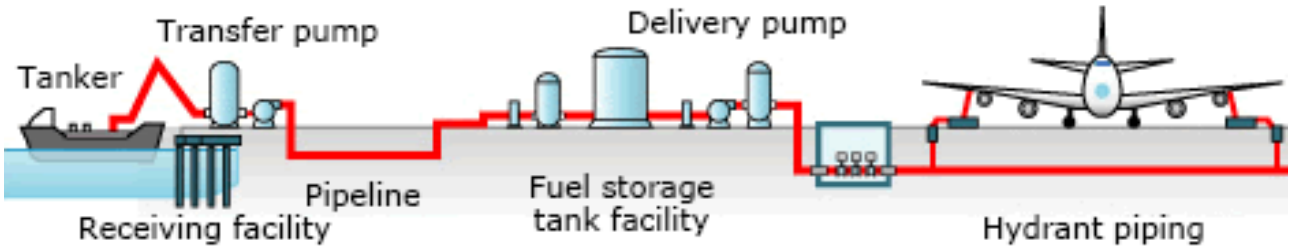

Figure 13.3: Aircraft refueling pipeline system[6].

As LNG has large differences in comparison to kerosene, current airport infrastructure may not be used to store or transfer this type of fuel. The storage temperatures and densities of both fuel sources are shown in Table 13.8, where it becomes clear that much larger fuel tanks will be needed for LNG storage. Additionally, the difference between temperatures at which kerosene and LNG must be stored is immense. To store the Zephyr One's fuel source, one must ensure appropriate insulation to achieve and maintain cryogenic temperatures, as LNG must be stored at circa -160°C. Note that, as efficient as an insulation may be, it will not keep such low temperatures on its own. "*LNG is stored as a "boiling cryogen," that is, it is a very cold liquid at its boiling point for the pressure it is being stored.*"[7] Therefore, when stored at constant pressure, LNG will stay at near constant temperature as long as the vapour boil off is allowed to exit the tank. Pipelines must also be adapted such to maintain cryogenic temperatures and liquefaction facilities must be introduced to ensure safe and effective refueling. Last but not least, leakage must be avoided at all cost, especially in case of possible contact with water, since the two elements may produce a violent reaction [87]. Finally, although LNG is generally more advantageous than kerosene, "*Methane slip during operations can lead to global warming as CH_4 has a higher greenhouse potential than CO_2, approximately 34 times compared to CO_2 over a 100-year period*" [88].

[6] `https://www.jfe-eng.co.jp/en/products/energy/ene06.html` [cited on 21 June 2021].
[7] `https://www.ch-iv.com/all-about-lng/` [cited on 21 June 2021].

Table 13.8: Storage temperatures and densities of LNG and kerosene.

Fuel tye	Storage temperature [°C]	Density [kg/m^3]
LNG	-160[8]	463.2[9]
Kerosene [89]	-40 to 38	775 to 840 (at 15°C)

Overall, it is clear that major infrastructural changes must be implemented to allow the design's operation and compatibility with current airports. Most of the fuel production, storage, and transportation will need to be updated, causing a major shift in the aviation industry, if it is to introduce LNG as an alternative fuel source on a larger scale [90].

13.2.2. Time Efficiency

Performance aside, the aircraft configuration must be used in the most efficient manner to benefit all stakeholders, including airline operators and airports. Consequently, turnaround time and ground operations must be optimised accordingly. As stated in requirement **EFMRA-SYS-AP-02**, the Zephyr One shall have a turnaround time of no more than 52 minutes in order to compete against the A320 family.

The structure of the aircraft is beneficial for achieving efficient turnaround operations. According to M. Schmidt [91], a Twin-Aisle (TA) aircraft configuration is more efficient than a Single-Aisle (SA) of similar passenger capacity for boarding time. Indeed, the TA configuration is proven to outperform the SA one by up to 50%. This is mainly due to fewer seat interference and slightly reduced walking distances. Furthermore, "switching from a SA layout to a TA configuration allows for a passenger flow separation into two different streams. This shortens the queue lengths and number of aisle interferences" [91]. Even though the Zephyr One does not qualify as a conventional twin-aisle aircraft, it is still expected that due to its V-shape and dual-fuselage configuration, the turnaround time will be very similar to the one of a TA configuration with comparable passenger capacity. In the effort to further reduce turnaround time, one may also optimise the usage of doors. When using both front and aft doors simultaneously for passenger processes, one could reduce boarding time between 30% to 35% instead of using only the front door [92].

Finally, when making use of a multi-purpose towing vehicle, such as the *SkyGate* vehicle, turnaround time may be further reduced [93], while also decreasing fuel consumption by up to 8% [94]. "*The vehicle combines the functions of a towing truck, a shuttle bus and a jetbridge into a single multi-functional vehicle driven by electric motors and controlled autonomously*" [91]. The idea is that while passengers disembark, *SkyGate* simultaneously tows the aircraft to its parking position. Hence, right after clearing the runway, the vehicle docks to the aircraft and starts towing it to the assigned gate. Since *SkyGate* operates electrically, the main engines are switched off, so fuel is saved and noise levels on the ground are reduced. Even though electric taxiing is already implemented in the design, this vehicle allows for faster boarding procedures and may also benefit the power budget by saving battery power from the electric taxiing system. More specifically, taxiing would be performed by the electric taxiing system, but after clearing the taxiway, the *SkyGate* vehicle would tow the Zephyr One while also disembarking passengers. Of course, this would only be possible at airports where the *SkyGate* vehicle is available. Elsewhere, taxiing and towing would both be facilitated by the electric taxiing system. In conclusion, the last requirement from Table 13.1 is largely expected to be met and even exceeds the expectations. In terms of time efficiency, the Zephyr One will be a fierce competitor for the A320.

[8] `https://www.ch-iv.com/all-about-lng/` [cited on 21 June 2021]

[9] `https://www.unitrove.com/engineering/tools/gas/liquefied-natural-gas-density` [cited on 21 June 2021]

13.2.3. Electric Taxiing

As detailed in Section 6.4.1, instead of using conventional towing trucks, the Zephyr One is equipped with an integrated electric taxiing system. The latter enables the aircraft to manoeuvre on the ground without requiring the use of main engines or any external vehicles for push-back. Removing this dependency allows to reduce turnaround time, since the aircraft would be autonomously taxiing. Furthermore, this also increases safety as the pilot is now in control of ground manoeuvring instead of relaying on towing trucks. In addition to taxiing, this system also enables automated push-back, once again increasing the autonomy of the design in regards to ground operations [78].

The electric taxiing system not only benefits turnaround time, but also reduces noise, emissions, and even fuel consumption, which are crucial in complying with Flightpath 2050 requirements. Safran claims that their electric taxiing system decreases fuel consumption by 4%, while NO_x and CO_2 emissions are estimated to be reduced by 51% and 61%, respectively[10]. With all these benefits in mind, the issue of power supply arises which leads to the logistical aspects of battery charging.

13.2.4. Battery Charging

As stated in Section 6.4.4 a total energy E_{bat} of 180.78 kWh is required from the batteries, resulting in a mass of 753.25 kg. Rechargeable lithium batteries will be used for this purpose and their charging time must be assessed to verify that it does not exceed the maximum turnaround time of 52 minutes. For this purpose, it was assumed that by the time the Zephyr One enters service, ultrafast charging points will be facilitated across most airports, providing a charging power P_{bat} between 350 to 450 kW [95]. Considering the batteries' depth of discharge (DoD) of 80%, one can easily estimate the charging time as shown in Equation 13.4. Note that an average value of 400 kW is taken for P.

$$\text{average charging time} = \frac{P_{\text{bat}} \cdot DoD}{E_{\text{bat}}} = \frac{180.78 \cdot 0.8}{400} \cdot 60 = 21.69 \text{ min } < 52 \text{ min} \tag{13.4}$$

The worst case scenario was also considered, as shown in Equation 13.5. Even with the minimum charging power, the maximum charging time remains much lower than the maximum required turnaround time of 52 minutes.

$$\text{max. charging time} = \frac{P_{\text{bat}} \cdot DoD}{E_{\text{bat, min}}} = \frac{180.78 \cdot 0.8}{350} \cdot 60 = 24.79 \text{ min } < 52 \text{ min} \tag{13.5}$$

As both charging times calculated above do not exceed the maximum turnaround time, recharging the batteries is proven to not be a limiting factor for requirement **EFMRA-SYS-AP-02**. Therefore, adding to Section 13.2.2, the requirement for turnaround time will be achieved by far and can be considered satisfied.

13.3. RAMS

In this section, the reliability, availability, maintainability and safety of the Zephyr One will be analysed. They will initially be analysed separately. However, it will rapidly become clear that they are inherently connected.

13.3.1. Reliability

Complete reliability assessment is not yet possible in this design stage, as there are still many unknowns in the design. However, it is possible to analyse and identify expected difference with relation to the reference aircraft.

[10] `https://www.safran-landing-systems.com/video/2355` [cited on 18 June 2021]

The first major difference with the reference aircraft is the more-electric aircraft architecture. This eliminates the need for complex hydraulic and pneumatic systems, and significantly reduces the number of moving parts. Furthermore, this decreases the chance of a leak, since the electric system is not reliant on pressurised fluids.

Another major difference with the reference aircraft is the propulsion system. Whilst the different fuel used should have little to no impact on the reliability of the engines, the SCR introduces a new subsystem compared to the reference aircraft. However, this system includes a limited number of moving parts and will therefore have minimal impact on the reliability.

The Flying-V aerodynamic concept is also a major differing factor. This concept increases the overall reliability of the aircraft, since elevators and ailerons are combined into elevons, thus reducing the number of potential failure points. Furthermore, the absence of high lift devices further decreases the number of moving parts and, thus, increases reliability.

13.3.2. Availability

In this subsection, the availability of all items required to successfully operate the aircraft will be assessed.

The availability is split into 3 types, the availability of materials required to build the aircraft, the availability of operational items, and that of trained personnel to fly and handle the aircraft. Since the aircraft uses no exotic materials, the availability of materials is presumed to be no issue.

The first of the critical operational items is the fuel. Since the aircraft can operate on LNG, fuel availability will not be an issue. However, in order to meet the CO_2 emission requirement, the aircraft will need to run mainly on synthetic methane. The availability of this form of methane might cause a problem, mainly in the earlier phases of the Zephyr One's service period. It is expected that in 2036 not all airports will have a supply of synthetic methane, however by 2050 more and more gas grids are expected to be converting from LNG to synthetic methane [96].

The next critical operational item considered is the reducing agent. Anhydrous amonia is already produced in large quantities for usage as a fertilizer in agriculture. Therefore, it is expected to be readily available for usage.

The final category considered is the operational personnel, including pilots, ground handling crew and cabin crew. The ground handling crew will have to be trained to be able to safely handle the liquid methane, as well as the rector fluid. Furthermore, ground maintenance crews will have to be trained for inspection and maintenance on the Zephyr One. Pilots will have to be trained in order to fly the Zephyr One in commercial service. To aid with this process, simulators will have to be designed and produced. Finally, cabin crew will have to be trained to handle the Zephyr One's unconventional cabin layout in case of an evacuation or other emergency.

13.3.3. Maintainability

Maintainability is an important factor in aircraft design, since long and and frequent maintenance overhauls are preferably avoided.

Structural maintenance technologies are driven by material selection. Similarly to any other aircraft, visual inspections should be performed before each flight in order to ensure no serious damage has been imposed on the structure. Furthermore, detailed inspections utilizing non-destructive testing for cracks can be performed.

Some methods are applicable for the entire aircraft assembly, and other methods can only be performed for detached components, such as engines or control surfaces. When the entire aircraft is investigated, eddy currents can be used in order to identify cracks near fasteners in metallic struc-

tures, and ultrasonic techniques can be utilised in order to detect delaminations in the composite components. X-ray methods could also be applied, but they require special equipment, specialists, and a cleared area. When the components are analysed individually, dye penetrants are suitable to detect cracks in metals (e.g engines), or components might be submerged in water in order to perform ultrasonic methods or apply magnetic ink methods. In case serious damage is detected, components should be replaced.

In general, the required maintenance can be expected to be similar to the maintenance required for conventional aircraft. However, there are some small but significant differences.

First of all, due to the absence of high-lift devices, and the elevons being employed instead of separate elevators and ailerons, the Zephyr One contains a lower amount of moving aerodynamic parts, thus requiring relatively less maintenance in these areas.

However, since the engines are placed on top of the aircraft, engine maintenance is significantly more difficult. Even for regular pre-flight checks, specialised equipment in order to reach and view into the engine is required. For regular scheduled maintenance, dedicated hangars with dedicated equipment for the Zephyr One will be required, due to the unconventional shape and engine placement.

The SCR system for NO_x emissions will not require significant maintenance, the tank will have to be structurally inspected, and the pumps will be checked and maintained in the same intervals as the fuel system pumps. The catalyst itself will have to be replaced every six to eight maintenance intervals [29]. During maintenance to the SCR system, measures to prevent inhalation of ammonia vapors will have to be taken.

13.3.4. Safety

The Zephyr One will comply with all current safety standards set out by CS-25 and ICAO. Therefore, the safety of the aircraft can be assumed to be equal to that of current aircraft. Whilst the aircraft contains several novel technology's, they will be thoroughly tested before the Zephyr One takes to the sky, and any issues with them will thus be detected and mitigated long before they can cause any safety concern.

Moreover, the aircraft features methane, as fuel source, which in some cases is more safer than regular jet fuel. This fuel is lighter than air and in case of engine fire this is good thing for safety. Due to the lightness of methane the fuel flow can be just shut off to extinguish the fire.

14 Financial and Competitive Analysis

For the Zephyr One to be successful, there needs to be sufficient demand for medium-range 200-seat aircraft and requirements on costs and a competitive market entry outlined in Section 14.1 need to be met next to the requirements on performance, noise and emissions. Figure 14.1 shows the process that is followed for the financial analysis. Building on the market analysis from the Baseline Report [2], in Section 14.2 the market analysis will be updated with the final design parameters of the Zephyr One in mind, followed by a discussion of the production quantity, which is driven by the market analysis, in Section 14.3. In Section 14.5 and Section 14.6, the production and development costs are discussed and combined into an estimate on the cost of goods estimate in Section 14.7. Using the aircraft sales price (ASP) outlined in Section 14.4, a return on investment (ROI) is computed for the Zephyr One in Section 14.8 concluding the financial analysis of the aircraft program. The analysis of program costs is followed by an analysis of the operating costs in Section 14.9 discussing the Direct Operating Costs (DOC), followed by an assessment on the disposal and recycling costs in Section 14.10 and a life cycle costs assessment in Section 14.11. The chapter is concluded with a competitive analysis discussing the unique selling points and comparisons with reference aircraft in Section 14.12.

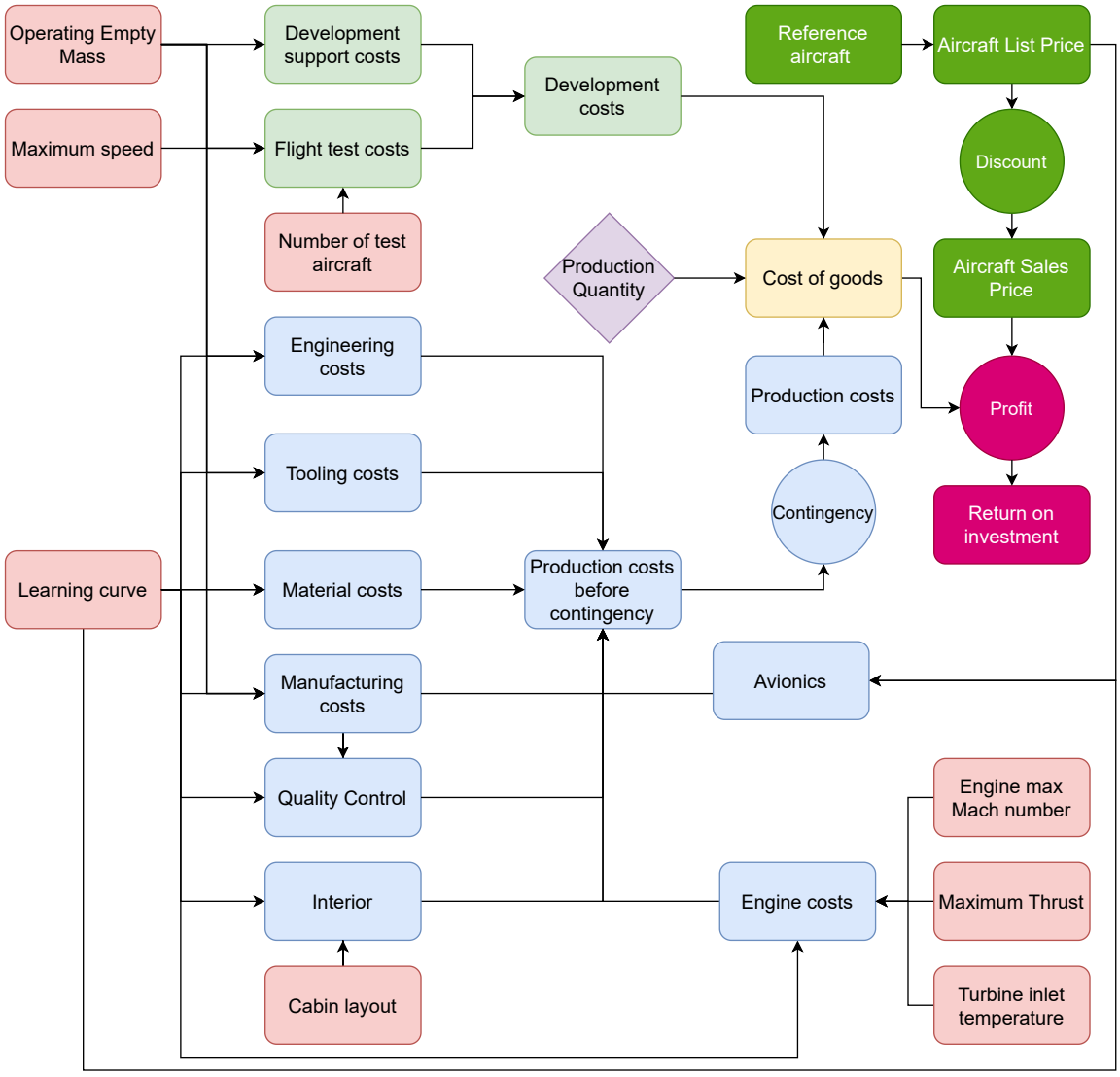

Figure 14.1: Estimation process return on investment, development and production costs.

14.1. Requirements

Table 14.1 shows the requirements where the following changes were made:

- **EFMRA-SYS-FR-01** has been superseded by **EFMRA-SYS-FR-01A** as the user requirement is set on the purchase price of the aircraft and not on the list price.
- **EFMRA-SYS-FR-02** has been superseded by **EFMRA-SYS-FR-02A** as block hour costs requirements are now set per hour and using a requirement with respect to the Airbus A321ceo instead of using an absolute cost requirements derived from data. The decision to eliminate an absolute value was made, because a unified estimation model for the Zephyr One and Airbus A321ceo will be used to estimate operating costs.
- The requirement on maintenance costs (**EFMRA-UR-09**) was given a system requirement identifier (**EFMRA-SYS-FR-06**).

Table 14.1: Requirements Zephyr One for financial and competitive analysis.

EFMRA-SYS-FR-01A	The aircraft shall have a sales price of not more than 100 million euros.
EFMRA-SYS-FR-02A	TThe aircraft shall have operational costs per seat no higher than the reference aircraft.
EFMRA-SYS-FR-03	The aircraft shall be available by 2036.
EFMRA-SYS-FR-06	The aircraft shall have no additional maintenance cost compared to the reference aircraft.

14.2. Market Analysis

In the market analysis presented in the Baseline Report [2], market trends and requirements for the Zephyr One were identified. Additionally, the market size and market share were estimated using the current market as a reference point. In support of the market analysis a Political, Economic, Sociological and Technological (PEST) analysis, a stakeholder analysis and an analysis on the strength, weaknesses, opportunities (SWOT) was carried out. With the final design parameters in place, the estimates on market demand and have been updated in this report in this section. The SWOT analysis will be updated in the Section 14.12.

14.2.1. Market Trends

Global trends that were identified [2] were long term increasing demand for air travel, despite the disruption form the pandemic. This shows resilience of the market. A PEST assessment by region showed that each region has its stronger and weaker points. Several weak points include unstable oil revenues affecting the Middle East, income inequality in South America, expected shortages of skilled technicians in Europe, trade tensions between China and the United States of America (USA) and political instability in the Middle East partially leading to irregularities in development of the tourism sector in parts of the region. Strong points include increasing transatlantic flights from and to North America, growth in route creation in Europe, increasing focus on development of tourism in the Middle East, growing middle classes in Asia and strong domestic markets within China and the USA while the domestic market in India is also growing.

During the pandemic, many airlines have received loans or guarantees from governments which has given governments leverage to demand bigger contributions from the airline industry to reduce emissions. This can be considered a break from the past when the influence on airlines was not as big.

In terms of aircraft fleets and networks several trends were observed as well. On the single aisle market the Baseline Report study found that airlines are upgauging meaning that smaller variants of

aircraft are replaced by bigger aircraft. On the wide body market, the opposite is happening where airlines are looking to dispatch smaller aircraft as networks have mostly shifted from hub-spoke models to point-to-point networks with a focus on serving secondary city-pairs, which are routes for which demands exists but deploying big aircraft is not always viable. Airlines are also focusing on frequency, thereby offering flexibility to travelers as multiple flights on smaller aircraft can be scheduled instead of a single flight on a big aircraft. Those trends come together around the 200-seat segment, which is what the Zephyr One is optimised for. The final relevant trend for the Zephyr One is the market penetration of low-cost carriers, which saw capacity grow by a factor 12 [97] between 2015 and 2017.

14.2.2. User Requirements

From the market analysis several user requirements were formulated. These user requirements include a maximum turnaround time of 52 minutes, the same gate and airport category as the A321, a one-class seating up to 240 passengers, up to 4.5 tons of revenue generating cargo and a design range of 6,150 km with possibilities to swap cargo containers for additional fuel tanks to enable transatlantic operations. For the service entry a target of 2036 was set, which paces with the replacement cycle of current generation single aisle aircraft and should give sufficient time to develop the Zephyr One.

14.2.3. Market Size

To establish the market demand for the Zephyr One, the current market has been analysed using data from Airbus [6], Boeing [98] and Japan Aircraft Development Corporation (JADC) [99]. The three parties estimate demand for passenger aircraft between 33,950 and 42,180 units. Boeing and Airbus forecast a 77% share for the single aisle segment, whereas JADC forecasts a 72% share giving a total of 24,500-32,270 deliveries in the single aisle segment. The average share for the single aisle segment is 75%. Boeing and Airbus do not define a share for large single aisle aircraft (LSA) such as the Zephyr One and A321. JADC has segmented the market further with a 170-229 seat segment, which includes aircraft such as the Airbus A321 and Boeing 737 MAX 9/10. For this segment, JADC expects demand for 11,500 units. This is 47% of all single aisle deliveries. It has been observed that the share of A321neo orders in the A320neo family order book is also 47%[1]. That serves as an indication that the percentage forecast by JADC carries credibility. Applying the percentage gives a demand forecast of 11,500-15,150 units for aircraft in the 170-229 seat segment.

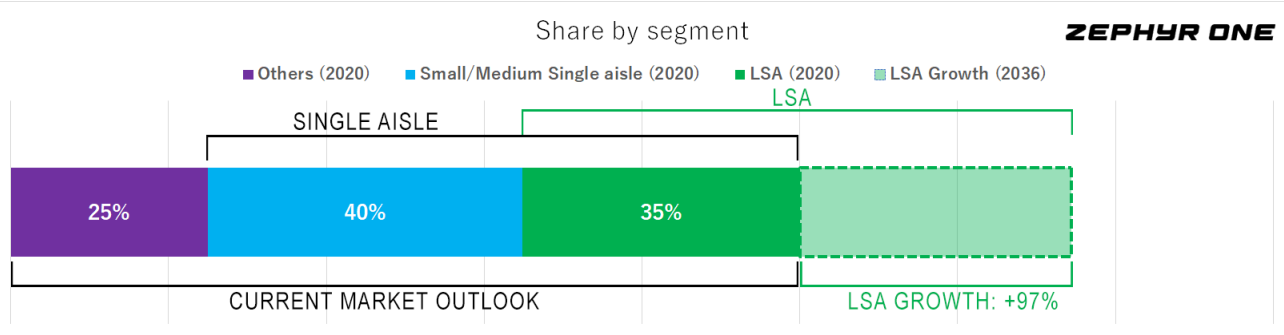

Figure 14.2: Share in demand by segment.

It should be noted that the forecast for up to 15,150 units holds for the coming 20 years while the Zephyr One is scheduled to enter service in 2036. Therefore, the demand forecast has been scaled using growth rates in forecast demand for single aisle aircraft over the past years. Between 2013 [100] and 2019 [101], the growth rate in forecast demand for single aisle aircraft was 4.65%. Applying

[1] https://www.airbus.com/content/dam/corporate-topics/publications/o&d/ODs-May-2021-Airbus-Commercial-Aircraft.xlsx [cited 16 June 2021]

this growth rate indicates that by 2036 the 20-year demand forecast for single aisle jets is set to rise by 97% as shown in Figure 14.2 to **22,750-30,000 units**.

14.2.4. Market Share

Initially, the Zephyr One targeted to have an average production rate of 10 aircraft per month, which is two thirds of the delivery rate for the Airbus A321neo. That production rate is based on current production numbers. Because it is expected that market demand will continue growing, the production rate estimate for the Zephyr One has been updated accordingly with a targeted average rate of approximately 20 aircraft per month. This would bring the market share of the Zephyr One to **15%-21%** with a total production quantity (PQ) of **4,750 units**.

14.3. Production Quantity

The production quantity (PQ) shown in Figure 14.1 as the purple square is established at 4,750 units in Section 14.2.4. The estimated production quantity might be conservative as a production run of 20 years has been assumed, while current engine option generations of the Airbus A320 and Airbus A330 have been in production for over 25 years. The production quantity plays an important role in calculating the profitability on the aircraft program. Therefore, underestimating the production quantity is deemed more acceptable than overestimating the production quantity.

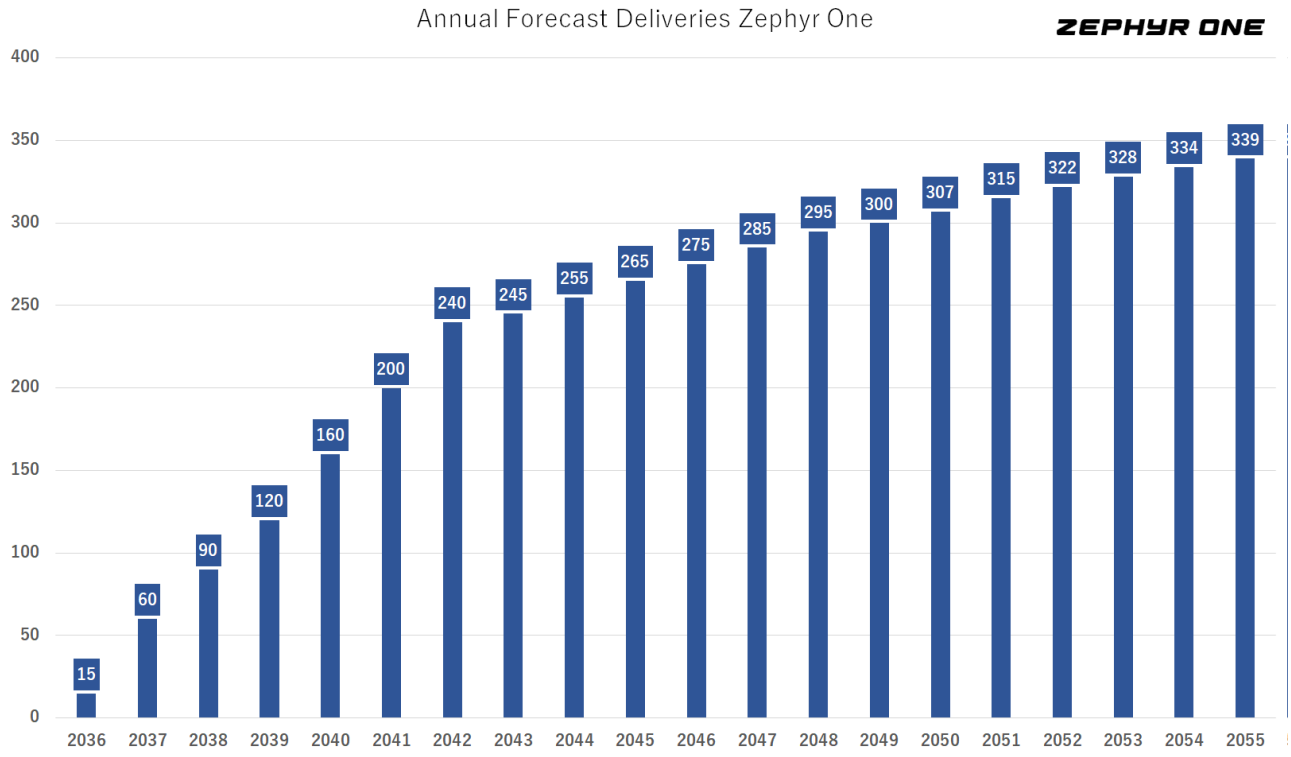

Figure 14.3: Annual forecast deliveries Zephyr One.

Figure 14.3 shows the envisioned production per year. Over the first 7 years of the program, the production will increase rapidly after which production will still increase but at a moderate pace. The average production rate will be slightly below 20 units per month with a production rate of 28.25 aircraft per month in 2055. As a reference, before and even during the pandemic Airbus and Boeing have been looking to increase production rates of their best selling single aisle aircraft to 70 aircraft per month[2]. By 2055, the Zephyr One will have a production rate that is 40% of the production rate

[2] https://centreforaviation.com/news/airbus-outlines-potential-to-raise-a320-production-to-70-per-month-by-1q202

that Airbus is aiming for by 2024, which is another sign that the forecasts for the Zephyr One are conservative but also keep in mind a challenging path to penetrate the market.

14.4. Aircraft Sales Price

The commercial aircraft industry is a cash intensive industry where narrow body aircraft are being listed[3] anywhere between $89.1 million and $134.9 million. For the Zephyr One, a user requirement (**EFMRA-SYS-FR-01A**) [102] on the acquisition costs was set. This requirement stipulated that the aircraft shall cost no more than €100 million, which is equivalent to $121.6 million using an exchange rate[4] of $1 being equal to €0.822403. To establish the aircraft list price (ALP) shown in the dark green boxes in Figure 14.1, Equation 14.1 based on Markish [103] was used. Equation 14.1 was adapted to take into consideration that the initial equation yields a 16.2% difference in pricing compared to the reference aircraft, even though there is no difference in capacity or range capability. This was deemed an unreasonable deviation, therefore a normalisation was applied.

$$ASP = \frac{0.735\left(\frac{Seats}{Seats_{ref}}\right)^{1.910} + 0.427\left(\frac{Range}{Range_{ref}}\right)}{1.162} \cdot Price_{ref} \tag{14.1}$$

Table 14.2: Input values and output for aircraft sales price.

	Unit	Zephyr One	Airbus A321neo
Seats	-	200	206
Range	km	6,484	5,589
Aircraft list price	$ millions	129.8	124.7
Aircraft sales price	$ millions	**64.9**	58.36

As a reference, the Airbus A321neo was used because this aircraft matches closely with the Zephyr One in terms of seating and range. Table 14.2 shows the inputs used to determine the ALP for the Zephyr One as well as the established ALP. An aircraft list price of $127.6 million expressed in 2021-dollars was found, which is 2.3% higher compared to the Airbus A321neo. The aircraft sales price (ASP) differs significantly from the ALP. The Airbus A321neo has an ASP of $58.4 million[5] marking a 53.2% discount on the ALP. The rule of thumb is that discounts of 50% are customary in the industry. Applying this to the Zephyr One gives a sales price of $64.9 million. This is 11.2% more expensive than the Airbus A321neo. It should, however, be noted that the Airbus A321neo is 9.5%[6] more expensive than the Airbus A321ceo and the Boeing 737 MAX 9 is 14.5%[7] more expensive than the Boeing 737-900ER. It can be concluded that going from one generation of aircraft to the other increases the market price by 10 to 15 percent. With that in mind, the price for the Zephyr One is compelling. Additionally, the Zephyr One has various advantages and strengths over competing aircraft that warrant a higher price tag. These unique selling points are discussed in Section 14.12 More importantly, it should be pointed out that the aircraft does meet the requirement on pricing (**EFMRA-SYS-FR-01A**).

[cited 11 June 2021]

[3] https://www.boeing.com/company/about-bca/#/prices[cited 4 June 2021]

[4] https://www.xe.com/currencyconverter/convert/?Amount=100&From=EUR&To=USD[cited 7 June 2021]

[5] https://www.myairtrade.com/resources/fleetstatus[cited 11 June 2021]

[6] https://www.airbus.com/content/dam/corporate-topics/publications/backgrounders/Airbus-Commercial-Aircraft-list-prices-2018.pdf[cited 11 June 2021]

[7] https://www.boeing.com/company/about-bca/#/prices[cited 11 June 2021]

14.5. Production Costs

The production costs shown in the blue boxes in Figure 14.1 are estimated in Section 14.5.1 to which a learning curve effect is applied in Section 14.5.2.

14.5.1. Production Cost Model

The production costs have been calculated using a modified production cost model based on the model by Raymer [104]. In this model costs for engineering, tooling, quality control and manufacturing are found by multiplying the number of hours multiplied by the hourly rates while material costs are estimated as a grand total. The aforementioned cost components are functions of the OEM and maximum speed of the aircraft. The engine cost are established using the maximum sea-level thrust, maximum engine Mach number and turbine inlet temperatures as input. The model has been supplemented by costs estimates for the interior [105] with parameters for the cabin layout discussed in Section 4.4.4 as inputs and avionics costs which are estimated as a function of the aircraft list price [106]. All cost components are expressed in constant 2021-dollars and combined in an estimate for the production costs to which contingency and fudge factors are applied.

Raymer advised fudge factors to be implemented to the hourly driven cost components based on material choice and to apply a 0.9 fudge factor for commercial aircraft designs. Given the unconventional design and need for contingency, the 0.9 fudge factor for the Zephyr One was not applied.

Table 14.3: Production costs Zephyr One in millions.

Component	Costs in millions	Percentage
Engineering	$3.1	5%
Tooling	$2.2	4%
Manufacturing	$9.8	17%
Quality Control	$1.4	2%
Engine production costs	$16.8	29%
Material costs	$5.8	10%
Avionics	$14.3	25%
Cabin	$4.7	8%
Total	**$58.1**	**100%**

Table 14.3 shows the cost breakdown for the Zephyr One. The production costs per aircraft are estimated at $58.1 million after five years of production at which production has matured.

14.5.2. Effect of Learning Curve

During manufacturing of aircraft, the earliest items boast higher production costs as the program is going through a learning curve. The learning curve captures the phenomenon of required labor or costs reducing by a certain percentage each time production doubles. Aerospace manufacturing has a typical learning curve of 85%[8] indicating that each time production increases, the labor required for production of the aircraft reduces by 15%.

[8] http://www.strategosinc.com/articles/strategy/learning_curves.htm [cited 11 June 2021]

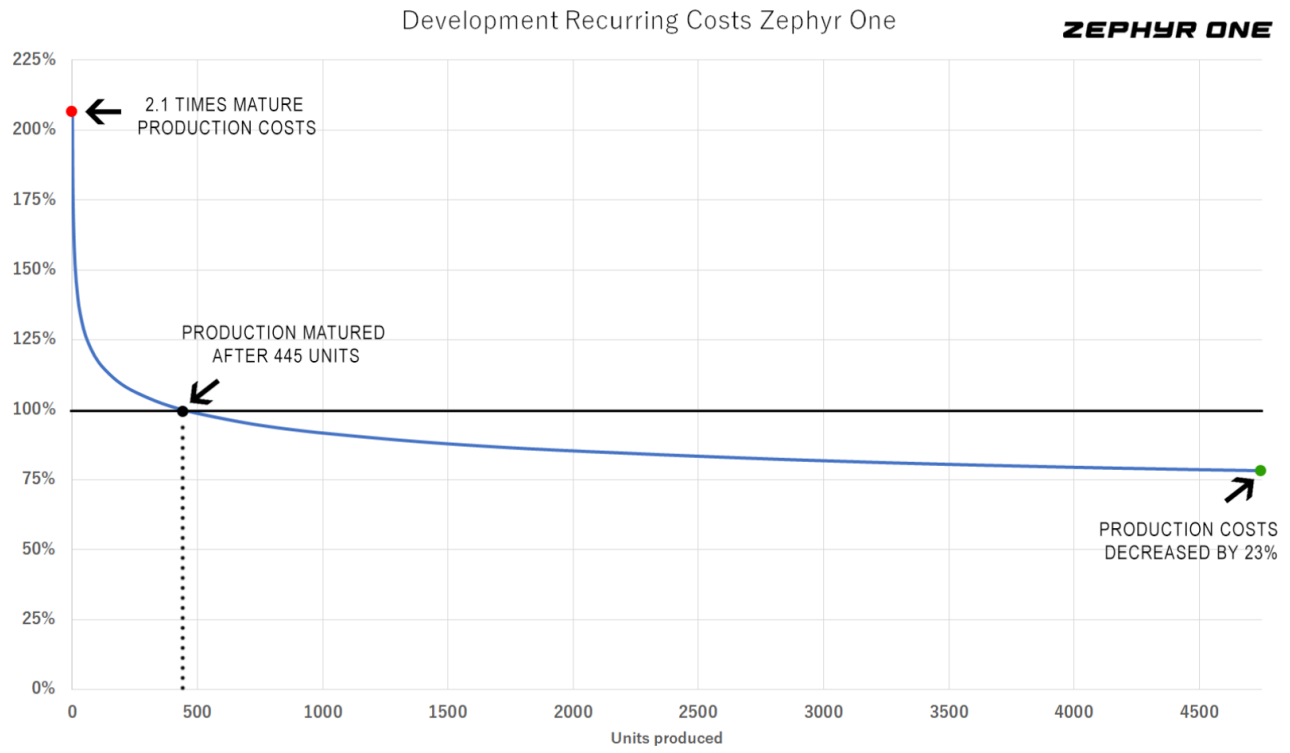

Figure 14.4: Learning curve Zephyr One.

For the Zephyr One, learning curves for labor, materials, engines and miscellaneous items were used. For labor, a learning curve of 85% was used while it was found that more efficient use of materials and miscellaneous items results in a 95% learning curve [107]. For production of the turbofans a learning curve of 92.7% [108] was applied as found in a study by II. Combining the learning curves for the various components results in an estimated learning curve of 91% for the Zephyr One. Figure 14.4 shows how costs develop compared to the mature cost point, which occurs after five years of production when 445 units have been produced. The aircraft produced early in the production run have costs that are 2.1 times the mature production costs, but these costs decrease rapidly until the mature point is reached. After 20 years of production, at the 4,750th aircraft, the production costs have decreased by 23% and average production costs are 50.5 million which is 13% lower than the production costs at the mature point.

14.6. Development Costs

To estimate the development costs, shown in the green boxes of Figure 14.1, two methods were utilised. One method by Raymer [104] based on the updated DAPCA V (Development And Procurement Cost of Aircraft) and a second method, which is the DAPCA model from 1987 [109]. Both methods have been applied with the number of test aircraft, maximum velocity and operating empty mass as inputs as shown in Figure 14.1. With a flight test program consisting of six aircraft, an OEM of 42.3 tons and a maximum speed of 876 km/h the development costs were estimated to be between $4.5 billion and $4.7 billion using the DAPCA method as well as the modified DAPCA method from Raymer. These figures are reasonable for perfect development cycles for conventional aircraft. However, the Zephyr One uses a unconventional design and has strict design requirements to satisfy the user requirements. Additionally, more recent aircraft programs have significantly exceeded development budget due to design complexity. With that in mind, a correction factor of two was applied. Resulting in development costs of $8.9 billion to $9.3 billion. The highest of these values was used for further cost computations.

Table 14.4: Backtest development costs in billions of dollars.

	DAPCA	Raymer	Actual	Δ DAPCA [%]	Δ Raymer [%]
Boeing 787	$10.4	$10.0	$18.9	+82%	+90%
Airbus A350	$10.9	$10.5	$18.9	+73%	+81%
Bombardier C Series	$4.0	$3.8	$6.1	+52%	+59%

To verify the accuracy of the DAPCA and Raymer models, development costs for the Boeing 787, Airbus A350 and Bombardier C Series (now Airbus A220) were compared to the results of the models when putting in the variables for each aircraft program. The results in Table 14.4 show that both methods have underestimated the development costs for recent aircraft developments, where the Raymer method underestimates the costs most. The Boeing 787, Airbus A350 and Bombardier C Series were chosen because those are new aircraft programs, while development costs for the Airbus A320neo and Boeing 737 MAX are not reflective as those are iterative designs. The correction factor of two has been maintained with a 80% correction for underestimation of the development costs and a 20% correction to facilitate additional development costs due to the unconventional aircraft design.

14.7. Cost of Goods

By combining the development cost of $9.3 billion and the production cost of $240 billion, the cost of the program ($COG_{program}$) is obtained. This figure of $249.4 billion is subsequently divided by the production quantity to obtain the average costs of goods (COG) shown in the yellow box in Figure 14.1 is obtained. The average costs per aircraft for production and amortized development are estimated at $52.5 million.

14.8. Return on Investment

Finalising the financial analysis for the aircraft program are the calculations of the profit and ROI shown in the pink boxes in Figure 14.1. The ROI is calculated using Equation 14.2.

$$ROI = \frac{(ASP - COG) \cdot PQ}{COG_{program}} \tag{14.2}$$

For the Zephyr One an ROI of 23.7% is forecast with profit margins, the profit expressed as a percentage of the revenues, of 19.1%.

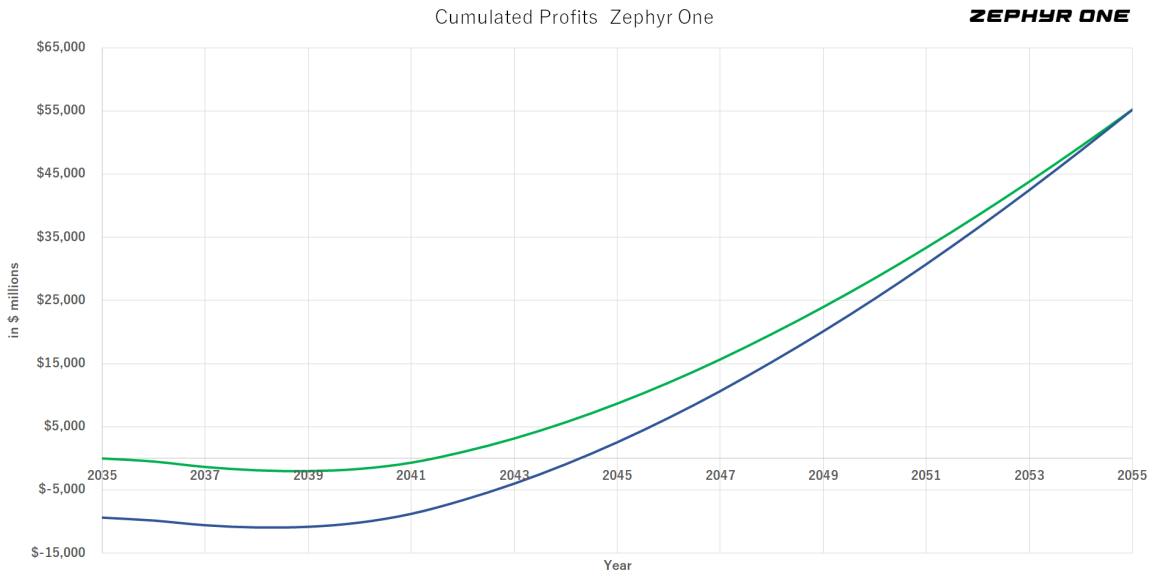

Figure 14.5: Cumulated profits Zephyr One.

Figure 14.5 shows two ways in which cumulative program profits have been computed. In the first method (green), the development costs are amortized over each unit that is to be produced. In the second method (blue), the development costs are recognized as a cost beforehand and are not amortized on each delivery. The result is that the initial program loss before a delivery has occurred is higher, but the booked profits on each delivery are also higher. The only way in which the methods differ is that it shifts the break-even point from 2039 to 2042.

Table 14.5: Summary financial metrics Zephyr One aircraft program.

	Unit	Value
Aircraft List Price	$ millions	129.8
Aircraft Sales Price	$ millions	64.9
Production Run	-	4,750
Revenues	$ billions	308.4
Production costs	$ billions	240.0
Development costs	$ billions	9.3
Program Profit	$ billions	59.0
Profit margin	-	19%
ROI	-	24%
Break-even point production	Year	2039
Break-even point aircraft production	Line number	235
Break-even point production program	Year	2042
Break-even point production program	Line number	672

Table 14.5 shows relevant information for the Zephyr One financial analysis, such as the ALP, ASP, production costs, development costs, revenues, profits. The table also shows the line number where revenues exceed not only the cost of producing the aircraft, but also the amortised development costs (break-even point) and aircraft program break-even point.

14.9. Direct Operating Costs

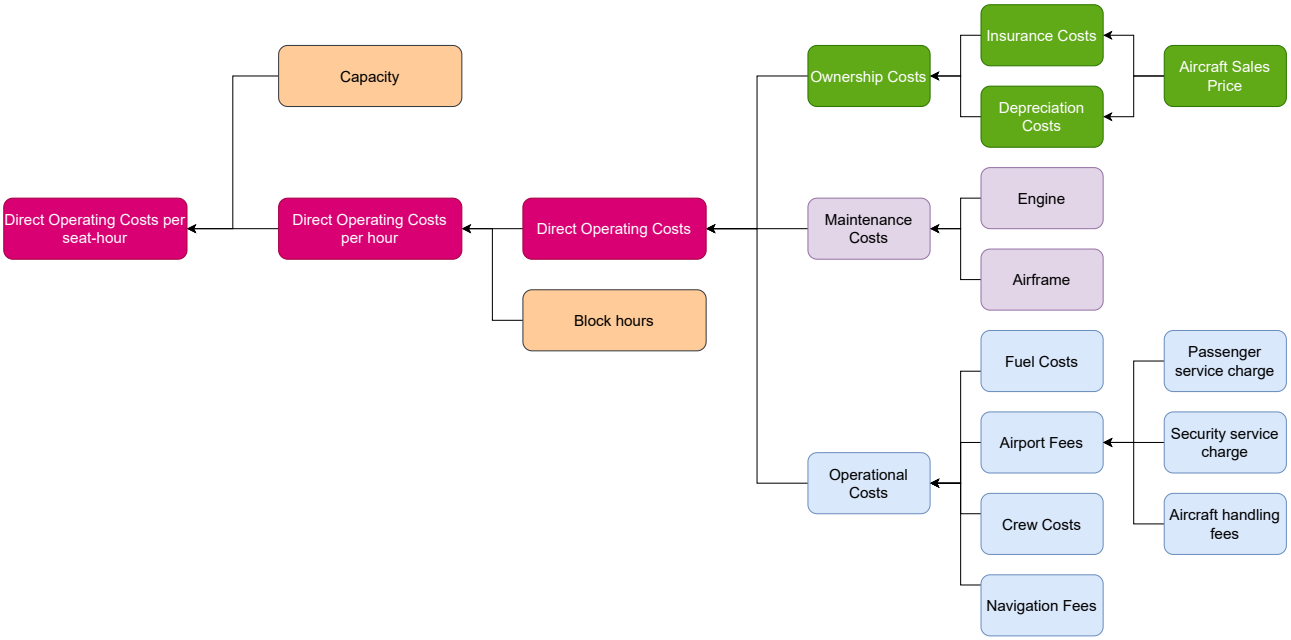

Figure 14.6: Direct Operating Costs diagram.

The DOC consists of three main cost components, namely the ownership costs, maintenance costs and operational costs. These costs are subsequently combined into a DOC figure. When dividing this number by the block hours, the time between closing the door at the departure airport and opening the door at the arrival airport, the DOC per block hour is obtained. This number can be normalised for the seating capacity of the aircraft by dividing the DOC per hour by the number of seats. The ownership costs depend on the aircraft sales price, which drives the insurance and depreciation costs while the maintenance costs are driven by engine maintenance cos and airframe maintenance costs. The operational costs are driven by fuel costs, airport fees, crew costs and navigation fee. The airport fees[9] are determined by the number of passengers carried and a combination of the MTOW and the noise category of the aircraft.

14.9.1. Ownership Costs

The insurance costs per block hour is calculated using Equation 14.4. An insurance rate of 1.5%[10] is used. This annual cost is amortized over the number of block hours (BHs) per year, calculated from the number of flights (n_{daily}) (**EFMRA-SYS-FR-04**) per day and block hours. The block hours (BH) per flight are calculated using the average stage length (ASL)[11] and the cruise velocity in Equation 14.3.

$$BH = \frac{ASL\cdot}{V_{cruise}} + \frac{43}{60} \tag{14.3}$$

$$\text{Insurance per BH} = \frac{1.5\% \cdot ASP \cdot 10^6}{n_{daily} \cdot 365 \cdot BH} \tag{14.4}$$

For the depreciation costs, a straight-line method shown in Equation 14.5 has been applied with a 10% residual value and 30 year economic life in mind.

$$\text{Depreciation per BH} = \frac{ASP \cdot 10^6 \cdot 0.9}{30 \cdot n_{daily} \cdot 365 \cdot BH} \tag{14.5}$$

14.9.2. Maintenance Costs

The total maintenance costs are estimated using Equation 14.6 outlined by Raymer [104] consisting of a cost component per Flight Hour (FH) and a component per Flight Cycle (FC), which is converted to an hourly rate. The costs are also split by airframe costs (C_a) and engine maintenance costs driven by the number of engines (N_e) and engine costs (C_e).

$$\text{Maintenance costs per BH} = 2\left(3.3 \cdot C_a + 14.2 + (58 \cdot C_e - 26.1)N_e) + \frac{4 \cdot C_a + 9.3 + (7.5 \cdot C_e + 5.6)N_e)}{BH}\right) \tag{14.6}$$

14.9.3. Operational Costs

The operational costs are subdivided into fuel costs, airport fees, crew costs and navigation fees. These cost components form the day to day operating costs for the aircraft.

Fuel Costs

The fuel costs are obtained from calculations with the Breguet Range equation as was performed in the Midterm Report [3] multiplied by the energy cost per kilogram and divided by the number of block

[9] https://www.schiphol.nl/en/download/b2b/1572597466/2qdMVyu742porlCDPH6NEB.pdf [cited 14 June 2021]

[10] http://wpage.unina.it/fabrnico/DIDATTICA/PGV_2012/MAT_DID_CORSO/08_Prestazioni/DOC_Jenkinson.pdf [cited 15 June 2021]

[11] https://web.mit.edu/airlinedata/www/2019%2012%20Month%20Documents/Revenue%20and%20Related/Passenger%20Revenue/System%20Passenger%20Revenue%20per%20Equivalent%20Seat%20Mile%20(PRESM).htm [cited 15 June 2021]

hours. For the Zephyr One, a fuel price per kg of $2.60 has been used based on data from Nelissen et al. [110].

Airport Fees

Airport charges can be calculated using various methods and these methods vary from airport to airport. For this project, the charges were computed using the fees set by Schiphol Airport for landing and take off as well as passenger service, which is based on the number of passengers. The aircraft handling fees are determined using the MTOM of the aircraft and the noise category (S1 to S7) for the aircraft with an associated rate. For the Zephyr One, the noise category used is S7 with an associated unit rate of $2.57 per ton.

$$\text{Airport handling per BH} = \frac{34.42 \cdot n_{passengers} + \frac{2.57 \cdot MTOM}{1000}}{BH} \tag{14.7}$$

Crew Costs

The crew costs are calculated with the rates from the Midterm report [3] and are shown in Table 14.6 along with the number of crew members in each role and the total hourly rate for the entire crew.

Table 14.6: Number of crew members and hourly rates.

	Crew	**Hourly rate**
Pilot	1	$275.00
First Officer	1	$180.00
Purser	1	$72.00
Flight Attendant	4	$60.00
Total	**7**	**$767.00**

Navigation Fees

The navigation fees are calculated with a method[12] utilised by EUROCONTROL consisting of a route charge and a terminal charge. The route charge depends on the MTOM and the distance flown through the airspace of a certain country multiplied by the unit rate that the country charges. Crossing the airspace of multiple countries means that various units rates apply. To simplify the calculation a $56.63 has been applied. For the terminal charge, which depends on the MTOM a unit rate of $230 has been used.

$$\text{Navigation fees} = 56.63 \cdot \sqrt{\frac{MTOM}{50000}} \frac{(ASL - 40)}{100} + \left(\frac{MTOM}{50000}\right)^{0.7} \cdot 230 \tag{14.8}$$

14.9.4. Total Direct Operating Costs

The cost components discussed in Section 14.9.3 are applied to the Zephyr One. The results are shown in Table 14.7 and compared to the Airbus A321ceo in Section 14.12.5.

[12] https://www.eurocontrol.int/archive_download/all/node/10683 [cited 15 June 2021]

Table 14.7: Direct Operating Costs Zephyr One.

Cost component	Value	Percentage
Ownership	$687	8%
Maintenance	$1,381	16%
Airport Handling	$1,391	16%
Navigation fees	$572	7%
Crew costs	$767	8%
Fuel costs	$3,779	45%
DOC per block hour	**$8,577**	**100%**

14.10. Disposal & Recycle Costs

This section provides an overview of the End-of-Life (EoL) aircraft economic management and explores into detail the Disposal & Recycle (D&R) costs. First, an overview of the current trends and common practices in aircraft EoL management will be given in Section 14.10.1. Section 14.10.2 covers the incentives for the airlines, operators and manufacturers to take into account the D&R processes. Finally, Section 14.10.3 gives an overview of the different economical aspects of the EoL and D&R processes.

14.10.1. End-of-Life Aircraft Management

The different EoL treatment strategies and their connections to each other are shown in Figure 14.7. Some additional comments regarding the component reuse, the recycling and the energy recovery process need to be made. The diagram and additional information are taken from a novel research on EoL process optimisation [111] and a D&R cost estimation study [112].

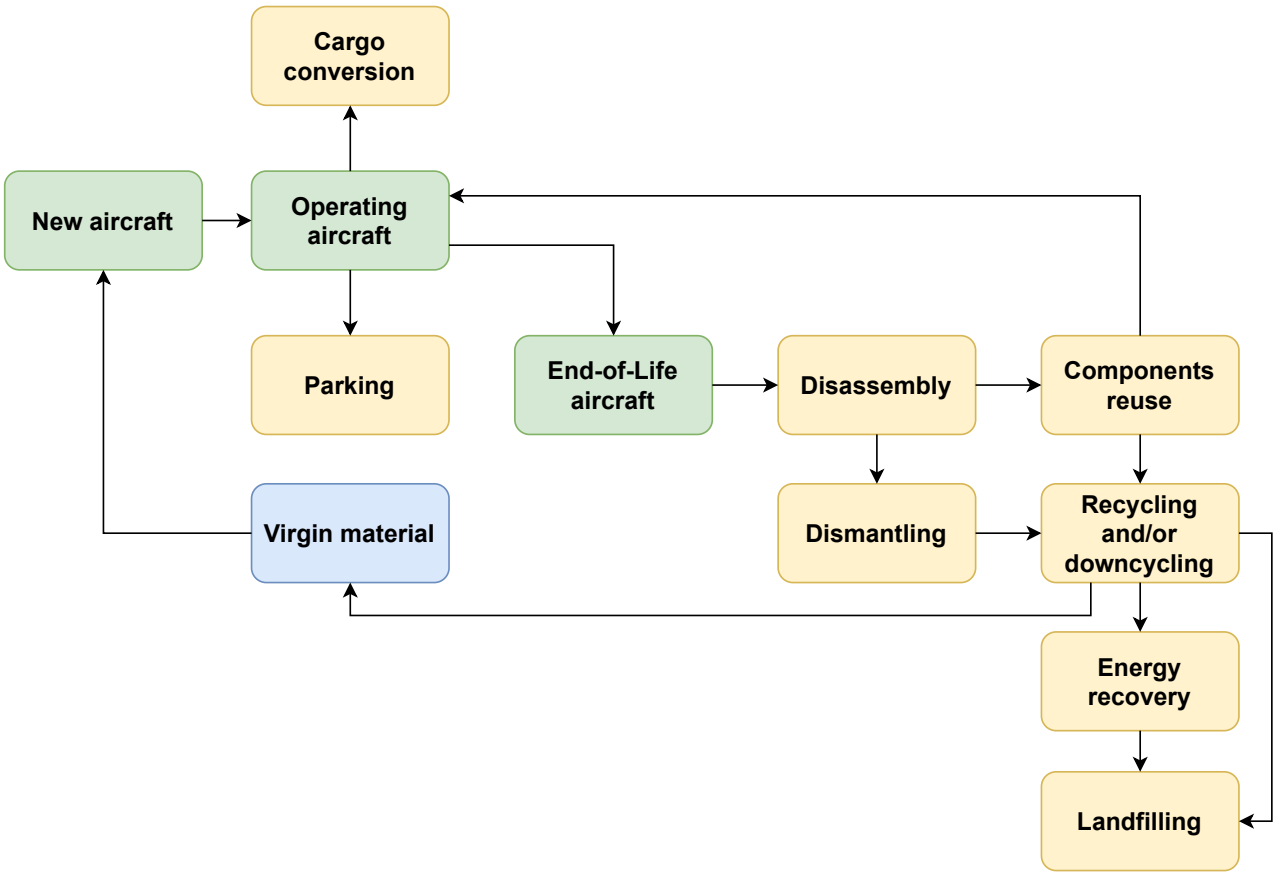

Figure 14.7: End-of-Life treatment strategies.

Components that will be re-used in other aircraft need to go through re-certification processes to comply with airworthiness authorities. Additionally, the energy recovery process does not necessarily happen. This process is only possible if non-recyclable materials can be be burned. If they can not, they go straight to land fills, without being used for energy production. Lastly, two types of recycling processes can be defined. Primary recycling makes use of scraps materials from manufacturing, while secondary recycling makes use of materials from disassembly and dismantling of decommissioned aircraft. When secondary recycling leads to lower quality, it is called downcycling, as opposed to recycling which leads quality equivalent to that of the original part. The lower quality is due to residual paints or glues and other components that can not be properly separated from the recycled part, either due to incomplete recycling methods or due to the nature of the part.

It should be noted that currently, the EoL management procedures are not regulated, and no responsibilities are clearly defined nor assigned to either manufacturers, owners or operators. As of now, these decisions are mostly profit-driven. A few other incentives will be given in Section 14.10.2. This profit-seeking decision-making is used by airlines and leasing companies, and relies heavily on their fleet planning, business model and business environmental conditions. Oliveira Junior et al. [111] provides two definitions of fleet planning. For the airlines, it consists of ”acquiring and managing their aircraft capacity to serve anticipated markets over a period of time with a view of maximising corporate wealth”. For the leasing company, it is about ”providing a portfolio of opportunity to profitably rent to organisations requiring flexible solution to their aircraft capacity needs”.

14.10.2. Incentives

As stated previously, the EoL processes are currently not regulated. Various reasons can be given in favour of conducting proper D&R and developing EoL strategies.

Some preliminary information should be given regarding aircraft decommissioning. A few numbers will illustrate the scale and the importance of D&R, all taken from a study on EoL support [111]. Between 2008 and 2014, 800 aircraft were retired annually, from a worldwide fleet of 25,000 units. New trends in aircraft operations estimate that an aircraft stays with its first operator around 10-12 years, which is roughly one fourth of the aircraft physical life and one third of the current average time spent in service.

Firstly, depending on various parameters, the D&R process can cover the entire aircraft residual value or larger. This can be ensured by recovering money through reselling reusable components and recycled parts. Proper planning can lead to EoL value creation. Additionally, using recycled materials is cheaper than using virgin materials.

Secondly, it can be part of the sustainability strategy to use recycled products. The sustainability considerations include, amongst other things, the potential damages to human health and the ecosystem quality. Next to that, a considerable amount of energy can be saved. Indeed, comparatively, recycling material is way less energy consuming than creating virgin material [112].

Lastly, bad EoL management can negatively affect company branding. Indeed, no airline, manufacturer or owner wants to be associated with a poorly decaying structure. On the contrary, current PR strategies rely on the advertisement of greener products or services, sometimes misleading their stakeholder in a process called greenwashing [113].

14.10.3. Cost Estimation and Economic Indicators

The economic viability and economic interest of conducting D&R processes is assessed in this section. The Cost Breakdown Structure (CBS) is shown in Figure 14.8. Some of its elements will further be analysed. This section is based on a research on aircraft D&R costs by Zhao et al. [112].

Before that, it should be noted that parking, storage and preservation of aircraft awaiting decom-

missioning procedures is not economically beneficial. Therefore, the economic viability of the EoL processes depends highly on the planning and management of the related operations. Poor management can lead to high fixed costs, as well as a drastic decrease of the aircraft's residual value.

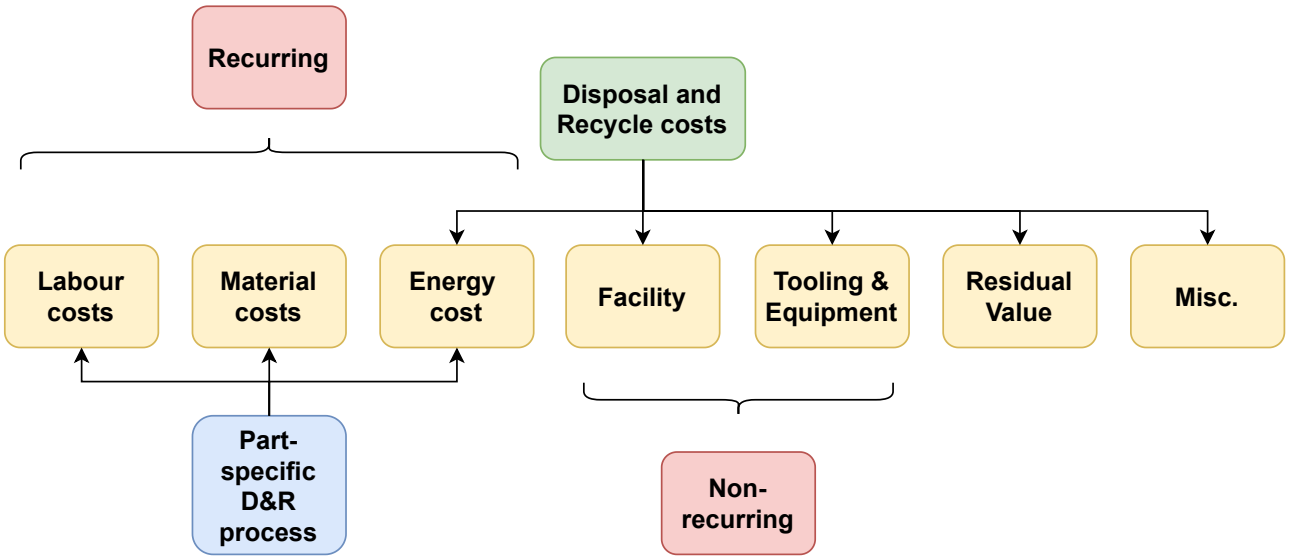

Figure 14.8: Cost Breakdown Structure for Disposal and Recycling.

As a rough estimate, the entire disposal costs of the aircraft should amount to 10% of the sales price, or approximately 1% of the entire life cycle costs. This sum can be broken down into different parts.

The recurring costs are part-specific, meaning that they vary depending on which aircraft sub-system is being disposed. The recurring costs include the labour costs, the material costs and the energy costs that is necessary for the recycling of the aircraft parts, before being able to re-certify, re-sell and reuse them. These costs occur for each aircraft and aircraft part going through the process, hence the recurring nature of the costs.

The non-recurring costs, on the other hand, are one-time costs related to the infrastructure required to perform the D&R process. The facility required as well as the tools and equipment are part of the non-recurring cost.

A major part of the D&R costs is the residual value. The residual value, as defined in Investopedia[13] is "the estimated value of a fixed asset at the end of its lease term or useful life". The residual value can be computed using Equation 14.9 found in [112].

$$C_{\text{residual}} = r_{\text{yearly}} \cdot P_{\text{residual}}(1+I)^{FY-FY_0} \cdot n_{\text{years}} \tag{14.9}$$

In the above equation, r_{yearly} is approximately 5% and $P_{residual}$ is roughly 10% of the aircraft price. FY and FY_0 represent the fiscal years of the start and end of DR operations, I indicates the inflation and n_{years} is the number of years of the start and end of flight operations.

The salvage cost is not to be mistaken with the residual value. The former is the value that can be obtained by reselling the recycled goods, so it includes the increase in value generated by the D&R process. The latter was described above and is the book value the operator or lessor has for an aircraft at the end of its life in service.

Even though the D&R process can lead to EoL value creation, the process itself has a cost, $C_{D\&R}$. An economic indicator can be established to evaluate the commercial viability of the D&R process and is shown in Equation 14.10.

[13] `https://www.investopedia.com/terms/r/residual-value.asp`, consulted June 15, 2021

$$I = \frac{C_{\text{salvage}} - C_{D\&R}}{P_{\text{residual}}(1+I)^{FY-FY_0}} \tag{14.10}$$

The D&R process also includes a learning factor, meaning that the economic benefits of recycling might appear later down the line rather than directly at the start. The mathematics of it are shown in Equation 14.11.

$$I_{\text{D\&R, learning}} = \frac{C_{\text{salvage}} - \left(\frac{Q}{Q_0}\right)^{log(r_{\text{learning}}-2)} C_{\text{D\&R, labour}}}{P_{\text{residual}}(1+I)^{FY-FY_0}} \tag{14.11}$$

A negative economic indicator indicates losses through the recycling process, while an indicator greater than one means that profit is made. If 0 < I < 1, then only part of the aircraft residual value is covered by the valorisation obtained through D&R. A comment and findings of Zhao et al. [112] is that the D&R process of the engine alone is more profitable than the D&R process of the entire aircraft. Additionally, profitability during the D&R process is only applicable for newer aircraft, as underlined in [111]. This is why integrated design is of prime importance: considering the EoL processes should be included in the conceptual phases as well.

14.10.4. Zephyr One D&R Financial Analysis

Benefits of using recycled materials | Recycling, re-certifying and reselling aircraft parts might present economic benefits. Some benefits can however also come from using recycled parts during manufacturing and assembly. According to [112], the use of recycled carbon fibers can decrease by up to 50% the price of material per pound. With regards to aluminum, primary recycling can lead to a save of 95% in energy consumption, while this number drops to 39% for secondary recycling.

Cost associated with conducting D&R | A quantitative financial analysis of the D&R costs of the Zephyr One is introduced here. Please note that this analysis is incomplete. Details of this statement and future recommendations will be provided later on in the section.

Table 14.8 shows the average dismantle cost of aircraft by type. The engine is separated from the rest of the aircraft, as it produces the most value when sold. It is therefore of interest to analyse it separately. The values from the table are taken from Table 1 in [112] and inflated with a 1.85% inflation rate to translate 2014-dollars to 2021-dollars, to make the comparison possible with the rest of this entire financial analysis. The total dismantle cost for a narrow body aircraft, corresponding with the Zephyr One, will be used in Equation 14.10 as $C_{D\&R}$. With this value and an assumed service life of 30 years, the required salvage value to obtain an economic indicator of 1 can be calculated.

For the Zephyr One, assuming that the aircraft is dismantled within two years of removal from service [14] the required salvage value to break-even on the D&R process is equal to **$7.3 million**.

Table 14.8: Average dismantle cost of aircraft by type, in 2021-dollars.

Type	Narrow body	Wide body	Regional jet
Aircraft	84,145	115,984	55,718
Engine	27,290	37,524	26,153
Total cost	**138,725**	**191,032**	**108,024**

[14] https://www.flightglobal.com/analysis/analysis-aircraft-retirement-wave-poses-challenges-for-recyclers/127188.article [cited 25 June 2021]

Table 14.9: Value of aircraft parts, in millions of 2021-dollars.

Type	Narrow body	Wide body	Regional jet
Aircraft	1.7	2.8	2.3
Engines (x2)	6.1	8.4	3.4

A similar approach is taken to construct Table 14.9. The original numbers are given in [112], in 2014-dollars and are converted to 2021-dollars.It can be concluded that the required salvage value to make profit off the D&R cycles of this aircraft **can be reached.** Without implementation of learning curve effects and a D&R process starting directly after removal from service, the economic indicator is equal to 1.2. It should be noted that costs for the D&R process can be reduced significantly when learning curve effects are applied. Separately, it should be noted that the profitability of the D&R process is highly dependent on the time between a recycling company taking possession of the aircraft and actually recycling the aircraft. The longer the aircraft remains with the recycling company without recycling, the lower the profit on the D&R process. The reason for this is that in the same way airlines and lessors have to depreciate the aircraft, recycling companies have to do the same for the aircraft they have in inventory.

Conclusions and recommendations | As stated previously, the method used in this section to assess the economic viability of D&R is not entirely accurate.

Firstly, the time that the aircraft spends in service is not taken into account, as the residual cost is fixed as the cost at the end of the economic life, irrespective of whether this happens after ten or thirty years. Oliveira et al. [111] showed however that the aircraft age in service and its maintenance status are the main components that determine value retention. Hence, this model is in itself not suited.

Secondly, the dismantling costs are assumed to be the entirety of the D&R costs, which is also far from correct. The D&R cost breakdown structure was detailed above in Section 14.10.3. The value of $C_{D\&R}$ in Equation 14.10 is therefore underestimated. It can thus be concluded that the model undershoots the required salvage value to be reached to break even in the D&R process.

While preliminary figures suggest that the D&R process can be profitable, considering other factors such as aircraft age, maintenance status and other costs factors not included in dismantling cost likely result in profitability on D&R to be more challenging and recycling companies should carefully establish maintenance status of aircraft and acquire those aircraft at attractive prices to turn a profit on D&R.

Aircraft recycling in practice | According to E-Cycle Environmental[15], general aviation aircraft are recyclable up to 70% on average, with 90% of the fuselage being recycled. Hundreds of tons of metal can be reused from the aircraft. The seats can also be worth between $450 to $5,000 so they are removed and reused as well. Besides that, what can not be recycled is either shredded, burned for energy recovery or disposed of in landfills. As explained above, the engines are worth the most when decommissioning the aircraft. Due to the current lack of regulations regarding EoL management and the fact that incentives are mostly economic, it might be that the potential to recycle an aircraft is lost. In other words, an aircraft can be made 75% recyclable as to comply with Flightpath 2050 requirements, if the operator or lessor does not see financial benefit to do so, they might not conduct proper EoL processes, hence not recycle the aircraft to its potential. This is due to the fact that, as explained above, re-selling leads to monetary gain, while generally, EoL processes of any other aircraft part is a cost rather than a gain. It is therefore more advantageous to only recycle the engine and dispose of the rest of the aircraft.

Recommendations for the future | Based on the previous paragraph, two main recommendations can be made. Firstly, it is apparent that thinking future-proof should be applied right away from the

[15] `http://www.ecycleenvironmental.com/recycling-blog/aircraft-recycling-product-destruction-profit-takeoff`, consulted June 06, 2021

conceptual phase to close the loop between aircraft manufacturers, lessors, operators and recycling companies. Another solution showed by Boeing is Overhaul programs, currently applied for landing gears, nacelles and control surfaces[16]. An incentive from the manufacturer or the maintenance company would be to have a combined maintenance and overhaul program, that will therefore be economically and logistically beneficial to both parties.

14.11. Life Cycle Costs

The components of the ASP, the DOC and D&R are combined into a life cycle cost assessment.These costs include the amortization of development costs, cost to produce the aircraft, the profit on production, the operating costs for airlines and the costs of D&R. What has also been considered is that aircraft maintenance costs are not constant over time. Typically have a newness phase which lasts around 7 years. During this phase maintenance costs are low. After 7 years maturity is reached and maintenance costs start to continue increasing slowly as the aircraft ages.

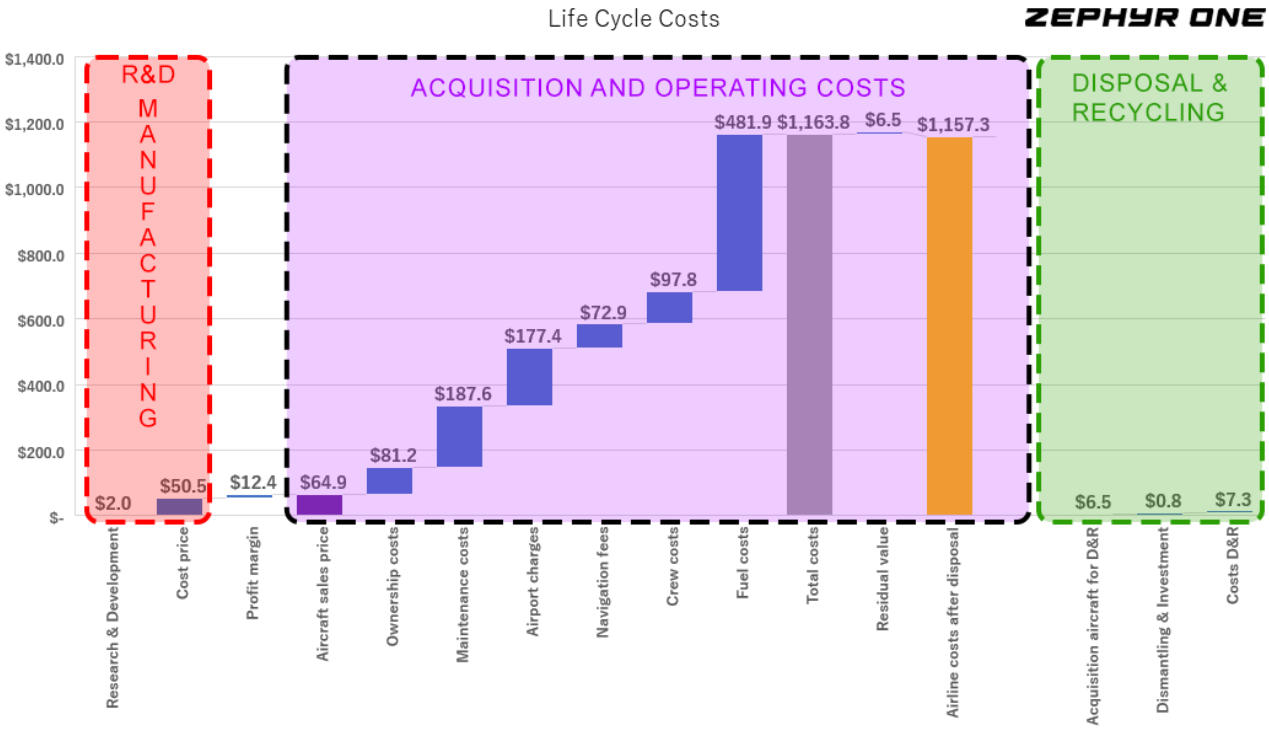

Figure 14.9: Life cycle costs Zephyr One.

The life cycle costs per aircraft are shown in figure Figure 14.9. The first two bars form the development and manufacturing cost per aircraft to which the profit margin of 19% has been added. Together, the first three bards form the ASP, followed by a composition of the airline operating costs, where the yellow bar shows the cost of operations including the acquisition of the aircraft and after the profit booked when selling the aircraft after its service life. Finalising the life cycle cost assessment, the D&R costs have been assessed. Over the entire life cycle, development and production costs (red shaded) account for only 4% of the life cycle costs, while operations of the aircraft (purple shaded) account for 95% and D&R (green shaded) accounts for 1%.

[16] https://www.boeingservices.com/parts/managed-part-and-repair-programs/exchange-programs/, [cited June 21, 2021]

14.12. Competitive Analysis

The Zephyr One has several unique selling points that are highlighted in this section and compared to competing aircraft. A stakeholder analysis has been carried out in Section 14.12.1 followed by an analysis on the strengths, weaknesses, opportunities and threats (SWOT) has been carried out in Section 14.12.2. The environmental parameters and comparisons with reference aircraft are discussed in Section 14.12.3. In Section 14.12.4, the versatile layout, comfort and range capability of the aircraft has been discussed followed by discussions on the DOC and revenue potential in Section 14.12.5 and Section 14.12.6. Together, these elements map the advantages and unique selling points of the Zephyr One.

14.12.1. Stakeholder Analysis

Identifying the parties that will influence the aircraft design, is an important step in the stakeholder analysis as it maps parties that could have an influence on the aircraft design. Stakeholders have been categorised by their impact on the aircraft design as well as their interest in the design in a power-interest matrix shown in Table 14.10. Several stakeholders are identified and are put in an influence and interest category.

Generally, airports and passengers have limited interest and influence on the design. However, regarding costs, their interests might also be considered high. Environmental organisations and communities near airports have a low influence on the design but a high interest in the design outcome with noise reduction and reduced emissions in mind. With regulations and taxes on emissions, governments have a high influence on the design while transportation agencies have a high influence as they are in charge of drafting certification requirement and certifying the aircraft. Manufacturers, airlines and lessors have a high interest and influence on the design process as the aircraft has to fulfil their operational and financial needs and fit in their strategic approach to sustainability.

Table 14.10: Power-Interest matrix.

	Low interest	High interest
High influence	• Government • Transportation agencies	• Manufacturers • Airlines • Lessors
Low influence	• Passengers • Airports	• Environmental organisations • Communities near airports

14.12.2. SWOT Analysis

The Zephyr One has several strengths and market opportunities making it a desired aircraft. However, it is also important to assess the weaknesses of the Zephyr One as well threats to the market. This has been done in Figure 14.10.

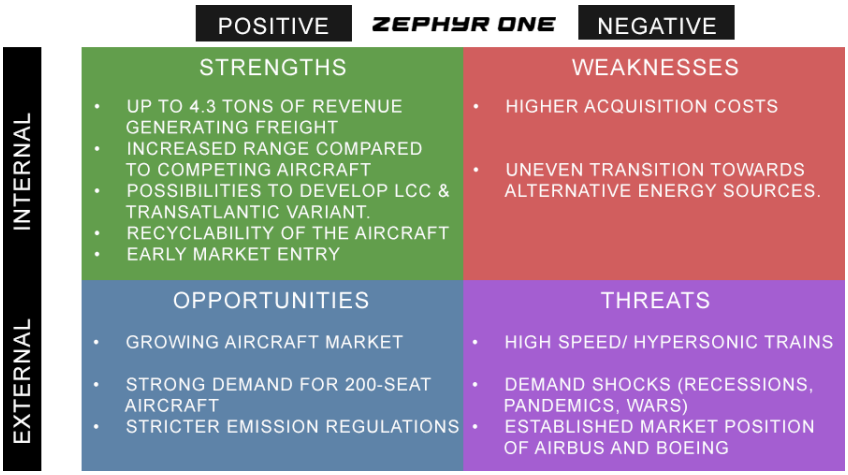

Figure 14.10: SWOT analysis Zephyr One.

One of the strengths of the Zephyr One is its ability to carry 4.3 tons of cargo. With increasing demand for air freight, as e-commerce sales continue to grow, having sufficient cargo capacity adds to the revenue potential as discussed in Section 14.12.6. Another strength of the Zephyr One is the possibility to create a high density configuration, which caters the needs of low-cost carriers while there also are opportunities to extend the range of the aircraft by exchanging the cargo containers for fuel tanks. With an increasing push on sustainability, the Zephyr One is designed with D&R processes in mind.

The strongest selling points of the Zephyr One is that it is a design with significant reductions in perceived noise levels and CO_2 and NO_x emissions with an early market entry. Airbus initially came up with ZEROe concepts that would have no emissions and would enter the market by 2035. However, recently Airbus stated[17] it does not expect hydrogen powered aircraft to enter the market until 2050. This is most likely related to the envisioned iterations for the Airbus A321neo and possible fuselage stretches of the Airbus A220 that would cover the 100-250 seat market with existing aircraft technologies. The service-entry target of 2036 is maintained for the Zephyr One making it the first aircraft built with sustainability as a primary driver.

Opportunities that can turn the Zephyr One into a success are growing demand for air travel with demand converging towards a 200-seat aircraft and stricter regulations on emissions. With reductions in emissions as a primary design driver, that should aid the Zephyr One capturing market share.

The Zephyr One also has some weaknesses. Although these weaknesses do not outweigh its strengths, they should still be addressed. In comparison to the Airbus A321neo, the Zephyr One has higher acquisition costs and there could be some challenges deploying the aircraft globally due to uneven transition towards alternative energy sources. Not all parts of the world will transition at the same rate, which could have consequences for dispatch flexibility for the Zephyr One. Over time it is expected that his weaknesses will fade as the transition gains traction globally.

Elements that could threaten the aircraft market in the coming decades are the rise of high speed and hyper-sonic trains, demand shocks caused by external factors such as recessions, wars, pandemics or political tensions. An external threat that threatens the Zephyr One is the established market position of Airbus and Boeing. Airbus and Boeing have crafted customer relations that go back decades and it will be difficult for the Zephyr One to break those relations from inception.

[17] https://eandt.theiet.org/content/articles/2021/06/airbus-to-keep-burning-jet-fuel-until-at-least-2050/ [cited 16 June 2021]

14.12.3. Environmentally Friendly

The Zephyr One is an environmentally friendly concept which will contribute to a future, more sustainable aviation industry. There are three main aspects in which the aircraft's sustainability can be assessed, namely noise, emissions, and material recyclability.

In terms of noise, the aircraft will not only comply with Flightpath 2050 requirements, but it is expected to surpass the imposed limits with even lower noise levels. The generated noise at fly-over, lateral, and approach measurement points are estimated to be 46, 65, and 67 dBA, while the maximum allowed levels are 59, 69, and 72 dBA, respectively. These are very low values which are expected to reduce the aircraft's impact on surrounding communities.

For both CO_2 and NO_x emissions, the Zephyr One meets the guidelines set out by Flightpath 2050. Depending on the ratio of LNG to synthetic methane, net CO_2 emissions can go all the way down to zero. Due to the innovative design used for NO_x emissions, a reduction of 95% compared to the reference aircraft can be achieved. Finally, the electric taxiing will allow for complete elimination of emissions during ground operations.

Because of the use of aluminium, the aircraft can be at least 80% recycled, which is in line with the current recyclability capabilities. Note however that even though the material choice makes the aircraft recyclable, due to certification costs, it does not automatically mean that recyclability is financially viable, but the Zephyr One has been designed with profitable recyclability and part re-use in mind.

14.12.4. Layout and Range

Versatile Layout

The Zephyr One can cater various markets; The aircraft has an increased cargo capacity catering for the growing demand to ship e-commerce products making it an integrated freight solution. Additionally, the aircraft can be configured in a high density configuration with up to 259 seats catering the growing share of low-cost carrier activity.

Range

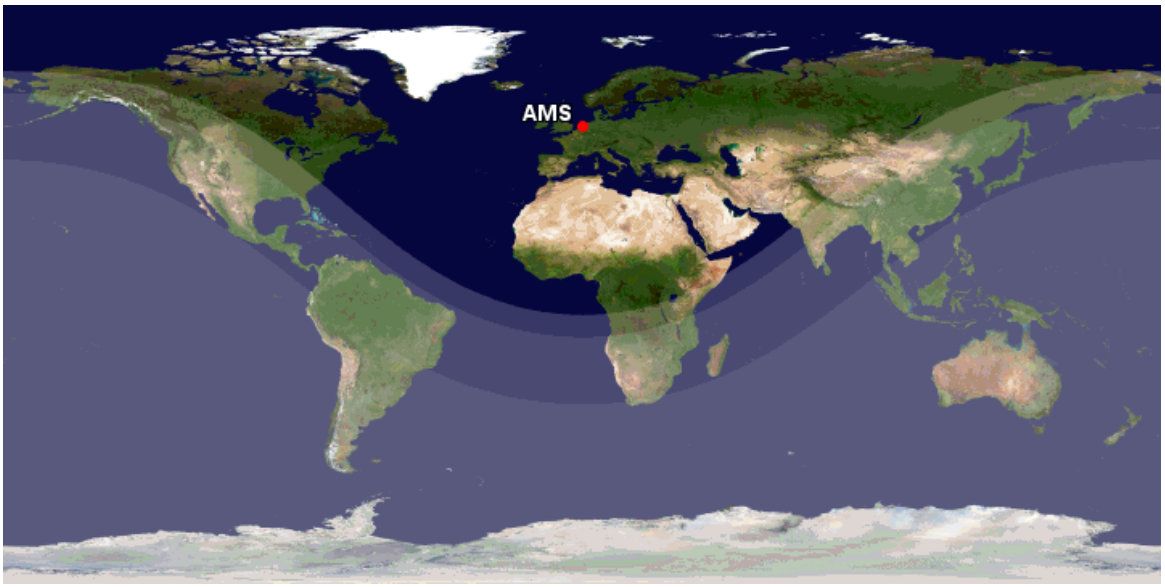

Figure 14.11: Dynamic range capability Zephyr One.

The Zephyr One has a range capability of 6,482 km at full payload. When the aircraft carries no cargo, the range increased towards 7,249 km enabling transatlantic flights, but mostly limited to flight from

one coast to the other. The range can be increased even further, up to 9,564 km, allowing for flights to destinations deeper into the mainlands shown in Figure 14.11.

Comfort

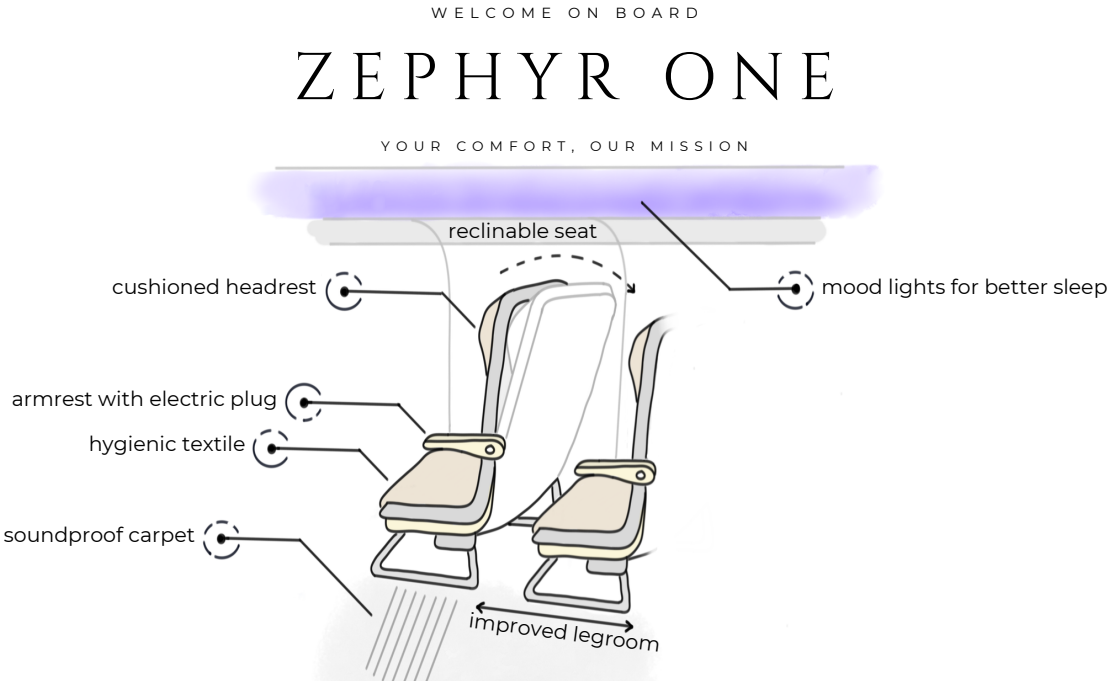

Figure 14.12: User experience aboard the Zephyr One.

Passenger comfort aboard the Zephyr One has been optimised to deliver premium user experience, as detailed on Figure 14.12. In addition to a cushioned headrest and more hygienic seat textile, the cabin is optimised for long-haul comfort on medium range flights. It indeed features a soundproof carpet to reduce noise from other passengers' movements during flight, as well as mood lights to ensure a more gentle jet lag. Comfort-wise, the legroom allocated is larger than that required by regulations and the seat is reclinable. There is also possibility to charge electric devices such as laptops and smartphones on board, to make sure passengers are fully equipped for transatlantic flight entertainment.

14.12.5. Direct Operating Costs

For the Zephyr One, a user requirement was set that the aircraft shall have no additional maintenance costs compared to the reference aircraft (**EFMRA-SYS-FR-06**). The maintenance costs per BH are calculated using the method by Raymer [104] with engine and airframe costs as an input. It was found that the Zephyr One has 11% lower maintenance costs compared to the A321ceo and 6% compared to A321neo. Thus, it can be concluded that the requirement on maintenance costs has been met.

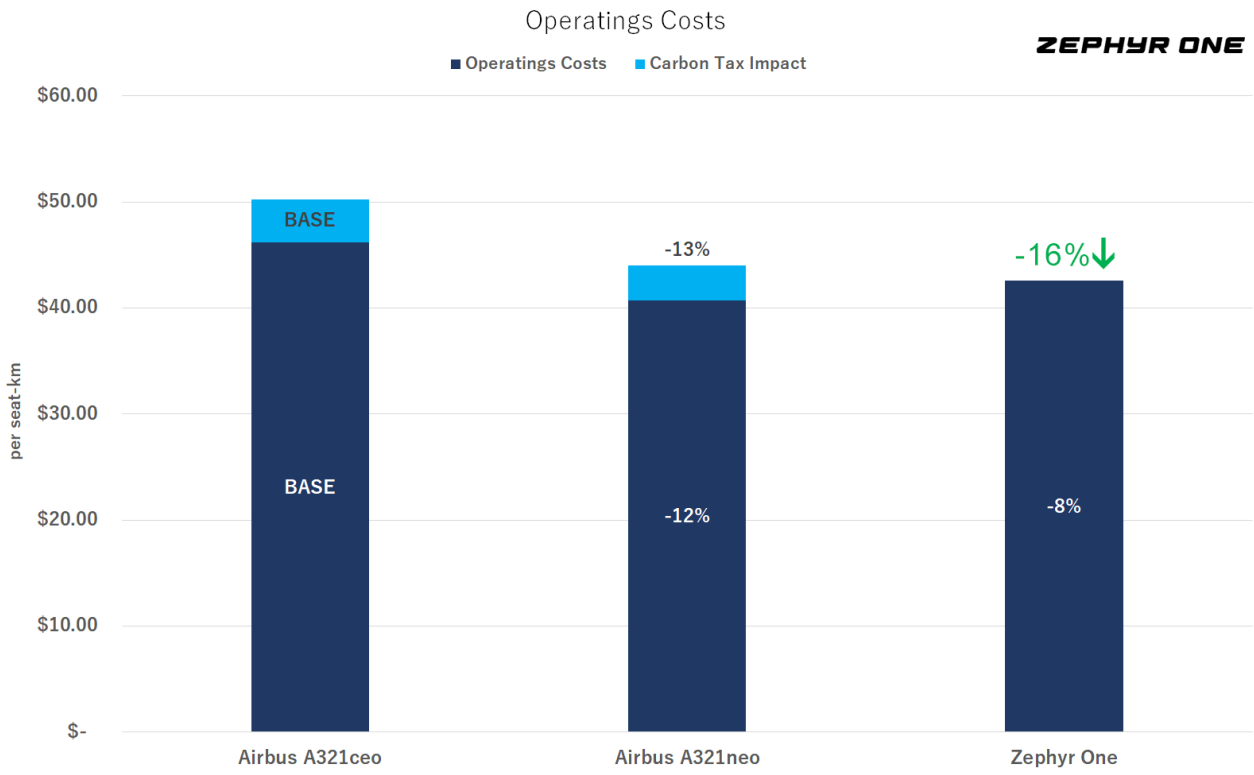

Figure 14.13: Direct Operating Costs Zephyr One and competitors.

The designers of the Zephyr One have set an even more ambitious goal aiming for equal or better total operating costs per block hour compared to the reference aircraft (**EFMRA-SYS-FR-02A**). Analysis shows that on a 1,906 km flight overall costs per seat-kilometer are **8% lower** for the Zephyr One compared to the A321ceo. It has been taken into consideration that in the future, governments might apply carbon taxes on current common energy sources to force a faster transition to sustainable fuels. When applying such carbon tax at a rate of 20%, the Zephyr One has **16% lower** costs compared the A321ceo and has a 3.2% advantage over the A321neo.

14.12.6. Revenue Potential

The competitive strength of an aircraft is often measured by comparing DOC figures per block hour or DOC figures per seat. However, it is also important to assess the revenue potential of the aircraft. This has been done by using ticket prices for economy and business class for a typical 1,100 km flight found on the website of KLM Royal Dutch Airlines and a cargo revenue of approximately $2.50[18] per kg. It was found that the revenue potential of the Zephyr One is **20% higher** compared to the A321ceo and **11%** higher compared to the A321neo. When cargo revenues are included, the revenue potential is even **25% higher** compared to the A321ceo and **22% higher** compared to the A321neo.

To obtain a more reflective measure of the revenue potential, the revenue potential has been expressed on a per-seat kilometer basis. Measured by seat-km, the Zephyr One has **9% higher** revenue compared to the A321ceo and **14% higher** when cargo revenue is included. In comparison to the A321neo, the Zephyr One has **12% higher** passenger revenue per seat-km and **24% higher** potential when cargo revenues are included. It can be concluded that the Zephyr One provides a significantly higher revenue per seat-km, which increases even more when cargo revenues are included.

[18] https://www.freightos.com/freight-resources/air-freight-rates-cost-prices/ [Cited 17 June 2021]

15 Risk Analysis

Managing risks is an important part of the design process. Improper risk management can lead to catastrophic failure of both the aircraft and the project. In this chapter, relevant risks will be identified, categorised and if needed, a mitigation strategy will be set up. Finally, a full risk map containing all identified risks will be presented. The risk map presented in this chapter is a combination of the risk registers obtained during the Baseline [2] and Midterm [3] reports, as well a few newly identified risks.

15.1. Risk Plan

In this section, the risk plan will be detailed. This risk plan was originally set up during the Baseline phase.

An important part of the technical management is accounting for and mitigating possible technical risks. In this section, a technical risk mitigation strategy will be detailed. Five types of risks will be considered. Safety risks, schedule or timeline risks, technical performance risks and operational risks. Some might fall under multiple categories, however, every risk will only be accounted for once.

All risks included in the risk mitigation plan will be categorised in four categories, based on their severity. In order to determine to which category a risk belongs, an estimation will be made. The categories used can be found in Table 15.1

Table 15.1: Risk severity categories for all risk types.

	Safety	**Timeline**	**Technical performance**	**Operational**
Catastrophic	Life-threatening situation	Delayed entry into service	One of user requirements not met/ potential to cause safety critical situation	Major operational issue, unable to perform mission
Critical	Non-life threatening safety impact	Delay in current design step	One of secondary requirements not met	Major operational impact
Marginal	Maintenance required	Re-allocation of resources needed	Sub-optimal performance	Small operational impact
Negligible	Negligible impact	Negligible impact	Negligible impact	Negligible impact

Furthermore, the risks will also be categorised in one of 5 categories, based on their likelihood of occurrence throughout the lifetime of an aircraft or throughout the design process, depending on the risk. In order to assign these categories, an estimation will be made. The categories used are the following:

- Very high: Likelihood greater than 70%.
- High: Likelihood between 50% and 70%

- Moderate: Likelihood between 30% and 50%
- Low: Likelihood between 1% and 30%
- Very low: Likelihood lower than 1%

The categorisation detailed above will be used to generate a risk map. If a potentially catastrophic risk has a likelihood of low or higher, it is deemed unacceptable. A critical risk is deemed unacceptable if the likelihood of occurrence is moderate or higher. Marginal risks are only deemed unacceptable if their likelihood is very high. Negligible risks are always accepted. If a risk falls into the unacceptable region, one of the following mitigation techniques will be used:

- Remove: Change a design decision, removing the associated risks.
- Reduce: Reduce the probability of occurrence, or the impact if it were to occur. e.g. design for redundancy.
- Accept: Accept the risk and closely monitor it, this is not an option for the safety risks.
- Transfer: Transfer or share the risk with a 3rd party, e.g. buying of the shelf parts instead of developing novel parts.

15.2. Risk Categorisation and Mitigation

Table 15.2: Risk categorisation and mitigation.

Identifier	Risk	Severity	Probability	Mitigation
		Safety Risks		
RS-01	Material fatigue might lead to structural failure	Catastrophic: Structural failure by material fatigue would have catastrophic effects for both the aircraft and the people on board.	Low: A plethora of research has been conducted into material fatigue and how to mitigate it, when proper design procedures are applied, the chance of material fatigue should be rather low.	In order to bring the risk of material fatigue down to an acceptable level, regular inspections of the airframe will have to be conducted once it is in service. This lowers the probability of occurrence to very low.
RS-02	Structural failure under high load during manoeuvres or bad weather	Catastrophic: Structural failure would mean loss of the aircraft en lives on board.	Very low: Safety factors are already included in the requirements driven by regulations. Therefore the probability of this occurring is very low.	/
RS-03	Control subsystem failure	Catastrophic: Failure of the control subsystem in any way would make the aircraft uncontrollable.	Very low: With proper design, the risk of an entire subsystem failing is rather small.	/

RS-04	Landing gear extension issue	Critical: A landing gear extension issue might cause a belly landing. This poses a significant risk to the aircraft.	Moderate: Landing gear extension mechanisms are complicated systems and rely on multiple auxiliary subsystems. Therefore an issue with it is rather likely.	In order to mitigate the risk of a landing gear extension issue, a second procedure for extension, using a different means of powering the extension will be considered. This lowers the probability of occurrence to very low.
RS-05	Communication issue with ATC	Critical: Communication with ATC is vital for safety and for compliance with the regulations	Low: Communication systems will be tested before the launch of the product, furthermore different means of communicating are built-in.	/
RS-06	Pilot error	Catastrophic: Since pilots have the final control over the aircraft, pilot error may lead to loss of the aircraft.	Low: Although pilot error is the main cause of accidents, accidents are very rare and therefore the likelihood is considered low.	In order to decrease the chance of pilot error, two pilots will operate the aircraft. Additionally, extensive autopilot systems, as well as warning systems, will be included. this will lower the chance to very low
RS-07	Evacuation difficulties	Critical: The atypical layout of the Flying-V might cause issues in case an evacuation is required, especially when there is a fire on one side.	Moderate: The probability of an evacuation is rather low, however, in case of an evacuation this issue is rather likely.	Include extra emergency exits, perform extensive ground testing of evacuation procedures. This lowers the likelihood to low.
RS-08	Methane leakage	Catastrophic: Methane poses a significant asphyxiation risk, as well as a fire or explosion risk inside the confined space of an aircraft. Furthermore, methane leaks release a considerable amount of greenhouse gas into the atmosphere[1].	Low: Methane leaks are relatively common throughout natural gas systems[2]. However, for an aircraft environment high certification and testing standards will be applied. Therefore, the likelihood is considered low.	Install methane sensors in the area of the fuel tank, consider a venting system for the surroundings of the fuel tank. This lowers the severity to critical.

[1] https://www.scientificamerican.com/article/methane-leaks-erase-some-of-the-climate-benefits-of-natural-gas/
[2] https://www.edf.org/climate/methane-studies

RS-09	Turbine blade burst	Critical: A turbine blade burst can render an engine inoperative, however, the engine cowling should contain the failure.	Low: Extensive ground test runs, including debris ingestion tests will be performed, therefore the likelihood will be low.	/
RS-10	In-flight ammonia leak	Critical: Anhydrous ammonia is an incredible toxic gas, however, since the tank is located outside the pressurised confines of the cabin, it should not leak into the cabin. Ammonia leakage will cause the SCR to stop working, increasing NO^x emissions.	Very low: Pressure tanks can be tested extensively on ground before entry into service.	/
RS-11	Ammonia leak during refueling	Catastrophic: Ammonia is an incredibly toxic gas, and a leakage on the ground during refueling can cause significant harm to everyone in the vicinity.	Low: Fuel systems can be extensively tested before entry into service, although human error connecting the refueling equipment is always a risk.	The refueling with the anhydrous ammonia will take place when there are no passengers in the aircraft, furthermore, the ground worker refueling the aircraft will have to wear protective equipment. This lowers the severity to marginal.
		Timeline Risks		
RT-01	Issue during testing requiring large reworks	Catastrophic: Testing is one of the latest phases of design, therefore there is little time left for significant redesign	Moderate: Since the aircraft will most likely include a number of novel systems, the chances of a flaw being discovered during testing are deemed moderate	In order to avoid an issue only being discovered during testing, extensive unit testing, as well as verification and validation, will be performed, lowering the likelihood to very low
RT-02	Too many innovative systems lead to design delay	Catastrophic: In case development of one of the novel systems cannot be developed in time, entry into service can be delayed.	Moderate: In order to meet emissions targets, a large number of innovative concepts will be required	In order to decrease the scheduling risk, TRL of components will be taken into account in the trade-off. This will lower the likelihood to low
RT-03	Delay during production	Catastrophic: Delays in production can most likely not be caught up before the foreseen launch date	Moderate: Production delays are quite common for new designs.	Manufacturing concerns will be taken into account during the design process, lower the likelihood to low

RT-04	Overrun of technical budget	Critical: An overrun of one of the technical budgets requires significant redesigns and can cause delays	Moderate: Original technical budgets have been set up early on in the design process, therefore the chance of a budget overrun is considered marginal	A contingency plan will be set up, lowering the severity to marginal
RT-05	Technology not at the level assumed for 2036	Critical: In case the technology is not at the level assumed before entry into service, some requirements might not be met.	Moderate: 2036 is still a long way off, and predicting the level of technology in the future is no exact science.	If possible, conservative estimates will be used, lowering the likelihood to very low.
		Technical performance risks		
RP-01	CO_2 Emission target not met	Catastrophic: This would mean one of the main user requirements is not met	Very low: This is one of the main driving user requirements that the design will be based on	/
RP-02	NO_X Emission target not met	Catastrophic: This would mean one of the main user requirements is not met	Very low: This is one of the main driving user requirements that the design will be based on	/
RP-03	Noise target not met	Catastrophic: This would mean one of the main user requirements is not met	Very low: This is one of the main driving user requirements that the design will be based on	/
RP-04	Sensor failure	Critical: A sensor failure could hamper the pilot or autopilot in controlling the plane, therefore this could lead to a safety issue	Moderate: An aircraft contains many sensors, therefore the chance of one failing throughout the lifetime of an aircraft is considered moderate	In order to reduce the severity to negligible, at least three redundant sensors will be used so that cross-validation is always possible
RP-05	Actuator failure	Critical: An actuator failure could lead to controllability issues, causing a safety concern	Moderate: An aircraft contains many actuators, therefore the chance of one throughout the lifetime of an aircraft is considered moderate	Critical actuators will be designed for redundancy, lower the severity to marginal
RP-06	Computer failure	Catastrophic: A computer failure can cause safety concerns, by virtue of disabling autopilot and causing fly by wire issues	Low: Extensive ground testing can be performed for computer systems.	A redundant, distributed computing setup will be used, lowering the probability to very low and severity to marginal

RP-07	Control issues	Critical: Not being able to perform certain manoeuvres might lead to operational inefficiencies.	Moderate: Controllability difficulties is one of the main drawbacks of a flying-V design, since it is a tailless design.	During the detailed design phase, special attention will be payed to the design of the control surfaces, lowering the likelihood to very low.
		Operational risks		
RO-01	Aircraft design does not fit in current airport infrastructure	Catastrophic: This would mean that the aircraft would be severely limited in what airports it can operate into	Very low: This will be taken into account in the design phase, therefore the likelihood of occurrence is very low	/
RO-02	Aircraft cannot use current airport equipment	Critical: This would drastically increase operating costs	High: With the high likelihood of using novel energy sources, some specialised ground will most likely be needed	This extra cost will be taken into account in the budget, lowering the severity to marginal
RO-03	Aircraft requires long turn-around	Critical: This would drastically increase both operating costs and decrease revenues	Low: Predicted turn-around time will be taken into account during design, however with novel concepts a higher turn-around time is possible	/
RO-04	Grey Methane	Critical: In case grey methane is supplied at the airport, the CO_2 emission requirements, which is a top level user requirement, will not be met. This will however have no further impact on the aircraft performance.	Moderate: At the moment of entry into service, many gas grids around the world will still be running on grey methane, or a mixture of grey and green methane. However, further along the lifespan of the aircraft, more and more grids will switch to higher concentrations of green methane.	Since the fuel supplied at the airport is not controlled by the manufacturer, this is a risk that will have to be accepted.

15.3. Risk Map

In Table 15.3 the final risk map including mitigation is presented. As can be observed, a number of risks remain in the red area. A mitigation strategy has however been considered, but was not sufficient to reduce the risk to an acceptable level. These risks will however be closely monitored.

Table 15.3: Risk map including mitigation.

	Very low	**Low**	**Moderate**	**High**	**Very High**
Catastrophic	RS-01, RS-02, RS-03, RS-07, RT-01, RP-01, RP-02, RP-03, RO-01,	RT-02, RT-03			
Critical	RS-04, RP-07, RS-10	RS-05, RO-03, RS-07, RS-08, RS-09, RT-05	RO-04		
Marginal	RP-06	RS-11	RT-04, RP-05	RO-02	
Negligible			RP-04		

16 Future Development

In this chapter the future development of the project is discussed. First of all, the project design and development logic is presented in Section 16.1. Then the production plan is given in Section 16.2. After this the project Gannt chart can be seen in Section 16.3. Finally, the sustainable development strategy is discussed in Section 16.4.

16.1. Project Design and Development Logic

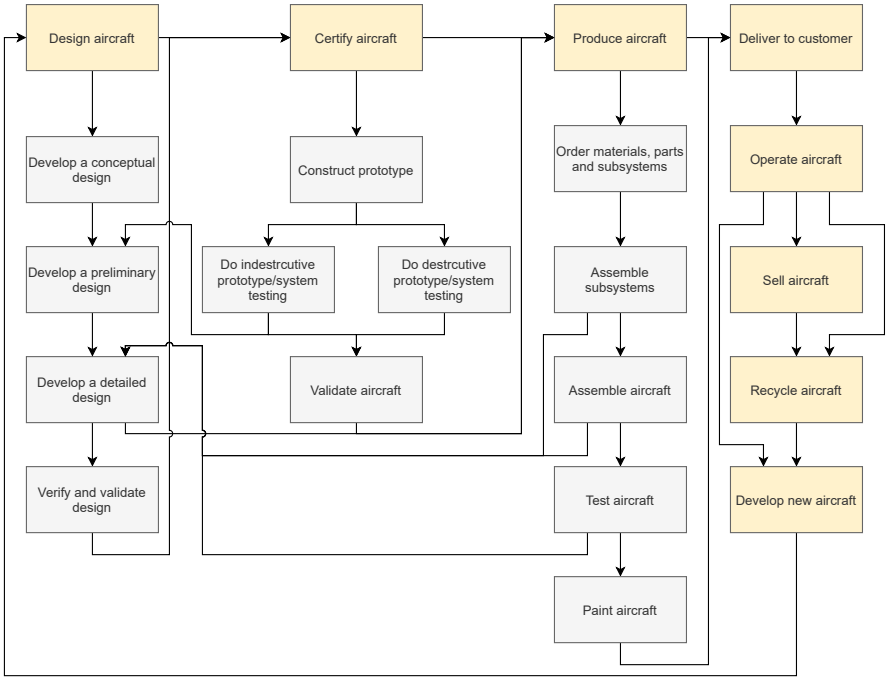

Figure 16.1: Project design and development logic diagram.

The project development logic is split into three main groups: design of the aircraft, certification of the aircraft and production of the aircraft. First of all, the design phase is split into three phases: conceptual design, preliminary design and detailed design [114]. The conceptual design stage has been done in the series of these reports. A preliminary design phase follows after that. During this phase the aircraft's design does not change too much, however, it goes into more detail, especially the structural and control design [114]. Additionally, a lot of test are done during this design phase. Usually test in wind tunnels are carried out, however, for this project acoustic and emissions test should also be done to verify that the design is capable of reaching the set out requirements. After this stage, depending on the success of the preliminary design, the project is frozen for the production of aircraft. In the detailed design phase very minor design is done, like the structure joining design. Finally, the design has to be verified and validated.

After the design phase the certification phase comes. This includes steps like constructing a prototype and doing destructive and nondestructive tests. Depending on the outcomes of these tests, the aircraft is either validated or it is returned to the preliminary design phase, to fix the problems.

Finally, after the aircraft is validated, it is time to produce it. First of all, the needed materials, parts and subsystems are ordered. Then the subsystems are assembled and the whole aircraft is assembled. After this the aircraft is tested, painted and delivered to the customer. During the assembly and

testing of aircraft some minor flaws or possible improvements could be found and the project could be brought back to the detailed design phase, however, this time the aircraft would not need the extensive certification and after improving the detailed design it could be bought back to the production phase.

Of course, after delivering the aircraft to the customer it is operated. The aircraft should operate for at least 30 years. Then it is either sold to another customer or recycled. Depending on the success of the aircraft, a development of the updated version of the aircraft can start during the operation of the original aircraft.

16.2. Production Plan

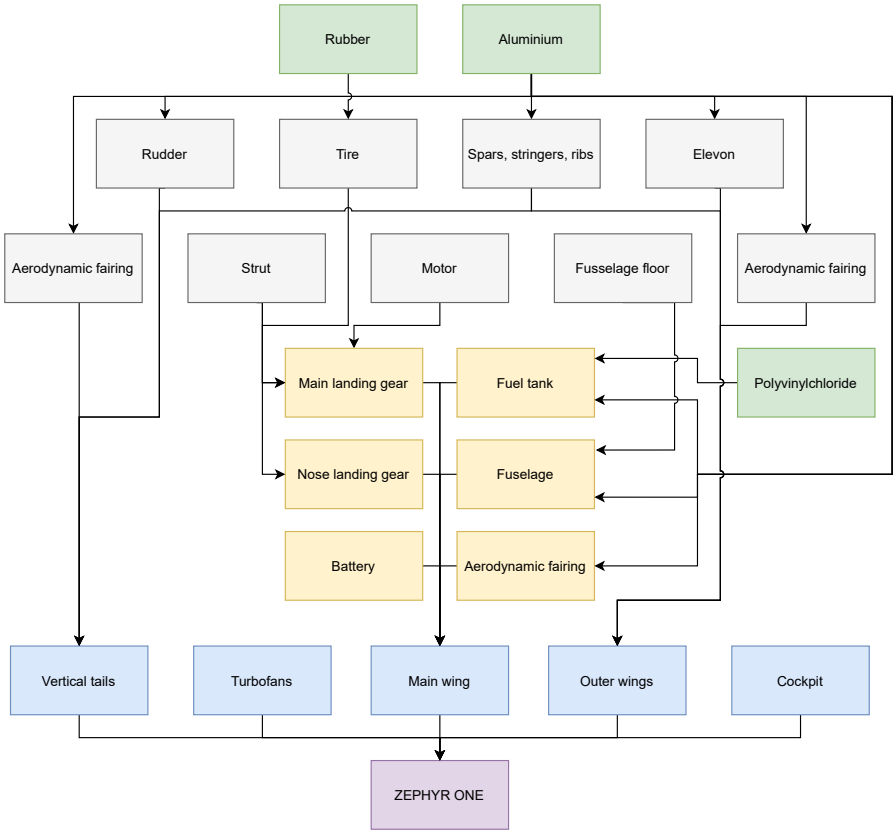

Figure 16.2: Aircraft production plan.

The production of aircraft is usually done in assemblies or subassemblies. This is also the case for Zephyr One. The aircraft production is split into five assemblies: vertical tail, turbofans, main wing, outer wings and cockpit. The main wing is the largest and most complex part of them wall. Thus, a bottleneck could form for this assembly. This could be countered by increasing the work force on this assembly or making more assembly lines. Of course, all of the assemblies and subassemblies would run in parallel to make the production more efficient.

Main wing part would be made out of these main subparts: aerodynamic fairing, fuselage, fuel tank, battery, main and nose landing gear. The landing gears would be assembled out of rubber tires, struts, and the main landing gear would feature motors for emission-free taxi. The motors would be ordered and not constructed on site. Also, the battery would be ordered. The fuselage, aerodynamic fairing and fuel tank would be mainly made out of aluminium and the fuel tank insulation would be made out of polyvinylchloride.

The outer wings and vertical tail would be constructed out of aerodynamic fairing, ribs, spars and stringers, which would be made out of aluminium. Additionally, the elevon would be fitted into the outer wings and rudder into the vertical tail. The production plan diagram is presented in Figure 16.2

16.3. Project Gantt Chart

The main project phases of the Zephyr One is: design, certification and production. It is expected that the design phase will take about 11 years. Boeing 777 had a design phase of about seven years [115], however, it has a lot of similarities with the Boeing fleet and a considerable amount of parts and systems can be reused. Zephyr One is a new generation aircraft and no similar aircraft exist for it. Thus, the design phase has to take more time due to the uniqueness of the aircraft. Certification phase for Zephyr One should take about 1.5 years. The Boeing 777 featured a approximately two year certification process [115] and A350 had just testing done for 14 months[1]. This is an ambitious goal, however, in order to offer the aircraft to the market at the best moment, this goal should be reached. It is also expected that the system tests will be carried out alongside the construction of the prototype. Finally, the production time of the first aircraft is estimated to be one year, which is close to the prototype construction time and the A350 first aircraft assembly time [116]. All in all, the first aircraft is expected at early 2035. The market analysis suggested that the best time for the aircraft to enter the market is 2036, leaving one year for highly likely delays. The production of Zephyr One should last till about 2056, and a newer version can be developed during the production phase. The Gantt chart of the project is presented in Figure 16.3.

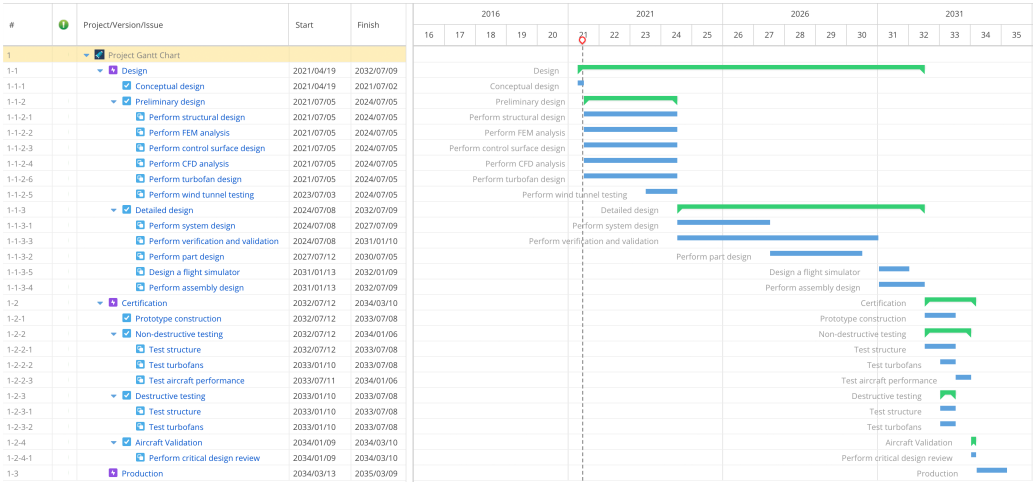

Figure 16.3: Project Gantt chart.

16.4. Sustainable Development Strategy

Sustainability was one of the main goals of the design of Zephyr One. The design focused mainly on the sustainability during the flight phase, however, the sustainability should be also addressed in other aircraft life phases. In this section, the sustainable development strategy regarding the general future design process is discussed. In addition to this, the strategies for manufacturing, end-of-life procedures, and fuel production are addressed in particular.

16.4.1. Future Design Process

In order to ensure the implementation of sustainability throughout the future design process, a strategy regarding sustainability is constructed that mirrors the one implemented throughout the DSE. Every major decision has to be backed up with detailed research regarding each option's impact on sustainability. Next, a fair trade-off between the different options with a variety of trade-off criteria must be performed to ensure that the correct choice is made. Finally, the effect of the winning option on sustainability must be quantified to ensure compliance with the requirements, and, if necessary, the process must be repeated.

[1] `https://www.airbus.com/aircraft/how-is-an-aircraft-built/test-programme-and-certification.html` [cited 15 June 2021]

16.4.2. Manufacturing

For more sustainable aircraft manufacturing process, the energy consumption has to be reduced [117]. The high amounts of energy used during manufacturing strongly correlates to larger amounts of emissions, as most of the energy comes from non renewable sources. The goal of the manufacturing of Zephyr One is to reduce the energy used, reduce waste produced, so energy would not be spent on waste, and use more sustainable energy sources.

A promising technology, which is currently being heavily developed, is additive manufacturing (AM). Currently this technology's application is quite limited, but it is expected that in the future this technology will be more widely used [118]. For Zephyr One AM would be beneficial for the turbofan, which features a lot of complex part. Additionally, it could be used for other less complex parts like control surfaces or landing gears. Regarding sustainability this the technology, which should be used, as most as possible, during manufacturing of the aircraft. It has been shown that AM needs less energy to manufacture aircraft parts [119].

Lean manufacturing is another philosophy, which should be implied in the manufacturing process. This manufacturing process focuses on the reduction waste or eliminating not value adding processes during manufacturing. Research has showed that this process strongly correlates to more sustainable manufacturing [120]. As less energy is wasted on not essential manufacturing process, the emission amount is reduced. Additionally, lean manufacturing is good way of increasing the profitability.

Finally, more renewable energy should be used for the manufacturing of Zephyr One. Currently the use of renewable energy is quite low compared to fossil fuel energy, however, it is expected that in the future renewable energy use will grow and the price of it will even drop more[2]. Fossil fuel energy prices is not dropping any more (in some cases even increasing) while the renewable energy prices are dropping due to the learning curve. Thus, it is expected that in the future the renewable energy will be more available and cheaper, thus, it likely that the Zephyr One will be manufactured with mainly renewable energy.

16.4.3. Fuel Production

The aircraft features the option for the use of LNG. This is not a sustainable option, still LNG emits less carbon dioxide into the atmosphere compared to jet fuel due to its higher energy density and higher hydrogen and carbon ration, but this option exists for customers to be flexible with fuel. The goal of Zephyr One is to be commercially viable, but also have an option to become more sustainable. Thus, the aim is to increase the the fraction of synthetic methane used for the Zephyr One. During the production of synthetic methane the carbon dioxide emitted during flight is absorbed to produce the methane [3]. With a more developed synthetic methane production line the Zephyr One will be able to switch fully to synthetic methane and the aircraft emissions will be absorbed during production. The price of synthetic methane should match LNG in 2050 and by that time the production line should be developed enough [121].

In order to have a fully sustainable fuel production, the transportation and sustainable resources should be used. First of all, the transportation of methane should not produce emissions. This can be possible by making production plants at airports and transporting it by methane pipes. Another option is having more central production plants and transporting it by other means of sustainable transport or investing a lot into methane pipes. On the other hand, with the current trends a sustainable transport is very achievable in the near future. Second of all, during methane production hydrogen is used [121]. This means that green or blue hydrogen should be used. This mean that the hydrogen should be produced from sustainable energy or the emissions should be captured and could be used for the production of methane.

[2] `https://ourworldindata.org/cheap-renewables-growth` [cited 15 June 2021]

17 Aircraft Verification & Validation

In this chapter the validation of the Zephyr One is done. This is done by checking, if the aircraft meets the set out requirements in the Baseline report [2]. Some of the requirements were not met, so the reason for not meeting them is presented in Section 17.1. The requirement compliance matrix is given in Section 17.2.

17.1. Feasibility Analysis

EFMRA-SYS-PF-08 has not been met because during the Baseline phase a value for a conventional aircraft was used, however, Flying-V configuration features a high sweep angle, so the aircraft can fly at higher Mach number. The goal of this requirement was to constraint the design not to from shock waves, so that no high drag would occur. This requirement was poorly made and should have been excluded in the Baseline, as other requirements constraint high amounts of drag.

EFMRA-SYS-SF-11.2 was not met, as it was changed to a diversion of 370.4 km. It was assumed that there will always be a diversion airport planned, thus, the aircraft was not designed for a flight plan without a diversion airport.

EFMRA-SYS-SF-01.3 and **EFMRA-SYS-SF-06.1** were not analysed, as they require a more complete design of the aircraft. No good sources were found to see if the aircraft meets **EFMRA-SYS-SF-12**, so it was also not analysed at this time. However, it is likely that the aircraft will meet these requirements.

EFMRA-SYS-SF-02 is currently not met because the aircraft cannot rotate during take-off, but with a more in depth analysis this requirement could be met.

17.2. Compliance Matrix

The compliance matrix is presented in Table 17.1, 17.2 and 17.3. Requirement codes highlighted in red mean that the requirement was not met and in in yellow means that the requirement compliance was not analysed (requirements with black cells are the requirement group parent requirement).

Table 17.1: Requirement compliance matrix.

Requirements		Compliance	
Performance requirements			
EFMRA-SYS-PF-01	The aircraft shall have a range of at least 6,150 km.	✓	Chapter 12
EFMRA-SYS-PF-02	The aircraft shall have a endurance of at least 6 h.	✓	Chapter 12
EFMRA-SYS-PF-03	The aircraft shall have a cruise speed of at least 830 km/h.	✓	Chapter 18
EFMRA-SYS-PF-04	The aircraft shall have a cruise altitude of at least 9,144 m.	✓	Chapter 18
EFMRA-SYS-PF-05	The aircraft shall have a take-off distance of at most 2,100 m.	✓	Chapter 12
EFMRA-SYS-PF-06	The aircraft shall have a landing distance of at most 1,500 m.	✓	Chapter 12
EFMRA-SYS-PF-07	The aircraft shall be able to carry at least 200 passengers and their luggage.	✓	Chapter 4
EFMRA-SYS-PF-08	The aircraft shall operate up to a Mach number of 0.8.	0.82	
EFMRA-SYS-PF-09	The aircraft shall have a rate of climb of at least 12.7 m/s.	✓	Chapter 12

Table 17.2: Requirement compliance matrix cont'd.

EFMRA-SYS-PF-10	The aircraft shall have a stall speed in landing configuration of no more than 55.8 m/s.	✓	Chapter 5
EFMRA-SYS-PF-11	The aircraft shall be able to carry up to 4.5 tons of cargo.	✓	Chapter 4
	Safety requirements		
EFMRA-SYS-SF-01	The aircraft shall comply with CS-25 climb gradient requirements.		
EFMRA-SYS-SF-01.1	The aircraft shall be capable of having a climb gradient of at least 1.2% during take-off.	✓	Chapter 12
EFMRA-SYS-SF-01.2	The aircraft shall be capable of having a climb gradient of at least 3.2% during an aborted landing.	✓	Chapter 12
EFMRA-SYS-SF-01.3	The aircraft shall be capable of having a climb gradient of at least 0% with one engine inoperative and with the landing gear retracted.		
EFMRA-SYS-SF-01.4	The aircraft shall be capable of having a climb gradient of at least 2.4% with one engine inoperative.	✓	Chapter 12
EFMRA-SYS-SF-02	The aircraft shall be stable and controllable.		
EFMRA-SYS-SF-03	The aircraft shall be capable of safely landing and taking-off with at most 37 km/h crosswind.	✓	Chapter 9
EFMRA-SYS-SF-04	The aircraft shall comply with CS-25 loading requirements.		
EFMRA-SYS-SF-04.1	A safety factor of 1.5 shall be applied for prescribed limit loads.	✓	Chapter 7
EFMRA-SYS-SF-04.2	The positive limit manoeuvring load factor shall not be less than 2.5.	✓	Chapter 7
EFMRA-SYS-SF-04.3	The negative limit manoeuvring load factor shall not be more than -1.	✓	Chapter 7
EFMRA-SYS-SF-05	In case of one aisle the aircraft shall not have more than 3 seats abreast on each side of the aisle in any one row.	✓	Chapter 4
EFMRA-SYS-SF-06	The aircraft shall comply with CS-25 climate control requirements.		
EFMRA-SYS-SF-06.1	At any time during the flight the aircraft shall be capable of providing at least 0.25 kg of fresh air per minute for each person on board.		
EFMRA-SYS-SF-06.2	The aircraft shall be capable of maintaining a cabin pressure altitude of at most 2438 m.	✓	Chapter 7
EFMRA-SYS-SF-7	The aircraft shall have an emergency fuel pump in case of failure of the main pump.	✓	Chapter 6
EFMRA-SYS-SF-8	The engine of the aircraft shall be separated by a firewall from the rest of the aircraft.	✓	Chapter 7
EFMRA-SYS-SF-10	The aircraft shall comply with CS-25 emergency exit requirements.		
EFMRA-SYS-SF-10.1	The emergency exits on the same side shall not be spaced more than 18.3 m apart.	✓	Chapter 4
EFMRA-SYS-SF-10.2	The aircraft shall have at least two Type I emergency exits on each side of the fuselage.	✓	Chapter 4
EFMRA-SYS-SF-10.3	The aircraft exits shall be designed for a 240 passenger capacity in one-class configuration.	✓	Chapter 4
EFMRA-SYS-SF-11	The aircraft shall comply with safety rules for reserve fuel/energy.		
EFMRA-SYS-SF-11.1	The aircraft shall have at least 5% of contingency fuel/energy.	✓	Chapter 12
EFMRA-SYS-SF-11.2	The aircraft shall have alternate fuel/energy to fly for at least 2 hours at cruise conditions.		370.4 km

Table 17.3: Requirement compliance matrix cont'd.

EFMRA-SYS-SF-11.3	The aircraft shall have final reserve fuel/energy to fly for at least 30 min at holding speed at an altitude of 450 m.	✓	Chapter 12
EFMRA-SYS-SF-12	The aircraft shall be able to achieve an ETOPS 180 certification.		
EFMRA-SYS-SF-13	Each passenger can be seated at a maximum angle of 18 degrees from the centre line without any special safety equipment	✓	Chapter 4
Flightpath 2050 requirements			
EFMRA-SYS-FP-01	The aircraft shall be at least 75% recyclable.	✓	Chapter 14
EFMRA-SYS-FP-02	The aircraft shall comply with Flightpath 2050 goals for noise.		
EFMRA-SYS-FP-02.1	The aircraft shall have a fly-over reference noise lower than 59 dBA.	✓	Chapter 11
EFMRA-SYS-FP-02.2	The aircraft shall have an approach reference noise lower than 72 dBA.	✓	Chapter 11
EFMRA-SYS-FP-02.3	The aircraft shall have a lateral reference noise lower than 69 dBA.	✓	Chapter 11
EFMRA-SYS-FP-03	The aircraft shall comply with Flightpath 2050 goals for emissions.		
EFMRA-SYS-FP-03.1	The aircraft shall produce no more than 2.917 kg/km of CO_2 emissions for its mission range.	✓	Chapter 6
EFMRA-SYS-FP-03.2	The aircraft shall produce no more than 0.0057 kg/km of NO_x emissions for its mission range.	✓	Chapter 6
EFMRA-SYS-FP-03.3	The aircraft shall produce no emissions while taxiing.	✓	Chapter 6
Airport requirements			
EFMRA-SYS-AP-01	The aircraft shall be able to operate at a 4C type aerodrome.		
EFMRA-SYS-AP-01.1	The aircraft shall have a wingspan no larger than 36.8 m.	✓	Chapter 13
EFMRA-SYS-AP-01.2	The aircraft shall have a tail height not larger than 13.7 m.	✓	Chapter 13
EFMRA-SYS-AP-02	The aircraft shall have a turn around time of no more than 52 min.	✓	Chapter 13
EFMRA-SYS-AP-03	The aircraft shall be compatible with existing ground material for the loading and unloading of passengers.	✓	Chapter 13
Financial requirements			
EFMRA-SYS-FR-01A	The aircraft shall cost not more than 100 million euros.	✓	Chapter 14
EFMRA-SYS-FR-02A	The aircraft shall have operational costs per seat no higher than the reference aircraft.	✓	Chapter 14
EFMRA-SYS-FR-03	The aircraft shall be available by 2036.	✓	Chapter 16
EFMRA-SYS-FR-04	The aircraft shall be able to perform 4 flights per day for medium haul operations.	✓	Chapter 14
EFMRA-SYS-FR-05	The aircraft shall have an operational life of at least 30 years.	✓	Chapter 14
EFMRA-SYS-FR-06	The aircraft shall have no additional maintenance cost compared to the reference aircraft.	✓	Chapter 14

18 Conclusion

The aim of this report was to present a conceptual technical design of Zephyr One and the steps taken to make the design. This was done by constructing codes for all systems, combining these codes and iterating. For most of the aircraft systems, like aerodynamics, structures, propulsion weight and configuration, this iteration was successful. All in all, Zephyr One meets the Flightpath 2050 goals for sustainability and it is also competitive for cost between other competing aircraft. The most important aircraft specifications are presented in Table 18.1.

The Zephyr One is 11% more expensive than the A321neo aircraft, but offers unparalleled reductions in perceived noise levels, NO_x and CO_2 emissions. The Zephyr One has superior range capability compared to competing aircraft making it suitable for medium and long range operations, improved passenger comfort but also catering low-cost carriers and its cargo capacity makes it an integrated freight solution. Furthermore, the aircraft is a safer investment as future taxes on fossil fuels will only strength its business case. Compared to the A321neo, the Zephyr One offers 3.2% lower costs per seat and 16% compared to the A321ceo reference aircraft. With the advantages of the Zephyr One outweighing the acquisition price disadvantage and an early service entry in 2035-2036, the Zephyr One will be able to capture a minimum of 4,750 sales giving it a 15%-21% market share.

Regarding the future of the project, the project should continue to the preliminary design phase. In this phase the structure and control and stability has to be analysed in much more detail. Also, CFD, FEM, and noise analyses should be done in this phase. As at this stage problems with elevators and landing gear were detected, in the upcoming phase design solution have to be come up with to fix these identified problems. First of all, currently the aircraft has rotation problems at take-off, thus, for future work, adjustments have to be made to make the aircraft rotate at take-off. Second of all, the landing gear height is 5 m, and in future this value should be reduced to make the aircraft more accessible. With the preliminary design and detailed design complete, the aircraft can undergo certification and a highly anticipated production of the first unit.

A lot of new concepts are being created with hydrogen. While hydrogen is a more sustainable fuel, it comes with some big drawbacks - low density and temperature of it. While hydrogen can become the leading aviation fuel in the long future, solutions need to be developed for the upcoming future, which are commercially viable. Zephyr One is that solution. While the Zephyr One is not as sustainable, as hydrogen aircraft, it offers the customer to choose the sustainability and profitability with use of LNG or synthetic methane and helps airports become better neighbors with reduced noise footprints. Thus, Zephyr One offers a viable small step towards a more sustainable but viable future catering the growing demand for air travel in a responsible manner.

Table 18.1: Aircraft specifications.

Dimensions	
Wingspan	36 m
Length	34 m
Height	12.77 m
Capacity	
Max seating	260
Typical seating 2-class	203
Max payload	25.3 ton

Performance	
Range	6,482 km
MTOM	81 ton
Max fuel mass	13.5 ton
Max thrust	240 kN
NO_x	2.4 g/km
Maximum noise	67 dBA (at approach)
Cruise speed	869 km/h
Cruise altitude	12.9 km

References

[1] Rainer Storn and Kenneth Price. *Differential Evolution-A Simple and Efficient Heuristic for Global Optimization over Continuous Spaces*. 1997, pp. 341–359.

[2] Dhierin-Perkash Bechai et al. *Baseline Report Environmentally Friendly Medium-Range Aircraft*. Tech. rep. Delft University of Technology, 2021.

[3] Dhierin-Perkash Bechai et al. *Midterm Report Environmentally Friendly Medium-Range Aircraft*. Tech. rep. Delft University of Technology, 2021.

[4] U. Schumann. "The impact of nitrogen oxides emissions from aircraft upon the atmosphere at flight altitudes—results from the aeronox project". In: *Atmospheric Environment* 31.12 (1997), pp. 1723–1733. issn: 1352-2310. doi: https://doi.org/10.1016/S1352-2310(96)00326-3.

[5] Mathias Basner et al. "Aviation Noise Impacts: State of the Science". In: *Noise and Health* 19.87 (), pp. 41–50. doi: 10.4103/nah.NAH_104_16.

[6] Airbus SAS. *Cities, Airports and Aircraft, 2019-2038*. 2019.

[7] András Sóbester and Andy J Keane. *Airfoil Design via Cubic Splines-Ferguson's Curves Revisited*. University of Southamption.

[8] Johannes Achleitner, Kai Rohde-Brandenburger, and Mirko Hornung. "Airfoil optimization with CST-parameterization for (un-)conventional demands". In: July 2018.

[9] Airbus SAS. *A321 AIRCRAFT CHARACTERISTICS AIRPORT AND MAINTENANCE PLANNING*. 2020.

[10] The Boeing Company. *737 MAX Airplane Characteristics for Airport Planning*. 2015.

[11] European Union Aviation Safety Agency. *Certification Specifications and Acceptable Means of Compliance for Large Aeroplanes CS-25*. 2020.

[12] NEA. *Survey on standard weights of passengers and baggage*. 2009.

[13] R. Vos, M.F.M. Hoogreef, and B.T.C. Zandbergen. *The Design of the Fuselage*.

[14] Daniel P. Raymer. *Aircraft Design: A Conceptual Approach*. Washington, D.C.: AIAA, 1992.

[15] J.A. Melkert and R. Vos. *Exam Aerospace Design and System Engineering Elements I, 20 April 2017*. 2017.

[16] W J Oosterom. "Flying-V Family Design". Delft University of Technology, Apr. 2021.

[17] Egbert Torenbeek. *Synthesis of Subsonic Airplane Design*. Delft: Delft University Press, 1982. isbn: 9024727243.

[18] F Faggiano. "Aerodynamic Design Optimization of a Flying V Aircraft". Delft University of Technology, Nov. 2016.

[19] G Bourget. "The effect of landing gear implementation on Flying V aerodynamics, stability and controllability". Delft University of Technology, June 2020.

[20] Martin Hepperle. *JavaFoil - Analysis of Airfoils*. 2021.

[21] D.E. Hoak. *USAF Stability and Control DATCOM*. 1960.

[22] F. Oliviero. *Aircraft aerodynamic analysis - Lift and Drag*. 2020.

[23] R.A. Viet. *Analysis of the flight characteristics of a highly swept cranked flying wing by means of an experimental test*. Delft University of Technology, 2019.

[24] M Palermo. "The Longitudinal Static Stability and Control Characteristics of a Flying V Scaled Model". Delft University of Technology, Feb. 2019.

[25] John D. Anderson. *Fundamentals of aerodynamics*. 5th. McGraw-Hill, Feb. 2011. isbn: 9780073398105.

[26] J Benad. "A new configuration for commercial passenger transport". In: (2015).

[27] J. E. Green. “Greener by Design — the technology challenge”. In: *The Aeronautical Journal (1968)* 106.1056 (2002), pp. 57–113. doi: 10.1017/S0001924000095993.

[28] N. Chandrasekaran and Abhijit Guha. “Study of prediction methods for NOx emission from turbofan engines”. In: *Journal of Propulsion and Power* 28 (1 Sept. 2012), pp. 170–180. issn: 15333876. doi: 10.2514/1.B34245.

[29] Prakash Prashanth et al. “Post-combustion emissions control in aero-gas turbine engines †”. In: (). doi: 10.1039/d0ee02362k.

[30] “Observations of Methane Emissions from Natural Gas-Fired Power Plants”. In: *Environmental Science and Technology* 53 (15 Aug. 2019), pp. 8976–8984. issn: 15205851. doi: 10.1021/acs.est.9b01875.

[31] Pavlos Rompokos et al. “Liquefied Natural Gas for Civil Aviation”. In: *Energies* 13.22 (2020). issn: 1996-1073. doi: 10.3390/en13225925.

[32] Milos Lukic et al. “Modelling and Analysis of an Aircraft On-board Electric Taxiing System”. In: Institute of Electrical and Electronics Engineers Inc., Aug. 2019. isbn: 9781728133980. doi: 10.1109/ICEMS.2019.8921709.

[33] “State of the Art of Electric Taxiing Systems”. In: Institute of Electrical and Electronics Engineers Inc., Jan. 2019. isbn: 9781538641927. doi: 10.1109/ESARS-ITEC.2018.8607786.

[34] Baumüller. *DST2 Synchronous Torque Motors*. Nürnberg GmbH, 2019.

[35] Pieter-Jan Proesmans. *Preliminary Propulsion System Design and Integration for a Box-Wing Aircraft Configuration - A Knowledge Based Engineering Approach*. Dec. 2019. doi: 10.13140/RG.2.2.24359.78242.

[36] M Holland. *PRESSURIZED NON-CIRCULAR MEMBER-EFFECT OF MEAN-LINE FORM*.

[37] E. Novitskaya et al. “Reinforcements in avian wing bones: Experiments, analysis, and modeling”. In: *Journal of the Mechanical Behavior of Biomedical Materials* 76 (Dec. 2017), pp. 85–96. issn: 18780180. doi: 10.1016/j.jmbbm.2017.07.020.

[38] Leen Zhang et al. *Review of automated fibre placement and its prospects for advanced composites*. June 2020. doi: 10.1007/s10853-019-04090-7.

[39] Alderliesten René. *Introduction to Aerospace Structures and Materials*. Open Textbook Library, 2018. doi: https://doi.org/10.5074/t.2018.003.

[40] A A R Broer. “Fatigue life prediction of carbon fibre-reinforced epoxy laminates using a single S-N curve”. Delft University of Technology, Apr. 2018.

[41] Steve Thompson. *MIL-HDBK-5J NOTICE 2 DEPARTMENT OF DEFENSE HANDBOOK METALLIC MATERIALS AND ELEMENTS FOR AEROSPACE VEHICLE STRUCTURES*. 2006.

[42] M O Lai and W G Ferguson. *Fracture Toughness of Aluminium Alloy 7075-T6 in the As-cast Condition*. 1985, pp. 133–138.

[43] Fanran Meng et al. “From aviation to aviation: Environmental and financial viability of closed-loop recycling of carbon fibre composite”. In: *Composites Part B: Engineering* 200 (2020). issn: 13598368. doi: 10.1016/j.compositesb.2020.108362.

[44] Naveen Jesu Arockiam, Mohammad Jawaid, and Naheed Saba. *Sustainable bio composites for aircraft components*. 2018. doi: 10.1016/B978-0-08-102131-6.00006-2.

[45] R K Schmidt. *Masters Thesis: A Semi-Analytical Weight Estimation Method for Oval Fuselages in Novel Aircraft Configurations*.

[46] Elmer Franklin Bruhn. *Analysis and design of flight vehicle structures*. Jacobs Pub., 1973.

[47] David Roylance. *Fatigue*. 2001.

[48] Xin Wang et al. “Automated crack detection for digital radiography aircraft wing inspection”. In: *Research in Nondestructive Evaluation* 22 (2 Apr. 2011), pp. 105–127. issn: 09349847. doi: 10.1080/09349847.2011.556543.

[49] J. Roskam. *Airplane design, Part I: Preliminary sizing of airplanes*. Lawrence, KS: DARcorp, 1990.

[50] Daniel Schiktanz. “Conceptual Design of a Medium Range Box Wing Aircraft”. MA thesis. Hamburg University of Applied Sciences, 2011.

[51] Mohammad H. Sadraey. *AIRCRAFT DESIGN A Systems Engineering Approach*. Chichester, United Kingdom: John Wiley Sons, 2013.

[52] J. Roskam and University of Kansas. *Airplane Design: Part 2 - preliminary configuration design and integration of the propulsion system*. DARcorporation, 1985.

[53] D. Scholz. *Aircraft Design: Empennage Sizing*. 2015.

[54] Gustavo Jorge Resende. “A Proposal of Tail and Control Surface Design”. UNIVERSIDADE FEDERAL DE UBERLÂNDIA FACULDADE DE ENGENHARIA MECÂNICA, 2019.

[55] Roberto Merino-Martinez et al. *The Cryo-V: Silent and Climate-Neutral Medium Range Aircraft Final DSE Report.* June 2020. doi: 10.13140/RG.2.2.31363.94241.

[56] International Civil Aviation Organisation. *Noise Certification Workshop*. 2004.

[57] Christoph Zellmann, Jean Wunderli, and Christian Paschereit. “The sonAIR Sound Source Model: Spectral Three-Dimensional Directivity Patterns in Dependency of the Flight Condition”. In: Aug. 2016.

[58] Federal Aviation Administration. *Aviation Noise Effects*. 1985.

[59] R. L. Bennett and K. S. Pearsons. *Handbook of aircraft noise metrics*. 1981.

[60] Martin R. Fink. *Airframe Noise Prediction Method*. Federal Aviation Administration, 1977.

[61] G.J.J. Ruijgrok. *Elements of Aviation Acoustics*. Stevinweg 1, 2628CN Delft: Delft University Press, 1993.

[62] Werner Dobrzynski et al. “Research at DLR towards airframe noise prediction and reduction”. In: *Aerospace Science and Technology* 12 (1 2008). issn: 12709638. doi: 10.1016/j.ast.2007.10.014.

[63] Roberto Merino-Martínez, John Kennedy, and Gareth J. Bennett. “Experimental study of realistic low–noise technologies applied to a full–scale nose landing gear”. In: *Aerospace Science and Technology* 113 (2021). issn: 12709638. doi: 10.1016/j.ast.2021.106705.

[64] Roberto Merino-Martínez et al. “Multi-approach study of nose landing gear noise”. In: *Journal of Aircraft* 57 (3 2020). issn: 15333868. doi: 10.2514/1.C035655.

[65] Lothar Bertsch. “Noise Prediction within Conceptual Aircraft Design Dissertation”. In: *DLR Research Report* (2013).

[66] “System noise assessment of a tube-and-wing aircraft with geared turbofan engines”. In: vol. 56. 2019. doi: 10.2514/1.C034935.

[67] L. Maurice. *Noise Levels for U.S. Certificated and Foreign Aircraft*. 2012.

[68] Nicolas E. Antoine and Ilan M. Kroo. “Aircraft optimization for minimal environmental impact”. In: *Journal of Aircraft* 41 (4 2004). issn: 15333868. doi: 10.2514/1.71.

[69] A. E. Vieira. “Improving Capabilities in Modeling Aircraft Noise Sources”. Delft University of Technology, June 2021.

[70] F.H.V Dewitte. “Aircraft Noise Shielding Assessment: The creation of a software tool to predict aircraft noise shielding”. Delft University of Technology, Apr. 2016.

[71] Paul Roling. *Airport Planning, Design and Operations - Aircraft Noise*.

[72] Daichi Toratani. “Study on Simultaneous Optimization Method for Trajectory and Sequence of Air Traffic Management”. PhD thesis. Mar. 2016. doi: 10.13140/RG.2.2.27308.46727.

[73] David H. Williams, Rosa M. Oseguera-Lohr, and Elliot T. Lewis. *Design and Testing of a Low Noise Flight Guidance Concept*. 2004.

[74] Eurocontrol. *European CCO/CDO Action Plan*. 2020.

[75] William E. Zorumski. *Aircraft Noise Prediction Program Theoretical Manual*. Langley Research Center, Hampton, Virginia: National Aeronautics and Space Administration, 1982.

[76] Ir. Joris Melkert. *Altitude effects on aircraft performance*.

[77] Paul Roling. *Airport Planning, Design and Operations - Airside Classification and Capacity*.

[78] Paul Roling. *Airport Planning, Design and Operations - Airport of the Future*.

[79] Alessandro Bombelli. *Air Transportation - Airport of the Future*.

[80] International Civil Aviation Organisation. *Aerodrome Design & Operations*. 2018.

[81] FAA. "Advisory Circular 150/5300-13A, Airport Design". In: 2006. Chap. Chapter 1.

[82] International Civil Aviation Organisation. *Aerodrome Design Manual*. 2005.

[83] Transport Canada Technical Evaluation Engineering. *Aircraft Classification Numbers*.

[84] Xiong Li et al. "Simulation Study on Runway Threshold Stagger and Utilization Pattern of Closely Spaced Parallel Runways". In: Jan. 2015. doi: 10.2991/icectt-15.2015.49.

[85] NATS. *Wake Turbulence*. 2017.

[86] International Civil Aviation Organisation. *Environmental Protection*. 2018.

[87] Pavlos Rompokos et al. "Liquefied Natural Gas for Civil Aviation". In: *Energies* 13.22 (2020). issn: 1996-1073. doi: 10.3390/en13225925.

[88] Arvind Gangoli Rao, Feijia Yin, and Henri G.C. Werij. "Energy Transition in Aviation: The Role of Cryogenic Fuels". In: *Aerospace* 7.12 (2020). issn: 2226-4310. doi: 10.3390/aerospace7120181.

[89] Chevron Products Company. *Aviation Fuels Technical Review*. 2007.

[90] Rasmus Ø. Gadsbøll. *The technical application of liquefied methane as an aviation fuel*. 2020.

[91] Michael Schmidt. "A review of aircraft turnaround operations and simulations". In: *Progress in Aerospace Sciences* 92 (May 2017). doi: 10.1016/j.paerosci.2017.05.002.

[92] Jörg Clemens Fuchte. "Enhancement of aircraft cabin design guidelines with special consideration of aircraft turnaround and short range operations". PhD thesis. DLR eV, 2014.

[93] UPM TUD INECO. *The Time-efficient Airport Concept*. 2013.

[94] DLR NLR and INECO. *The Ultra-Green Airport Concept – An operational concept for 2050 and beyond*. 2013.

[95] Simone Y. ten Have, Konstantinos Gkiotsalitis, and Karst T. Geurs. "Investigating the Future of Ultrafast Charging: A Choice Experiment in the Netherlands". In: *World Electric Vehicle Journal* 11.4 (2020). issn: 2032-6653. doi: 10.3390/wevj11040070.

[96] Jachin Gorre, F. Ortloff, and Charlotte van Leeuwen. "Production costs for synthetic methane in 2030 and 2050 of an optimized Power-to-Gas plant with intermediate hydrogen storage". In: *Applied Energy* 253 (Nov. 2019), p. 113594. issn: 03062619. doi: 10.1016/j.apenergy.2019.113594.

[97] The Boeing Company. *Current Market Outlook 2018-2037*. 2018.

[98] The Boeing Company. *Current Market Outlook 2020-2039*. 2020.

[99] Japan Aircraft Development Corporation. *Worldwide Market Forecast 2020-2040*. 2021.

[100] The Boeing Company. *Current Market Outlook 2013-2032*. 2013.

[101] The Boeing Company. *Current Market Outlook 2019-2038*. 2019.

[102] Feijia Yin and Roberto Merino-Martinez. *Project Guide Design Synthesis Exercise ENVIRONMENTALLY FRIENDLY MEDIUM-RANGE AIRCRAFT*. 2021.

[103] Jacob Markish. *Valuation Techniques for Commercial Aircraft Program Design*. 2002.

[104] Daniel P. Raymer. *Aircraft Design: A Conceptual Approach*. Playa del Rey, California: AIAA, 2012.

[105] SGI Aviation. *The financial impact of extending or reducing a lease*.

[106] Kennet Bandelier. *Aging Aircraft and Obsolete Avionics Chapter Summit 2011*. 2011.

[107] Jacob Markish. “Valuation Techniques for Commercial Aircraft Program Design”. Massachusetts Institute of Technology, June 2002.

[108] William Albert Young II. “Learning Rates With Confidence Limits For Jet Engine Manufacturing Processes and Part Families From Noisy Data”. The School of Eletrical Engineering et al., Nov. 2005.

[109] R Hess and H Romanoff. *Aircraft Airframe Cost Estimating Relationships: All Mission Types”*. Dec. 1987.

[110] Dagmar Nelissen et al. *Availability and costs of liquefied bio- and synthetic methane*. 2020.

[111] Flavio Soares de Oliveira Junior et al. “A practical approach to support end-of-life commercial aircraft parking, market relocation, retirement and decommissioning strategic decisions”. In: *International Journal of Production Research* (2020).

[112] XiaoJia Zhao et al. “Aircraft Disposal and Recycle Cost Estimation”. In: *Advances in Transdisciplinary Engineering* 4 (2016), pp. 685–694.

[113] Sebastião Vieira de Freitas Netto et al. *Concepts and forms of greenwashing: a systematic review*. 2020. doi: 10.1186/s12302-020-0300-3.

[114] Jr John D. Anderson. *Aircraft Performance and Design*. New Delhi, India: Tata McGraw-Hill, 2010.

[115] Niels Jørgensen. “THE BOEING 777: DEVELOPMENT LIFE CYCLE FOLLOWS ARTIFACT”. In: (2006).

[116] Airbus SAS. *A320 FAMILY: the most successful aircraft family ever*. 2021.

[117] Martin Bornschlegl, Markus Bregulla, and Jörg Franke. “Methods-Energy Measurement – An approach for sustainable energy planning of manufacturing technologies”. In: *Journal of Cleaner Production* 135 (2016), pp. 644–656. issn: 0959-6526. doi: https://doi.org/10.1016/j.jclepro.2016.06.059.

[118] Markus Korpela et al. “Additive Manufacturing—Past, Present, and the Future”. In: *Technical, Economic and Societal Effects of Manufacturing 4.0: Automation, Adaption and Manufacturing in Finland and Beyond*. Ed. by Mikael Collan and Karl-Erik Michelsen. Cham: Springer International Publishing, 2020, pp. 17–41. isbn: 978-3-030-46103-4. doi: 10.1007/978-3-030-46103-4_2.

[119] Runze Huang et al. “Energy and emissions saving potential of additive manufacturing: the case of lightweight aircraft components”. In: *Journal of Cleaner Production* 135 (2016), pp. 1559–1570. issn: 0959-6526. doi: https://doi.org/10.1016/j.jclepro.2015.04.109.

[120] Sri Hartini and Udisubakti Ciptomulyono. “The Relationship between Lean and Sustainable Manufacturing on Performance: Literature Review”. In: *Procedia Manufacturing* 4 (2015). Industrial Engineering and Service Science 2015, IESS 2015, pp. 38–45. issn: 2351-9789. doi: https://doi.org/10.1016/j.promfg.2015.11.012.

[121] Jachin Gorre, Felix Ortloff, and Charlotte van Leeuwen. “Production costs for synthetic methane in 2030 and 2050 of an optimized Power-to-Gas plant with intermediate hydrogen storage”. In: *Applied Energy* 253 (2019), p. 113594. issn: 0306-2619. doi: https://doi.org/10.1016/j.apenergy.2019.113594.